pH-responsive polymers for nucleic acid and vaccine delivery

David James Peeler

A dissertation

submitted in partial fulfillment of the

requirements for the degree of

Doctor of Philosophy

University of Washington

2019

Reading Committee:

Suzie H. Pun, Chair

Drew L. Sellers, Co-chair

Patrick S. Stayton

Program Authorized to Offer Degree:

Bioengineering

i

University of Washington

Abstract

pH-responsive polymers for nucleic acid and vaccine delivery

David James Peeler

Chair of the Supervisory Committee

Suzie H. Pun

Department of Bioengineering

Biomacromolecules such as nucleic acids and peptides have great potential as therapeutics but must overcome many challenging biological barriers to succeed in the clinic. In this work, we present several investigations of stimulus-responsive polymers developed to navigate both extracellular and intracellular barriers to biologic drug delivery. We begin with a review of past applications of pH-responsive chemistries in nucleic acid delivery (**Chapter 1**). After screening a panel of lytic peptides in a pH-sensitive polymer conjugate system that mediates endosomal escape of plasmid cargo (**Chapter 2**), we evaluate the most promising gene delivery vector in a mouse model of traumatic brain injury (**Chapter 3**). Our efforts to develop engineered stem cells transplants as alternatives to gene delivery are then discussed (**Chapter 4**). Finally, we adapt our pH-responsive polymer for the delivery of peptide vaccine cargo (**Chapter 5**) and detail future directions to further improve antigen and adjuvant delivery with polymers (**Chapter 6**).

TABLE OF CONTENTS

i

LIST OF FIGURES

LIST OF TABLES

ACKNOWLEDGEMENTS

I am first and foremost grateful to **Suzie Pun** for being my greatest inspiration, my greatest source of confidence, my strongest champion, and my part-time counselor. Your dedicated leadership and ever-loving trust have given me the strength to dream and pursue dreams, and your thoughtful insights have sharpened my mind and inspired my life's work. I am so grateful that you gave me this opportunity, and so proud to be a part of your academic family forever.

I am profoundly grateful to the many people who have given me so much, in so many ways, over the past five years. Although I am unable to thank all of you in this document, and in no way would this thanks ever be able to express the depth of my gratitude and love, I am specifically grateful:

To my co-mentor **Drew Sellers**, who is one of the realest people I've ever met. I'm so glad I had you around to tell me it like it was anytime I was struggling in a mire of anxiety. You've taught me much of what I know about science in both practical and philosophical terms, and I'll always be grateful for the many pushes you gave me to go out on a limb and test new ideas. I'll most remember our spontaneous brainstorms and KEXP listening parties.

To my committee member and part-time mentor, **Pat Stayton**, for his generous collaboration, mentorship, and comradery. You've always made me feel like a part of your academic family, and I look forward to one day putting my feet on your ceiling to cement that.

To my undergraduate research assistants **Salina Thai** and **Nicholas Luera**, whose optimism and dedication made our time together as fun as it was rewarding. You taught me how to teach, you tolerated me (impressive!), and you made this work possible. I'm so excited to see where you go and I'm here for you forever.

To my earliest mentors at the University of Washington: **Floyd Karp, Jojo Das, Anna Blakney, Kim Woodrow,** and **Nataly Kacherovsky**. You put my feet on the ground and my hands in motion at a critical junction, and I'll always remember your support. Similarly, I am thankful for **Brynn Olden, Gary Liu,** and **Bob Lamm**, who welcomed me into the Pun lab family with open arms and became my friends for life. You are each incredible role models and I'm lucky to have spent so much of my time here with you.

To my chemistry mentors **Yilong Cheng, Selvi Srinavisan,** and **Anthony Convertine**, for equipping me with the skills to realize the designs we spent so much time talking about, and for your encouragement and respect at every stage of my development as a polymer chemist.

To my collaborators **Albert Yen, Charlie Roco, Alex Rosenberg, Anna Kuchina, Georg Seelig, Phil Horner, Liza Severs**, and members of the **Pun lab** for generous support, stimulating creative discussions, and for sharing your passion in the pursuit of scientific greatness.

To my fellow bioengineers **Alex Jiao, Eric Swanson, Hannah Frizzell, Alissa Bleem, Hal Holmes, Amy Oreskovic, Daniel Corbett, Alex Prossnitz,** and **Lars Crawford**, for forging the closest friendships I'm likely to hold in this life. You have all inspired me to be a better scientist and a better human being and it's been a straight up blast spending every week[end] with you.

To my brothers **Ian Blumenthal, Kristian Eschenburg**, and **Zak Wescoe**, for holding me up and for holding me accountable; for always being down to get down; and for the family we created. We've shared every type of moment together and my love for you will last my lifetime. Also, for the record, you really shouldn't have done that, he's just a boy.

To my sister **Julie** for joining me on this journey of life and understanding that which only you can. I will always live to make you as proud as you make me and look forward to that which awaits us further down this long, long road.

To **Sara Keller**, for engaging with me in the greatest process without end. You are the frame through which I see the future I want to create, the peace of the present I live in, and you are embedded at the core of many of the best moments of my past. Thank you for your love.

To my mother **Donna** and my father **John** for their unconditional love and support that have instilled me with a love of learning, an understanding of my value, and a desire to embody love to the world. I am forever grateful for the way you raised me, and I know I will never depart from it.

DEDICATION

To the memory of my grandfather Donald Walker, PhD for his passion for science, nature, art, and family; and to my grandmother Shirley Walker for nurturing the same in me.

Chapter 1. PH-SENSITIVE POLYMERS AS DYNAMIC MEDIATORS OF BARRIERS TO NUCLEIC ACID DELIVERY

Abstract

The non-viral delivery of exogenous nucleic acids (NA) into cells for therapeutic purposes has rapidly matured into tangible clinical impact. Synthetic polymers are particularly attractive vectors for NA delivery due to their relatively inexpensive production compared to viral alternatives and their highly tailorable chemical properties; indeed, many preclinical investigations have revealed the primary biological barriers to non-viral NA delivery by systematically varying polymeric material properties. This review focuses on applications of pH-sensitive chemistries that enable polymeric vectors to serially address multiple biological barriers to NA delivery. In particular, we focus on recent innovations with *in vivo* evaluation that dynamically enable colloidal stability, cellular uptake, endosomal escape, and nucleic acid release. We conclude with a summary of successes to date and projected areas for impactful future research.

1.1 INTRODUCTION

Biology is fundamentally organized by the propagation, regulation, and expression of nucleic acids (NA).[1] With every new insight into the molecular mechanisms of this central dogma, delivery of exogenous NA into cells becomes a more powerful therapeutic prospect.[2,3] Indeed, at least 1,250 clinical trials focused on "gene therapy" were initiated between 2007 and 2017 worldwide, with a steady average of 114 trials per year.[4] Over 70% of all known, categorized gene therapy clinical trials have been conducted with viral NA delivery vectors, at least 20% have administered naked NA, but less than 5% have utilized synthetic non-viral vectors.[4] However, recent successes like FDA approval of the first non-viral siRNA drug, Onpattro®,[5] confirm that non-viral materials can deliver NA in clinically meaningful doses. Descriptions of the categories of therapeutic nucleic acids, the benefits of non-viral versus viral delivery, the classes of synthetic materials used as non-viral delivery vectors, and the fundamental challenges facing the non-viral delivery field have been discussed at length in other reviews.[6–12]

It is important to note that successful intracellular nucleic acid delivery requires all of the following: 1) extracellular protection of NA cargo 2) carrier stability 3) cellular uptake 4) cytosolic

delivery and 5) release of NA cargo. Polymers stand out among the many classes of non-viral vectors in part due to the vast diversity of polymeric synthesis and modification chemistries that can tailor material properties to address biological barriers to NA delivery. For example, polycations (polymers with many functional groups that are positively charged at neutral pH, e.g. polyethyleneimine [PEI]) have attracted much interest due to their inherent electrostatic abilities to condense NA into "polyplexes" and promote cellular uptake.[13]

In this review we highlight a specific subset of "responsive" polymers[14–16] that impart property changes to NA delivery vectors triggered by changes in physiological pH. Importantly, these responses enable vectors to dynamically address serial barriers to NA delivery that otherwise have solutions at odds with each other (**Figure 1.1**). This review is organized around three critical "balancing acts" that pH-sensitive strategies negotiate to improve polymeric NA delivery: extracellular stability versus cell internalization, extracellular stability versus nucleic acid release, and endosomal escape versus low cell toxicity.
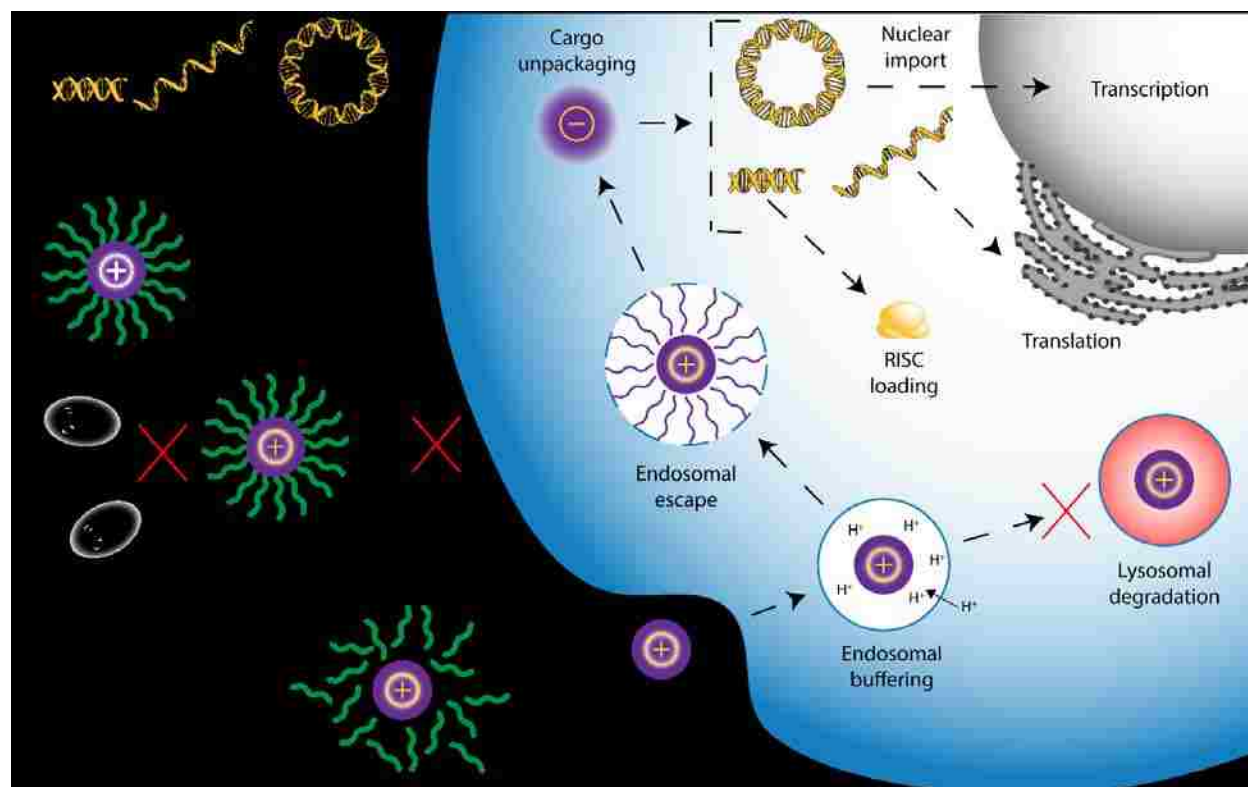
Figure 1.1 An overview of the barriers that nucleic acid delivery systems face and pH-sensitive polymer responses that have been employed to balance them.

Figure 1.2 outlines the predominant pH-sensitive chemistries applied in the subjects of this review; interested parties may wish to consult additional reviews on the topic.[17–19] Due to the vast work in this field we have focused on a few illustrative examples of pH-responsive polymeric carriers from the recent literature and apologize to those whose work are not covered. In particular, pH-sensitive lipoplexes and lipopolyplexes are outside the scope of this review and are covered by other recent reviews.[12,20,21]

Figure 1.2 Major pH-sensitive chemistries.
(A) Bonds that are hydrolyzed in acidic conditions. For maleic anhydride derivatives: cis-aconitic anhydride (R_2 = H, R_3 = CH$_2$-COOH); citraconic anhydride (R_2 = H, R_3 = CH$_3$); dimethyl maleic anhydride (R_2 = CH$_3$, R_3 = CH$_3$). **(B)** Examples of functional groups that protonate in acidic conditions and their functions.

1.2 METHODS FOR BALANCING EXTRACELLULAR COLLOIDAL STABILITY WITH CELL INTERNALIZATION

For systemic administration applications, it is critical for polyplexes to maintain colloidal stability in blood circulation conditions in order to reach target cells and avoid toxicity that often results from lung accumulation of polyplex aggregates. As with all colloidal suspensions of nanoparticles, polyplexes are susceptible to Van der Waals force-induced aggregation that increases as a function

of particle concentration and decreases as a function of the strength of repulsive electrostatic forces and steric hindrances. Because the repulsive net positive surface charge of binary polyplexes is screened in physiological salt conditions, chemical modifications that increase steric repulsion between polyplexes have been widely investigated to increase particle stability.[7]

Incorporation of highly flexible, hydrophilic functional groups like poly(ethylene glycol) (PEG) and hyaluronic acid (HA) or zwitterions like carboxybetaine (PCB) and poly(2-methacryloyloxyethyl phosphorylcholine) (PMPC) has been shown to effectively stabilize polyplexes in physiological salt concentrations. [22–25] In addition, hydrophilic functional groups have been shown to reduce serum protein adsorption, which mitigates polyplex unpackaging and/or rapid clearance by cells of the innate immune system.[22–25] Although PEG has long been the *de facto* steric stabilizer of choice, it is becoming increasingly clear that widespread pre-existing immunity to PEG in humans may limit the clinical application of designs incorporating this material.[26,27] Biomimetic alternatives like dextran sulfate[25,28] and hyaluronic acid[29,30] or synthetic zwitterionic materials like PCB[31] and PMPC[24] have already demonstrated promise as alternative "stealth" coatings for polyplexes and would also benefit from further development involving dynamic, pH-responsive strategies discussed mainly in the context of PEG below.

Early investigations of polycation PEGylation revealed that the length of PEG chains, the density of the displayed PEG brush layer, and the chemical route to PEG incorporation all dramatically affect the primary useful properties of cationic polyplexes.[22,32] While balancing polycation molecular weight (MW) and structure with PEG MW, brush density, and structure can yield polyplexes that condense nucleic acid into serum-stable nanoparticles, material properties that convey steric shielding are fundamentally at odds with those that mediate efficient cellular association and uptake.[33,34] This dichotomy is well represented by an early example from the literature, where the modification of just 10% of the primary amines in 25 kDa PEI with 5 kDa PEG yielded polyplexes incapable of transfection.[35] Thus, dynamic strategies are needed in order to sequentially navigate the primary extracellular barriers to nucleic acid delivery: colloidal stability, cellular targeting, and cellular uptake.

One such strategy incorporates steric shielding through electrostatically reversible or acid-cleavable linkages to imbue polyplexes with extracellular colloidal stability that is released in the event of a decrease in environmental pH.[36] (**Figure 1.3**) If delivered intravenously, polyplexes employing this strategy have the added benefit of selective de-shielding and targeted uptake in mildly acidic extracellular microenvironments found in conditions of ischemia or inflammation. To our knowledge there are no reports of pH-mediated inflammation targeting polyplexes to compare to equivalent small molecule carriers[37]; however, the relatively acidic ($6.5 < \text{pH} < 7.2$)[38] extracellular tumor microenvironment has been targeted through several creative designs.
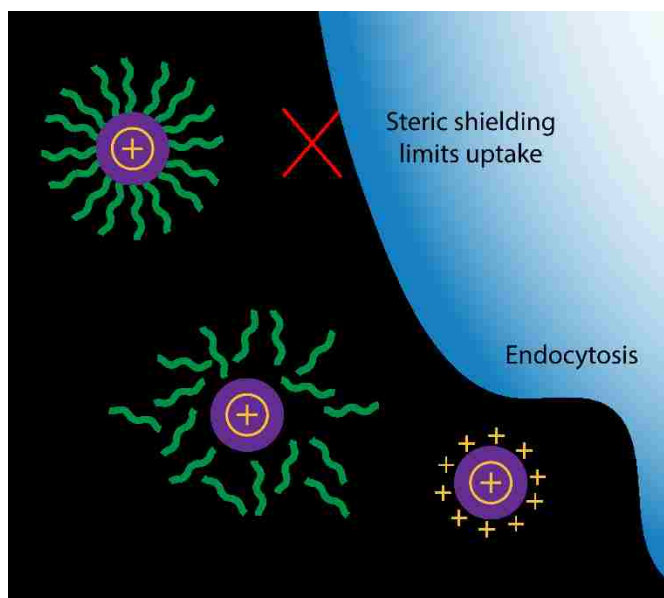
Figure 1.3 Methods for balancing extracellular colloidal stability with cell internalization

Modifying polyplexes with dense shields of flexible, hydrophilic polymers creates steric hindrances that not only prevent aggregation in serum but also limit interactions with cellular membranes. Endocytosis can be enhanced in acidic microenvironments by the release of the shield and/or charge switching to increase positive particle charge through the application of pH-sensitive chemistries. (Adapted from reference [39])

1.2.1   *Reversible shielding with hydrophilic shells conjugated via acid-cleavable linkers*

Several pH-degradable chemistries (hydrazone, Schiff base, acetal, ketal) have all been applied to the "PEG dilemma" of reversible polyplex shielding and provide insights into the general rules that govern the success of pH sensitive approaches *in vivo*.

A PEG-hydrazone-PEI conjugate bearing an EGFR ligand was the first reversible PEG design to achieve greater tumor transfection than non-reversibly shielded designs with the same targeting ligand.[40] Although an intriguing proof of concept, the reversibly shielded construct also demonstrated higher transfection in all other organs investigated relative to the non-reversibly shielded construct, with an overall biodistribution of transfection more similar to the unshielded, untargeted construct. Other homologs (acetal and ketal linkages) designed for more rapid pH-triggered degradation were reported soon thereafter.[41,42] While both of these constructs demonstrated equivalent transfection to unshielded polyplexes *in vitro* and improved biocompatibility, *in vivo* transfection results were not presented in the reports.

Other reversible-shielding designs that utilize Schiff base (SB) linkages between PEG-PEI constructs have demonstrated mixed results, perhaps also due to the even greater instability of the SB bond relative to other pH-sensitive bonds such as the oxime.[43,44] For example, Guan et al. formed PEI/poly-l-glutamic acid/DNA ternary nanoparticles and crosslinked excess PEI amines with PEG-bis(aldehyde) to both sterically and physically stabilize the particles with pH-sensitive bonds.[45] While charge neutralization with poly(glutamic acid) had a dramatic impact on construct biodistribution and target gene knockdown, further incorporation of PEG through SB did not greatly improve CT26 tumor reduction. In a later study, mPEG-aldehyde modified PEI showed increased tumor transfection relative to naked PEI polyplexes; however, it is difficult to assess the importance of the SB linkage as no non-cleavable PEG coating was tested.[46] Jiang et al recently showed that polyplexes formed from PEG-SB-PEI can achieve even greater colloidal stability through the electrostatic association of hydrophobic small molecule tetraphenylene-$(COOH)_4$ (TPE).[47] SB-PEGylation was shown to be sufficient to limit *in vivo* toxicity following tail vein injection but PEG-SB-PEI-TPE constructs demonstrated 10- and 12-fold higher luciferase expression in xenograft A549 tumors relative to naked PEI or PEG-SB-PEI without TPE. Although a later section of this review will discuss the importance of hydrophobic polyplex modifications in more depth, it is worth noting here that inclusion of hydrophobic groups may also increase the stability of pH-sensitive linkages to external hydrophilic groups as a result of particle compaction and decreased hydration.

1.2.2 *Enhanced cellular uptake of stabilized complexes by charge switching*

Polyplexes typically are comprised of a molar excess of positively charged polymeric amino groups to bind phosphate groups of nucleic acid for effective condensation (N:P, or amine to phosphate ratio, > 1). Thus, polyplexes display a net positive surface charge that may be used to electrostatically layer additional functional materials (such as PEG shields) bearing a negatively charged component to form "ternary" complexes. Disruption of ternary electrostatic interactions via pH-dependent protonation has been used to dissociate shielding material or shift material properties to enhance uptake in a number of creative ways.

Reversible addition of a PEG layer to polyplex through a pH-sensitive electrostatic interaction was first demonstrated through coating of pre-formed pDNA/PEI polyplexes with PEG2k coupled to 3 kDa sulfonamide oligomers.[48] Such oligomeric sulfonamides are negatively charged at pH 7.4 but neutral when protonated at pH < 6.8. Sulfonamide protonation led to apparent dissociation of the PEG shield and enabled greater *in vitro* transfection efficiency of the ternary complex in pH 6.6 media than in pH 7.4 media. Despite showing lower transfection than standard PEI polyplexes, this initial effort also showed that reversible PEG shielding could improve the toxicity profile of polyplexes at neutral pH *in vitro*.

Following in the footsteps of a large body of work utilizing maleic anhydride derivatives to reverse the charge of polycations,[49] Yang et al used a negatively charged 2,3-dimethylmaleic anhydride (DMMA)-modified poly(cystamino-phosphoester)-bl-mPEG2k copolymer to form ternary complexes with ssPEI800/siRNA polyplexes.[50] The authors demonstrate that DMMA cleavage at pH 6.8 reveals cystamino-phosphoester primary amines and switches the outer layer charge to net positive. Thus, enhanced cell uptake is mediated by both PEG dissociation and locally increased positive charge. The pH-sensitive PEG-releasing polyplexes achieve 2-fold enhancement of siRNA uptake and 2.5-fold enhancement of Plk1 mRNA knockdown relative to insensitive polyplexes in an MDA-MB-231 xenograft tumor model. Although systemic biodistribution is not reported, both sensitive and insensitive PEGylated complexes achieve much higher tumor uptake and knockdown then uncoated PEI polyplexes, reinforcing the importance of steric serum stabilization in IV polyplex administration.

In contrast to strategies that utilize PEG as a shielding agent, Chen et al synthesized OEAL/PEI/DNA ternary complexes that respond to pH < 6.8 with the dissociation of a zwitterionic outer layer (OEAL = oligoethylenimine-poly(l-aspartate)-poly(l-lysine)).[51] Protonation of OEAL carboxylic acids yielded dramatic charge switching from a zeta potential of −19 mV at pH 7.4 to +21 mV at pH 6.8. The authors show pH-selective enhancement in DNA uptake and 20-fold enhanced luciferase expression by cells transfected in pH 6.8 media relative to transfection in pH 7.4 media *in vitro*. When complexed with therapeutic pDNA and repeatedly injected intratumorally in a hind flank HeLa xenograft tumor, the charge reversing ternary complexes elicited a larger decrease in tumor volume relative to unshielded PEI polyplexes and non-reversibly shielded PEI polyplexes. Although the difference was not statistically significant, this zwitterionic strategy circumvents antibody response to PEG[52] and may be better suited for the treatment of a different tumor model through IV administration.

In conclusion, these examples demonstrate the inherent difficulty in balancing the need for steric shielding in blood with sensitive and specific shield release at slightly acidic pH. Serum stable polyplexes have rapidly improved in the past decade and multifunctional materials have enabled progress towards the goal of tumor-sensing transfection. Nonetheless, in order to maximize translation potential, non-viral delivery materials need to move beyond PEG-based strategies.[26,27] Alternatively, selecting an alternative route of polyplex administration (e.g. intratumoral, intradermal, intracerebroventricular) may provide sufficient targeting while forgoing the need for extreme steric stabilization. Application of pH-mediated de-shielding for targeted transfection of inflamed tissues should also provide a route to less frequent dosing than current steroidal and non-steroidal inflammatory drugs.[37]

1.3 METHODS FOR BALANCING EXTRACELLULAR STABILITY WITH NUCLEIC ACID RELEASE

Just as hydrophilic shielding modifications that enable extracellular polyplex stability can limit intracellular access, strategies that enhance polyplex stability and uptake have been shown to limit intracellular nucleic acid release. For example, while increasing the N:P ratio of a given polyplex formulation or utilizing a polycation with high MW can lead to smaller polyplexes that are rapidly endocytosed, these polyplexes can be too tightly complexed with inefficient release of cargo in the cytoplasm or nucleus.[53] Schaffer and Lauffenburger demonstrated that polyplexes formed from lower MW polycations readily unpackage their contents in the cytoplasm due to cation exchange with endogenous mRNA, spermine, and chromosomal DNA.[53] While optimizing polycation MW may seem a simple strategy to engineer the precise balance of extracellular stability and intracellular instability, high MW vectors (bPEI$_{25k}$-PEG$_{5k}$) have been shown to can unpackage prematurely in organs with highly anionic extracellular matrix (ECM) like the liver.[54] Moreover, additional strategies for cargo packaging beyond electrostatics are warranted because polycation molecular weight and toxicity are typically directly correlated.[55] This section will discuss pH-responsive solutions to this stability dilemma in the context of three polyplex strategies: 1) reversible hydrophobization 2) polymer degradation and 3) charge-switching. (**Figure 1.4**)
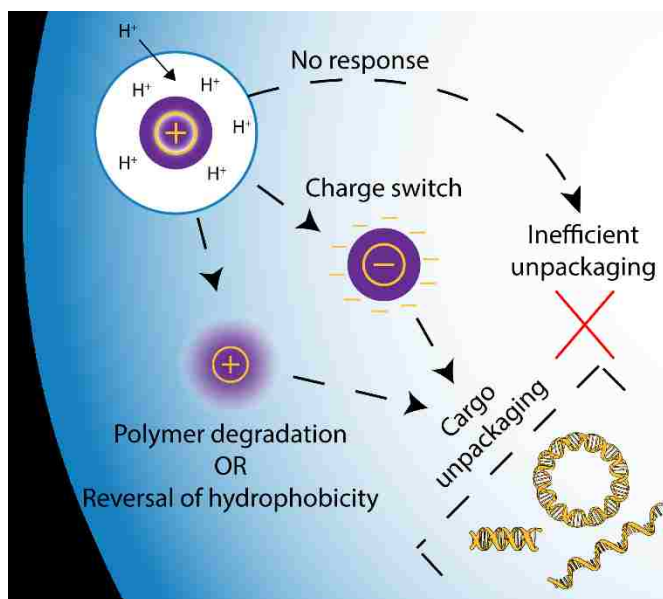
Figure 1.4 Methods for pH-sensitive nucleic acid release.

Assuming endosomal escape can occur, high MW polycations must incorporate an active mechanism for cargo unpackaging, especially when non-electrostatic (e.g. hydrophobic) material properties are utilized for polyplex stabilization.

1.3.1 *Reversible hydrophobization*

Hydrophobic modification can improve polyplex serum stability and adsorptive endocytosis by endowing the complexes with amphipathic characteristics.[56] Improved circulation time and higher transfection efficiency relative to naked PEI was first reported for PEI hydrophobized with amino acids such as alanine[57] and tyrosine[58] or aliphatic chains of varying length.[59,60] Incorporation of relatively hydrophobic yet biodegradable poly(lactic acid) (PLA) or poly(ε-caprolactone) (PCL) blocks has also been shown to aid nucleic acid encapsulation while improving biocompatibility.[61–63] Several groups have also shown that poly-β-amino esters bearing hydrophobic alkyl tails can incorporate helper PEG-lipids that increase serum stability and alter biodistribution *in vivo*.[64,65] Of the examples listed above, only the hydrolytically-degradable polymers possess an additional (albeit slow) mechanism for nucleic acid release beyond highly inefficient cation exchange. Responsive chemistries, including acid-cleavable linkers and protonatable functional groups, are among the tools used to selectively enhance polyplex unpackaging through the release or reversal of hydrophobic modifications.

Our group addressed the need for selective, rapid release of hydrophobic modifications by linking hydrophobic and polycationic polymer blocks with an intracellularly-reducible disulfide bond. These polymers displayed high extracellular stability and significantly higher transfection *in vivo* compared to a non-reducible control polymer.[66] In order to obviate concerns that the cytoplasmic release of hydrophobic polymer chains could affect cell viability, we next developed reversibly hydrophobized polycationic micelles based on pH-sensitive small molecule capping agents.[67] In this diblock copolymer design, the first block provided hydrophilic steric stabilization and cationic nucleic acid condensation while the second block was grafted with methoxy benzoic imine that drove hydrophobic micelle assembly. We showed that polymeric benzoic imines were rapidly hydrolyzed at pH 5.5 to generate primary amine groups, which enabled a switch from hydrophobic to hydrophilic properties, micelle disassembly, and cytoplasmic release of fluorescently labeled DNA. Although the pH-sensitive polymer demonstrated greater *in vivo* luciferase transfection than

either bPEI20k or a polymer grafted with a pH-insensitive phenyl cap, it is difficult to determine whether this enhancement was due to enhanced vehicle disassembly or enhanced endosomal escape as a result of conversion from neutrally charged imines to positively charged primary amines.

In addition to acid-cleavable linkages, protonatable groups can be used to mitigate pH-responsive destabilization of hydrophobic polyplex cores. Building on work initiated by the Stayton group,[68,69] the Duvall group has investigated copolymerization of 2-(dimethylamino)ethyl methacrylate (DMAEMA) with varying amounts of butyl methacrylate (BMA) to simultaneously optimize polyplex stabilization and endosomal lysis.[70] Even though pDMAEMA pKa and therefore siRNA loading capacity was reduced with higher BMA content, this strategy enabled the simultaneous usage of a polycation for nucleic acid loading and as a pH-responsive trigger for complex disassembly and endosomal escape. As a hydrophilic PEG block was present in all formulations tested, this study also illustrates the additive importance of all three forms of colloidal polyplex stabilization discussed thus far in this review. Numerous other studies have applied a wide array of variously substituted tertiary amine monomers to elucidate the impact of monomer structure,[71] monomer copolymerization,[72] and polymer block ordering[73] in multiparameter optimizations of polyplex stability and endosomal escape. In these cases, the tertiary amine monomers are hydrophobic and contribute to polyplex stability when unprotonated at neutral pH but become hydrophilic and participate in endosomal buffering when protonated at pH below their pKa. One common lesson is that incorporation of monomers with pKa above extracellular pH is required for efficient nucleic acid condensation and cellular uptake, but the ratio and ordering of these monomers alongside those with endosomal pKa can be tuned to achieve greater endosomal escape than that of constitutively protonated homopolymers.

1.3.2 *Polymer degradation*

Many pH- and hydrolysis-sensitive cationic polymers have been developed in an effort to improve the biodegradation, clearance, and thereby safety of transfection reagents. Summarizing the full panel and chemistry of all functional groups utilized in these approaches is beyond the scope of this review, but a brief list must include: amides (e.g. polypeptides), carbamates, carbonates, phosphoesters, phosphazenes, and esters (e.g. orthoesters, PHP, PAGA, PBAE). Most confer an

additional level of safety beyond bPEI while equaling or exceeding its transfection efficiencies in serum-free conditions; however, none of these designs can surpass all the barriers to gene delivery in a single material formulation.[74] In addition, since bulk hydrolysis typically occurs over the course of hours, many pH-sensitive strategies have been investigated to provide more rapid polyplex degradation following endocytosis.

Modifications to enhance the degradability of the main backbone of PEI were among the first investigated. Kim et al first demonstrated that low MW PEI polymerized with PEG succinimidyl succinate was first much less toxic than non-degradable PEI of similar MW.[75] Later efforts utilizing diacrylate-PEG crosslinkers enabled the creation of better controlled, higher MW degradable PEI with efficiencies exceeding that of non-degradable PEI.[76,77] Modification of PEI primary amines with an acid-degradable dimethyl ketal linkage conferred hydrophobicity to the polyplexes and improved their safety.[78,79] Ketalization increased nucleic acid complexation efficiency of LMW PEI, likely due to hydrophobic packing. However, both complexation and dissociation of nucleic acids by HMW PEI was hindered by ketalization due to the stiff structure and high charge density present after pH-mediated side chain degradation. Thus, in the absence of charge conversion, backbone degradation appears to be a more efficient mechanism for achieving nucleic acid release.

Poly-β-amino esters (PBAEs) are among the most widely used biodegradable polycations due to their large potential for structural diversity and their inherent hydrophobic nature at neutral pH. Although PBAEs become hydrophilic and swell when they are ionized below pH 6.5, first generation PBAEs paradoxically degraded more rapidly at pH 7.4 than at pH 5.1.[80] Crosslinking PBAE with methyl ketal crosslinkers achieved rapid degradation in acidic pH but poor uptake and transfection due to these particular material's negative zeta potential.[81,82] Later generations of PBAEs have further succeeded by incorporating many of the design strategies mentioned in this review, including: the identification of capping agents that promote uptake and endosomal escape;[83] mixed formulations of non-PEGylated PBAE and PBAE-PEG copolymers to enable plasmid condensation and tissue penetration;[84] and the incorporation of reducible linkages that enable rapid intracellular particle dissociation and miRNA release.[85] It is also interesting to note

that pre-mixed PBAE/DNA nanoparticles have been shown to retain transfection efficiency when re-constituted after lyophilization for several months.[86]

The dynamic covalent bond formed between phenylboronic acids (PBA) and diols has attracted increased attention as a mechanism for polyplex disassembly as both pH and diol affinity can be used to trigger bond dissociation.[87,88] For example, low MW PEI grafted with either PBA or galactose can be mixed to form biocompatible high MW PEI ("crossPEI").[89] In this study, the authors further modified the crossPEI with a star PEG and additional PBA moieties to convey serum stability and targeting to upregulated sialic acid glycoproteins on CT-26 tumors, respectively. The authors demonstrate that PBA surface-modified polyplexes achieve an impressive 2-fold enhancement of polyplex uptake and significant reduction in tumor volume relative to untargeted PEGylated constructs with the same core. However, *in vitro* gel retardation assays showed that this design was likely hindered by inefficient DNA release.

Kataoka et al recently expanded on this concept by forming crosslinked polyplex micelles of PEG-*b*-PAsp(DET) grafted with either 4-carboxy-3-fluorophenylboronic acid (FPBA) or d-gluconamide (GlcAm).[90] Due to charge reduction inherent to this grafting approach, the authors had to carefully balance crosslinking ratio with charge density. Again, pH-mediated disassembly was not very efficient (only 10-15% of strands were released during pH drop *in vitro*); however, ATP-mediated GlcAm displacement in the cytoplasm led to very efficient unpackaging. Crosslinked micelles demonstrated impressive six-fold enhanced luciferase transfection *in vitro* relative to control PEG-*b*-PAsp(DET) polyplexes. Crosslinked micelle cellular uptake was agnostic to the presence of heparin on cell surfaces, indicating that uptake was driven by the particle's positive zeta potential in contrast to PBA-mediated ECM targeting in the previously mentioned example.

1.3.3 *Charge switching vectors for nucleic acid unpackaging*

Tertiary and quaternary amines employed by polycations for nucleic acid condensation are constitutively protonated and thus tightly associated with nucleic acid phosphate groups at both extracellular and intracellular pH. Although some competitive displacement of nucleic acid by endogenous, negatively charged intracellular species has been demonstrated for low MW

polycations, this exchange is limited by high MW vectors.[53] Responsive chemistries that shift the charge of polyplexes towards net neutral or negative values have thus been explored as methods for enhanced cargo unpackaging and intracellular activity. In order to balance efficacy and biocompatibility, an ideal charge-switching vector will: 1) convert charges on biologically relevant time scales (within minutes) 2) fully neutralize all positive charge and 3) generate no cytotoxic byproducts.

Initial applications of charge-converting chemistries (e.g. hydrolysis of positively charged functional groups) for polyplex unpackaging successfully generated fully neutralizing and highly biocompatible polyplexes, yet limited transfection efficiencies as a result of slow charge conversion (<50% charge conversion in less than 20 hours).[31,91,92] The approaches cited depend on pH-insensitive ester hydrolysis, which has proved difficult to accelerate without compromising extracellular vector stability.[93–95] Recently, the Wender and Waymouth groups demonstrated exceptionally high mRNA transfection with cationic oligo(carbonate-b-α-amino ester)s that achieve charge neutralization, nucleic acid unpackaging, and endosomal escape.[96] Organocatalytic ring-opening polymerization (OROP) was utilized to synthesize a hydrophobic block containing various alkyl side-chains, followed by OROP of morpholin-2-ones with various amine substitutions for nucleic acid condensation. As all hydrophobic monomers were linked by carbonate bonds and all positively charged amines convert to neutrally charged amides during α-amino ester self-immolation, this work represents an interesting application of both reversible hydrophobization and charge conversion strategies. Importantly, the authors demonstrate that polyplex disassembly and endosomal escape, not uptake, are the critical bottlenecks to mRNA expression. Similar to other carbonate materials that are unstable at alkaline pH, the oligomers described above degraded in minutes at pH 7.4. However, mRNA polyplexes were stable for 2 hours at pH 7.4 (and achieved transfection *in vivo*) due to decreased deprotonation and thus self-immolation. Further optimization of oligomer hydrophobic blocks of these materials has resulted in increased transfection in the lymphocytes beyond commercially available reagents.[97] In addition to alkaline pH-responsive materials, we suggest that acid-sensitive chemistries that initiate charge reduction or neutralization could also provide a simple route to rapid intracellular polyplex unpackaging due to endosomal pH.

1.4 METHODS FOR BALANCING POTENT ENDOSOMAL ESCAPE WITH LOW NON-SPECIFIC CELL TOXICITY

After navigating the extracellular barriers to delivery and achieving endocytosis, polyplexes must also escape endosomal trafficking in order to avoid lysosomal degradation and to release their nucleic acid cargo into the cytoplasm.[98] (**Figure 1.5**) Viruses evolved functional mechanisms for exiting endosomes millions of years ago;[99,100] in contrast, endosomal escape remains a bottleneck in the development of non-viral gene delivery to this day.[10,101] The vast majority of non-viral strategies that address endosomal release are predicated on a response to decreases in pH mediated by ATP-dependent proton pumps during endosomal maturation.[102] In particular, the widespread availability of polycations like PEI and pDMAEMA has facilitated their use as "all-in-one" multifunctional gene delivery vectors.[8] The tertiary amines of pDMAEMA have an average pKa of 7.5, which enables not only endocytosis but also "proton sponge" endosomal buffering that results in a combination of rapid osmotic swelling, membrane destabilization, and endosomal rupture in some cell types.[103,104] Many structurally diverse monomers that protonate within the endosome (e.g. imidazoles) have been shown to provide enhanced endosomal escape relative to PEI/PLL/pDMAEMA and have been reviewed elsewhere.[102,105] However, it is well documented that endosomal escape mediated by the proton sponge effect is not only very inefficient (1-2%) but also highly variable based on cell type specific properties such as endosomal size and membrane leakiness.[106–108] Thus, as the true mechanism[109] and even the existence[110] of proton sponge effects remain the matter of continuing debate, this review will primarily focus on proton sponge-independent strategies for pH-dependent endosomal escape.
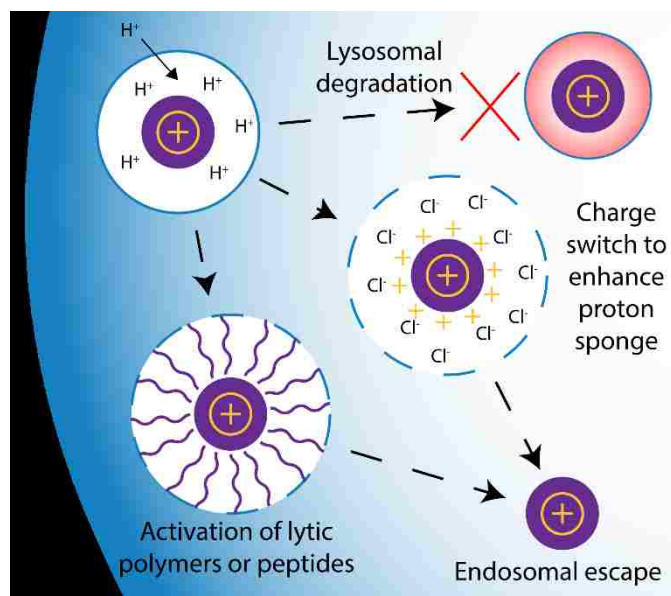
Figure 1.5 Endosomal escape is required for cytoplasmic access.
Carriers have been developed that utilize pH-sensitive chemistries to 1) charge switch to enhance the proton sponge and to 2) display amphipathic materials with lytic properties.

1.4.1 *Charge switching for enhanced proton sponge*

Modification of an amine with a maleic anhydride derivative (Figure 2) results in a negative charge at neutral pH that is quickly converted back to a positively charged amine through cleavage of the maleic amide at acidic pH. Several groups have utilized this chemistry to construct ternary complexes that convert from net neutral or negative charge to net positive charge exclusively in the endosome, thereby minimizing toxicity due to polycation interaction with extracellular membranes and dually enhancing proton sponge endosomolysis.[111–116]

The Kataoka group has demonstrated that ternary complexes formed from cis-aconitylamide (Aco) modified pAsp(DET), unmodified pAsp(DET), and plasmid DNA show enhanced endosomal escape and transfection relative to both simple pAsp(DET) polyplexes and non-charge converting ternary complexes.[111] A block copolymer of PEG and charge converting pAsp(DET-Aco) was later utilized to enhance the endosomal escape of calcium phosphate siRNA nanoprecipitates.[112] This approach is especially notable for its lack of any cationic charge at neutral pH, which led to significantly higher endosomal escape, target knockdown, and biocompatibility than non-converting ternary complexes. Subsequent work that enhanced the rate of Aco hydrolysis resulted

16

in further increases in silencing efficiency, presumably due to earlier release from endosome before recycling to the cell surface could occur.[113]

Similar approaches have conveyed enhanced transfection efficiencies to ternary complexes formed from a wide variety of gene delivery vehicles, including: cis-aconitic anhydride-masked poly(allylamine) + PEI + gold nanoparticles[114]; citraconic anhydride-masked PEI + iron oxide nanoparticles[115]; citraconic anhydride-masked poly(allylamine) + chitosan.[116]

1.4.2 *Responsive hydrophobization of endosomolytic polymers*
Despite improvements in proton sponge strategies for endosomal escape like those mentioned above, alternative escape mechanisms that do not solely rely on endosomal buffering have the potential to achieve cell-type agnostic escape that is also more rapid and efficient. The application of pH-responsive polymers that gain amphipathic properties and membrane lytic activity upon protonation at endosomal pH has shown great promise as an alternative means of endosomal rupture.

Initial biophysical investigations by Tirrell et al demonstrated that poly(2-alkylacrylic acid) polymers such as poly(2-ethylacrylic acid) (PEAA) could solubilize lipid membranes once protonated at slightly acidic pH ~ 6.3 through hydrophobically driven micellization processes analogous to those evolved in membrane-lytic peptides like melittin.[117,118] Murthy et al. investigated a slightly more hydrophobic polymer, poly(propyl acrylic acid) (PPAA), which was found to disrupt red blood cells 15 times more efficiently than PEAAc at pH 6.1[119] and to enhance lipopolyplex gene transfer much more than other 2-alkylacrylic acid polymers.[120] Importantly, these mechanisms have inherent selectivity towards endosomal versus cytoplasmic membranes because they rapidly transition back to a hydrophilic, non-lytic state at cytoplasmic pH following endosomal escape. However, their negative charge at neutral pH intrinsically complicates their use in simple cationic polyplex systems. Block polymerization of pDMAEMA (for siRNA condensation) followed by copolymerization of PPAA, DMAEMA, and butyl methacrylate (BMA) enabled the formation of micelles with a neutrally charged second block that could undergo pH-sensitive disassembly and endosomal escape.[68,69] The observation that increased polymeric BMA content was directly correlated with greater siRNA knockdown efficiency eventually led to

the development of lytic polymers without PPAA, where a copolymerized core of DMAEMA and BMA was sufficient to achieve pH-responsive endosomal escape.[70] The Duvall group has most recently optimized the hydrophilic corona of these micelleplexes to include zwitterionic phosphorylcholine (PMPC) in place of PEG, further increasing the already high siRNA delivery efficiency and systemic biocompatibility of these systems.[24]

Others have used acid-cleavable linkages to incorporate lytic polymers in a variety of interesting polyplex carriers including polyion complex micelles[121], comb polycations[122], and β-cyclodextrins.[123] An important consideration in translational use of these materials is feasibility for large scale and reproducible synthesis and formulation.

1.4.3 *Responsive display or activation of non-polymeric membrane lytic agents*

Non-polymeric lytic agents such as small molecules and peptides have been applied to polyplex endosomal escape with great success. Again, a key challenge in these systems is the complete limitation of membrane-disrupting activity to the endosome so as to prevent off-target toxicity. Two main pH-sensitive strategies have emerged: 1) masking of lytic agents with acid-degradable protecting groups and 2) encapsulation of lytic agents in polymeric micelles that dissociate upon protonation. A few interesting strategies utilizing small molecule drugs to enhance endosomal escape have been recently reviewed;[124] thus, for the purposes of brevity we will limit our discussion in this section to peptide-enabled endosomal escape.

Many researchers have enhanced polyplex uptake and endosomal escape through the incorporation of unmodified membrane lytic peptides such as melittin,[125,126] KALA,[127] gp41,[128] or diphtheria toxin.[129] However, all of these designs are dose-limited by toxicity that results from non-specific interaction with cellular membranes. Peptides that offer sequence-dependent enhanced membrane destabilization at acidic pH versus neutral pH, such as influenza hemaglutinnin-derived HA-2 conjugated to PLL,[130] engineered melittin analogs conjugated to PEI,[131] or various applications of GALA,[132] have indeed shown reduced carrier toxicity but only convey modest enhancements in transfection efficiency.

Protection of amino acid side chains with acid-cleavable groups is an alternative strategy to restrict lytic peptide activity to endosomes that avoids potentially deleterious alterations to primary

peptide sequences. Rozema et al pioneered the usage of maleic anhydride groups to reversibly mask lysine residues thought to contribute to melittin's interactions with membranes.[133] Wagner's group developed conjugates of masked-melittin and PEGylated PLL for siRNA delivery;[134,135] unfortunately, these nanoparticles were prone to aggregation and induced severe, acute liver and abdominal toxicity in mice.[136] Unimeric, "dynamic polyconjugates" have enjoyed more success in part due to their small size.[137] In this design, pH-responsive masking groups reversibly inactivate a lytic polymer chain that is directly conjugated to siRNA. The use of targeting ligands and PEG as masking groups endows additional functionality and stability to the conjugates without compromising its endosomal escape properties. This design was moved to clinical trials by Arrowhead Pharmaceuticals after demonstrating impressive knockdown in non-human primates.[138] Current designs have replaced the lytic polymer component of the original dynamic polyconjugate with a masked melittin-like peptide that will serve as the primary conjugate scaffold.[139]

Polymer-mediated, pH-sensitive micellar encapsulation of lytic agents provides another method for endosomal release that may offer greater selectivity and safety profiles in comparison to acid-labile protecting groups. We recently reported a self-assembling block copolymer that responds to endosomal acidification with the revelation of melittin conjugated to a reversibly hydrophobic polymer block.[140] This Virus-Inspired Polymer for Endosomal Release (VIPER) combines serum stable nucleic acid condensation with pH-sensitive display of a potent lytic peptide to achieve safe and highly efficient plasmid and siRNA delivery *in vivo*.[140–142] Importantly, we avoid both non-specific extracellular lysis and enzyme-mediated peptide degradation by concealing peptides in the hydrophobic micelle core until environmental pH drops to < 6.4 in maturing endosomes. Our most recent work with this system investigated how variation in lytic peptide size, net charge, hydrophobicity, isoelectric point, and polymer conjugation would affected micelle stability, endosomolysis, and transfection efficiency.[142] We have demonstrated that the sharp pH-transition of VIPER exerts highly sensitive control over peptide-mediated membrane lysis, such that polymer-peptide conjugates with more potent lytic peptides achieved more effective transfection *in vivo*. Future work seeks to apply this technology as a mechanism for the efficient endosomal escape of additional biomacromolecular cargos.

1.5   CONCLUSION: ACHIEVEMENTS AND CHALLENGES

It is clear from the examples above that polymer chemistry has enabled investigators to better understand and overcome barriers to nucleic acid delivery. In addition to control over molecular weight, monomer incorporation, and polymer structure (among many other variables), the application of pH-sensitive chemistries in polycation design has yielded a new generation of highly-tuned carriers that are responsive to extra- and intracellular cues. These dynamic carriers achieve much higher transfection *in vivo* than earlier static, single-property carriers as a result of their ability to overcome serial roadblocks that require dramatic material property changes within narrow timeframes. Indeed, the fact that some recent designs are able to overcome endosomal barriers that have long remained key limitations in non-viral success is not only encouraging but also a testament to the decades of work that have elucidated reproducible strategies to manage extracellular barriers to delivery.

As there are currently no clinically approved polymer nucleic acid carriers, much work remains to realize their broad potential. In order to effectively balance properties that overcome multiple barriers simultaneously, systematic iteration within a chosen synthetic framework may yield insight into which chemistries yield the greatest multifunctional benefit. One such inspiring study involved a massive, multi-parameter optimization to improve the therapeutic index (TI) of poly(vinyl ether) terepolymer siRNA conjugates by varying pH-labile PEG shielding, pH-labile targeting ligand conjugation, and protonatable imidazole/pirazole/carboxylic acid incorporation. In the end, incorporation of a specific ratio of 1-methyl-2-imidazole provided the largest increase in TI as a result of enhanced endosomal escape, yet again underlining the relatively large importance of intracellular barriers.[143]

Despite the exciting progress in siRNA delivery and the immense therapeutic prospects of gene silencing, there remains a large need for materials that can deliver nucleic acids that express proteins (e.g. mRNA, pDNA), especially in post-mitotic cells. Although mRNA is actively translated in both mitotic and post-mitotic cells, it has been well-documented that mRNA is more difficult to deliver *in vivo* compared to pDNA or even siRNA due to its large size, extreme flexibility, immunogenicity, and high susceptibility to hydrolytic and nuclease degradation.[144,145] However, lessons may be learned from pDNA delivery, as demonstrated in a recent work where

hydrophobic properties conveyed enhanced serum stability and transfection following systemic administration.[63]

Efforts to improve translocation of pDNA through the nuclear envelope have mostly focused on the conjugation of NLS peptides to carriers and plasmids, which has yielded highly variable levels of success.[146–148] Taking nuclear entry into account when addressing other barriers could simultaneously improve the efficiency of breaching this limitation. For example, since polyplex-containing endosomal vesicles are concentrated in perinuclear region, selectively delaying endosomal escape could improve nuclear uptake by allowing for longer vesicular trafficking towards the nucleus.[149] Moreover, improving vector unpackaging in the cytoplasm should enable sequence-mediated nuclear localization (e.g. EBV oriP; SV40) by increasing plasmid access for transcription proteins that bind to and transport plasmids to the nucleus.[150] Certain polymers have also demonstrated increased nuclear translocation of plasmids containing NFκB–binding sites due to material-based activation of NFκB signaling.[151] Lastly, certain small molecule drugs have shown promise in the manipulation of the nuclear barrier. Glucocorticoid priming of human mesenchymal stem cells enhanced PEI plasmid transfection efficiency 3-fold and prolonged transgene expression compared to transfection without glucocorticoids, in part due to increased cellular (5-fold) and nuclear (6–10-fold) DNA uptake.[152] Pharmacological inhibition of epigenetic processes has recently been shown to both enhance the amount of plasmid DNA delivered to the nucleus and also limit plasmid silencing by preventing interaction with endogenous histones.[153] Co-delivery of plasmid and small molecule HDAC inhibitors therefore represents a novel approach to overcome unaddressed epigenetic barriers on the other side of the nuclear pore.

Finally, the development and widespread adoption of methods for the quantification of delivery efficiency at each aforementioned barrier are necessary in order for the field to gain fundamental understanding of the material properties that beget success at those barriers. For example, Dahlman et al have pioneered an inspirational approach that utilizes the encapsulation and subsequent sequencing of DNA barcodes to enable the *in vivo* screening of thousands of vector formulations for biodistribution and transfection efficiency.[154,155] High-throughput investigations of intracellular barriers has proved more challenging. While there are a vast array of complementary methods for the analysis of where, when, and how endosomal escape occurs, few studies employ

multiple techniques to unravel the temporal and spatial dynamics of vector trafficking.[156] Although detailed investigations involving highly labor intensive live cell tracking microscopy techniques have provided invaluable insights into the inefficiencies of non-viral delivery,[157–159] the development of higher throughput techniques would likely enhance the frequency of these investigations.

BIBLIOGRAPHY

(1)   Crick, F. Central Dogma of Molecular Biology. *Nature* **1970**, *227* (5258), 561–563.

(2)   Behr, J. P. Synthetic Gene-Transfer Vectors. *Acc. Chem. Res.* **1993**, *26* (5), 274–278.

(3)   Behr, J.-P. Synthetic Gene Transfer Vectors II: Back to the Future. *Acc. Chem. Res.* **2012**, *45* (7), 980–984.

(4)   Edelstein, M. Gene Therapy Clinical Trials Worldwide http://www.abedia.com/wiley/vectors.php (accessed Sep 23, 2018).

(5)   A Triumph of Perseverance over Interference. *Nat. Biotechnol.* **2018**, *36* (9), 775–775.

(6)   Mulligan, R. C. The Basic Science of Gene Therapy. *Science (80-.).* **1993**, *260*, 926–932.

(7)   Hwang, S. J.; Davis, M. E. Cationic Polymers for Gene Delivery: Designs for Overcoming Barriers to Systemic Administration. *Curr. Opin. Mol. Ther.* **2001**, *3* (2), 183–191.

(8)   Pack, D. W.; Hoffman, A. S.; Pun, S.; Stayton, P. S. Design and Development of Polymers for Gene Delivery. *Nat. Rev. Drug Discov.* **2005**, *4* (7), 581–593.

(9)   Scholz, C.; Wagner, E. Therapeutic Plasmid DNA versus SiRNA Delivery: Common and Different Tasks for Synthetic Carriers. *J. Control. Release* **2012**, *161* (2), 554–565.

(10)   Lächelt, U.; Wagner, E. Nucleic Acid Therapeutics Using Polyplexes: A Journey of 50 Years (and Beyond). *Chem. Rev.* **2015**, 150415062557000.

(11)   Schroeder, A.; Levins, C. G.; Cortez, C.; Langer, R.; Anderson, D. G. Lipid-Based Nanotherapeutics for SiRNA Delivery. *J. Intern. Med.* **2010**, *267* (1), 9–21.

(12)   Rezaee, M.; Oskuee, R. K.; Nassirli, H.; Malaekeh-Nikouei, B. Progress in the Development of Lipopolyplexes as Efficient Non-Viral Gene Delivery Systems. *J. Control. Release* **2016**, *236*, 1–14.

(13)   Boussif, O.; Lezoualc'h, F.; Zanta, M. A.; Mergny, M. D.; Scherman, D.; Demeneix, B.; Behr, J. P. A Versatile Vector for Gene and Oligonucleotide Transfer into Cells in Culture and in Vivo: Polyethylenimine. *Proc. Natl. Acad. Sci.* **1995**, *92* (16), 7297–7301.

(14)   Hoffman, A. S. Stimuli-Responsive Polymers: Biomedical Applications and Challenges for Clinical Translation. *Adv. Drug Deliv. Rev.* **2013**, *65* (1), 10–16.

(15)   Shim, M. S.; Kwon, Y. J. Stimuli-Responsive Polymers and Nanomaterials for Gene Delivery and Imaging Applications. *Adv. Drug Deliv. Rev.* **2012**, *64* (11), 1046–1059.

(16)   Pezzoli, D.; Candiani, G. Non-Viral Gene Delivery Strategies for Gene Therapy: A "Ménage à Trois" among Nucleic Acids, Materials, and the Biological Environment. *J. Nanoparticle Res.* **2013**, *15* (3), 1523.

(17)   Park, I.-K.; Singha, K.; Arote, R. B.; Choi, Y.-J.; Kim, W. J.; Cho, C.-S. PH-Responsive Polymers as Gene Carriers. *Macromol. Rapid Commun.* **2010**, *31* (13), 1122–1133.

(18)   Kocak, G.; Tuncer, C.; Bütün, V. PH-Responsive Polymers. *Polym. Chem.* **2017**, *8* (1), 144–176.

(19)   Bazban-Shotorbani, S.; Hasani-Sadrabadi, M. M.; Karkhaneh, A.; Serpooshan, V.; Jacob, K. I.; Moshaverinia, A.; Mahmoudi, M. Revisiting Structure-Property Relationship of PH-Responsive Polymers for Drug Delivery Applications. *J. Control. Release* **2017**, *253*, 46–63.

(20)   Heinrich, C.; Blum, R.; Gascón, S.; Masserdotti, G.; Tripathi, P.; Sánchez, R.; Tiedt, S.; Schroeder, T.; Götz, M.; Berninger, B. Directing Astroglia from the Cerebral Cortex into Subtype Specific Functional Neurons. *PLoS Biol.* **2010**, *8* (5).

(21)   Zhao, Y. Lipid Nanoparticles for Gene Delivery. *Adv. Genet.* **2014**, *88*, 13–36.

(22)   Finsinger, D.; Remy, J. S.; Erbacher, P.; Koch, C.; Plank, C. Protective Copolymers for

Nonviral Gene Vectors: Synthesis, Vector Characterization and Application in Gene Delivery. *Gene Ther.* **2000**, *7* (14), 1183–1192.

(23) Xiu, K.-M.; Zhao, N.-N.; Yang, W.-T.; Xu, F.-J. Versatile Functionalization of Gene Vectors via Different Types of Zwitterionic Betaine Species for Serum-Tolerant Transfection. *Acta Biomater.* **2013**, *9* (7), 7439–7448.

(24) Jackson, M. A.; Werfel, T. A.; Curvino, E. J.; Yu, F.; Kavanaugh, T. E.; Sarett, S. M.; Dockery, M. D.; Kilchrist, K. V.; Jackson, A. N.; Giorgio, T. D.; et al. Zwitterionic Nanocarrier Surface Chemistry Improves SiRNA Tumor Delivery and Silencing Activity Relative to Polyethylene Glycol. *ACS Nano* **2017**, *11* (6), 5680–5696.

(25) Poon, Z.; Lee, J. B.; Morton, S. W.; Hammond, P. T. Controlling in Vivo Stability and Biodistribution in Electrostatically Assembled Nanoparticles for Systemic Delivery. *Nano Lett.* **2011**, *11* (5), 2096–2103.

(26) Park, K. Impact of Anti-PEG Antibodies on PEGylated Nanoparticles Fate in Vivo. *J. Control. Release* **2018**, *287*, 257.

(27) Li, B.; Yuan, Z.; Hung, H. C.; Ma, J.; Jain, P.; Tsao, C.; Xie, J.; Zhang, P.; Lin, X.; Wu, K.; et al. Revealing the Immunogenic Risk of Polymers. *Angewandte Chemie - International Edition*. Wiley-Blackwell October 15, 2018, pp 13873–13876.

(28) Perrino, C.; Lee, S.; Choi, S. W.; Maruyama, A.; Spencer, N. D. A Biomimetic Alternative to Poly(Ethylene Glycol) as an Antifouling Coating: Resistance to Nonspecific Protein Adsorption of Poly(L-Lysine)-Graft- Dextran. *Langmuir* **2008**, *24* (16), 8850–8856.

(29) Ito, T.; Iida-Tanaka, N.; Koyama, Y. Efficient in Vivo Gene Transfection by Stable DNA/PEI Complexes Coated by Hyaluronic Acid. *J. Drug Target.* **2008**, *16* (4), 276–281.

(30) He, Y.; Cheng, G.; Xie, L.; Nie, Y.; He, B.; Gu, Z. Polyethyleneimine/DNA Polyplexes with Reduction-Sensitive Hyaluronic Acid Derivatives Shielding for Targeted Gene Delivery. *Biomaterials* **2013**, *34* (4), 1235–1245.

(31) Sinclair, A.; Bai, T.; Carr, L. R.; Ella-Menye, J. R.; Zhang, L.; Jiang, S. Engineering Buffering and Hydrolytic or Photolabile Charge Shifting in a Polycarboxybetaine Ester Gene Delivery Platform. *Biomacromolecules* **2013**, *14* (5), 1587–1593.

(32) Gref; Lück; Quellec; Marchand; Dellacherie; Harnisch; Blunk; Müller. "Stealth" Corona-Core Nanoparticles Surface Modified by Polyethylene Glycol (PEG): Influences of the Corona (PEG Chain Length and Surface Density) and of the Core Composition on Phagocytic Uptake and Plasma Protein Adsorption. *Colloids Surf. B. Biointerfaces* **2000**, *18* (3–4), 301–313.

(33) Mishra, S.; Webster, P.; Davis, M. E. PEGylation Significantly Affects Cellular Uptake and Intracellular Trafficking of Non-Viral Gene Delivery Particles. *Eur. J. Cell Biol.* **2004**, *83*, 97–111.

(34) Kursa, M.; Walker, G. F.; Roessler, V.; Ogris, M.; Roedl, W.; Kircheis, R.; Wagner, E. Novel Shielded Transferrin−Polyethylene Glycol−Polyethylenimine/DNA Complexes for Systemic Tumor-Targeted Gene Transfer. *Bioconjug. Chem.* **2003**, *14* (1), 222–231.

(35) Nguyen, H. K.; Lemieux, P.; Vinogradov, S. V; Gebhart, C. L.; Guérin, N.; Paradis, G.; Bronich, T. K.; Alakhov, V. Y.; Kabanov, A. V. Evaluation of Polyether-Polyethyleneimine Graft Copolymers as Gene Transfer Agents. *Gene Ther.* **2000**, *7* (2), 126–138.

(36) Meyer, M.; Wagner, E. PH-Responsive Shielding of Non-Viral Gene Vectors. *Expert Opin. Drug Deliv.* **2006**, *3* (5), 563–571.

(37) Li, C.; Li, H.; Wang, Q.; Zhou, M.; Li, M.; Gong, T.; Zhang, Z.; Sun, X. PH-Sensitive Polymeric Micelles for Targeted Delivery to Inflamed Joints. *J. Control. Release* **2017**, *246*, 133–141.

(38) Helmlinger, G.; Yuan, F.; Dellian, M.; Jain, R. K. Interstitial PH and PO2 Gradients in Solid Tumors in Vivo: High-Resolution Measurements Reveal a Lack of Correlation. *Nat. Med.* **1997**, *3* (2), 177–182.

(39) Peeler, D. J.; Sellers, D. L.; Pun, S. H. PH-Sensitive Polymers as Dynamic Mediators of Barriers to Nucleic Acid Delivery. *Bioconjug. Chem.* **2018**.

(40) Walker, G. F.; Fella, C.; Pelisek, J.; Fahrmeir, J.; Boeckle, S.; Ogris, M.; Wagner, E. Toward Synthetic Viruses: Endosomal PH-Triggered Deshielding of Targeted Polyplexes Greatly Enhances Gene Transfer in Vitro and in Vivo. *Mol. Ther.* **2005**, *11* (3), 418–425.

(41) Knorr, V.; Allmendinger, L.; Walker, G. F.; Paintner, F. F.; Wagner, E. An Acetal-Based PEGylation Reagent for PH-Sensitive Shielding of DNA Polyplexes. *Bioconjug. Chem.* **2007**, *18* (4), 1218–1225.

(42) Knorr, V.; Ogris, M.; Wagner, E. An Acid Sensitive Ketal-Based Polyethylene Glycol-Oligoethylenimine Copolymer Mediates Improved Transfection Efficiency at Reduced Toxicity. *Pharm. Res.* **2008**, *25* (12), 2937–2945.

(43) Ulrich, S.; Boturyn, D.; Marra, A.; Renaudet, O.; Dumy, P. Oxime Ligation: A Chemoselective Click-Type Reaction for Accessing Multifunctional Biomolecular Constructs. *Chem. - A Eur. J.* **2014**, *20* (1), 34–41.

(44) Kolli, S.; Wong, S.-P.; Harbottle, R.; Johnston, B.; Thanou, M.; Miller, A. D. PH-Triggered Nanoparticle Mediated Delivery of SiRNA to Liver Cells in Vitro and in Vivo. *Bioconjug. Chem.* **2013**, *24* (3), 314–332.

(45) Guan, X.; Guo, Z.; Lin, L.; Chen, J.; Tian, H.; Chen, X. Ultrasensitive PH Triggered Charge/Size Dual-Rebound Gene Delivery System. *Nano Lett.* **2016**, *16* (11), 6823–6831.

(46) Guan, X.; Guo, Z.; Wang, T.; Lin, L.; Chen, J.; Tian, H.; Chen, X. A PH-Responsive Detachable PEG Shielding Strategy for Gene Delivery System in Cancer Therapy. *Biomacromolecules* **2017**, *18* (4), 1342–1349.

(47) Jiang, Z.; Chen, Q.; Yang, X.; Chen, X.; Li, Z.; Liu, D.-E.; Li, W.; Lei, Y.; Gao, H. Polyplex Micelle with PH-Responsive PEG Detachment and Functional Tetraphenylene Incorporation to Promote Systemic Gene Expression. *Bioconjug. Chem.* **2017**, *28* (11), 2849–2858.

(48) Sethuraman, V. A.; Na, K.; Bae, Y. H. PH-Responsive Sulfonamide/PEI System for Tumor Specific Gene Delivery: An in Vitro Study. *Biomacromolecules* **2006**, *7* (1), 64–70.

(49) Lee, Y.; Fukushima, S.; Bae, Y.; Hiki, S.; Ishii, T.; Kataoka, K. A Protein Nanocarrier from Charge-Conversion Polymer in Response to Endosomal PH. *J. Am. Chem. Soc.* **2007**, *129* (17), 5362–5363.

(50) Yang, X.-Z.; Du, J.-Z.; Dou, S.; Mao, C.-Q.; Long, H.-Y.; Wang, J. Sheddable Ternary Nanoparticles for Tumor Acidity-Targeted SiRNA Delivery. *ACS Nano* **2012**, *6* (1), 771–781.

(51) Chen, J.; Dong, X.; Feng, T.; Lin, L.; Guo, Z.; Xia, J.; Tian, H.; Chen, X. Charge-Conversional Zwitterionic Copolymer as PH-Sensitive Shielding System for Effective Tumor Treatment. *Acta Biomater.* **2015**, *26*, 45–53.

(52) Knop, K.; Hoogenboom, R.; Fischer, D.; Schubert, U. S. Poly(Ethylene Glycol) in Drug Delivery: Pros and Cons as Well as Potential Alternatives. *Angew. Chemie Int. Ed.* **2010**,

49 (36), 6288–6308.

(53) Schaffer, D. V.; Fidelman, N. A.; Dan, N.; Lauffenburger, D. A. Vector Unpacking as a Potential Barrier for Receptor-Mediated Polyplex Gene Delivery. *Biotechnol. Bioeng.* **2000**, *67* (5), 598–606.

(54) Burke, R. S.; Pun, S. H. Extracellular Barriers to in Vivo PEI and PEGylated PEI Polyplex-Mediated Gene Delivery to the Liver. *Bioconjug. Chem.* **2008**, *19* (3), 693–704.

(55) Chu, D. S. H.; Schellinger, J. G.; Shi, J.; Convertine, A. J.; Stayton, P. S.; Pun, S. H. Application of Living Free Radical Polymerization for Nucleic Acid Delivery. *Acc. Chem. Res.* **2012**, *45* (7), 1089–1099.

(56) Liu, Z.; Zhang, Z.; Zhou, C.; Jiao, Y. Hydrophobic Modifications of Cationic Polymers for Gene Delivery. *Prog. Polym. Sci.* **2010**, *35* (9), 1144–1162.

(57) Thomas, M.; Klibanov, A. M. Enhancing Polyethylenimine's Delivery of Plasmid DNA into Mammalian Cells. *Proc. Natl. Acad. Sci.* **2002**, *99* (23), 14640–14645.

(58) Creusat, G.; Zuber, G. Self-Assembling Polyethylenimine Derivatives Mediate Efficient SiRNA Delivery in Mammalian Cells. *Chembiochem* **2008**, *9* (17), 2787–2789.

(59) Neamnark, A.; Suwantong, O.; Remant Bahadur, K. C.; Hsu, C. Y. M.; Supaphol, P.; Uludağ, H. Aliphatic Lipid Substitution on 2 KDa Polyethylenimine Improves Plasmid Delivery and Transgene Expression. *Mol. Pharm.* **2009**, *6* (6), 1798–1815.

(60) Dehshahri, A.; Oskuee, R. K.; Shier, W. T.; Hatefi, A.; Ramezani, M. Gene Transfer Efficiency of High Primary Amine Content, Hydrophobic, Alkyl-Oligoamine Derivatives of Polyethylenimine. *Biomaterials* **2009**, *30* (25), 4187–4194.

(61) Yue, X.; Qiao, Y.; Qiao, N.; Guo, S.; Xing, J.; Deng, L.; Xu, J.; Dong, A. Amphiphilic Methoxy Poly(Ethylene Glycol)-b-Poly(ε-Caprolactone)-b- Poly(2-Dimethylaminoethyl Methacrylate) Cationic Copolymer Nanoparticles as a Vector for Gene and Drug Delivery. *Biomacromolecules* **2010**, *11* (9), 2306–2312.

(62) Zheng, M.; Librizzi, D.; Kiliç, A.; Liu, Y.; Renz, H.; Merkel, O. M.; Kissel, T. Enhancing in Vivo Circulation and SiRNA Delivery with Biodegradable Polyethylenimine-Graft-Polycaprolactone-Block-Poly(Ethylene Glycol) Copolymers. *Biomaterials* **2012**, *33* (27), 6551–6558.

(63) Capasso Palmiero, U.; Kaczmarek, J. C.; Fenton, O. S.; Anderson, D. G. Poly(β-Amino Ester)-Co-Poly(Caprolactone) Terpolymers as Nonviral Vectors for MRNA Delivery In Vitro and In Vivo. *Adv. Healthc. Mater.* **2018**, *7* (14), 1800249.

(64) Kaczmarek, J. C.; Kauffman, K. J.; Fenton, O. S.; Sadtler, K.; Patel, A. K.; Heartlein, M. W.; DeRosa, F.; Anderson, D. G. Optimization of a Degradable Polymer-Lipid Nanoparticle for Potent Systemic Delivery of MRNA to the Lung Endothelium and Immune Cells. *Nano Lett.* **2018**, *18* (10), acs.nanolett.8b02917.

(65) Wu, C.; Li, J.; Wang, W.; Hammond, P. T. Rationally Designed Polycationic Carriers for Potent Polymeric SiRNA-Mediated Gene Silencing. *ACS Nano* **2018**, *12* (7), 6504–6514.

(66) Wei, H.; Volpatti, L. R.; Sellers, D. L.; Maris, D. O.; Andrews, I. W.; Hemphill, A. S.; Chan, L. W.; Chu, D. S. H.; Horner, P. J.; Pun, S. H. Dual Responsive, Stabilized Nanoparticles for Efficient in Vivo Plasmid Delivery. *Angew. Chemie - Int. Ed.* **2013**, *52* (20), 5377–5381.

(67) Cheng, Y.; Sellers, D. L.; Tan, J.-K. Y.; Peeler, D. J.; Horner, P. J.; Pun, S. H. Development of Switchable Polymers to Address the Dilemma of Stability and Cargo Release in Polycationic Nucleic Acid Carriers. *Biomaterials* **2017**, *127*, 89–96.

(68) Convertine, A. J.; Benoit, D. S. W.; Duvall, C. L.; Hoffman, A. S.; Stayton, P. S.

Development of a Novel Endosomolytic Diblock Copolymer for SiRNA Delivery. *J. Control. Release* **2009**, *133* (3), 221–229.

(69) Convertine, A. J.; Diab, C.; Prieve, M.; Paschal, A.; Hoffman, A. S.; Johnson, P. H.; Stayton, P. S. PH-Responsive Polymeric Micelle Carriers for SiRNA Drugs. *Biomacromolecules* **2010**, *11* (11), 2904–2911.

(70) Nelson, C. E.; Kintzing, J. R.; Hanna, A.; Shannon, J. M.; Gupta, M. K.; Duvall, C. L. Balancing Cationic and Hydrophobic Content of PEGylated SiRNA Polyplexes Enhances Endosome Escape, Stability, Blood Circulation Time, and Bioactivity in Vivo. *ACS Nano* **2013**, *7* (10), 8870–8880.

(71) Engler, A. C.; Bonner, D. K.; Buss, H. G.; Cheung, E. Y.; Hammond, P. T. The Synthetic Tuning of Clickable PH Responsive Cationic Polypeptides and Block Copolypeptides. *Soft Matter* **2011**, *7* (12), 5627–5637.

(72) Zhou, J.; Wu, Y.; Wang, C.; Cheng, Q.; Han, S.; Wang, X.; Zhang, J.; Deng, L.; Zhao, D.; Du, L.; et al. PH-Sensitive Nanomicelles for High-Efficiency SiRNA Delivery in Vitro and in Vivo: An Insight into the Design of Polycations with Robust Cytosolic Release. *Nano Lett.* **2016**, *16* (11), 6916–6923.

(73) Wang, C.; Du, L.; Zhou, J.; Meng, L.; Cheng, Q.; Wang, C.; Wang, X.; Zhao, D.; Huang, Y.; Zheng, S.; et al. Elaboration on the Distribution of Hydrophobic Segments in the Chains of Amphiphilic Cationic Polymers for Small Interfering RNA Delivery. *ACS Appl. Mater. Interfaces* **2017**, *9* (38), 32463–32474.

(74) Nguyen, D. N.; Green, J. J.; Chan, J. M.; Langer, R.; Anderson, D. G. Polymeric Materials for Gene Delivery and DNA Vaccination. *Adv. Mater.* **2009**, *21* (8), 847–867.

(75) Ahn, C. H.; Chae, S. Y.; Bae, Y. H.; Kim, S. W. Biodegradable Poly(Ethylenimine) for Plasmid DNA Delivery. *J. Control. Release* **2002**, *80* (1–3), 273–282.

(76) Forrest, M. L.; Koerber, J. T.; Pack, D. W. A Degradable Polyethylenimine Derivative with Low Toxicity for Highly Efficient Gene Delivery. *Bioconjug. Chem.* **2003**, *14* (5), 934–940.

(77) Mi, R. P.; Ki, O. H.; In, K. H.; Myung, H. C.; Jae, W. N.; Yun, J. C.; Chong, S. C. Degradable Polyethylenimine-Alt-Poly(Ethylene Glycol) Copolymers as Novel Gene Carriers. *J. Control. Release* **2005**, *105* (3), 367–380.

(78) Shim, M. S.; Kwon, Y. J. Controlled Delivery of Plasmid DNA and SiRNA to Intracellular Targets Using Ketalized Polyethylenimine. *Biomacromolecules* **2008**, *9* (2), 444–455.

(79) Shim, M. S.; Kwon, Y. J. Controlled Cytoplasmic and Nuclear Localization of Plasmid DNA and SiRNA by Differentially Tailored Polyethylenimine. *J. Control. Release* **2009**, *133* (3), 206–213.

(80) Lynn, D. M.; Langer, R. Degradable Poly(β-Amino Esters): Synthesis, Characterization, and Self-Assembly with Plasmid DNA. *J. Am. Chem. Soc.* **2000**, *122*, 10761–10768.

(81) Sankaranarayanan, J.; Mahmoud, E. A.; Kim, G.; Morachis, J. M.; Almutairi, A. Multiresponse Strategies to Modulate Burst Degradation and Release from Nanoparticles. *ACS Nano* **2010**, *4* (10), 5930–5936.

(82) Guk, K.; Lim, H.; Kim, B.; Hong, M.; Khang, G.; Lee, D. Acid-Cleavable Ketal Containing Poly(β-Amino Ester) for Enhanced SiRNA Delivery. *Int. J. Pharm.* **2013**, *453* (2), 541–550.

(83) Green, J. J.; Langer, R.; Anderson, D. G. A Combinatorial Polymer Library Approach Yields Insight into Nonviral Gene Delivery. *Accounts of Chemical Research*. NIH Public

Access June 2008, pp 749–759.

(84) Mastorakos, P.; Song, E.; Zhang, C.; Berry, S.; Park, H. W.; Kim, Y. E.; Park, J. S.; Lee, S.; Suk, J. S.; Hanes, J. Biodegradable DNA Nanoparticles That Provide Widespread Gene Delivery in the Brain. *Small* **2016**, *12* (5), 678–685.

(85) Lopez-Bertoni, H.; Kozielski, K. L.; Rui, Y.; Lal, B.; Vaughan, H.; Wilson, D. R.; Mihelson, N.; Eberhart, C. G.; Laterra, J.; Green, J. J. Bioreducible Polymeric Nanoparticles Containing Multiplexed Cancer Stem Cell Regulating MiRNAs Inhibit Glioblastoma Growth and Prolong Survival. *Nano Lett.* **2018**, *18* (7), 4086–4094.

(86) Tzeng, S. Y.; Guerrero-Cázares, H.; Martinez, E. E.; Sunshine, J. C.; Quiñones-Hinojosa, A.; Green, J. J. Non-Viral Gene Delivery Nanoparticles Based on Poly(β-Amino Esters) for Treatment of Glioblastoma. *Biomaterials* **2011**, *32* (23), 5402–5410.

(87) Cambre, J. N.; Sumerlin, B. S. Biomedical Applications of Boronic Acid Polymers. *Polymer (Guildf).* **2011**, *52* (21), 4631–4643.

(88) Brooks, W. L. A.; Sumerlin, B. S. Synthesis and Applications of Boronic Acid-Containing Polymers: From Materials to Medicine. *Chem. Rev.* **2016**, *116* (3), 1375–1397.

(89) Kim, J.; Lee, Y. M.; Kim, H.; Park, D.; Kim, J.; Kim, W. J. Phenylboronic Acid-Sugar Grafted Polymer Architecture as a Dual Stimuli-Responsive Gene Carrier for Targeted Anti-Angiogenic Tumor Therapy. *Biomaterials* **2016**, *75*, 102–111.

(90) Yoshinaga, N.; Ishii, T.; Naito, M.; Endo, T.; Uchida, S.; Cabral, H.; Osada, K.; Kataoka, K. Polyplex Micelles with Phenylboronate/Gluconamide Cross-Linking in the Core Exerting Promoted Gene Transfection through Spatiotemporal Responsivity to Intracellular PH and ATP Concentration. *J. Am. Chem. Soc.* **2017**, *139* (51), 18567–18575.

(91) Zhang, X. X.; Prata, C. A. H.; Berlin, J. A.; McIntosh, T. J.; Barthelemy, P.; Grinstaff, M. W. Synthesis, Characterization, and in Vitro Transfection Activity of Charge-Reversal Amphiphiles for DNA Delivery. *Bioconjug. Chem.* **2011**, *22* (4), 690–699.

(92) Sun, B.; Lynn, D. M. Release of DNA from Polyelectrolyte Multilayers Fabricated Using "charge-Shifting" Cationic Polymers: Tunable Temporal Control and Sequential, Multi-Agent Release. *J. Control. Release* **2010**, *148* (1), 91–100.

(93) Prata, C. A. H.; Zhao, Y.; Barthelemy, P.; Li, Y.; Luo, D.; McIntosh, T. J.; Lee, S. J.; Grinstaff, M. W. Charge-Reversal Amphiphiles for Gene Delivery. *J. Am. Chem. Soc.* **2004**, *126* (39), 12196–12197.

(94) Liu, X.; Yang, J. W.; Miller, A. D.; Nack, E. A.; Lynn, D. M. Charge-Shifting Cationic Polymers That Promote Self-Assembly and Self-Disassembly with DNA. *Macromolecules* **2005**, *38* (19), 7907–7914.

(95) Carr, L. R.; Jiang, S. Mediating High Levels of Gene Transfer without Cytotoxicity via Hydrolytic Cationic Ester Polymers. *Biomaterials* **2010**, *31* (14), 4186–4193.

(96) McKinlay, C. J.; Vargas, J. R.; Blake, T. R.; Hardy, J. W.; Kanada, M.; Contag, C. H.; Wender, P. A.; Waymouth, R. M. Charge-Altering Releasable Transporters (CARTs) for the Delivery and Release of MRNA in Living Animals. *Proc. Natl. Acad. Sci.* **2017**, *114* (4), E448–E456.

(97) McKinlay, C. J.; Benner, N. L.; Haabeth, O. A.; Waymouth, R. M.; Wender, P. A. Enhanced MRNA Delivery into Lymphocytes Enabled by Lipid-Varied Libraries of Charge-Altering Releasable Transporters. *Proc. Natl. Acad. Sci.* **2018**, *115* (26), E5859–E5866.

(98) Sahay, G.; Alakhova, D. Y.; Kabanov, A. V. Endocytosis of Nanomedicines. *Journal of*

Controlled Release. NIH Public Access August 3, 2010, pp 182–195.

(99) Kay, M. A.; Glorioso, J. C.; Naldini, L. Viral Vectors for Gene Therapy: The Art of Turning Infectious Agents into Vehicles of Therapeutics. *Nat. Med.* **2001**, *7* (1), 33–40.

(100) Lagache, T.; Danos, O.; Holcman, D. Modeling the Step of Endosomal Escape during Cell Infection by a Nonenveloped Virus. *Biophys. J.* **2012**, *102* (5), 980–989.

(101) Stewart, M. P.; Lorenz, A.; Dahlman, J.; Sahay, G. Challenges in Carrier-Mediated Intracellular Delivery: Moving beyond Endosomal Barriers. *Wiley Interdiscip. Rev. Nanomedicine Nanobiotechnology* **2016**, *8* (3), 465–478.

(102) Varkouhi, A. K.; Scholte, M.; Storm, G.; Haisma, H. J. Endosomal Escape Pathways for Delivery of Biologicals. *J. Control. Release* **2011**, *151* (3), 220–228.

(103) Agarwal, S.; Zhang, Y.; Maji, S.; Greiner, A. PDMAEMA Based Gene Delivery Materials. *Mater. Today* **2012**, *15* (9), 388–393.

(104) Sonawane, N. D.; Szoka, F. C.; Verkman, A. S.; Szoka, R. C.; Verkman, A. S. Chloride Accumulation and Swelling in Endosomes Enhances DNA Transfer by Polyamine–DNA Polyplexes. *J. Biol. Chem.* **2003**, *278* (45), 44826–44831.

(105) Midoux, P.; Pichon, C.; Yaouanc, J.-J.; Jaffrès, P.-A. Chemical Vectors for Gene Delivery: A Current Review on Polymers, Peptides and Lipids Containing Histidine or Imidazole as Nucleic Acids Carriers. *Br. J. Pharmacol.* **2009**, *157* (2), 166–178.

(106) Won, Y.-Y.; Sharma, R.; Konieczny, S. F. Missing Pieces in Understanding the Intracellular Trafficking of Polycation/DNA Complexes. *J. Control. Release* **2009**, *139* (2), 88–93.

(107) Rehman, Z. ur; Hoekstra, D.; Zuhorn, I. S. Mechanism of Polyplex- and Lipoplex-Mediated Delivery of Nucleic Acids: Real-Time Visualization of Transient Membrane Destabilization without Endosomal Lysis. *ACS Nano* **2013**, *7* (5), 3767–3777.

(108) Vermeulen, L. M. P.; Brans, T.; Samal, S. K.; Dubruel, P.; Demeester, J.; De Smedt, S. C.; Remaut, K.; Braeckmans, K. Endosomal Size and Membrane Leakiness Influence Proton Sponge-Based Rupture of Endosomal Vesicles. *ACS Nano* **2018**, *12* (3), 2332–2345.

(109) Benjaminsen, R. V; Mattebjerg, M. A.; Henriksen, J. R.; Moghimi, S. M.; Andresen, T. L. The Possible "proton Sponge " Effect of Polyethylenimine (PEI) Does Not Include Change in Lysosomal PH. *Mol. Ther.* **2013**, *21* (1), 149–157.

(110) Vermeulen, L. M. P.; De Smedt, S. C.; Remaut, K.; Braeckmans, K. The Proton Sponge Hypothesis: Fable or Fact? *European Journal of Pharmaceutics and Biopharmaceutics*. Elsevier August 1, 2018, pp 184–190.

(111) Lee, Y.; Miyata, K.; Oba, M.; Ishii, T.; Fukushima, S.; Han, M.; Koyama, H.; Nishiyama, N.; Kataoka, K. Charge-Conversion Ternary Polyplex with Endosome Disruption Moiety: A Technique for Efficient and Safe Gene Delivery. *Angew. Chemie - Int. Ed.* **2008**, *47* (28), 5163–5166.

(112) Pittella, F.; Zhang, M.; Lee, Y.; Kim, H. J.; Tockary, T.; Osada, K.; Ishii, T.; Miyata, K.; Nishiyama, N.; Kataoka, K. Enhanced Endosomal Escape of SiRNA-Incorporating Hybrid Nanoparticles from Calcium Phosphate and PEG-Block Charge-Conversional Polymer for Efficient Gene Knockdown with Negligible Cytotoxicity. *Biomaterials* **2011**, *32* (11), 3106–3114.

(113) Maeda, Y.; Pittella, F.; Nomoto, T.; Takemoto, H.; Nishiyama, N.; Miyata, K.; Kataoka, K. Fine-Tuning of Charge-Conversion Polymer Structure for Efficient Endosomal Escape of SiRNA-Loaded Calcium Phosphate Hybrid Micelles. *Macromol. Rapid Commun.* **2014**, *35* (13), 1211–1215.

(114) Guo, S.; Huang, Y.; Jiang, Q.; Sun, Y.; Deng, L.; Liang, Z.; Du, Q.; Xing, J.; Zhao, Y.; Wang, P. C.; et al. Enhanced Gene Delivery and SiRNA Silencing by Gold Nanoparticles Coated with Charge-Reversal Polyelectrolyte. *ACS Nano* **2010**, *4* (9), 5505–5511.

(115) Mok, H.; Veiseh, O.; Fang, C.; Kievit, F. M.; Wang, F. Y.; Park, J. O.; Zhang, M. PH-Sensitive SiRNA Nanovector for Targeted Gene Silencing and Cytotoxic Effect in Cancer Cells. *Mol. Pharm.* **2010**, *7* (6), 1930–1939.

(116) Han, L.; Tang, C.; Yin, C. Enhanced Antitumor Efficacies of Multifunctional Nanocomplexes through Knocking down the Barriers for SiRNA Delivery. *Biomaterials* **2015**, *44*, 111–121.

(117) Thomas, J. L.; Tirrell, D. A. Polyelectrolyte-Sensitized Phospholipid Vesicles. *Acc. Chem. Res.* **1992**, *25*, 336–342.

(118) Thomas, J. L.; Barton, S. W.; Tirrell, D. A. Membrane Solubilization by a Hydrophobic Polyelectrolyte: Surface Activity and Membrane Binding. *Biophys. J.* **1994**, *67* (3), 1101–1106.

(119) Murthy, N.; Robichaud, J. R.; Tirrell, D. A.; Stayton, P. S.; Hoffman, A. S. The Design and Synthesis of Polymers for Eukaryotic Membrane Disruption. *J. Control. Release* **1999**, *61* (1–2), 137–143.

(120) JONES, R. A.; CHEUNG, C. Y.; BLACK, F. E.; ZIA, J. K.; STAYTON, P. S.; HOFFMAN, A. S.; WILSON, M. R. Poly(2-Alkylacrylic Acid) Polymers Deliver Molecules to the Cytosol by PH-Sensitive Disruption of Endosomal Vesicles. *Biochem. J.* **2003**, *372* (1), 65–75.

(121) Yessine, M. A.; Dufresne, M. H.; Meier, C.; Petereit, H. U.; Leroux, J. C. Proton-Actuated Membrane-Destabilizing Polyion Complex Micelles. *Bioconjug. Chem.* **2007**, *18* (3), 1010–1014.

(122) Lin, Y. L.; Jiang, G.; Birrell, L. K.; El-Sayed, M. E. H. Degradable, PH-Sensitive, Membrane-Destabilizing, Comb-like Polymers for Intracellular Delivery of Nucleic Acids. *Biomaterials* **2010**, *31* (27), 7150–7166.

(123) Durmaz, Y. Y.; Lin, Y. L.; El-sayed, M. E. H. Development of Degradable, PH-Sensitive Star Vectors for Enhancing the Cytoplasmic Delivery of Nucleic Acids. *Adv. Funct. Mater.* **2013**, *23* (31), 3885–3895.

(124) Joris, F.; De Smedt, S. C.; Raemdonck, K. Small Molecules Convey Big Messages: Boosting Non-Viral Nucleic Acid Delivery with Low Molecular Weight Drugs. *Nano Today* **2017**, *16*, 14–29.

(125) Ogris, M.; Carlisle, R. C.; Bettinger, T.; Seymour, L. W. Melittin Enables Efficient Vesicular Escape and Enhanced Nuclear Access of Nonviral Gene Delivery Vectors. *J. Biol. Chem.* **2001**, *276* (50), 47550–47555.

(126) Schellinger, J. G.; Pahang, J. a; Johnson, R.; Chu, D. S.; Sellers, D. L.; Maris, D. O.; Convertine, A. J.; Stayton, P. S.; Horner, P. J.; Pun, S. H. Melittin-Grafted HPMA-Oligolysine Based Copolymers for Improved Gene Delivery. *Biomaterials* **2013**, *34* (9), 2318–2326.

(127) Min, S.-H.; Lee, D. C.; Lim, M. J.; Park, H. S.; Kim, D. M.; Cho, C. W.; Yoon, D. Y.; Yeom, Y. Il. A Composite Gene Delivery System Consisting of Polyethylenimine and an Amphipathic Peptide KALA. *J. Gene Med.* **2006**, *8* (12), 1425–1434.

(128) Kwon, E. J.; Bergen, J. M.; Pun, S. H. Application of an HIV Gp41-Derived Peptide for Enhanced Intracellular Trafficking of Synthetic Gene and SiRNA Delivery Vehicles. *Bioconjug. Chem.* **2008**, *19* (4), 920–927.

(129) Kakimoto, S.; Hamada, T.; Komatsu, Y.; Takagi, M.; Tanabe, T.; Azuma, H.; Shinkai, S.; Nagasaki, T. The Conjugation of Diphtheria Toxin T Domain to Poly(Ethylenimine) Based Vectors for Enhanced Endosomal Escape during Gene Transfection. *Biomaterials* **2009**, *30* (3), 402–408.

(130) Wagner, E.; Plank, C.; Zatloukal, K.; Cotten, M.; Birnstiel, M. L. Influenza Virus Hemagglutinin HA-2 N-Terminal Fusogenic Peptides Augment Gene Transfer by Transferrin–polylysine–DNA Complexes: Toward a Synthetic Virus-like Gene-Transfer Vehicle. *Proc. Natl Acad. Sci. Usa* **1992**, *89* (17), 7934–7938.

(131) Boeckle, S.; Fahrmeir, J.; Roedl, W.; Ogris, M.; Wagner, E. Melittin Analogs with High Lytic Activity at Endosomal PH Enhance Transfection with Purified Targeted PEI Polyplexes. *J. Control. Release* **2006**, *112* (2), 240–248.

(132) Li, W.; Nicol, F.; Szoka, F. C. GALA: A Designed Synthetic PH-Responsive Amphipathic Peptide with Applications in Drug and Gene Delivery. *Advanced Drug Delivery Reviews*. Elsevier April 23, 2004, pp 967–985.

(133) Rozema, D. B.; Ekena, K.; Lewis, D. L.; Loomis, A. G.; Wolff, J. A. Endosomolysis by Masking of a Membrane-Active Agent (EMMA) for Cytoplasmic Release of Macromolecules. *Bioconjug. Chem.* **2003**, *14* (1), 51–57.

(134) Meyer, M.; Zintchenko, A.; Ogris, M.; Wagner, E. A Dimethylmaleic Acid–melittin-Polylysine Conjugate with Reduced Toxicity, PH-Triggered Endosomolytic Activity and Enhanced Gene Transfer Potential. *J. Gene Med.* **2007**, *9* (9), 797–805.

(135) Meyer, M.; Philipp, A.; Oskuee, R.; Schmidt, C.; Wagner, E. Breathing Life into Polycations: Functionalization with PH-Responsive Endosomolytic Peptides and Polyethylene Glycol Enables SiRNA Delivery. *J. Am. Chem. Soc.* **2008**, *130* (11), 3272–3273.

(136) Meyer, M.; Dohmen, C.; Philipp, A.; Kiener, D.; Maiwald, G.; Scheu, C.; Ogris, M.; Wagner, E. Synthesis and Biological Evaluation of a Bioresponsive and Endosomolytic SiRNA−Polymer Conjugate. *Mol. Pharm.* **2009**, *6* (3), 752–762.

(137) Rozema, D. B.; Lewis, D. L.; Wakefield, D. H.; Wong, S. C.; Klein, J. J.; Roesch, P. L.; Bertin, S. L.; Reppen, T. W.; Chu, Q.; Blokhin, A. V; et al. Dynamic PolyConjugates for Targeted in Vivo Delivery of SiRNA to Hepatocytes. *Proc. Natl. Acad. Sci. U. S. A.* **2007**, *104* (32), 12982–12987.

(138) Wooddell, C. I.; Rozema, D. B.; Hossbach, M.; John, M.; Hamilton, H. L.; Chu, Q.; Hegge, J. O.; Klein, J. J.; Wakefield, D. H.; Oropeza, C. E.; et al. Hepatocyte-Targeted RNAi Therapeutics for the Treatment of Chronic Hepatitis B Virus Infection. In *Molecular Therapy*; American Society of Gene & Cell Therapy, 2013; Vol. 21, pp 973–985.

(139) Hou, K. K.; Pan, H.; Schlesinger, P. H.; Wickline, S. A. A Role for Peptides in Overcoming Endosomal Entrapment in SiRNA Delivery - A Focus on Melittin. *Biotechnol. Adv.* **2015**, *33* (6 Pt 1), 931–940.

(140) Cheng, Y.; Yumul, R. C.; Pun, S. H. Virus-Inspired Polymer for Efficient In Vitro and In Vivo Gene Delivery. *Angew. Chemie - Int. Ed.* **2016**, *55* (39), 12013–12017.

(141) Feldmann, D. P.; Cheng, Y.; Kandil, R.; Xie, Y.; Mohammadi, M.; Harz, H.; Sharma, A.; Peeler, D. J.; Moszczynska, A.; Leonhardt, H.; et al. In Vitro and in Vivo Delivery of SiRNA via VIPER Polymer System to Lung Cells. *J. Control. Release* **2018**, *276*, 50–58.

(142) Peeler, D. J.; Thai, S. N.; Cheng, Y.; Horner, P. J.; Sellers, D. L.; Pun, S. H. PH-Sensitive Polymer Micelles Provide Selective and Potentiated Lytic Capacity to Venom Peptides for

Effective Intracellular Delivery. *Biomaterials* **2018**, *in press*, 235–244.

(143) Guidry, E. N.; Farand, J.; Soheili, A.; Parish, C. A.; Kevin, N. J.; Pipik, B.; Calati, K. B.; Ikemoto, N.; Waldman, J. H.; Latham, A. H.; et al. Improving the In Vivo Therapeutic Index of SiRNA Polymer Conjugates through Increasing PH Responsiveness. *Bioconjug. Chem.* **2014**, *25* (2), 296–307.

(144) Kaczmarek, J. C.; Kowalski, P. S.; Anderson, D. G. Advances in the Delivery of RNA Therapeutics: From Concept to Clinical Reality. *Genome Medicine*. December 27, 2017, p 60.

(145) Sergeeva, O. V.; Koteliansky, V. E.; Zatsepin, T. S. MRNA-Based Therapeutics - Advances and Perspectives. *Biochem. Biokhimiia* **2016**, *81* (7), 709–722.

(146) Cartier, R.; Reszka, R. Utilization of Synthetic Peptides Containing Nuclear Localization Signals for Nonviral Gene Transfer Systems. *Gene Therapy*. Nature Publishing Group February 22, 2002, pp 157–167.

(147) Escriou, V.; Carrière, M.; Scherman, D.; Wils, P. NLS Bioconjugates for Targeting Therapeutic Genes to the Nucleus. *Advanced Drug Delivery Reviews*. Elsevier February 10, 2003, pp 295–306.

(148) Dean, D. A.; Strong, D. D.; Zimmer, W. E. Nuclear Entry of Nonviral Vectors. *Gene Therapy*. Nature Publishing Group June 28, 2005, pp 881–890.

(149) Mishra, S.; Webster, P.; Davis, M. E. PEGylation Significantly Affects Cellular Uptake and Intracellular Trafficking of Non-Viral Gene Delivery Particles. *Eur. J. Cell Biol.* **2004**, *83* (3), 97–111.

(150) Wilson, G. L.; Dean, B. S.; Wang, G.; Dean, D. A. Nuclear Import of Plasmid DNA in Digitonin-Permeabilized Cells Requires Both Cytoplasmic Factors and Specific DNA Sequences. *J. Biol. Chem.* **1999**, *274* (31), 22025–22032.

(151) Yang, Z.; Sahay, G.; Sriadibhatla, S.; Kabanov, A. V. Amphiphilic Block Copolymers Enhance Cellular Uptake and Nuclear Entry of Polyplex-Delivered DNA. *Bioconjug. Chem.* **2008**, *19* (10), 1987–1994.

(152) Kelly, A. M.; Plautz, S. A.; Zempleni, J.; Pannier, A. K. Glucocorticoid Cell Priming Enhances Transfection Outcomes in Adult Human Mesenchymal Stem Cells. *Mol. Ther.* **2016**, *24* (2), 331–341.

(153) Christensen, M. D.; Nitiyanandan, R.; Meraji, S.; Daer, R.; Godeshala, S.; Goklany, S.; Haynes, K.; Rege, K. An Inhibitor Screen Identifies Histone-Modifying Enzymes as Mediators of Polymer-Mediated Transgene Expression from Plasmid DNA. *J. Control. Release* **2018**, *286*, 210–223.

(154) Paunovska, K.; Gil, C. J.; Lokugamage, M. P.; Sago, C. D.; Sato, M.; Lando, G. N.; Gamboa Castro, M.; Bryksin, A. V.; Dahlman, J. E. Analyzing 2,000 in Vivo Drug Delivery Data Points Reveals Cholesterol Structure Impacts Nanoparticle Delivery. *ACS Nano*. American Chemical Society July 20, 2018, p acsnano.8b03640.

(155) Dahlman, J. E.; Kauffman, K. J.; Xing, Y.; Shaw, T. E.; Mir, F. F.; Dlott, C. C.; Langer, R.; Anderson, D. G.; Wang, E. T. Barcoded Nanoparticles for High Throughput in Vivo Discovery of Targeted Therapeutics. *Proc. Natl. Acad. Sci.* **2017**, *114* (8), 2060–2065.

(156) Martens, T. F.; Remaut, K.; Demeester, J.; De Smedt, S. C.; Braeckmans, K. Intracellular Delivery of Nanomaterials: How to Catch Endosomal Escape in the Act. *Nano Today*. Elsevier June 1, 2014, pp 344–364.

(157) Rehman, Z. ur; Hoekstra, D.; Zuhorn, I. S. Mechanism of Polyplex- and Lipoplex-Mediated Delivery of Nucleic Acids: Real-Time Visualization of Transient Membrane

Destabilization without Endosomal Lysis. *ACS Nano* **2013**, *7* (5), 3767–3777.

(158) Wittrup, A.; Ai, A.; Liu, X.; Hamar, P.; Trifonova, R.; Charisse, K.; Manoharan, M.; Kirchhausen, T.; Lieberman, J. Visualizing Lipid-Formulated SiRNA Release from Endosomes and Target Gene Knockdown. *Nat. Biotechnol.* **2015**, *33* (8), 870–876.

(159) Kettling, U.; Koltermann, A.; Schwille, P.; Eigen, M. Real-Time Enzyme Kinetics Monitored by Dual-Color Fluorescence Cross-Correlation Spectroscopy. *Proc. Natl. Acad. Sci. U. S. A.* **1998**, *95* (4), 1416–1420.

Chapter 2. PH-SENSITIVE POLYMER MICELLES PROVIDE SELECTIVE AND POTENTIATED LYTIC CAPACITY TO VENOM PEPTIDES FOR EFFECTIVE INTRACELLULAR DELIVERY

Abstract

Endocytosed biomacromolecule delivery systems must escape the endosomal trafficking pathway in order for their cargo to exert effects in other cellular compartments. Although endosomal release is well-recognized as one of the greatest barriers to efficacy of biologic drugs with intracellular targets, most drug carriers have relied on cationic materials that passively induce endosomal swelling and membrane rupture with low efficiency. To address the endosome release challenge, our lab has developed a diblock copolymer system for nucleic acid delivery that selectively displays a potent membrane-lytic peptide (melittin) in response to the pH drop during the endosomal maturation. To further optimize this system, we evaluated a panel of peptides with reported lytic activity in comparison to melittin. Nineteen different lytic peptides were synthesized and their membrane-lytic properties at both neutral and acidic pH characterized using a red blood cell hemolysis assay. The top five performing peptides were then conjugated to our pH-sensitive diblock copolymer via disulfide linkers and used to deliver a variety of nucleic acids to cultured mammalian cells as well as *in vivo* to the mouse brain. We demonstrate that the sharp pH-transition of VIPER compensates for potential advantages from pH-sensitive peptides, such that polymer-peptide conjugates with poorly selective but highly lytic peptides achieve safe and effective transfection both *in vitro* and *in vivo*. In addition, peptides that require release from polymer backbones for lysis were less effective in the VIPER system, likely due to limited endosomal reducing power of target cells. Finally, we show that certain peptides are potentiated in lytic ability by polymer conjugation and that these peptide-polymer constructs are most effective *in vivo*.

2.1   INTRODUCTION

Selective endosomal membrane disruption technology remains the "missing key" in most intracellular delivery vehicles for biologic therapeutics. While viral vectors possess efficient mechanisms for endosomal escape,[1,2] few, if any, synthetic systems offer matching levels of cytosolic delivery efficiency for macromolecular drugs such as nucleic acids.[3–5]   Moreover, the

commercial availability of polycationic materials like polyethylenimine (PEI) and poly(2-dimethylaminoethyl methacrylate) (pDMAEMA) has facilitated their widespread use as all-in-one multifunctional gene delivery vectors.[6–8] A model polycation, pDMAEMA's average pKa value of 7.5 enables partial protonation in the extracellular environment that promotes endocytosis and also "proton sponge" endosomal buffering that enables rapid osmotic swelling, membrane destabilization, and endosomal rupture in some cell types.[9,10] However, it is well documented that endosomal escape mediated by the proton sponge effect is not only very inefficient (1-2%) but also highly variable based on cell type specific properties (e.g. endosomal size and membrane leakiness).[10–12] The insufficiencies of passive, polycationic approaches in endosomal escape motivate the development of active escape strategies and materials that are more efficient, cell-type agnostic, and amenable to *in vivo* biomacromolecule delivery.

Advances in controlled polymerization technologies have enabled the facile synthesis of polymeric materials with more complex behavior.[13,14] For example, Jianjun Cheng's group recently reported helical polypeptides with potent endosomal release properties that are effective in *in vivo* CRISPR/Cas9 delivery.[15,16] Inspired by adenovirus' endosomal escape mechanism, which involves capsid rearrangement after cellular internalization to display membrane-lytic protein VI,[17,18] we recently reported a self-assembling block copolymer that responds to endosomal acidification by revealing a membrane-lytic peptide that is conjugated to a reversibly hydrophobic polymer block.[19] This Virus-Inspired Polymer for Endosomal Release (VIPER) combines highly sensitive and tunable state-switching polymeric materials[20–23] with reducible conjugation of the potent lytic peptide melittin to achieve safe and highly efficient plasmid and siRNA delivery *in vivo*.[19,24] In comparison to the many strategies for active endosomal escape reviewed in depth elsewhere,[5,25] relatively few have employed the bioconjugation of membrane-lytic/pore-forming peptides to drug carriers, likely due to off-target lysis.[26–35] Moreover, past efforts have only utilized a select number of the many lytic peptides described in the literature and much remains unknown about the peptide conjugate properties that may be optimized to improve drug delivery.

In this work, we present our expansive effort to (i) directly compare 19 reported membrane-lytic or cell penetrating peptides for their pH-dependent hemolytic activity, (ii) elucidate the impact of 5 select peptide sequences on resulting self-assembly properties of peptide-polymer conjugates, and (iii) evaluate the resulting materials for *in vitro* and *in vivo* gene transfer. (**Figure 1.1**) We hypothesized that the backbone polymer of the VIPER system could serve as an effective scaffold for covalent conjugation and selective endosomal display of a wide variety of lytic peptides, thereby enabling a broad investigation into the peptide properties that enhance both polymer micellization and endosomolysis. In contrast to the vast majority of lytic peptide literature that has focused on the identification of peptides with dual antimicrobial potency and minimal lysis of mammalian cell membranes, we revisited this rich literature with a specific search for peptides with the ability to destabilize mammalian cell membranes. Because peptides in the VIPER system are concealed in the hydrophobic micelle core until environmental pH drops to < 6.4 in maturing endosomes, our pH-responsive polymer system should avoid non-specific extracellular lysis and enzyme-mediated peptide degradation before reaching its target. However, it is unknown how sequence-dependent variation in lytic peptide size, net charge, hydrophobicity, isoelectric point, and polymer conjugation would affect micelle stability, endosomolysis, and ultimately nucleic acid cargo delivery. We demonstrate that the sharp pH-transition of VIPER compensates for potential advantages from pH-sensitive peptides, such that polymer-peptide conjugates with poorly selective but highly lytic peptides achieve safe and effective transfection both *in vitro* and *in vivo*. Moreover, we show that certain peptides are poorly lytic in polymer-conjugated form such that the *in vivo* delivery efficiency of our disulfide conjugation system depends on the endosomal reducing power of target cells.
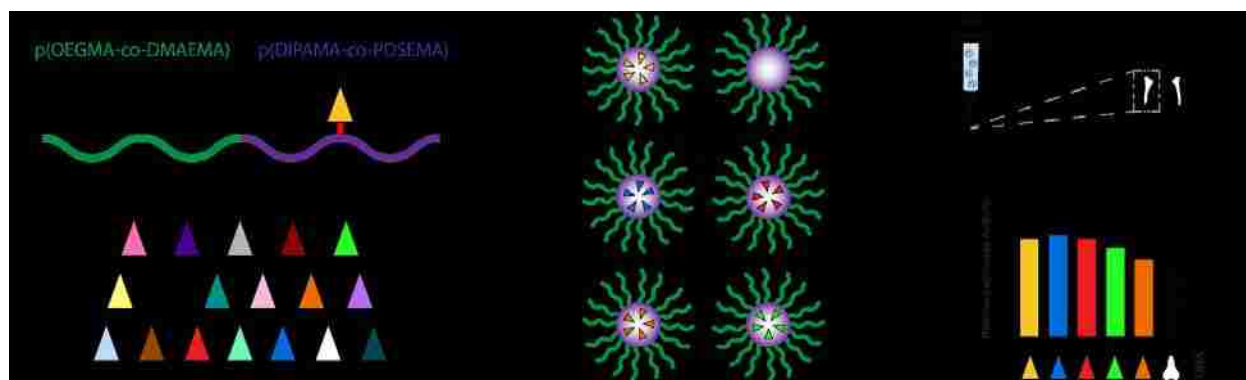
Figure 2.1 Strategy for comparison of the transfection efficiency of lytic peptide polymer conjugates.[36]

2.2   MATERIALS AND METHODS

2.2.1   *Materials*

RAFT CTA 4-cyanopentanoic acid dithio-benzoate (CPADB), N,N′-Azobisisobutyronitrile (AIBN), anhydrous N,N'-dimethylacetamide (DMAc, HPLC, 99.9%), methanol (MeOH, HPLC, 99.9%), and methylene chloride (DCM, HPLC, 99.9%) were purchased from Sigma-Aldrich and used without further purification. Pyridyl disulfide ethyl methacrylate (PDSEMA) was synthesized as described previously.[23] 2-(Dimethylamino)ethyl methacrylate (DMAEMA) and oligo(ethylene glycol) monomethyl ether methacrylate (OEGMA, Mn = 300 and pendent EO units DP 4~5), and 2-Diisopropylaminoethyl methacrylate (DIPAMA) were purchased from Sigma-Aldrich and were purified by passing through a column filled with basic alumina to remove the inhibitor prior to polymerization. Nile Red was purchased from ACROS Organics. Endotoxin-free plasmid pCMV-Luc™ (ProMega) and pmaxGFP™ (Lonza) were purified with the Qiagen Plasmid Giga kit (Qiagen) according to the manufacturer's protocol.

2.2.2   *Peptide synthesis*

Lytic peptides (**Table 2.1**) were synthesized through solid phase peptide synthesis (SPPS) using a CEM Liberty Blue microwave peptide synthesizer (Matthews, NC) at 0.25 mmol scale using standard Fmoc amino acids and NovaPEG Rink Amide Resin (Millipore). Peptides were cleaved from the resin in a trifluoroacetic acid (TFA) cocktail with 5% dimethoxybenzene, 2.5% triisopropylsilane, and 2.5% ethanedithiol. Water was included at 2.5% for peptides containing arginine. Crude peptide was precipitated twice in cold diethyl ether and purified by reverse-phase HPLC using 0.1% TFA water and acetonitrile to >95% purity. Peptide molecular mass was determined by MALDI-TOF at the University of Washington Department of Medicinal Chemistry Mass Spectrometry Center. Peptide hydrophobicity was calculated as the average of each sequence's amino acid values using the Eisenberg scale.[37]

2.2.3   In vitro *hemolysis of peptides*

A hemolysis assay was used to determine the lytic potency of synthesized peptides at pHs corresponding to extracellular (pH 7.4) and endosomal (pH 5.5) compartments using methods derived from others' work with endosomolytic polymers.[22] Briefly, plasma from human blood was removed by centrifugation, red blood cells (RBCs) were washed three times with 150 mM NaCl,

and resuspended in 100 mM phosphate buffer (PB) at pH 7.4, or 5.5. Peptides were then incubated with RBC suspensions at various concentrations (0.012-100 µM) in a sealed 96-well V-bottom plate for 1 h at 37 °C. After centrifugation, the released hemoglobin (supernatant) was transferred to a new plate and the absorbance at 541 nm was measured by with a plate reader. Percent hemolysis was calculated relative to the positive control (1% Triton X-100). Experiments were performed in triplicate and EC50 (50% hemolysis) values were determined using a four-parameter dose-response curve fit in Prism software (Graph Pad Software).

2.2.4 *Cell culture*

HeLa cells (ATCC CCL-2) were maintained in Gibco Dulbecco's Modified Eagle's Medium (DMEM) supplemented with 10% fetal bovine serum and penicillin/streptomycin. A549 cells (ATCC CCL-185) were cultured and transfected in F-12K medium supplemented with 10% FBS and 1% penicillin/streptomycin (P/S). PC-12 cells (ATCC CRL-1721) were cultured and seeded in growth medium (F-12K medium supplemented with 15% horse serum, 2.5% fetal bovine serum, and 1% P/S). For differentiation to a neuron-like phenotype and subsequent transfection, cells were cultured in differentiation medium (F-12K medium supplemented with 1% horse serum, 100 ng/mL nerve growth factor, and 1% P/S). Z310 cells[38] were cultured and transfected in high glucose 1:1 DMEM:F12K medium supplemented with 10% FBS, 1% P/S, 40 ug/mL gentamicin, and 10 ng/mL nerve growth factor. Cells were passaged every three days or when 75% confluent and seeded to reach 75-90% confluency at time of transfection.

2.2.5 *Polymer synthesis and characterization*

Block copolymer p(OEGMA$_{8.60}$-*co*-DMAEMA$_{50.0}$)-*bl*-p(DIPAMA$_{25.32}$-*co*-PDSEMA$_{1.00}$) ("control polymer", CP) was prepared with RAFT polymerization and purified by dialysis as in previous work.[19] ^{1}H NMR spectra were recorded on a Bruker AV 500 (Bruker Corporation) nuclear magnetic resonance (NMR) instrument in deuterated chloroform (CDCl3). The molecular weight and molecular weight distribution (PDI) of the polymers were determined by size exclusion chromatography (SEC). To prepare materials for SEC analysis, the purified polymer was dissolved at 10 mg/mL in running buffer (0.15 M sodium acetate buffered to pH 4.4 with acetic acid) for analysis by SEC. Samples were then applied to an OHpak SB-804 HQ column (Shodex) in line with a miniDAWN TREOS light scattering detector (Wyatt) and a OptiLab rEX refractive index

detector (Wyatt). Absolute molecular weight averages (M_w and M_n) was calculated using ASTRA software (Wyatt).

2.2.6 *Conjugation of lytic peptides to block copolymer*

Lytic peptides were conjugated to CP through disulfide exchange as described in our previous work with slightly altered reaction conditions.[19] CP (10 mg, 0.625 µmol groups) was dissolved in 500 µL MeOH for each conjugate. Then, 1 equivalent (relative to PDS groups) of each peptide was added to the polymer stocks and purged with argon at room temperature for 5 min. The reaction was sealed and monitored by UV at 343 nm for the release of 2-thiopyridine (**Supplemental Figure 2.7**). Each reaction mixture was then diluted 10-fold in 0.15 M sodium acetate (pH 4.4) and then concentrated to the original volume on an Amicon 10 kDa centrifugal filter. Each polymer-peptide conjugate (PPC) was washed three times and then passed through a PD-10 column to ensure removal of unreacted peptide prior to lyophilization. Conjugation efficiency was confirmed by analysis of residual pyridyl disulfide (PDS) content as previously reported with slight adaptation.[29] Briefly, aqueous CP or PPC solutions (2 mg/mL) were reduced with DTT (10 mM, 37 °C, 30 min), releasing one pyridine-2-thiol molecule per PDSEMA group left unreacted. Small molecule pyridine-2-thiol was purified from the polymer with a 3 kDa cut-off Amicon spin filter (Millipore) and the UV-Vis absorbance of the flow-through was measured with a Nanodrop One (Thermo Fisher). Percent reacted PDSEMA was calculated according to the equation in **Supplemental Table 2.3**.

2.2.7 *Micelle formation and characterization*

Polymer micelles were formed through rapid pH-transition as in previous work.[19] Briefly, up to 20 mg of PPC was dissolved in 190 µL of 200 mM monobasic sodium phosphate (~pH 5.4), followed by addition of 810 µL of 200 mM dibasic sodium phosphate to bring the pH to 7.4. Micelles were allowed to form overnight before buffer exchange to nanopure distilled water on a 10 kDa cutoff Amicon centrifugal filter (Millipore) and stored at 4 °C as a 20 mg/mL solution until future use.

Critical micelle concentrations were determined using Nile Red as previously reported.[39] Micelle solutions at concentrations varying from 0.5 to 1024 mg/L were added to dry Nile Red and incubated for 24 hr before fluorescence intensity (excitation/emission: 556/625 nm) was recorded

using an Infinite 200 PRO plate reader (Tecan). As shown in a representative plot in **Supplemental Figure 2.9**, linear regression was separately performed on flat and exponential regions of fluorescence intensity; the CMC was taken to be x-value at the intersection of these lines for each sample. A slightly altered version of the Nile Red assay described above was performed to determine the pH transition point where micelles disassemble due to cooperative protonation of DIPAMA: micelle concentration was fixed at 0.2 mg/mL and incubation phosphate buffer pH was varied from 5.2 to 7.4 in increments of 0.2 pH units.

Micelle size was determined by dynamic light scattering using a ZetaPLUS instrument (Brookhaven Instruments Corporation). Micelle stock solutions were diluted to 0.1 mg/mL in 800 µL 150 mM phosphate buffered saline (PBS; pH 7.4) and measured in triplicate after 30 min incubation at room temperature.

2.2.8 *Preparation and characterization of DNA polyplexes*

Polyplexes were formed by adding polymer to DNA solution followed by 30 min incubation at room temperature. For the gel retardation assay, polyplexes with various N/P ratios were loaded onto a 1% agarose gel containing TAE buffer (40 µmM tris-acetate, 1 mM EDTA) and 0.5 µg/mL ethidium bromide, and were electrophoresed at 100 V for 40 min before imaging on a UV transilluminator. The size and surface charge of the polyplexes were also tested on a ZetaPLUS instrument; polyplexes (1 µg DNA, 20 µL solution, N/P = 5) were diluted in 800 µL in 10 mM NaCl and measured in triplicate.

2.2.9 In vitro *hemolysis of polymer-peptide conjugates*

Peptide-polymer conjugates (PPCs) were assayed as described above for peptides. PPCs were also tested in the presence of 10 mM glutathione (GSH) to determine whether PPCs recovered lytic potency upon peptide liberation from the polymer backbone. RBCs were first suspended in 20 mM GSH PB to give 10 mM GSH final when mixed with polymer dilutions. It should be noted that pH 6.0 was used in place of pH 5.5 in this assay because RBCs were damaged during incubation with GSH at pH 5.5 but not at pH 6.0. Concentration ranges and all other methods were otherwise performed identically to the assay described above for peptides.

2.2.10 In vitro *plasmid transfection*

For pmaxGFP™ transfection, HeLa cells were seeded at a density of 25,000 cells/well in complete cell culture medium in 24-well plates. Cells were first incubated at 37 °C, 5% CO_2 for 16 h. Polyplexes were prepared at different N/P ratios using 1 µg of pmaxGFP™ pDNA (0.1 mg/mL) and allowed to rest for at least 10 min. Each polyplex solution was then added dropwise directly to each well (in triplicate). After 4 h, cells were washed with PBS and given fresh complete cell culture medium. After 40 additional hours, cells were washed with PBS, trypsinized and pelleted at $300 \times$ g for 5 min at 4 °C. Cells were washed once more with PBS, resuspended in Zombie Violet™ viability dye (BioLegend) diluted 500-fold in PBS, and incubated at room temperature for 10 min. Cells were washed twice with cold 1% BSA in PBS and analyzed using an Attune NxT flow cytometer (Thermo Fisher). Singlet cell events were serially gated to analyze viable (Violet-) and transfected (GFP+) cells as shown in **Supplemental Figure 2.12**. Transfection efficiency is reported as the mean percentage of single cells that were GFP+/Violet-. Luciferase transfection was performed at N/P 5 in the same manner as above. HeLa, A549, and Z310 cells were seeded at 25,000 cells/well and transfected 16 h after seeding. PC-12 cells were seeded at 50,000 cells/well in growth media, exchanged to differentiation media after 16 h, and transfected in fresh differentiation media 3 d after initiation of differentiation. Polyplexes formed with commercially available branched polyethyleneimine (bPEI; MW = 20 kDa; Sigma) were also included as a control group in each transfection assay. At time of harvest (48 h post-transfection), cells were washed once in PBS and lysed directly in the plate using Reporter Lysis Buffer (ProMega). Lysates were subjected to one freeze-thaw cycle and clarified by centrifugation at 14,000 g for 10 m at 4 °C. Clarified lysate was assayed for luminescence with luciferase substrate (ProMega) using a plate reader and relative light units (RLU) were normalized by protein content as determined by BCA Protein Assay Kit (Pierce). All experiments were performed in triplicate and variance is reported as the standard deviation of the mean.

2.2.11 In vivo *luciferase plasmid transfection in the brain*

All animal procedures were completed according to protocols approved by the Institutional Animal Care and Use Committee at the University of Washington. Intracerebroventricular (ICV) injection was performed as described before.[40] Polyplex formulations were prepared in 5% glucose solution containing 2.5 µg of luciferase plasmid DNA (N/P 10). Female C57/Bl6 mice (8 wk old) were

anesthetized by intraperitoneal injection of Avertin (500 mg/kg body weight). After craniotomy, a burr hole (1 mm diameter) was made on the right-side of the skull using a dental drill, and 10 µL of polyplex was stereotaxically injected (Bregma, -0.5mm; Medial/Lateral, 1.0mm; Dorsal/Ventral, 1.8mm) using a 33 gauge Hamilton syringe. The injection was made at 2 µL/min and the syringe was kept in the injection site for 2 min to prevent backflow prior to needle removal. After two days, brain compartments were harvested as distinct tissues (left, right and hind brain) from mice and collected in lysis buffer supplemented with protease inhibitors (Roche, Nutley, NJ). Three freeze-thaw cycles were performed in liquid nitrogen, tissues were mechanically homogenized, and lysate was cleared by centrifugation at 21,000 g for 15 min at 4 °C. Clarified lysate was assayed in the same manner described for the in vitro assays. Thus, gene expression was reported as the average RLU/mg protein for each brain region with error reported as the standard deviation of the mean. Whole brain gene expression was calculated as the sum of RLU/mg values of all regions per brain. N=4 for Melittin, C6M3, MEP-2, CP; N=3 for CMA-2, FL-20, DNA.

2.2.12 *Histology and epifluorescence microscopy*

Polyplexes formulated with pmaxGFP™ and either CP or VIPER (melittin-PPC) were administered by intraventricular injection to mice as described above (N=2). Two days post-injection, mice were euthanized and perfused intracardially with 0.9% saline followed by 4% paraformaldehyde in 0.1 M phosphate buffer. After perfusion and fixation, the brains were excised and equilibrated to 30% sucrose in phosphate buffer. Brains were embedded in OCT and sectioned into 30 µm-thick coronal slices. For immunofluorescent labeling, slides were rinsed with PBS and blocked in PBS, 0.3% TritonX- 100, 2% bovine serum albumin (BSA) for 1 h. Primary antibodies (mouse anti-Tuj1 [1:500, Biolegend]; chicken anti-GFAP [1:500, Millipore]) were applied to the tissue sections in PBS, 0.3% TritonX-100, 2% BSA overnight at 4 °C. Sections were rinsed three times for 20min in TBS, 0.1% Tween 20 and species appropriate secondary antibodies conjugated with fluorophore were incubated in PBS, 0.1% Tween 20, and 2% donkey serum for 2 h. Sections were rinsed three times for 20min in TBS–Tween, with the last rinse containing the nuclear marker, 4′,6-diamidino-2-phenylindole (DAPI; 0.5 µg/ml). Sections were then mounted onto glass slides, sealed and cover-slipped with polyvinyl alcohol, and imaged using an epifluorescence microscope.

Hematoxylin and eosin (H&E) staining and imaging was performed on unstained, dry-mounted tissue slices by the University of Washington Histology and Imaging Core.

2.2.13 *Statistical analysis*

All statistical analyses were performed in Prism software (Graph Pad Software, La Jolla, CA) using a two-tailed Student's t- test with unequal variance and Welch's correction. All EC50 values were determined from curve fits with $R^2 > 0.95$.

2.3 RESULTS AND DISCUSSION

2.3.1 *Lytic peptide selection and synthesis*

We conducted an intensive review of literature describing venom-derived antimicrobial peptides and synthetic derivatives, focusing on peptides that are as small or smaller than melittin (~2.9 kDa and 27 a.a.) yet reported to display similarly potent hemolytic activity. We also sought to diversify our panel by selecting peptides that differed from melittin in regards to hydrophobicity (e.g. FL-20), isolectric point (e.g. CMA-2), net charge (e.g. IsCT), and pH-dependent lytic behavior (e.g. C6M3). Peptides containing cysteine (e.g. defensins) were excluded so that a C-terminal cysteine could be added to facilitate polymer conjugation via pyridyl disulfide exchange as in previous work with cysteine-modified melittin.[19] A final panel of 19 lytic and cell-penetrating peptides (**Table 2.1**) were synthesized via solid phase peptide synthesis (SPPS) on Rink Amide resin, purified by HPLC, and characterized by MALDI-TOF mass spectrometry before further testing.

Table 2.1 Key properties of the 19 peptides evaluated in this work.
Peptides are listed in order of decreasing membrane lytic activity (hemolysis) at pH 5.5.[36]

Peptide	Biological origin	Amino acid sequence	# AA	Molecular weight	EC$_{50}$ (µM) pH 5.5	EC$_{50}$ (µM) pH 7.4	pH(I)	Net charge pH 7	Net charge pH 5	Hydro-phobicity	Ref
Melittin	Bee venom	GIGAVLKVLTTGLPALISWIKRKRQQC	27	2949.76	5	6	12.2	6	6	0.09	19
C6M3	Synthetic	RLWHLLWRLWRRLHRLLRC	19	2681.00	6	>100	12.8	7	9	-0.23	41,42
MEP-2	Bee venom	GFLSILKKVLKVMAHMKC	18	2043.80	12	16	11.2	5	6	0.22	43
CaLL	Synthetic hybrid	KWKLFKKIFKRIVQRIKDFLRC	22	2892.52	13	9	12.0	9	9	-0.25	44
CMA-2	Melittin	GIGAVLKVLTTGLPALISWIHHHHEEC	27	2929.46	14	9	7.4	0	4	0.35	29
FL-20	Florae/Melittin	GIGAILKVLATGLPTLISWIC	21	2136.60	16	30	10.1	2	2	0.61	45
EB1	Penetratin	LIRLWSHLIHIWFQNRRLKWKKKC	24	3205.11	18	9	12.5	8	10	-0.22	46
Meucin-18	Scorpion venom	FFGHLFKLATKIIPSLFQC	19	2207.25	20	12	10.7	3	4	0.39	47
LAH	KALA/synthetic	KKLAHALHLLALLWLHLAHALKKAC	25	2811.39	20	>100	11.2	5	9	0.34	48
V681-S11K	Synthetic	KWKSFLKTFKKAVKTVLHTALKAISSC	27	3064.24	22	10	11.5	8	9	0.04	49
Endoporter	Synthetic	LHKLLHHLLHHLHKLLHHLHHLLHKLC	27	3374.48	31	>100	11.0	5	16	0.12	50
Crabrolin	Hornet venom	FLALILRKIVTALC	14	1571.86	38	16	11.4	3	3	0.42	51
LPE3-1	GALA/melittin	GWWLALAEAEAEALALASWIKRKRQQC	27	3099.13	75	>100	9.9	2	2	0.02	52
Aurein1.2	Southern bell frog	GLFDIIKKIAESFC	14	1582.70	95	98	8.8	1	1	0.24	30
IsCT	Scorpion venom	ILGKIWEGIKSLFC	14	1604.71	>100	57.5	10.0	2	2	0.31	53
Lyco-L17E	M-lycotoxin	IWLTALKFLGKHAAKHEAKQQLSKLC	26	2962.34	>100	>100	10.9	5	7	-0.03	28
HE	Magainin 2	GIHHWLHSAHEFGEHFVHHIMNSC	24	2860.38	>100	>100	6.8	0	5.5	0.19	54
SPFK	Bovine semen	PKLLKTFLSKWIGC	14	1631.82	>100	>100	11.1	4	4	0.23	55
TAT	HIV	YGRKKRRQRRRC	12	1661.20	>100	>100	12.4	9	9	-1.77	56

2.3.2   In vitro *hemolysis of lytic peptides*

Lytic peptides functionalized with a C-terminal cysteine were first evaluated with a standard hemolysis assay for direct comparison of membrane-lytic ability. In this assay, red blood cell lysis is quantified by monitoring hemoglobin release through absorption measurements. Although conjugated peptides are expected to reside in the hydrophobic core of VIPER micelles until disassembly at pH 6.4, we hypothesized that peptides with minimal lytic activity at neutral pH and high lytic activity at acidic pH would confer additional safety and endosomolytic selectivity. Thus, peptide hemolysis was tested at both extracellular (7.4) and endosomal (5.5) pH in order to prioritize polymer conjugation according to hemolytic potency at acidic pH (**Table 2.1**). Indeed, many peptides displayed much less potent hemolysis (e.g. SPFK) or no pH-selective lysis (e.g. CMA-2) compared to reported values when tested in our hands, although the discrepancy in potency may be due to the addition of a C-terminal cysteine or assay differences such as the species of red blood cell used. Peptides with redundant characteristics were eliminated and four peptides with potent hemolytic activity at acidic pH were selected for conjugation to the VIPER polymer

backbone (**Figure 2.2**): FL-20 (short melittin homolog with greater hydrophobicity); CMA-2 (melittin homolog with identical length but neutral isolectric point); MEP-2 (bee venom-derived and similar in charge to melittin but shorter in length); and C6M3 (shorter than melittin, selectively lytic at low pH, but greater positive charge).
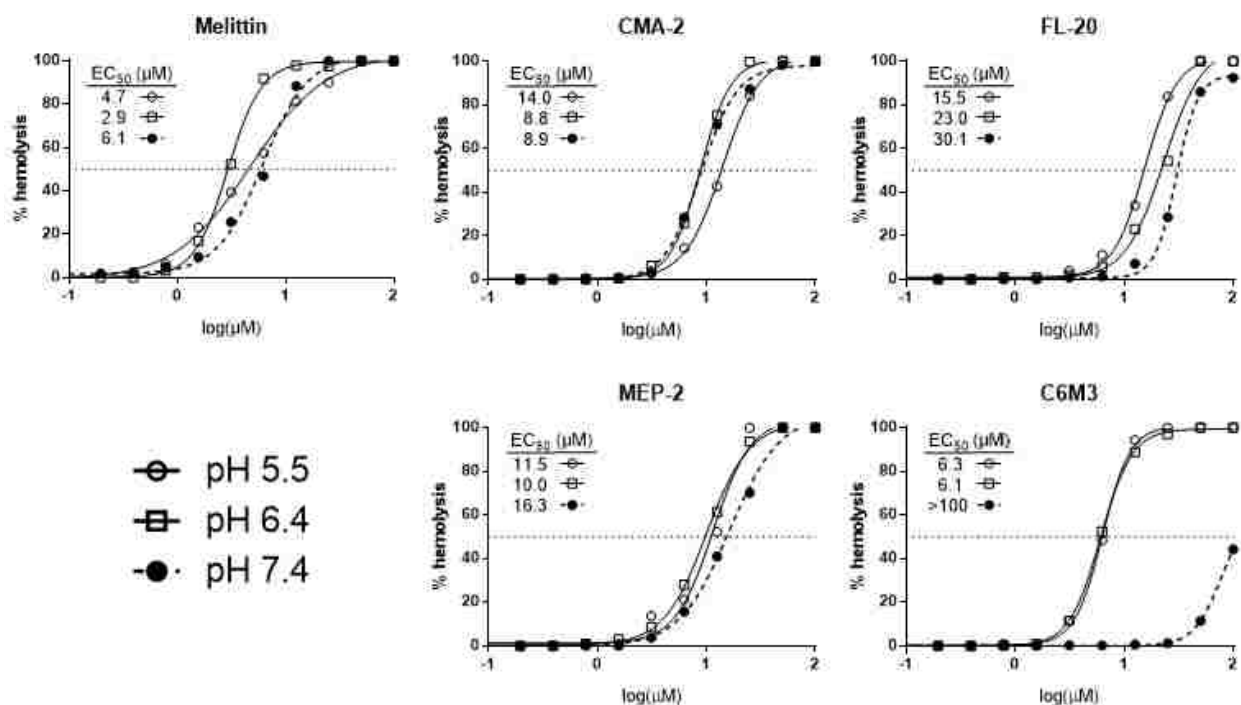
Figure 2.2 Lytic peptide hemolysis at various pH.
Peptides were incubated with human red blood cells at pH 7.4, 6.4, or 5.5 and hemolysis measured by UV absorbance at 541 nm relative to the positive control, 0.1% Triton X-100.[36]

2.3.3   *Polymer synthesis and characterization*

VIPER block copolymers with the general block formula of p(OEGMA-co-DMAEMA)-b-p(DIPAMA-co-PDSEMA) were synthesized using reversible addition-fragmentation chain transfer (RAFT) polymerization according to protocols established in previous work.[19] Molecular weight analysis via GPC revealed a monodisperse polymerization product characteristic of living polymerization (Đ = 1.19), while 1H NMR analysis confirmed nearly identical monomer composition relative to the previously reported polymer. (**Supplemental Figure 2.6**) All experiments,   p(OEGMA8.60-co-DMAEMA50.0)-b-p(DIPAMA25.32-co-PDSEMA1.00)   is referred to hereafter as the control polymer (CP); various polymer-peptide conjugates (PPCs) are referred to by the name of the respective peptide conjugate.

2.3.4 *Micelle formation and characterization*

We first characterized the impact of varied peptide biochemical properties such as size, isoelectric point, and hydrophobicity on PPC micelle size and pH-dependent stability. Micelle diameter as determined by DLS was consistent across all PPCs (21.7-26.0 nm), indicating that VIPER micelles can encapsulate peptides with a variety of biochemical properties and molecular weights without affecting size (**Table 2.2**). The critical micelle concentration of PPCs was determined using a Nile Red encapsulation assay (**Table 2.2**, **Supplemental Figure 2.9**); the CMCs of all 6 polymers (control and five peptide conjugates) were all in relatively narrow range of 46.2 mg/L (for CMA-2 PPC) to 59.4 mg/L (for FL-20 PPC).

We next monitored micelle disassembly as a function of pH between 5.4 and 7.2 in 0.2 pH unit increments using the Nile Red encapsulation assay. Again, micelle disassembly for all 6 polymers occurred within a narrow range of pH of 6.38 to 6.47, dominated by the pKa of the p(DIPAMA) block (**Table 2.2**, **Supplemental Figure 2.10**). Notably, the most hydrophobic PPC (FL-20) displayed a lower and more gradual pH transition than CP, while all other PPCs transitioned sharply at approximately the same pH as the melittin PPC. Thus, increasing micelle core hydrophobicity effectively lowered monomer pKa as a result of decreased water and ion transport that limits "all-or-nothing" cooperative protonation characteristic of charge/state-switching polymeric micelles.[57–60]

Table 2.2 Micelle and polyplex characterization.
Critical micelle concentration (CMC) and pH transition point as determined by a Nile Red encapsulation assay. Micelle and polyplex diameter as determined by DLS. Polyplex Zeta potential as determined by electrophoretic mobility.[36]

Polymer or Conjugate	CMC (mg/L)	pH transition point	Micelle diameter (nm)	Polyplex diameter (nm)	Polyplex Zeta potential (mV)
CP	46.9	6.38	21.7 ± 1.9	112.4 ± 4.2	16.2 ± 3.3
Melittin	49.9	6.41	22.7 ± 1.9	$133.0 \pm 3.4*$	17.8 ± 1.7
CMA-2	46.2	6.47	26.0 ± 1.2	108.3 ± 3.2	16.3 ± 1.4
FL-20	59.4	6.34	24.1 ± 1.5	103.3 ± 9.4	12.8 ± 1.0
MEP-2	54.1	6.40	22.7 ± 2.0	$141.5 \pm 1.5*$	15.4 ± 4.3
C6M3	52.6	6.42	23.8 ± 2.1	127.8 ± 17.9	19.4 ± 1.3

$* = p < 0.05$

2.3.5 *Characterization of DNA polyplexes*

PPC and CP polyplexes formed by electrostatic complexation of cationic micelles with plasmid DNA were characterized by gel retardation (DNA condensation), DLS (diameter), and electrophoretic mobility (zeta potential/surface charge). Imaging polyplex gel retardation showed that all PPCs fully condensed plasmid DNA (pDNA) at N/P 2, while CP condensed pDNA at N/P 1 (**Supplemental Figure 2.11**). Since only the number of polymeric tertiary amines was used to determine the N/P ratio (same mass concentration used for each polymer), the difference in N/P required for full DNA condensation is attributed to the mass of peptide present in PPC samples as in previous work.[19]

Statistical analysis of polyplex DLS Z-avg diameters revealed that MEP-2 and melittin PPC polyplexes had significantly larger diameters compared to CP. (**Table 2.2**) However, all diameters were between 105-145 nm and therefore typically representative of polyplexes described by our lab and others.[4,19,24] Because peptides are conjugated to the polymer chains that occupy the micelle core at neutral pH, the lack of statistically significant differences in zeta potential (surface charge) between CP and PPC polyplexes is also unsurprising. However, the most hydrophobic PPC (FL-20) registered the lowest surface charge of polyplexes tested (12.8 mV), which was significantly lower than that of the PPC with the highest net peptide charge (C6M3, 19.4 mV; $p = 0.0028$).

2.3.6 In vitro *hemolysis of polymer-peptide conjugates*

PPC-mediated hemolysis of human RBCs was evaluated in buffer conditions mimicking various cellular compartments to determine which PPCs possessed specificity for lytic behavior in acidic endosomes. The majority of literature support the claims that the cytoplasm is a reducing environment with high concentrations of glutathione (1-10 mM GSH) and relatively neutral pH (7.4),[61,62] while endosomes are essentially as oxidative as the extracellular space (1-100 µM GSH) but establish pH as low as pH 5.4 through ATP-dependent proton pumps.[63–65] Thus, we tested PPC hemolysis without GSH at pH 7.4 (extracellular mimic) and pH 5.5 (endosomal mimic), as well as with 10 mM GSH at pH 7.4 (cytoplasm mimic) and pH 6 (non-physiologic control; see note in

Section 2.2.9). A broad range of polymer concentrations spanning four orders of magnitude (0.01 to 100 µM polymer) was tested (**Figure 2.3A**; **Supplemental Figure 2.8**).

No hemolysis was observed at pH 7.4 without GSH for all samples, confirming that lytic peptides remain hidden inside the DIPAMA micelle core in extracellular environments (**Figure 2.3A**). Hemolysis was observed only at high concentrations of melittin and MEP-2 PPCs (>10 µM) at pH 7.4 in the presence of GSH, likely due to GSH penetration into the micelle core and subsequent release of small amounts of lytic peptide (**Supplemental Figure 2.8**). Most interestingly, in endosomal mimicking conditions (acidic pH without GSH), the EC_{50}s of the three melittin-like PPCs tested (melittin, CMA-2, FL-20) were lower than the corresponding peptide-only EC_{50}s (2.0, 2.3, 1.9 µM, respectively), whereas the EC_{50}s of MEP-2 and C6M3 PPCs increased relative to peptide-only values (23.5, 22.9 µM, respectively) (**Figure 2.3B**). We hypothesized that certain peptide sequences must be released from the polymer backbone to retain lytic activity and tested this hypothesis by conducting the PPC hemolysis assay at acidic pH with 10 mM GSH. As expected, all EC_{50} values of GSH-reduced PPCs at acidic pH are similar that of the free peptide at acidic pH (**Figure 2.3B**; **Supplemental Figure 2.8**). This fact indicates that melittin-like PPCs may be better suited to endosomal lysis than MEP-2 or C6M3 as a result of the former's ability to retain and/or enhance peptide activity following conjugation to a polymer backbone through disulfide bond. Importantly, no hemolysis was observed for the control polymer (CP) at any concentration tested in any condition, demonstrating that the polymer backbone itself is non-lytic and therefore all lysis observed in PPC samples was peptide mediated.
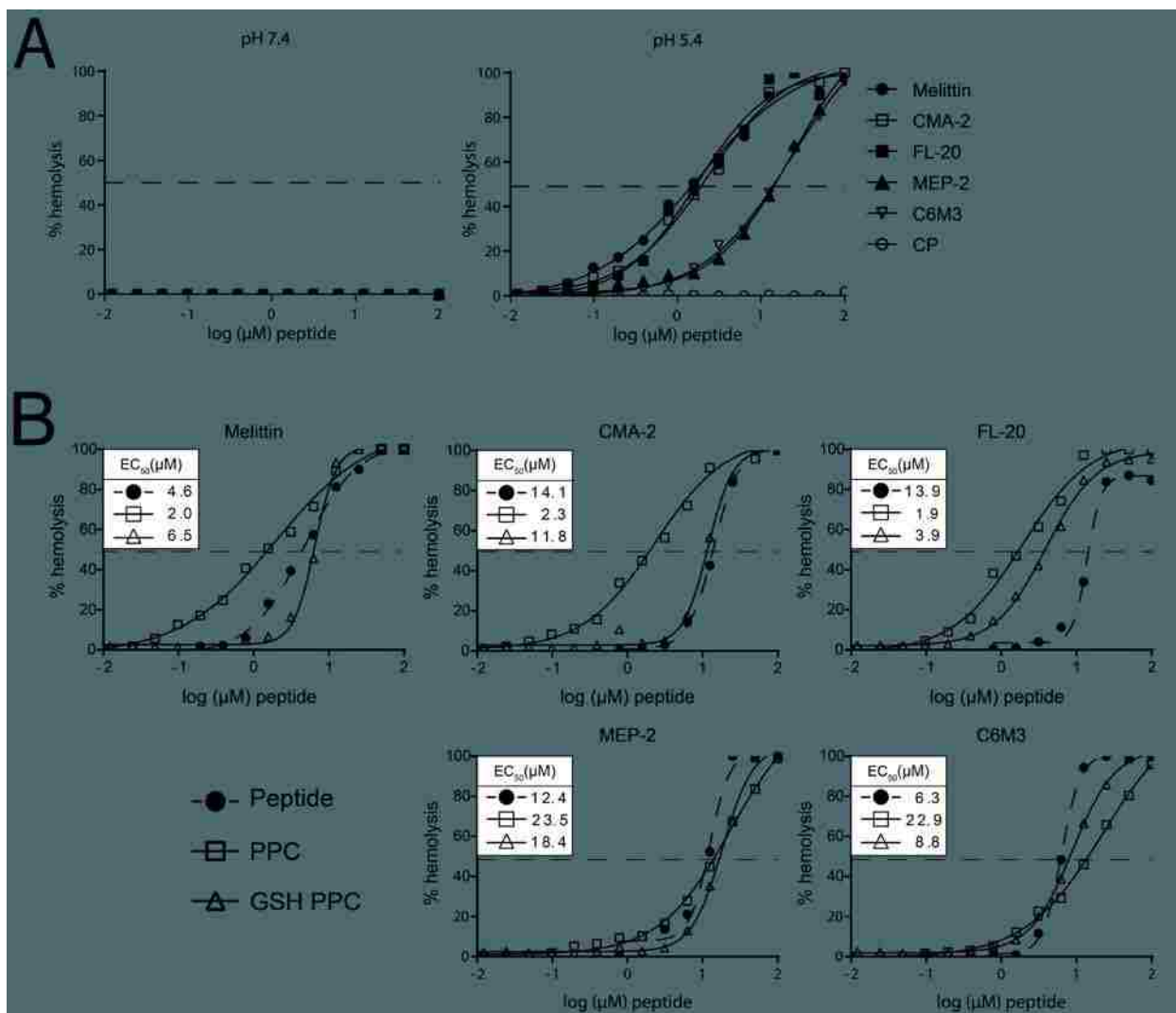
Figure 2.3 Peptide-polymer conjugate (PPC) hemolysis.
(A) PPC hemolysis at various pH. **(B)** Compiled low pH hemolysis curves of free peptide, non-reduced peptide-polymer conjugates, and reduced peptide polymer conjugates. Polymers were incubated with red blood cells at various effective peptide concentrations at pH 7.4 and pH 5.4 for 1 h. For CP, an equivalent concentration of polymer was used in place of PPC concentration. Hemolysis was monitored by UV absorbance for released hemoglobin at 541 nm.[36]

2.3.7   In vitro *plasmid transfection*

Next the gene transfer efficiency and cell compatibility of PPCs were tested in cultured mammalian cells. HeLa cells were transfected in serum-containing media with PPC polyplexes formulated at various N/P ratios with pmaxGFP™ plasmid (**Figure 2.4A**; **Supplemental Figure 2.12**). Cell viability decreased with increasing N/P as expected, but was acceptable (>75%) even at the highest N/P (N/P 8) tested. Moreover, no significant differences in viability were observed

49

between any PPC and CP at each N/P. Therefore, the previously observed cytotoxicity was not due to the presence of a particular lytic peptide as we had hypothesized, but rather due to charge-dependent toxicity associated with increased p(DMAEMA) content.[66,67] All PPCs transfected exceptionally well even in the presence of serum proteins (>60% GFP$^+$) at N/P 5 and above and were significantly more effective than CP (<20% GFP$^+$) at all N/P tested (p < 0.002), confirming results from our previous work that pH-dependent display of the lytic peptide is required for efficient transfection.[19,24] Of the PPCs, CMA-2, FL-20, MEP-2, and melittin transfected with >96% efficiency, while C6M3 transfected with 76% efficiency at N/P 8. The reduced transfection efficiency of C6M3 is likely due to compromised lytic activity when conjugated to the polymer backbone (**Figure 2.3B**). Since peptides are susceptible to lysosomal protease degradation that increases in activity as pH decreases to pH 5.5,[68–70] C6M3 activity may be compromised by degradation at the pH required for membrane lysis.

PPC transfection efficiency was also screened in several other cells lines using a luciferase plasmid in order to confirm the cell type-agnostic nature of our active endosomal escape mechanism. We conducted this screen at N/P 5 because transfection at this N/P yielded the largest total number of GFP+ cells in the previous studies. We chose to compare HeLa cells, A549 cells (which have larger endosomes than HeLa cells[12]), ventricular zone choroid plexus epithelial Z310 cells[38], and neuron-like 3-day differentiated PC-12 cells.[71] The resulting trends in transfection mirror those of the HeLa GFP transfection in that melittin, CMA-2, FL-20, and MEP-2 PPCs transfect more efficiently than C6M3 PPC (**Figure 2.4B**) and transfect with 1-3 orders of magnitude greater efficiency than "proton sponge" control polymers (CP, 20 kDa bPEI) in all cell types tested. These results demonstrate the broad applicability of our lytic peptides and highlight the large impact that "active" endosomal escape strategies and can have on non-viral gene delivery.
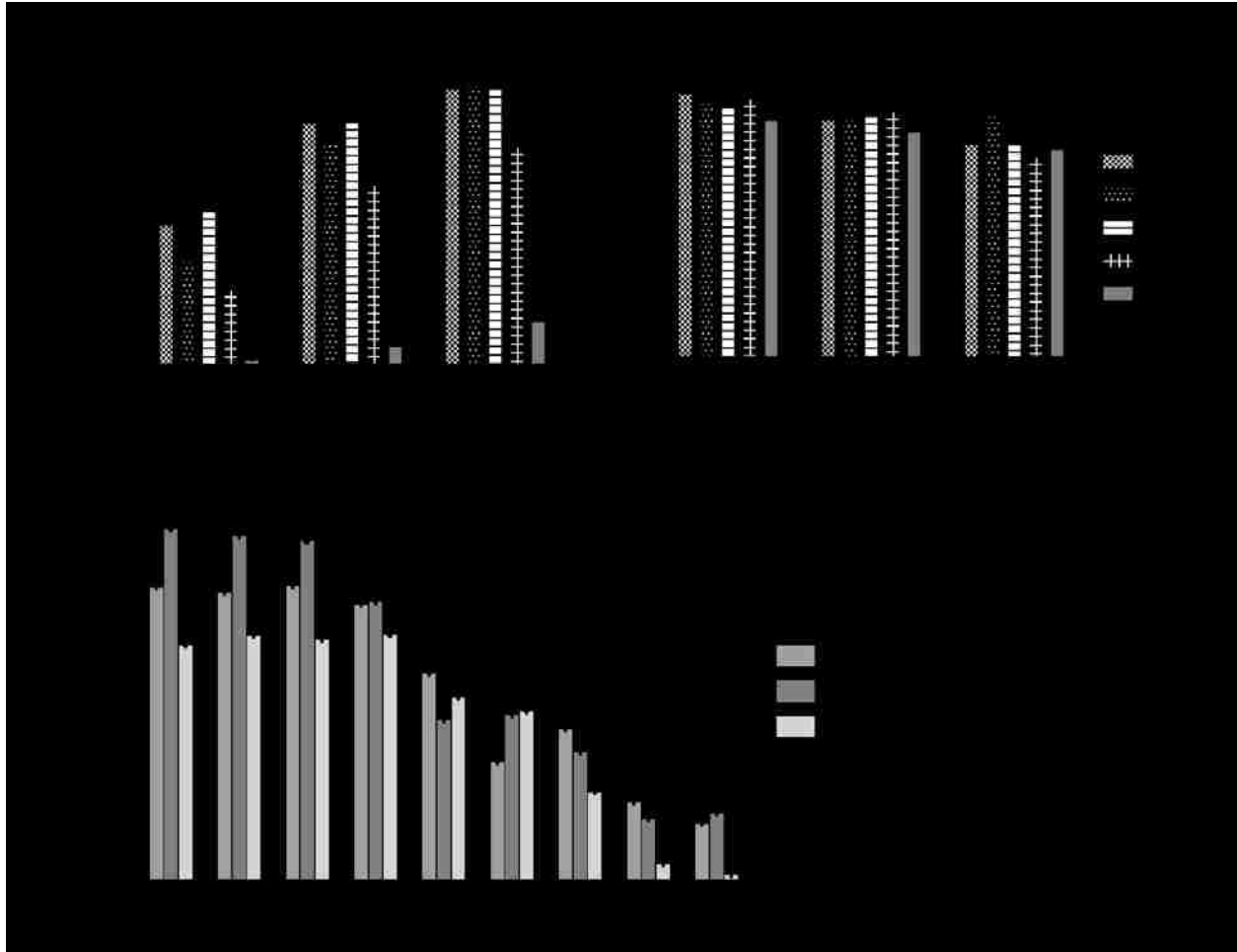
Figure 2.4 *In vitro* plasmid transfection

 (A) HeLa transfection viability and GFP expression efficiency. Transfection efficiency of CP and PPCs to HeLa cells in serum-containing media as determined by flow cytometry analysis of GFP expression 48 hours post transfection. Cell viability was determined by flow cytometry using Zombie Violet staining. All values are reported as mean ± SD. (N =3; * = p < 0.002) **(B)** Relative luciferase activity in cell lysates 48 h after transfection with N/P 5 polyplexes. All values are reported as mean ± SD with significance in comparison to CP, bPEI, DNA, and cells only. (N =3; * = p < 0.002)

2.3.8   In vivo *plasmid transfection in the brain*

As all PPCs displayed excellent transfection efficiencies *in vitro*, we evaluated *in vivo* delivery efficiency by delivering polyplexes formed with the reporter luciferase plasmid to the mouse brain by intracerebroventricular (ICV) injection (**Figure 2.5**). This route of administration enables access to neural progenitor cells (NPCs) which reside in the subventricular zone (SVZ) and extend foot processes through the choroid plexus epithelium.[72] We are interested in transfection to this region with our non-viral vector because expression of transcription and growth factors in SVZ

NPCs has shown therapeutic promise as a means for the regeneration of cortical neurons following ischemic injury.[73–77] We have previously shown that dividing NPCs can be transfected by N/P 10 polyplexes delivered through this administration route, [78] and have achieved higher transfection in the right brain over the left after injection into the right ventricle.[40,79,80] In this study we observed no significant differences between transfection in the left and right brains for any polymer tested (**Supplemental Figure 2.13**). Importantly, overall transfection efficiency was highest for PPCs that achieved potent lysis at low pH without GSH (i.e. melittin and its homologs CMA-2 and FL-20). Thus, cells transfected in the brain from intraventricular polyplex delivery likely do not have sufficient endosomal GSH levels to release disulfide conjugated peptides from PPCs.
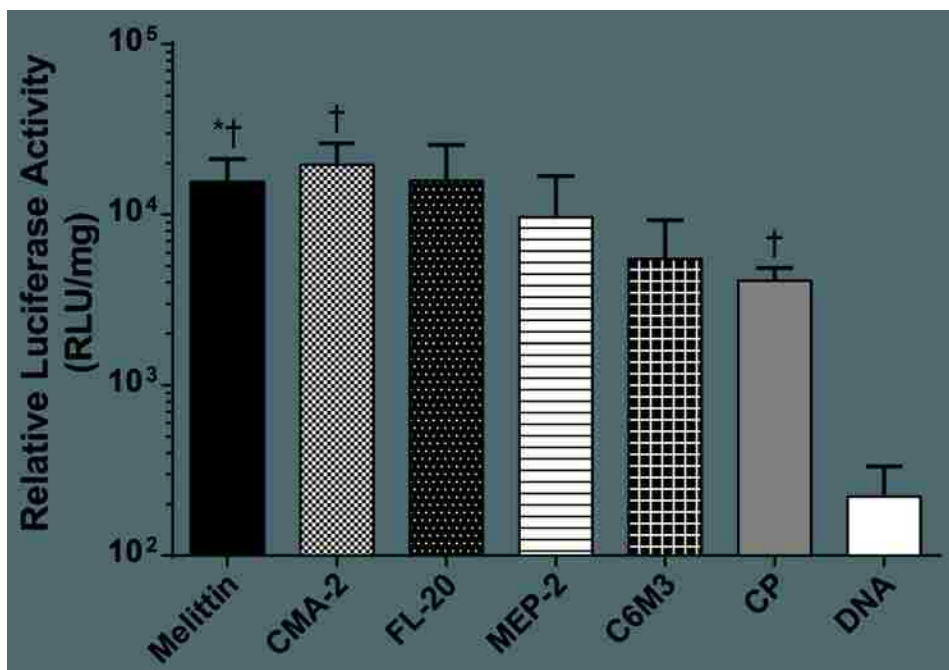
Figure 2.5 Luciferase activity in whole brain lysates 48 h after ICV injection of N/P 10 polyplexes. N=3-4; Data are plotted as the mean + SD. Statistical significance derived from Student's t-test comparing expression to one of two controls. (* $p < 0.05$ vs CP; † $p < 0.05$ vs DNA)

Epifluorescence microscopy was also used to analyze the distribution of transfection in a separate *in vivo* study where mice received polyplexes formulated with pmaxGFP™ and either CP or melittin PPC. We observed greater transfection for brains receiving PPC polyplexes but saw similar localization of transfection throughout the SVZ for both treatments (**Supplemental Figure 2.14**). It is not surprising that both polyplexes (CP and melittin PPC) undergo non-specific uptake along the SVZ epithelial barrier because association with cellular membranes and endocytosis of polyplexes is driven by their positive surface charge.[81] Although co-localization was not observed

between transfected cells (GFP$^+$) and either Tuj1 (neuronal marker) or GFAP (glial marker), transfection was observed predominantly in the periventricular space throughout the brain as in our previous studies with other polycations.[80] Transfection of cells in the subventricular zone was also observed for melittin PPC polyplex-treated animals. Finally, injections were well-tolerated by the animals and H&E staining revealed neither gross toxicity nor major tissue disruption along the needle track (**Supplemental Figure 2.15**). These results confirm that lytic peptides are well-protected in polyplexes *in vivo* and that transfection efficiency *in vivo* correlates with the lytic activity of non-reduced PPCs.

2.4   CONCLUSION

Herein we report the synthesis and evaluation of a panel of synthesized lytic peptides and the transfection capabilities they convey to acid-sensitive block copolymer micelles. Peptide polymer conjugates (PPCs) created from selected lytic peptides all demonstrated pH-dependent lysis and significantly enhanced *in vitro* transfection relative to unconjugated polymer, indicating that various peptide sequences may be encapsulated in VIPER micelles and are sufficient for endosomal escape. Surprisingly, only melittin-like PPCs showed greater hemolysis at pH 5.5 than their corresponding free peptides, implying that polymer-conjugated peptides may have enhanced lytic properties as a function of peptide sequence. As these most potently hemolytic PPCs also achieved the highest transfection *in vivo*, we conclude that only certain lytic peptides are able to promote endosomal escape when covalently conjugated to a polymer backbone. In summary, these data show that our pH-responsive micelle system exerts highly sensitive control over peptide-mediated membrane lysis regardless of the pH-responsiveness of the peptide conjugate, further establishing this technology as an active, universal mechanism for the endosomal escape of nucleic acid cargo.

2.5 SUPPLEMENTAL INFORMATION

Supplemental Figure 2.6 Polymer characterization by GPC and ^{1}H NMR.

Polymer	Formula	$M_n{}^a$	$M_n{}^b$	$Đ^b$
Block 1	p(OEGMA$_{8.60}$-co-DMAEMA$_{50.00}$)	10706	15940	1.064
Block 2	p(OEGMA$_{8.60}$-co-DMAEMA$_{50.0}$)-b-p(DIPAMA$_{25.32}$-co-PDSEMA$_{1.00}$)	16072	22520	1.194

a Determined by 1H NMR; b Obtained by GPC.
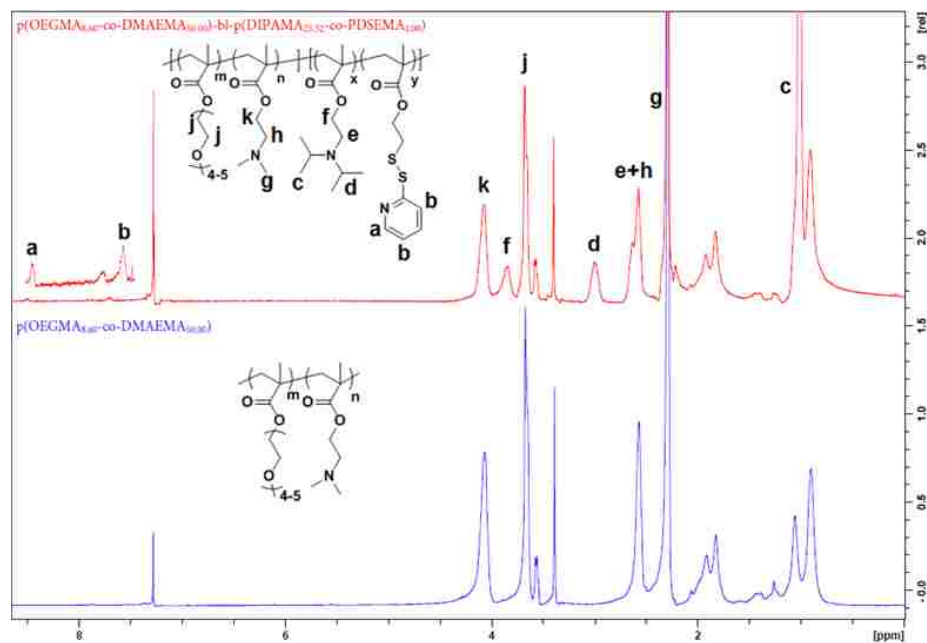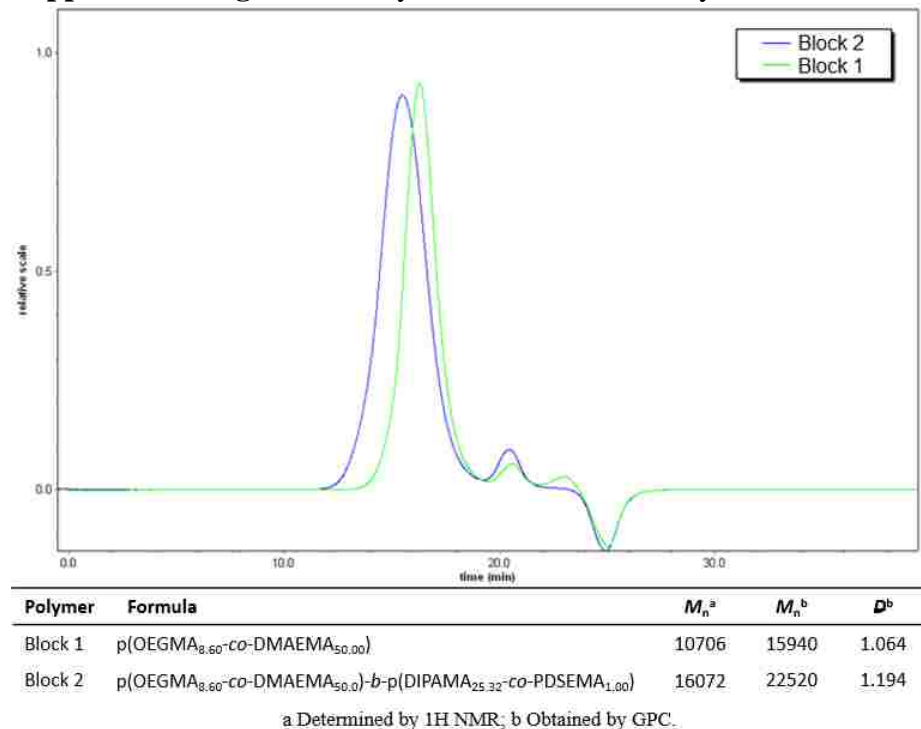
Supplemental Figure 2.7 Schematic of peptide-polymer conjugation by disulfide exchange.
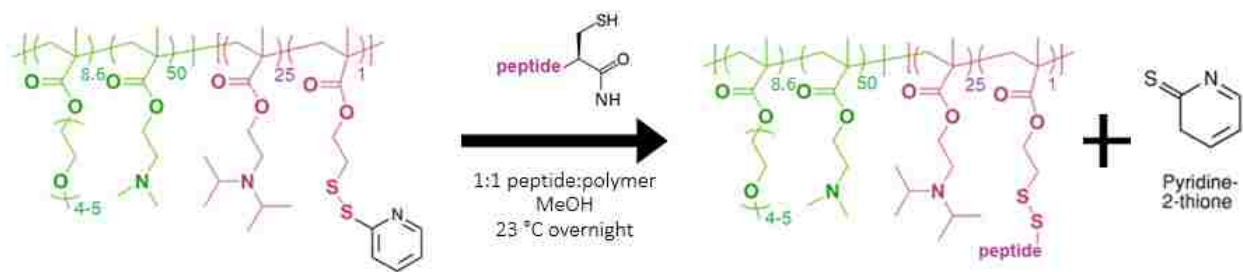
Supplemental Figure 2.8 PPC hemolysis at various pH in the presence of 10 mM GSH. Polymers were incubated with red blood cells at various effective peptide concentrations at pH 7.4 and pH 6 for 1 h in the presence of 10 mM GSH. For CP, an equivalent concentration of polymer was used in place of PPC concentration. Hemolysis was monitored by UV absorbance for released hemoglobin at 541 nm.
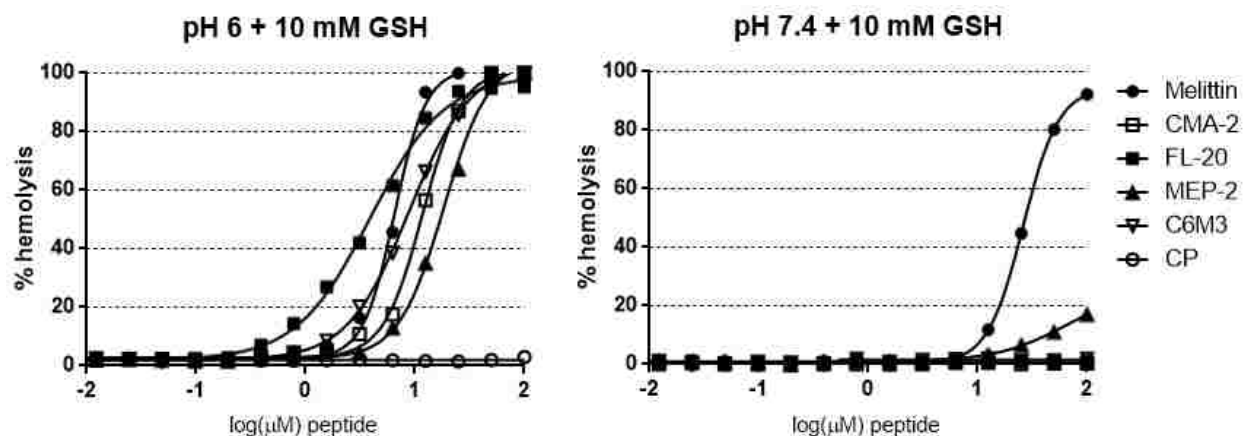
Supplemental Table 2.3 Quantification of peptide conjugation via analysis of residual PDSEMA content.

Conjugate	Abs$_{343}$	% PDSEMA reacted
Unreacted	0.41	0
Melittin	0.02	95
CMA-2	0.08	81
FL-20	0.02	95
C6M3	0.10	76
MEP-2	0.00	100

$$\% \, PDSEMA \, reacted = 100 * \left(1 - \frac{Sample_{abs343}}{Unreacted_{abs343}} \right)$$

Supplemental Figure 2.9 Representative results of two CMC assays.
Micelle solutions at concentrations varying from 0.5 to 1024 mg/l were added to dry Nile Red
and incubated for 24 hr before fluorescence intensity (excitation/emission: 556/625 nm) was
recorded. Linear regression was separately performed on flat and exponential regions of
fluorescence intensity; the CMC was taken to be x-value at the intersection of these lines for
each sample.
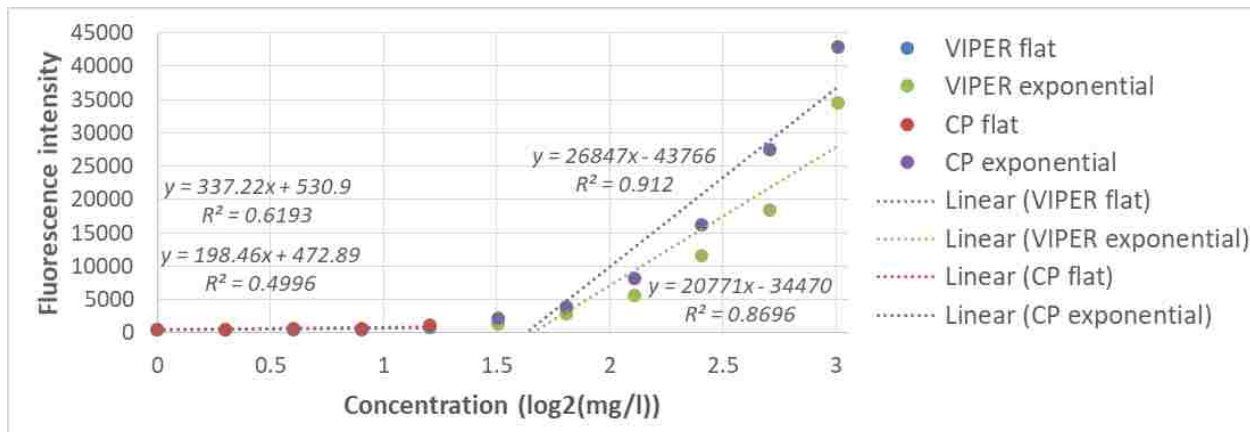
Supplemental Figure 2.10 Determination of micelle disassembly transition pH.

Micelles (0.2 mg/mL; CMC = 0.07 mg/mL) were incubated in phosphate buffers of varying pH
with1 µM Nile Red for 24 hr and then fluorescence intensity was measured (ex. 556 nm em. 625
nm). Fluorescence intensity is dependent on the amount of encapsulated Nile Red which is
directly correlated to the number of intact polymeric micelles.

Supplemental Figure 2.11 Gel retardation of plasmid DNA by CP and PPCs.
Polymer stocks were diluted to give a variety of molar ratios between tertiary amines (polymer, N) and phosphate groups (DNA, P) relative to a 0.1 mg/mL plasmid DNA stock. Polymer and DNA were mixed, incubated at room temperature for 10 minutes, and then run on a 1% agarose gel at 110 V for 30 min before imaging on a UV transilluminator.

Supplemental Figure 2.12 Representative flow cytometry transfection data.
(A) Representative flow cytometry gating on negative control samples and **(B)** GFP histogram plots of HeLa transfection at N/P 8 (above). Singlet cell events were serially gated to analyze viable (Violet-) and transfected (GFP+) cells.

Sample	Count	GFP-A+
Melittin	5837	91.7
FL20	3662	92.1
CMA2	3366	90.7
MEP2	5258	87.7
C6M3	6029	65.3
CP	6018	2.71
NoTreat	13915	0.014

Supplemental Figure 2.13 Relative luciferase activity in various brain compartment lysates 48 h after ICV injection of N/P 10 polyplexes.

N=3-4; Data are plotted as the mean + SD. Statistical significance was derived from Student's t-test comparing expression in each brain compartment to one of two corresponding controls. (* $p < 0.05$ vs CP; ** $p < 0.01$ vs CP; † $p < 0.05$ vs DNA; †† $p < 0.01$ vs DNA)
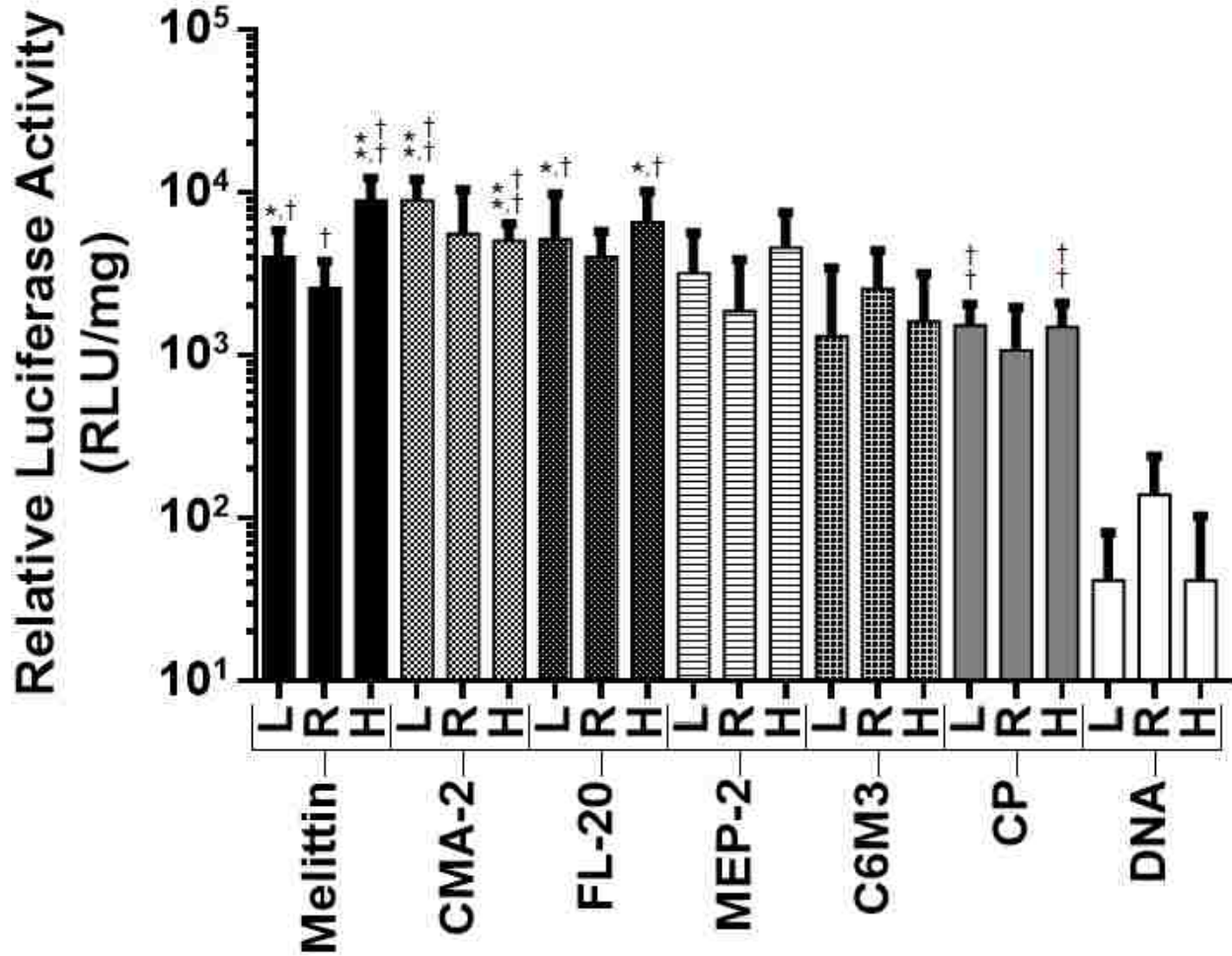
Supplemental Figure 2.14 Epifluorescence micrographs of cells expressing GFP in a region rostral to the site of polyplex injection.
Brains injected with polyplexes formed with control polymer (A-E) had fewer transfected cells (GFP$^+$, green) than brains injected with polyplexes formed with melittin PPC (F-I). In both cases, transfection is primarily localized to the vicinity near the ventricle wall, with some penetration into the subventricular zone (I) observed for the melittin PPC. Scale bar = 100 µm.
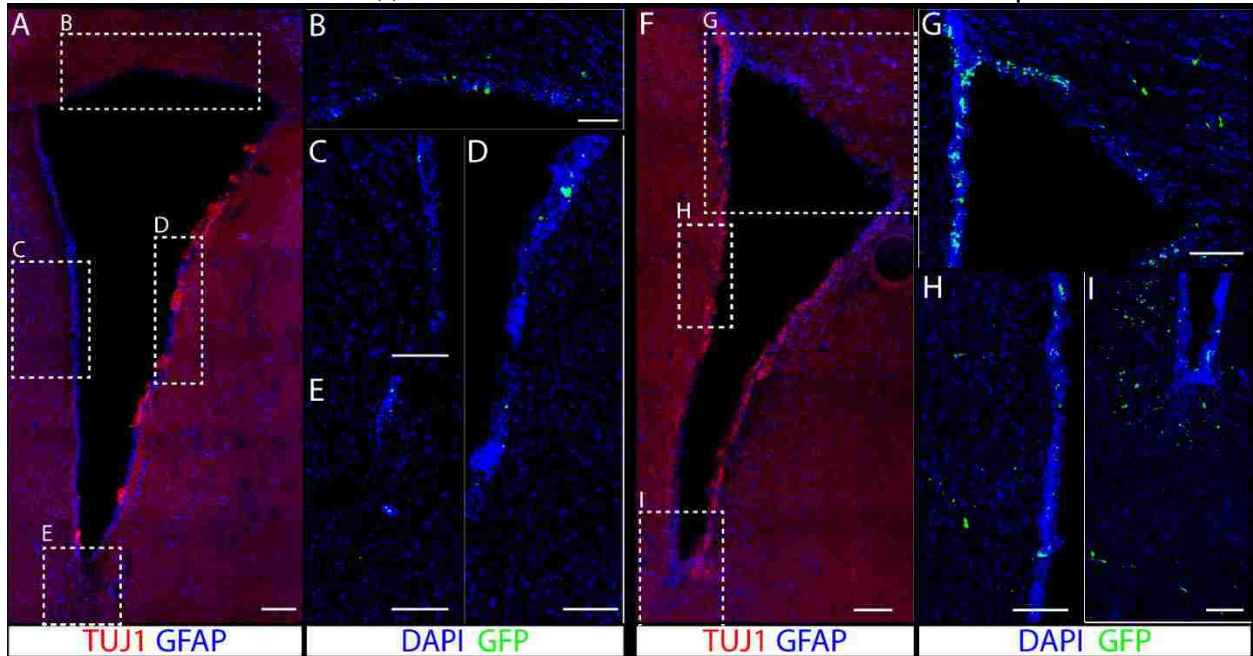
Supplemental Figure 2.15 Digital micrographs of brain tissue stained with H & E at the site of melittin-PPC polyplex injection.
Although the stain displays large-scale artifacts due to slide preparation (**A** 1.25X, **B** 5X; scale bar = 1 mm), the path of the needle is visible at high magnification (**C** 20X; scale bar = 100 µm) as a small, straight track of red stain indicative of local capillary rupture. Aside from local damage due to the injection, all other tears are a result of slide preparation and no other signs of tissue damage or inflammation were observed.
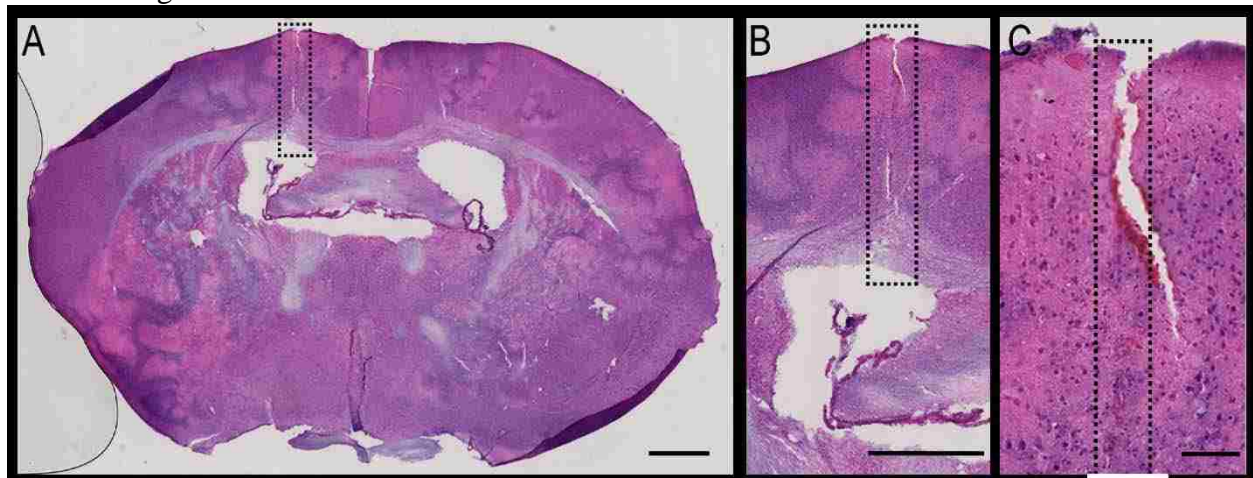
BIBLIOGRAPHY

(1)   Kay, M. A.; Glorioso, J. C.; Naldini, L. Viral Vectors for Gene Therapy: The Art of Turning Infectious Agents into Vehicles of Therapeutics. *Nat. Med.* **2001**, *7* (1), 33–40.

(2)   Lagache, T.; Danos, O.; Holcman, D. Modeling the Step of Endosomal Escape during Cell Infection by a Nonenveloped Virus. *Biophys. J.* **2012**, *102* (5), 980–989.

(3)   Stewart, M. P.; Lorenz, A.; Dahlman, J.; Sahay, G. Challenges in Carrier-Mediated Intracellular Delivery: Moving beyond Endosomal Barriers. *Wiley Interdiscip. Rev. Nanomedicine Nanobiotechnology* **2016**, *8* (3), 465–478.

(4)   Lächelt, U.; Wagner, E. Nucleic Acid Therapeutics Using Polyplexes: A Journey of 50 Years (and Beyond). *Chem. Rev.* **2015**, 150415062557000.

(5)   Pack, D. W.; Hoffman, A. S.; Pun, S.; Stayton, P. S. Design and Development of Polymers for Gene Delivery. *Nat. Rev. Drug Discov.* **2005**, *4* (7), 581–593.

(6)   Van De Wetering, P.; Moret, E. E.; Schuurmans-Nieuwenbroek, N. M. E.; Van Steenbergen, M. J.; Hennink, W. E. Structure-Activity Relationships of Water-Soluble Cationic Methacrylate/Methacrylamide Polymers for Nonviral Gene Delivery. *Bioconjug. Chem.* **1999**, *10* (4), 589–597.

(7)   Agarwal, S.; Zhang, Y.; Maji, S.; Greiner, A. PDMAEMA Based Gene Delivery Materials. *Mater. Today* **2012**, *15* (9), 388–393.

(8)   Boussif, O.; Lezoualc'h, F.; Zanta, M. A.; Mergny, M. D.; Scherman, D.; Demeneix, B.; Behr, J. P. A Versatile Vector for Gene and Oligonucleotide Transfer into Cells in Culture and in Vivo: Polyethylenimine. *Proc. Natl. Acad. Sci.* **1995**, *92* (16), 7297–7301.

(9)   Akinc, A.; Thomas, M.; Klibanov, A. M.; Langer, R. Exploring Polyethylenimine-Mediated DNA Transfection and the Proton Sponge Hypothesis. *J. Gene Med.* **2005**, *7* (5), 657–663.

(10)   Won, Y.-Y.; Sharma, R.; Konieczny, S. F. Missing Pieces in Understanding the Intracellular Trafficking of Polycation/DNA Complexes. *J. Control. Release* **2009**, *139* (2), 88–93.

(11)   Rehman, Z. ur; Hoekstra, D.; Zuhorn, I. S. Mechanism of Polyplex- and Lipoplex-Mediated Delivery of Nucleic Acids: Real-Time Visualization of Transient Membrane Destabilization without Endosomal Lysis. *ACS Nano* **2013**, *7* (5), 3767–3777.

(12)   Vermeulen, L. M. P.; Brans, T.; Samal, S. K.; Dubruel, P.; Demeester, J.; De Smedt, S. C.; Remaut, K.; Braeckmans, K. Endosomal Size and Membrane Leakiness Influence Proton Sponge-Based Rupture of Endosomal Vesicles. *ACS Nano* **2018**, *12* (3), 2332–2345.

(13)   Chu, D. S. H.; Schellinger, J. G.; Shi, J.; Convertine, A. J.; Stayton, P. S.; Pun, S. H. Application of Living Free Radical Polymerization for Nucleic Acid Delivery. *Acc. Chem. Res.* **2012**, *45* (7), 1089–1099.

(14)   Lee, D. C.; Prossnitz, A. N.; Lamm, R. J.; Boydston, A. J.; Pun, S. H. Dual Polymerizations: Untapped Potential for Biomaterials. *Adv. Healthc. Mater.* **2018**, *in revisio*.

(15)   Wang, H.-X.; Song, Z.; Lao, Y.-H.; Xu, X.; Gong, J.; Cheng, D.; Chakraborty, S.; Park, J. S.; Li, M.; Huang, D.; et al. Nonviral Gene Editing via CRISPR/Cas9 Delivery by Membrane-Disruptive and Endosomolytic Helical Polypeptide. *Proc. Natl. Acad. Sci. U. S. A.* **2018**, 201712963.

(16)   Gabrielson, N. P.; Lu, H.; Yin, L.; Li, D.; Wang, F.; Cheng, J. Reactive and Bioactive Cationic α-Helical Polypeptide Template for Nonviral Gene Delivery. *Angew. Chemie Int.*

Ed. **2012**, *51* (5), 1143–1147.

(17)   Wiethoff, C. M.; Nemerow, G. R. Adenovirus Membrane Penetration: Tickling the Tail of a Sleeping Dragon. *Virology* **2015**, *479–480*, 591–599.

(18)   Wiethoff, C. M.; Wodrich, H.; Gerace, L.; Nemerow, G. R. Adenovirus Protein VI Mediates Membrane Disruption Following Capsid Disassembly. *J. Virol.* **2005**, *79* (4), 1992–2000.

(19)   Cheng, Y.; Yumul, R. C.; Pun, S. H. Virus-Inspired Polymer for Efficient In Vitro and In Vivo Gene Delivery. *Angew. Chemie - Int. Ed.* **2016**, *55* (39), 12013–12017.

(20)   Zhou, K.; Wang, Y.; Huang, X.; Luby-Phelps, K.; Sumer, B. D.; Gao, J. Tunable, Ultrasensitive PH-Responsive Nanoparticles Targeting Specific Endocytic Organelles in Living Cells. *Angew. Chem. Int. Ed. Engl.* **2011**, *50* (27), 6109–6114.

(21)   Murthy, N.; Chang, I.; Stayton, P. S.; Hoffman, A. S. PH-Sensitive Hemolysis by Random Copolymers of Alkyl Acrylates and Acrylic Acid. *Macromol. Symp.* **2001**, *172*, 49–55.

(22)   Murthy, N.; Robichaud, J. R.; Tirrell, D. A.; Stayton, P. S.; Hoffman, A. S. The Design and Synthesis of Polymers for Eukaryotic Membrane Disruption. *J. Control. Release* **1999**, *61* (1–2), 137–143.

(23)   Wilson, J. T.; Keller, S.; Manganiello, M. J.; Cheng, C.; Lee, C.-C.; Opara, C.; Convertine, A.; Stayton, P. S. PH-Responsive Nanoparticle Vaccines for Dual-Delivery of Antigens and Immunostimulatory Oligonucleotides. *ACS Nano* **2013**, *7* (5), 3912–3925.

(24)   Feldmann, D. P.; Cheng, Y.; Kandil, R.; Xie, Y.; Mohammadi, M.; Harz, H.; Sharma, A.; Peeler, D. J.; Moszczynska, A.; Leonhardt, H.; et al. In Vitro and in Vivo Delivery of SiRNA via VIPER Polymer System to Lung Cells. *J. Control. Release* **2018**, *276*, 50–58.

(25)   Varkouhi, A. K.; Scholte, M.; Storm, G.; Haisma, H. J. Endosomal Escape Pathways for Delivery of Biologicals. *J. Control. Release* **2011**, *151* (3), 220–228.

(26)   Ogris, M.; Carlisle, R. C.; Bettinger, T.; Seymour, L. W. Melittin Enables Efficient Vesicular Escape and Enhanced Nuclear Access of Nonviral Gene Delivery Vectors. *J. Biol. Chem.* **2001**, *276* (50), 47550–47555.

(27)   Meyer, M.; Zintchenko, A.; Ogris, M.; Wagner, E. A Dimethylmaleic Acid–melittin-Polylysine Conjugate with Reduced Toxicity, PH-Triggered Endosomolytic Activity and Enhanced Gene Transfer Potential. *J. Gene Med.* **2007**, *9* (9), 797–805.

(28)   Akishiba, M.; Takeuchi, T.; Kawaguchi, Y.; Sakamoto, K.; Yu, H. H.; Nakase, I.; Takatani-Nakase, T.; Madani, F.; Gräslund, A.; Futaki, S. Cytosolic Antibody Delivery by Lipid-Sensitive Endosomolytic Peptide. *Nat. Chem.* **2017**, *9* (8), 751–761.

(29)   Boeckle, S.; Fahrmeir, J.; Roedl, W.; Ogris, M.; Wagner, E. Melittin Analogs with High Lytic Activity at Endosomal PH Enhance Transfection with Purified Targeted PEI Polyplexes. *J. Control. Release* **2006**, *112* (2), 240–248.

(30)   Li, M.; Tao, Y.; Shu, Y.; LaRochelle, J. R.; Steinauer, A.; Thompson, D.; Schepartz, A.; Chen, Z. Y.; Liu, D. R. Discovery and Characterization of a Peptide That Enhances Endosomal Escape of Delivered Proteins in Vitro and in Vivo. *J. Am. Chem. Soc.* **2015**, *137* (44), 14084–14093.

(31)   Schellinger, J. G.; Pahang, J. a; Johnson, R.; Chu, D. S.; Sellers, D. L.; Maris, D. O.; Convertine, A. J.; Stayton, P. S.; Horner, P. J.; Pun, S. H. Melittin-Grafted HPMA-Oligolysine Based Copolymers for Improved Gene Delivery. *Biomaterials* **2013**, *34* (9), 2318–2326.

(32)   Kwon, E. J.; Bergen, J. M.; Pun, S. H. Application of an HIV Gp41-Derived Peptide for Enhanced Intracellular Trafficking of Synthetic Gene and SiRNA Delivery Vehicles.

Bioconjug. Chem. **2008**, *19* (4), 920–927.

(33)   Wagner, E.; Plank, C.; Zatloukal, K.; Cotten, M.; Birnstiel, M. L. Influenza Virus Hemagglutinin HA-2 N-Terminal Fusogenic Peptides Augment Gene Transfer by Transferrin–polylysine–DNA Complexes: Toward a Synthetic Virus-like Gene-Transfer Vehicle. *Proc. Natl Acad. Sci. Usa* **1992**, *89* (17), 7934–7938.

(34)   Kakimoto, S.; Hamada, T.; Komatsu, Y.; Takagi, M.; Tanabe, T.; Azuma, H.; Shinkai, S.; Nagasaki, T. The Conjugation of Diphtheria Toxin T Domain to Poly(Ethylenimine) Based Vectors for Enhanced Endosomal Escape during Gene Transfection. *Biomaterials* **2009**, *30* (3), 402–408.

(35)   Min, S.-H.; Lee, D. C.; Lim, M. J.; Park, H. S.; Kim, D. M.; Cho, C. W.; Yoon, D. Y.; Yeom, Y. Il. A Composite Gene Delivery System Consisting of Polyethylenimine and an Amphipathic Peptide KALA. *J. Gene Med.* **2006**, *8* (12), 1425–1434.

(36)   Peeler, D. J.; Thai, S. N.; Cheng, Y.; Horner, P. J.; Sellers, D. L.; Pun, S. H. PH-Sensitive Polymer Micelles Provide Selective and Potentiated Lytic Capacity to Venom Peptides for Effective Intracellular Delivery. *Biomaterials* **2018**, *in press*, 235–244.

(37)   Eisenberg, D.; Schwarz, E.; Komaromy, M.; Wall, R. Analysis of Membrane and Surface Protein Sequences with the Hydrophobic Moment Plot. *J. Mol. Biol.* **1984**, *179* (1), 125–142.

(38)   Zheng, W.; Zhao, Q. Establishment and Characterization of an Immortalized Z310 Choroidal Epithelial Cell Line from Murine Choroid Plexus. *Brain Res.* **2002**, *958* (2), 371–380.

(39)   Dong, H.; Dong, C.; Xia, W.; Li, Y.; Ren, T. Self-Assembled, Redox-Sensitive, H-Shaped Pegylated Methotrexate Conjugates with High Drug-Carrying Capability for Intracellular Drug Delivery. *Med. Chem. Commun.* **2014**, *5* (2), 147–152.

(40)   Cheng, Y.; Wei, H.; Tan, J. Y.; Peeler, D. J.; Maris, D. O.; Sellers, D. L.; Horner, P. J.; Pun, S. H. Nano-Sized Sunflower Polycations As Effective Gene Transfer Vehicles. *Small* **2016**, 1–9.

(41)   Jafari, M.; Xu, W.; Naahidi, S.; Chen, B.; Chen, P. A New Amphipathic, Amino-Acid-Pairing (AAP) Peptide as SiRNA Delivery Carrier: Physicochemical Characterization and in Vitro Uptake. *J. Phys. Chem. B* **2012**, *116* (44), 13183–13191.

(42)   Xu, W.; Pan, R.; Zhao, D.; Chu, D.; Wu, Y.; Wang, R.; Chen, B.; Ding, Y.; Sadatmousavi, P.; Yuan, Y.; et al. Design and Evaluation of Endosomolytic Biocompatible Peptides as Carriers for SiRNA Delivery. *Mol. Pharm.* **2015**, *12* (1), 56–65.

(43)   Čeřovský, V.; Hovorka, O.; Cvačka, J.; Voburka, Z.; Bednárová, L.; Borovičková, L.; Slaninová, J.; Fučík, V. Melectin: A Novel Antimicrobial Peptide from the Venom of the Cleptoparasitic Bee *Melecta Albifrons*. *ChemBioChem* **2008**, *9* (17), 2815–2821.

(44)   Fox, M. A.; Thwaite, J. E.; Ulaeto, D. O.; Atkins, T. P.; Atkins, H. S. Design and Characterization of Novel Hybrid Antimicrobial Peptides Based on Cecropin A, LL-37 and Magainin II. *Peptides* **2012**, *33* (2), 197–205.

(45)   Tan, Y.-X.; Chen, C.; Wang, Y.-L.; Lin, S.; Wang, Y.; Li, S.-B.; Jin, X.-P.; Gao, H.-W.; Du, F.-S.; Gong, F.; et al. Truncated Peptides from Melittin and Its Analog with High Lytic Activity at Endosomal PHenhance Branched Polyethylenimine-Mediated Gene Transfection. *J. Gene Med.* **2012**, *14*, 214–250.

(46)   Lundberg, P.; El-Andaloussi, S.; Sütlü, T.; Johansson, H.; Langel, Ü. Delivery of Short Interfering RNA Using Endosomolytic Cell-Penetrating Peptides. *FASEB J.* **2007**, *21* (11), 2664–2671.

(47) Gao, B.; Sherman, P.; Luo, L.; Bowie, J.; Zhu, S. Structural and Functional Characterization of Two Genetically Related Meucin Peptides Highlights Evolutionary Divergence and Convergence in Antimicrobial Peptides. *FASEB J.* **2009**, *23* (4), 1230–1245.

(48) Lan, Y.; Langlet-Bertin, B.; Abbate, V.; Vermeer, L. S.; Kong, X.; Sullivan, K. E.; Leborgne, C.; Scherman, D.; Hider, R. C.; Drake, A. F.; et al. Incorporation of 2,3-Diaminopropionic Acid into Linear Cationic Amphipathic Peptides Produces PH-Sensitive Vectors. *Chembiochem* **2010**, *11* (9), 1266–1272.

(49) Chen, Y.; Mant, C. T.; Farmer, S. W.; Hancock, R. E. W.; Vasil, M. L.; Hodges, R. S. Rational Design of Alpha-Helical Antimicrobial Peptides with Enhanced Activities and Specificity/Therapeutic Index. *J. Biol. Chem.* **2005**, *280* (13), 12316–12329.

(50) Bartz, R.; Fan, H.; Zhang, J.; Innocent, N.; Cherrin, C.; Beck, S. C.; Pei, Y.; Momose, A.; Jadhav, V.; Tellers, D. M.; et al. Effective SiRNA Delivery and Target MRNA Degradation Using an Amphipathic Peptide to Facilitate PH-Dependent Endosomal Escape. *Biochem. J.* **2011**, *435* (2), 475–487.

(51) Krishnakumari, V.; Nagaraj, R. Antimicrobial and Hemolytic Activities of Crabrolin, a 13-Residue Peptide from the Venom of the European Hornet, Vespa Crabro, and Its Analogs. *J. Pept. Res.* **1997**, *50* (2), 88–93.

(52) Kashiwada, A.; Mizuno, M.; Hashimoto, J. PH-Dependent Membrane Lysis by Using Melittin-Inspired Designed Peptides. *Org. Biomol. Chem.* **2016**, *14* (26), 6281–6288.

(53) Dai, L.; Corzo, G.; Naoki, H.; Andriantsiferana, M.; Nakajima, T. Purification, Structure–function Analysis, and Molecular Characterization of Novel Linear Peptides from Scorpion Opisthacanthus Madagascariensis. *Biochem. Biophys. Res. Commun.* **2002**, *293* (5), 1514–1522.

(54) Wakabayashi, N.; Yano, Y.; Kawano, K.; Matsuzaki, K. A PH-Dependent Charge Reversal Peptide for Cancer Targeting. *Eur. Biophys. J.* **2017**, *46* (2), 121–127.

(55) Sitaram, N.; Subbalakshmi, C.; Nagaraj, R. Structural and Charge Requirements for Antimicrobial and Hemolytic Activity in the Peptide PKLLETFLSKWIG, Corresponding to the Hydrophobic Region of the Antimicrobial Protein Bovine Seminalplasmin. *Int. J. Pept. Protein Res.* **1995**, *46* (2), 166–173.

(56) Vivès, E.; Brodin, P.; Lebleu, B. A Truncated HIV-1 Tat Protein Basic Domain Rapidly Translocates through the Plasma Membrane and Accumulates in the Cell Nucleus. *J. Biol. Chem.* **1997**, *272* (25), 16010–16017.

(57) Wang, C.; Wang, Y.; Li, Y.; Bodemann, B.; Zhao, T.; Ma, X.; Huang, G.; Hu, Z.; DeBerardinis, R. J.; White, M. A.; et al. A Nanobuffer Reporter Library for Fine-Scale Imaging and Perturbation of Endocytic Organelles. *Nat Commun* **2015**, *6*.

(58) Whitesides, G. M.; Mathias, J. P.; Seto, C. T. Molecular Self-Assembly and Nanochemistry: A Chemical Strategy for the Synthesis of Nanostructures. *Science* **1991**, *254* (5036), 1312–1319.

(59) Li, Y.; Zhao, T.; Wang, C.; Lin, Z.; Huang, G.; Sumer, B. D.; Gao, J. Molecular Basis of Cooperativity in PH-Triggered Supramolecular Self-Assembly. *Nat. Commun.* **2016**, *7*, 13214.

(60) Li, Y.; Wang, Z.; Wei, Q.; Luo, M.; Huang, G.; Sumer, B. D.; Gao, J. Non-Covalent Interactions in Controlling PH-Responsive Behaviors of Self-Assembled Nanosystems. *Polym. Chem.* **2016**, *7* (38), 5949–5956.

(61) Rietsch, A.; Beckwith, J. The Genetics of Disulfide Bond Metabolism. *Annu. Rev. Genet.*

1998, *32* (1), 163–184.

(62) Schafer, F. Q.; Buettner, G. R. Redox Environment of the Cell as Viewed through the Redox State of the Glutathione Disulfide/Glutathione Couple. *Free Radic. Biol. Med.* **2001**, *30* (11), 1191–1212.

(63) Feener, E. P.; Shen, W. C.; Ryser, H. J. Cleavage of Disulfide Bonds in Endocytosed Macromolecules. A Processing Not Associated with Lysosomes or Endosomes. *J. Biol. Chem.* **1990**, *265* (31), 18780–18785.

(64) Go, Y.-M.; Jones, D. P. Redox Compartmentalization in Eukaryotic Cells. *Biochim. Biophys. Acta* **2008**, *1780* (11), 1273–1290.

(65) Santra, S.; Kaittanis, C.; Santiesteban, O. J.; Perez, J. M. Cell-Specific, Activatable, and Theranostic Prodrug for Dual-Targeted Cancer Imaging and Therapy. *J. Am. Chem. Soc.* **2011**, *133* (41), 16680–16688.

(66) Lv, H.; Zhang, S.; Wang, B.; Cui, S.; Yan, J. Toxicity of Cationic Lipids and Cationic Polymers in Gene Delivery. *J. Control. Release* **2006**, *114* (1), 100–109.

(67) Verbaan, F. J.; Bos, G. W.; Oussoren, C.; Woodle, M. C.; Hennink, W. E.; Storm, G. A Comparative Study of Different Cationic Transfection Agents for in Vivo Gene Delivery after Intravenous Administration. *J. Drug Deliv. Sci. Technol.* **2004**, *14* (2), 105–111.

(68) Barrett, A. J.; Kirschke, H. Cathepsin B, Cathepsin H, and Cathepsin L. *Methods Enzymol.* **1981**, *80 Pt C*, 535–561.

(69) Seglen, P. O.; Bohley, P. Autophagy and Other Vacuolar Protein Degradation Mechanisms. *Experientia* **1992**, *48* (2), 158–172.

(70) Cuervo, A. M.; Dice, J. F. Lysosomes, a Meeting Point of Proteins, Chaperones, and Proteases. *J. Mol. Med.* **1997**, *76* (1), 6–12.

(71) Greene, L. A.; Tischler, A. S. Establishment of a Noradrenergic Clonal Line of Rat Adrenal Pheochromocytoma Cells Which Respond to Nerve Growth Factor. *Proc. Natl. Acad. Sci. U. S. A.* **1976**, *73* (7), 2424–2428.

(72) Ihrie, R. A.; Álvarez-Buylla, A. Lake-Front Property: A Unique Germinal Niche by the Lateral Ventricles of the Adult Brain. *Neuron* **2011**, *70* (4), 674–686.

(73) Arvidsson, A.; Collin, T.; Kirik, D.; Kokaia, Z.; Lindvall, O. Neuronal Replacement from Endogenous Precursors in the Adult Brain after Stroke. *Nat. Med.* **2002**, *8* (9), 963–970.

(74) Kolb, B.; Morshead, C.; Gonzalez, C.; Kim, M.; Gregg, C.; Shingo, T.; Weiss, S. Growth Factor-Stimulated Generation of New Cortical Tissue and Functional Recovery after Stroke Damage to the Motor Cortex of Rats. *J Cereb Blood Flow Metab* **2006**, *27* (5), 983–997.

(75) Faiz, M.; Acarin, L.; Villapol, S.; Schulz, S.; Castellano, B.; Gonzalez, B. Substantial Migration of SVZ Cells to the Cortex Results in the Generation of New Neurons in the Excitotoxically Damaged Immature Rat Brain. *Mol. Cell. Neurosci.* **2008**, *38* (2), 170–182.

(76) Zheng, W.; ZhuGe, Q.; Zhong, M.; Chen, G.; Shao, B.; Wang, H.; Mao, X.; Xie, L.; Jin, K. Neurogenesis in Adult Human Brain after Traumatic Brain Injury. *J. Neurotrauma* **2013**, *30* (22), 1872–1880.

(77) Saha, B.; Peron, S.; Murray, K.; Jaber, M.; Gaillard, A. Cortical Lesion Stimulates Adult Subventricular Zone Neural Progenitor Cell Proliferation and Migration to the Site of Injury. *Stem Cell Res.* **2013**, *11* (3), 965–977.

(78) Kwon, E. J.; Lasiene, J.; Jacobson, B. E.; Park, I.-K.; Horner, P. J.; Pun, S. H. Targeted Nonviral Delivery Vehicles to Neural Progenitor Cells in the Mouse Subventricular Zone.

Biomaterials **2010**, *31* (8), 2417–2424.

(79)   Cheng, Y.; Sellers, D. L.; Tan, J.-K. Y.; Peeler, D. J.; Horner, P. J.; Pun, S. H. Development of Switchable Polymers to Address the Dilemma of Stability and Cargo Release in Polycationic Nucleic Acid Carriers. *Biomaterials* **2017**, *127*, 89–96.

(80)   Tan, J.-K. Y.; Pham, B.; Zong, Y.; Perez, C.; Maris, D. O.; Hemphill, A.; Miao, C.; Matula, T. J.; Mourad, P. D.; Wei, H.; et al. Microbubbles and Ultrasound Increase Intraventricular Polyplex Gene Transfer to the Brain. *J. Control. Release* **2016**.

(81)   Sahay, G.; Alakhova, D. Y.; Kabanov, A. V. Endocytosis of Nanomedicines. *Journal of Controlled Release*. NIH Public Access August 3, 2010, pp 182–195.

Chapter 3. POLYPLEX TRANSFECTION FROM INTRACEREBROVENTRICULAR DELIVERY IS NOT SIGNIFICANTLY AFFECTED BY TRAUMATIC BRAIN INJURY

Abstract

Traumatic brain injury (TBI) is largely non-preventable and often kills or permanently disables its victims. Because current treatments for TBI merely ameliorate secondary effects of the initial injury like swelling and hemorrhaging, strategies for the induction of neuronal regeneration are desperately needed. Recent discoveries regarding the TBI-responsive migratory behavior and differentiation potential of neural progenitor cells (NPCs) found in the subventricular zone (SVZ) have prompted strategies targeting gene therapies to these cells to enhance neurogenesis after TBI. We have previously shown that plasmid polyplexes can non-virally transfect SVZ NPCs when directly injected in the lateral ventricles of uninjured mice. We describe the first reported intracerebroventricular transfections mediated by polymeric gene carriers in a murine TBI model and investigate the anatomical parameters that dictate transfection through this route of administration. Using both luciferase and GFP plasmid transfections, we show that the time delay between injury and polyplex injection directly impacts the magnitude of transfection efficiency, but that overall trends in the location of transfection are not affected by injury. Confocal microscopy of quantum dot-labeled plasmid uptake *in vivo* reveals association between our polymers and negatively charged NG2 chondroitin sulfate proteoglycans of the SVZ extracellular matrix. We further validate that glycosaminoglycans but not sulfate groups are required for polyplex uptake and transfection *in vitro.* These studies demonstrate that non-viral gene delivery

is impacted by proteoglycan interactions and suggest the need for improved polyplex targeting materials that penetrate brain extracellular matrix to increase transfection efficiency *in vivo*.

3.1   INTRODUCTION

Approximately 1.7 million people suffer a traumatic brain injury (TBI) each year in the United States alone, injuries that can result in death or permanent disability while costing the healthcare system over $50 billion annually. [1,2] While focal TBI is initiated as an acute blunt-force trauma to the exterior of the skull that causes immediate cortical zone cell death, larger ischemic or swollen regions then develop throughout the cortex that produce permanent scarring and neuron loss.[3] The current standard of care for TBI seeks to curtail these secondary damages by limiting bleeding and inflammation but requires prompt implementation and does not ultimately restore the function of the neural tissue lost to injury.[4] This is in part because injured neurons in the central nervous system (CNS) demonstrate virtually no endogenous regenerative capacity, unlike injured axons in the peripheral nervous system.[5] Thus, therapeutic strategies for the regeneration and integration of neurons at the site of injury could greatly impact patient recovery after TBI.

While stem cell transplantation therapies for tissue regeneration in the CNS have rapidly progressed into clinical study,[6] gene therapies that manipulate endogenous neural progenitor cells (NPCs) with transcription or growth factors offer a promising alternative.[7–9] Compared to cultured cell therapies used as transplants, "direct reprogramming" approaches are more cost effective, less toxic, and promise access to different neuronal subtypes that may repair damaged nerve circuits with greater efficacy.[8,10] Interestingly, it has been shown that a variety of injuries including TBI stimulate the endogenous reservoir of NPCs in the subventricular zone (SVZ) to

proliferate and migrate to the site of injury in adult rodents, primates, and humans.[11–14] Upon

arrival in the TBI cortex, these cells primarily differentiate into astrocytes but also a small number

of neurons, resulting in minor improvements to motor and sensory function in rodents.[15,16]

While naturally-occurring neurogenesis is not enough to restore function following TBI, it

motivates research that will enhance the proliferation, migration, and differentiation of SVZ NPCs

into cortical neurons.[8,10] Although intracerebroventricular (ICV) retrovirus injection has shown

initial promise as a means for endogenous NPC reprogramming,[17] viral strategies are

translationally limited by their immunogenicity, genetic cargo capacity, and complex

manufacturing processes in comparison to non-viral methods.[18,19] Thus, we seek to augment

the NPC repair response through non-viral transfection of therapeutic genes in SVZ NPCs through

ICV injection of polyplexes.

We have previously demonstrated delivery of reporter plasmids to cells of the SVZ in healthy

mice;[20,21] however, very little is known about the impact of TBI on *in vivo* transfection. In this

work, we utilize our most promising polymeric gene carrier (VIPER[21,22]) to deliver various

plasmid cargoes through ICV injection in a controlled cortical impact (CCI) mouse model of TBI.

Although the clinical etiology of TBI is extremely diverse, CCI offers promise as a translational

model that generates reproducible and quantifiable cognitive and motor deficits in mice that mimic

human symptoms.[23,24] As a first step towards therapeutic transfection after TBI, we first

optimize the timing of transfection post-injury using luciferase reporter plasmids in order to

capitalize on the dynamic cellular proliferation response to injury. We next analyze the distribution

of GFP transfection after injury in various brain regions contacting the ventricular space through

confocal microscopy, and then further investigate extracellular barriers to gene delivery in these

regions through a combined *in vivo* and *in vitro* approach. This work highlights the significant hurdles between current non-viral transfection approaches and therapeutic transfection after CCI in mice and establishes guidelines for future vector development.

3.2   EXPERIMENTAL SECTION

3.2.1   *Material sourcing and polymer synthesis*

Endotoxin-free plasmid pCMV-Luc™ (ProMega) and pMAX-GFP™ (Lonza) were purified with the Qiagen Plasmid Giga kit (Qiagen) according to the manufacturer's protocol. EdU (5-ethynyl-2'-deoxyuridine) purchased from Lumiprobe was dissolved at 10 mg/mL in saline by heating at 80 °C for 10 min before storage at -20 °C in 0.22 µm sterile-filtered aliquots until use. All chemicals used for polymer and peptide synthesis were purchased from either Sigma Aldrich or Thermo Fisher Scientific and used without further purification as previously described.[18] The block copolymer p(OEGMA8.6-co-DMAEMA50.0)-bl-p(DIPAMA25.3-co-[PDSEMA-g-melittin]1.0) termed "VIPER" was prepared and characterized in previous work.[18]

3.2.2   *Controlled Cortical Impact (CCI)*

All animal procedures were completed according to protocols approved by the Institutional Animal Care and Use Committee at the University of Washington. Moderate CCI was performed on female C57Bl/6 mice (8 wk old) using a custom electromechanical impactor described by the Ohio State University ESCID Contusion Model.[23] Briefly, in this model, a 3.5 mm by 3.5 mm craniotomy is performed followed by exposure of the dura via electric drilling of a burr hole (centered 1 mm medial/lateral, -1.5 mm rostral/caudal to Bregma). A 2 mm wide metal probe attached to the contusion device is lowered onto the dura covering the motor cortex until contact is visualized by

the dampening of force oscillations on an oscilloscope. Brain deformation of 0.8 mm at a velocity of 5 m/sec is performed with a slope of 0.3 V/ms; actual displacement and mean force are recorded for each impact. Bleeding is dried with gauze, gel foam is used to patch the burr hole, and staples are utilized for skin closure prior to recovery and analgesia. While the primary necrotic injury occupies the somatosensory and parietal association cortexes, the secondary injury zone comprised of inflammation and disrupted blood-brain-barrier function extends into the hippocampus.[24,25] (**Supplemental Figure 3.6**) This overall moderate injury leads to significant motor and learning deficits that can be reliably evaluated through behavioral assessment.[26]

3.2.3   In vivo *plasmid transfection in the brain*

Intracerebroventricular (intraventricular) injection was performed as described before.[27] Polyplex formulations were prepared in 5% glucose solution containing 2.5 µg of plasmid DNA (N/P 10) by vigorously pipetting polymer into DNA and resting the mixture for at least 10 minutes. Female C57/Bl6 mice (8 wk old) were anesthetized by intraperitoneal injection of Avertin (500 mg/kg body weight). After craniotomy, a burr hole (1 mm diameter) was made on the right-side of the skull using a dental drill, and 10 µL of polyplex was stereotaxically injected (Bregma, -0.5mm; Medial/Lateral, 1.0mm; Dorsal/Ventral, 1.8mm) using a 33 gauge Hamilton syringe. The injection was made at 2 µL/min and the syringe was kept in the injection site for 2 min to prevent backflow prior to needle removal. When used, EdU was injected intraperitoneally at a dose of 50 mg/kg 8 h after transfection.

For luciferase plasmid transfections, brain compartments were harvested 48 h after transfection as distinct tissues (left, right and hind brain) from mice and collected in lysis buffer supplemented

with protease inhibitors (Roche). Three freeze-thaw cycles were performed in liquid nitrogen, tissues were mechanically homogenized, and lysate was cleared by centrifugation at 21,000 g for 15 min at 4 °C. Clarified lysate was assayed for luminescence with luciferase substrate (ProMega) using a plate reader and relative light units (RLU) were normalized by protein content as determined by BCA Protein Assay Kit (Pierce). Thus, gene expression was reported as the average RLU/mg protein for each brain region with error reported as the standard deviation of the mean. Whole brain gene expression was calculated as the sum of RLU/mg values of all regions per brain.

For GFP plasmid or QD585-labeled luciferase plasmid transfection, mice were euthanized 48 h or 1 h after transfection, respectively, and perfused intracardially with 0.9% saline followed by 4% paraformaldehyde in 0.1 M phosphate buffer. Brains were then processed for histology as described below.

3.2.4 *Histology and confocal microscopy*

After perfusion and fixation, brains were excised and equilibrated to 30% sucrose in phosphate buffer. Brains were embedded in OCT and sectioned into 30 µm-thick coronal slices stored floating in PBS. For immunofluorescent labeling, slices were rinsed with PBS and blocked in PBS, 0.3% Triton X-100, 2% bovine serum albumin (BSA) for 1 h. If performing click chemistry staining of EdU, slices were washed three times with PBS, incubated for 30 m in labeling cocktail (1 µM N_3-Cy5 [Click Chemistry Tools], 1 mM $CuSO_4$, 100 mM sodium ascorbate), and then washed three times in TBS before proceeding.[28] Primary antibodies (chicken anti-GFAP [1:500, Millipore AB5541]; rabbit anti-Iba1 [1:500, Wako 019-19741]; rabbit anti-NG2 [1:500, Millipore AB5320]) were applied to the tissue sections in PBS, 0.3% TritonX-100, 2% BSA overnight at 4 °C. Sections

71

were rinsed three times for 20min in TBS, 0.1% Tween 20 and species appropriate secondary antibodies conjugated with fluorophore were incubated in PBS, 0.1% Tween 20, and 2% donkey serum for 2 h. Sections were rinsed three times for 20min in TBS–Tween, with the last rinse containing the nuclear marker, 4′,6-diamidino-2-phenylindole (DAPI; 0.5 µg/ml). Sections were then mounted onto glass slides, sealed and cover-slipped with polyvinyl alcohol, and imaged using a custom Leica SP8X confocal scanning laser microscope housed at the W. M. Keck Microscopy Center at the University of Washington Medical Center.

3.2.5 *Conjugation of luciferase plasmid DNA with QD585*

Luciferase plasmid was labeled with Qdot™ 585 Streptavidin Conjugate (QD585, ThermoFisher) utilizing the DNA-intercalating crosslinker Psoralen-PEO-biotin (ThermoFisher) as previously described with minor protocol modifications.[29] In brief, the psoralen crosslinker (20 mM in DMSO) was diluted 1:100 v/v with luciferase plasmid DNA (2 mg/mL in water) and irradiated using a 50 W longwave UV lamp for 1 h at room temperature. The plasmid was ethanol/acetate precipitated and biotin content verified to be in excess of 1000 biotins/plasmid using the Quant*Tag™ Biotin Kit (Vector Laboratories) and a Nanodrop spectrophotometer (ThermoFisher). Strep-QD585 solution was mixed with biotinylated plasmid at 1:1 molar ratio and incubated at room temperature overnight. Plasmids were ethanol/acetate precipitated to remove unconjugated Strep-QD585 and resuspended in 5% glucose for use in transfection. Conjugation purity was verified by gel electrophoresis and the degree of conjugation was determined to be between 0.5-1 QD585/pLuciferase using the HS dsDNA Qubit assay (ThermoFisher) to quantify DNA concentration and a fluorescence plate reader to quantify QD585 concentration via a custom standard curve.

3.2.6 *Cell culture and in vitro plasmid uptake and transfection*

CHO cells (K1 wt ATCC# CCL-61; pgsE-606 ATCC# CRL-2246; pgsA-745 ATCC# CRL-2242) were maintained at 37 °C/5% CO_2 in F-12K base media (Gibco) supplemented with 10% fetal bovine serum and penicillin/streptomycin and passaged every three days or when 75% confluent. Cells were seeded at a density of 25,000 cells/well in 24-well plates and incubated overnight before assay. Polyplexes were prepared at N/P 5 with 1 µg QD585-pLuciferase (for uptake studies) or 1 µg pMAX-GFP™ pDNA (for transfection studies) and allowed to rest for at least 10 min. Each polyplex solution was then added dropwise directly to each well (in triplicate). In uptake studies, cells were washed twice with PBS and lifted with trypsin for analysis by flow cytometry at either 2, 4, or 8 h after polyplex addition. In transfection studies, cells were given fresh complete medium after 4 h incubation with polyplexes and analyzed by flow cytometry 48 h after transfection. Singlet cell events recorded on an Attune NxT flow cytometer (ThermoFisher) were gated using untreated cells to determine %QD585+ or %GFP+ (**Supplemental Figure 3.9**). All experiments were performed in at least biological triplicate and variance is reported as the standard deviation of the mean.

3.2.7 *Polyplex unpackaging assays*

VIPER or bPEI polyplexes were formulated with pLuciferase at N/P 10 and incubated in the presence of various concentrations of heparan sulfate or chondroitin sulfate sodium salt (Sigma) for 30 min at 37 °C. Samples were then loaded onto a 0.5% agarose gel containing TAE buffer (40 µmM tris-acetate, 1 mM EDTA) and 0.5 µg/mL ethidium bromide, and were electrophoresed at 110 V for 30 min before imaging on a UV transilluminator.

3.2.8 *Statistical analysis*

All statistical analyses were performed in Prism software (Graph Pad Software, La Jolla, CA) using a two-tailed Student's t- test with unequal variance and Welch's correction.

3.3 RESULTS AND DISCUSSION

3.3.1 *Luciferase transfection in the brain following controlled cortical impact (CCI)*

We first investigated whether overall intraventricular polyplex transfection efficiency was altered by CCI. We hypothesized that the length of time between injury and transfection could dramatically alter transfection efficiency due to both physical changes in brain anatomy that evolve with the primary and secondary injury over time (e.g. edema, inflammation)[3,30] and due to increased mitosis among the neuroprogenitor cells (NPCs) of the subventricular zone (SVZ).[11] It has been reported that SVZ NPC proliferation is enhanced as soon as 1 day post injury (DPI) and peaks sometime between 3 and 7 DPI in various rodent models of TBI.[11,13,31,32] Because nuclear uptake and expression of plasmid DNA often depends on mitosis,[33] we hypothesized that timing transfection to coincide with peak SVZ NPC proliferation would maximize transfection efficiency and eventually therapeutic benefit. Thus, we performed CCI and then intraventricular transfection of luciferase plasmid ipsilateral to the injury at various DPI, followed by harvest and *in vitro* luciferase detection in brain lysates 48 h after transfection. (**Figure 3.1**)
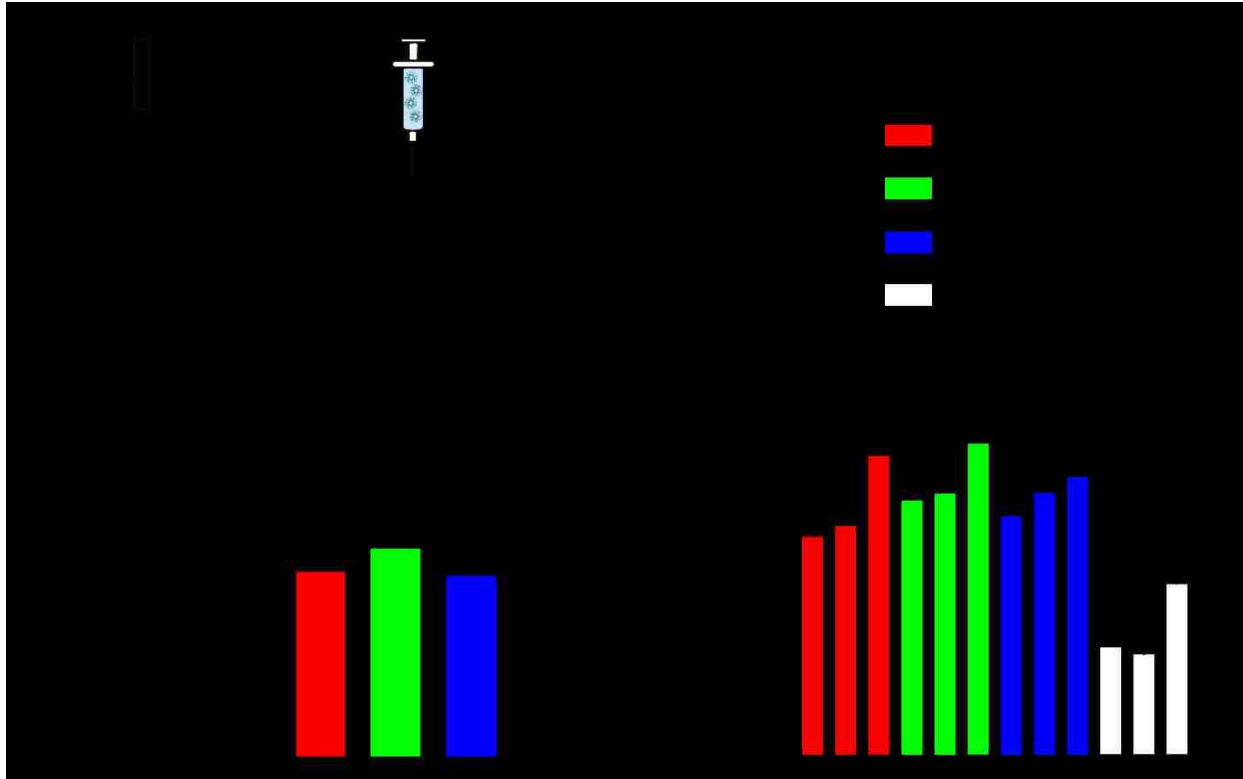
Figure 3.1 Transfection efficiency of polyplexes injected intraventricularly at various time points after CCI.
Relative luciferase activity in homogenized brains displayed as a sum of all brain regions (A) and by brain compartment (B). Data are plotted as mean $\pm$ SD where N = 3-4 mice. (* $p < 0.05$)

We observed that CCI increased subsequent transfection at all time points tested relative to transfection in uninjured mice. (**Figure 3.1A**) Although increases in transfection efficiency were not statistically significantly different between groups, we did observe a trend of increasing transfection with increased time post injury that peaked at 3 DPI, in agreement with past studies identifying this time point at the peak of SVZ proliferation.[32] The relative distribution of transfection among brain compartments was not altered by TBI, with the lowest transfection observed in the left brain (contralateral to injection) and the highest transfection observed in the hind brain in all groups. (**Figure 3.1B**) This is in agreement with our past data from uninjured mice,[18] and is likely a result of polyplex drainage into the fourth ventricle via the flow of cerebral

spinal fluid (CSF).[34–36] Thus, CCI does not dramatically alter intraventricular transfection, and may even potentiate transfection if performed 3 DPI.

3.3.2 *Distribution of GFP transfection by anatomical location and cell type*

Encouraged by these results, we next sought to determine whether CCI influences the cell types that are transfected in specific anatomical locations in the brain. Thus, we performed intraventricular delivery of polyplexes in both injured and uninjured mice using a plasmid encoding GFP, chased transfection with an intraperitoneal injection of EdU to metabolically label mitotic cells, and processed brains for confocal microscopy 48 h after transfection. (**Figure 3.2**) As we observed in the luciferase study that intraventricular transfections were poorly tolerated at 7 DPI, we only moved forward with comparisons between mice transfected without injury or at 1 or 3 DPI. Transfection among EdU+ dividing cells of the SVZ was not drastically altered by injury, and was (in all groups) less frequent than in previous studies by our group with other polymers.[17] (**Figure 3.2A-C**)
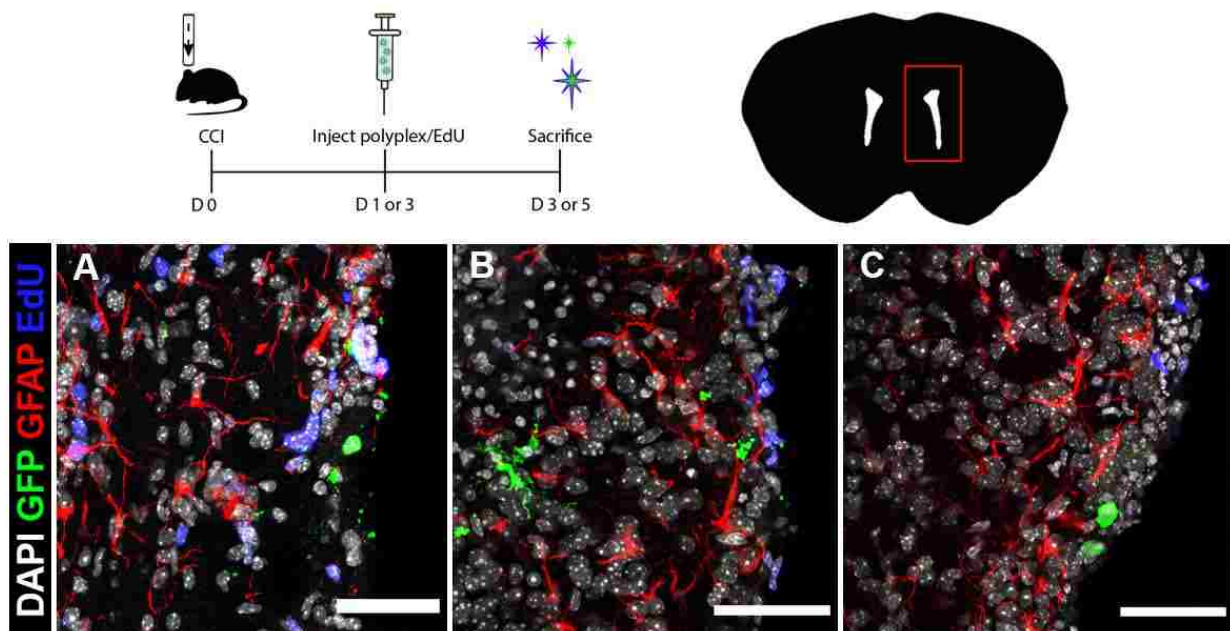
Figure 3.2 Immunohistochemistry and EdU click-labeling reveal that CCI does not dramatically change proliferation or transfection in the SVZ.
Confocal micrographs of the SVZ region following transfection with plasmid encoding GFP and fluorescent staining for GFAP and EdU. Mice were transfected without injury (A), 1 DPI (B), or 3 DPI (C), EdU was administered IP 8 h after transfection, and mice were sacrificed and perfused 48 h after transfection. Images are representative of results from N = 4 mice per group. Scale bar = 50 µm.

In qualitative agreement with luciferase transfection data, we observed slightly more GFP+ cells in mice transfected 3 DPI than in mice transfected 1 DPI or without injury, with the greatest frequency of transfection observed in the fimbria and at the base of the hippocampus within 1 mm of the injury on the rostral-caudal axis independent of injury. (**Figure 3.3**, **Supplemental Figure 3.7**) Almost all transfected cell were found at interfaces of tissue and CSF (e.g. hippocampus and striatum; fimbria and ventricle), indicating that polyplexes did not penetrate tissue but were instead disseminated by CSF flow to various ventricle-facing surfaces. Indeed, relatively little transfection was observed rostral to the injection site compared to transfection observed in regions caudal to the injection, echoing distribution patterns identified by luciferase transfection and underlining the impact of CSF circulation. Other groups have reported similarly narrow distribution near CSF interfaces for both cationic and neutrally charged nanoparticles with diameters ~100 nm, indicating that both surface charge and size can limit nanoparticle penetration through brain tissue following direct intrathecal or intraventricular injection.[37–40]

We observed heterogeneous transfection of various cell types dependent on the region investigated but independent of injury. For example, we observed transfection of morphologically complex cells resembling oligodendrocytes in the fimbria in all mice (**Figure 3.3A**) but were unable to identify the cells that were consistently transfected at the base of the hippocampus (**Figure 3.3B**). Although we did observe transfection of some GFAP+ astrocytes, in no cases were transfected

cells Iba1+ microglia. (**Supplemental Figure 3.8**) In summary, although the rate of transfection was much lower than we expected, we observed that only specific anatomical regions of the brain are transfected following intraventricular injection and that CCI does increase the number of cells transfected in these regions.
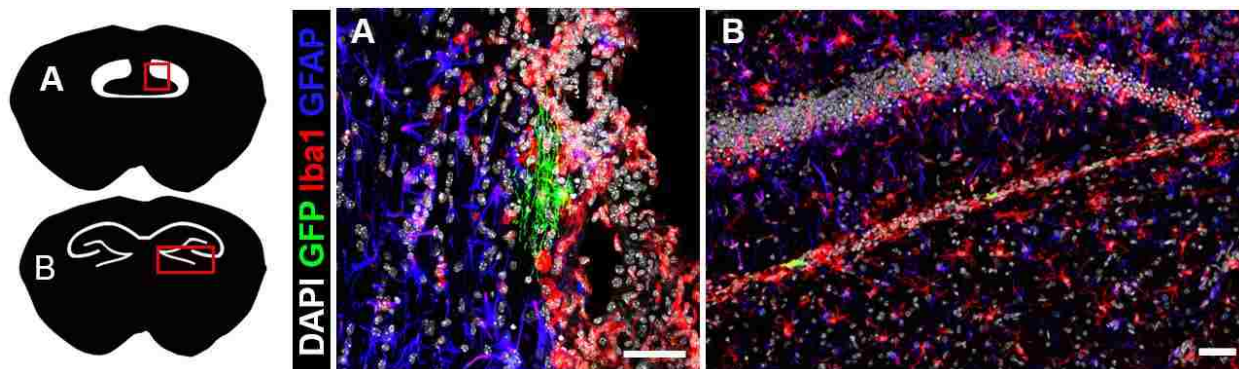
Figure 3.3 Transfection observed primarily in specific anatomic regions of CSF-tissue interfaces. Confocal micrographs of the fimbria (A) and the base of the hippocampus (B) following transfection 3 DPI with plasmid encoding GFP and fluorescent staining for GFAP and Iba1. Scale bar = 50 µm.

3.3.3 *Quantum dot labeling reveals extracellular barriers to plasmid uptake*

Drawing on our experience investigating extracellular barriers to gene delivery following intravenous injection, we hypothesized that poor cellular uptake or premature polyplex unpackaging could also limit transfection in the ventricular space. We have previously shown that some cationic polymers will forgo the condensation of plasmid DNA in favor of electrostatic interactions with negatively charged extracellular matrix (ECM) components (e.g. glycosaminoglycans), thereby releasing unpackaged DNA outside the cell, coating the cell surface with polymer, and ultimately achieving very little intracellular plasmid uptake.[29] Fluorescent labeling of plasmids with a small number of ultra-bright quantum dots (QDs) enables the detection of individual plasmids delivered by polyplexes *in vivo* without drastically altering polyplex properties.[41] We transfected QD-plasmid conjugates in healthy mice to better characterize the

localization of plasmid cargo following intraventricular polyplex injection. We observed identical patterns in plasmid uptake as observed in GFP transfection, with most QD-plasmid found in the fimbria. (**Figure 3.4**)
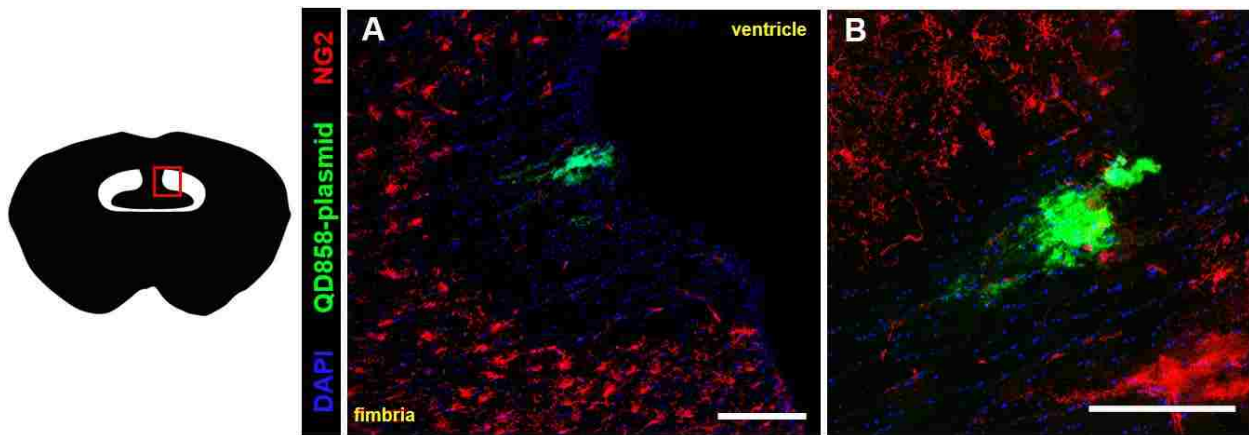
Figure 3.4 Plasmid delivery patterns mimic regional patterns of transfection and are driven by electrostatic interactions with sulfated proteoglycans.
Confocal micrographs at low (A) and high (B) magnification of the fimbria following transfection with QD585-conjugated luciferase plasmid and fluorescent staining for NG2 chondroitin sulfate proteoglycan. Scale bar = 200 µm.

Interestingly, all tissue within a ~200 µm radius of QD-plasmid displayed very little immunofluorescent staining for NG2, an extracellular chondroitin sulfate proteoglycan that is ubiquitously expressed throughout the brain and upregulated following TBI.[42] As there is still some, but limited, NG2 staining in the tissue proximal to the plasmid, we hypothesize that this "blast radius" could be the result of electrostatic coating of sulfated glycosaminoglycan domains with VIPER chains that prevents antibody staining. We previously observed that fluorescently-labeled polyethylenimine binds to liver ECM after systemic administration.[29] Taken together, these observations strongly suggest that VIPER's transfection is limited by premature polyplex unpackaging through electrostatic interactions with ECM components in neural tissue.

3.3.4 *Plasmid transfection and uptake in ECM mutant cell lines*

In order to better understand which ECM components VIPER interacts with, we next performed *in vitro* GFP plasmid transfection in several mammalian cell lines with mutations in various glycosaminoglycan (GAG) synthetic pathways. We selected the Chinese hamster ovary (CHO) K1 cell line derivative pgsE-606, which carries mutations in N-sulfotransferase that decrease the degree of GAG sulfation 3-5 fold, and the CHO pgsA-745 line, which carries a mutation in xylosyltransferase that completely eliminates GAG synthesis.[43,44] We transfected K1 wildtype (wt), pgsE-606, and pgsA-745 CHO cells with pMAX-GFP/VIPER polyplexes at N/P 5 in serum containing media and quantified the percentage of viable cells that were GFP+ by flow cytometry two days after transfection. Our results show that VIPER transfects wt and pgsE-606 cells with similar efficiency at N/P 5 (36% vs 46% GFP+), and that this efficiency is significantly decreased in pgsA-745 cells (3% GFP+). (**Figure 3.5A**)

To determine whether transfection efficiency was dictated by plasmid uptake, we next performed mock-transfections using polyplexes formulated with QD585-pLuciferase and quantified intracellular QD585+ signal using flow cytometry at various time points. (**Figure 3.5B**) Plasmid uptake increased with polyplex incubation time for all cell types, but while wt and pgsE-606 cells demonstrated near total uptake at 4 h (72% and 76%, respectively), only a small fraction of pgsA-745 cells contained plasmid even after 8 h incubation (17%). Moreover, the overall shift in QD585 median fluorescence intensity (MFI) from 0-8 h was significantly lower in pgsA-745 cells (6.3-fold) compared to wt and pgsE-606 cells (16.5- and 20.5-fold, respectively), indicating that the total number of plasmids taken up by pgsA-745 cells was low. (**Figure 3.5C**; **Supplemental Figure 3.9**) These data demonstrate that VIPER polyplex uptake is enhanced by electrostatic

proteoglycan interactions at the cell surface and that polyplex uptake efficiency dictates transgene expression. Furthermore, we suggest that VIPER polyplexes may also be attracted to unproductive proteoglycan interactions with GAG-rich ECM that could hamper CNS tissue penetrance *in vivo*.
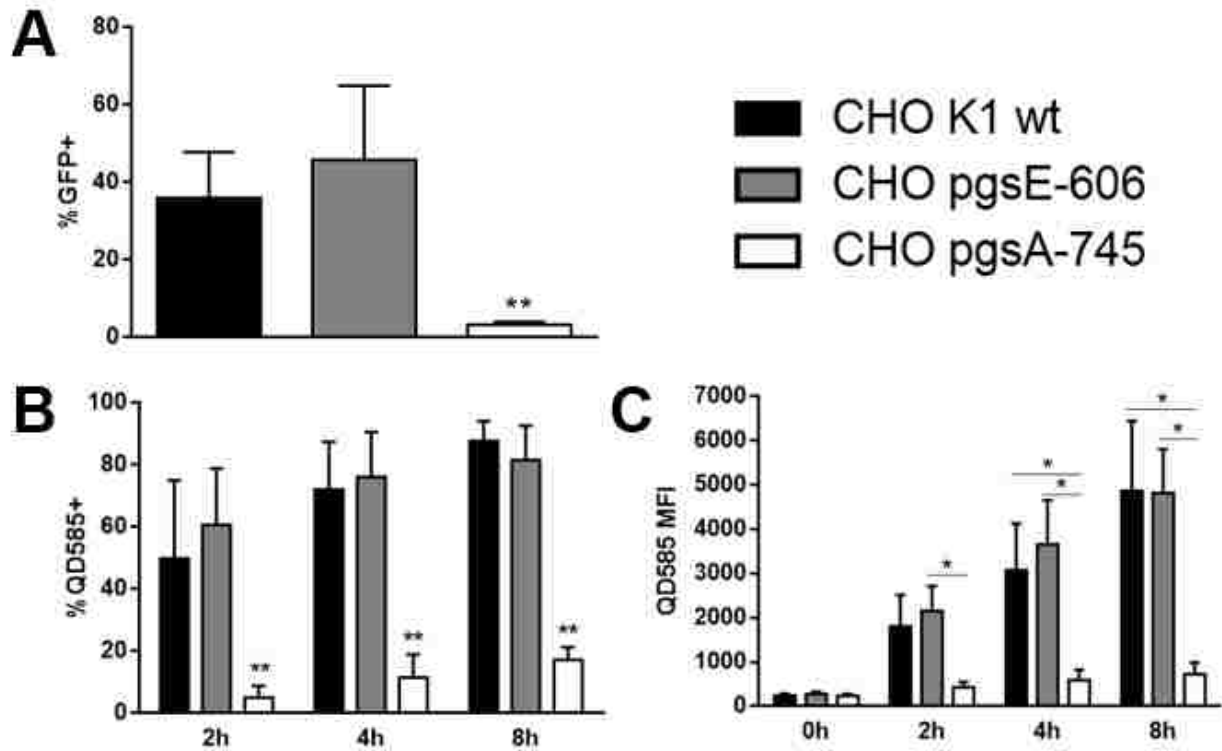
Figure 3.5 *In vitro* plasmid transfection and uptake in GAG mutant CHO cell lines.
Flow cytometry was used to quantify GFP+ cells 48 h after pMAX-GFP polyplex addition (A) or to quantify the percentage of QD585+ cells at various times after QD585-pLuciferase polyplex addition (B). The average median fluorescent intensity (MFI) of QD585 signal in single cells increased with uptake over time (C). Data are plotted as the mean ± SD of ≥ 3 experiments and statistical significance derived from Student's t-test (* $p < 0.05$; ** $p < 0.01$).

The charge density, pKa, and molecular weight of both GAGs and polycations are known to have differentially positive and negative effects on polyplex transfection.[46–48] As demonstrated by previous studies, GAGs are required for polyplex uptake,[47] yet heparin sulfate proteoglycan can lead to premature polyplex unpackaging by out-competing DNA binding with polycations.[46,48] In this study, we observed a drastic reduction of VIPER uptake and transfection in GAG deficient cells, but transfection and uptake are not adversely affected in pgsE-606 cells lacking proteoglycan

sulfation. In order to determine if sulfate interactions could lead to polyplex unpackaging, we incubated VIPER or bPEI polyplexes (N/P 10) with varying concentrations of either heparan sulfate or chondroitin sulfate. (**Supplemental Figure 3.10**) While neither VIPER nor bPEI polyplexes were unpackaged by chondroitin sulfate (5 mg/mL), both VIPER and bPEI polyplexes were unpackaged at 100 µg/mL heparan sulfate, which corroborates prior experiments that demonstrated charge density may differentiate GAG-polyplex interactions.[46] Taken together with *in vivo* NG2 staining (**Figure 3.4**) and *in vitro* transfection data (**Figure 3.5**), these results indicate that VIPER requires GAGs for transfection, but that the highly GAG-rich ECM of neural tissue may limit VIPER penetration or cause unpackaging *in vivo*. Future work will be needed to determine which GAG interactions dominate VIPER transfection *in vivo*, and whether polycations with different amine fucntional groups (i.e. primary or secondary amines)[49] or charge densities[50] would better suited for CNS transfection.

3.4   CONCLUSION

Herein we present the first investigation of intraventricular polyplex transfection following controlled cortical impact in mice. Using a custom polymer we previously reported to yield high luciferase plasmid expression in the brain, we show that CCI slightly increases overall transfection efficiency and that the distribution of transfection throughout the major compartments of the brain is unaffected by CCI, but polyplexes do not penetrate deep into brain tissue. We demonstrate that this pattern of distribution is not dependent on injury but may be a direct result of interactions between VIPER and ECM proteoglycans. Given that chondroitin sulfate proteoglycan upregulation has been implicated as a potential therapeutic target in TBI, this work motivates future polymer designs that can take advantage of charge-charge interactions for polyplex targeting

without sacrificing plasmid uptake, perhaps by increasing polycation charge density or altering polycation pKa. In summary, we report that polyplex-mediated plasmid transfection is largely unaffected by CCI in mice but that extracellular barriers to delivery must be accounted for in order to transfect therapeutically relevant numbers of cells in the intraventricular space.

3.5 SUPPLEMENTAL INFORMATION

Supplemental Figure 3.6 Controlled Cortical Impact (CCI) induces blood-brain barrier (BBB) disruption and peripheral immune invasion.
CCI is performed with constant velocity and consistent displacement using an OSU impactor. In the top panels, immunohistochemistry shows that albumin extravasation increases with time post-injury (PI), confirming BBB disruption that mimics secondary injury in human TBI. In the bottom panels, H&E staining shows transient infiltration of the primary injury by inflammatory peripheral immune cells at 30 min PI that begins to contract as soon as 4 hr PI, behavior also consistent with human TBI.
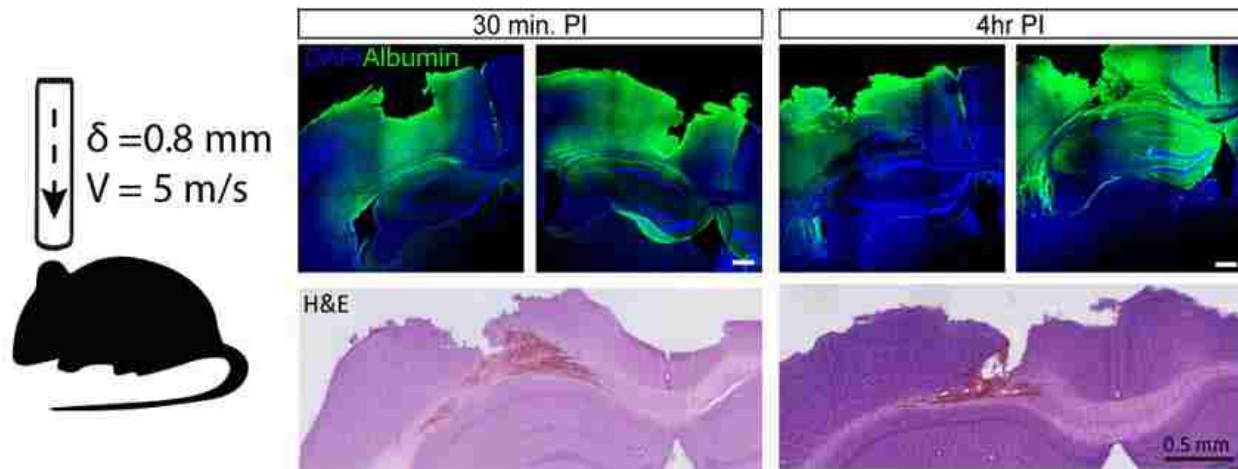
Supplemental Figure 3.7 Transfection primarily found at the interface of hippocampus and striatum in 3 DPI mice.
Scale bar = 100 µm.
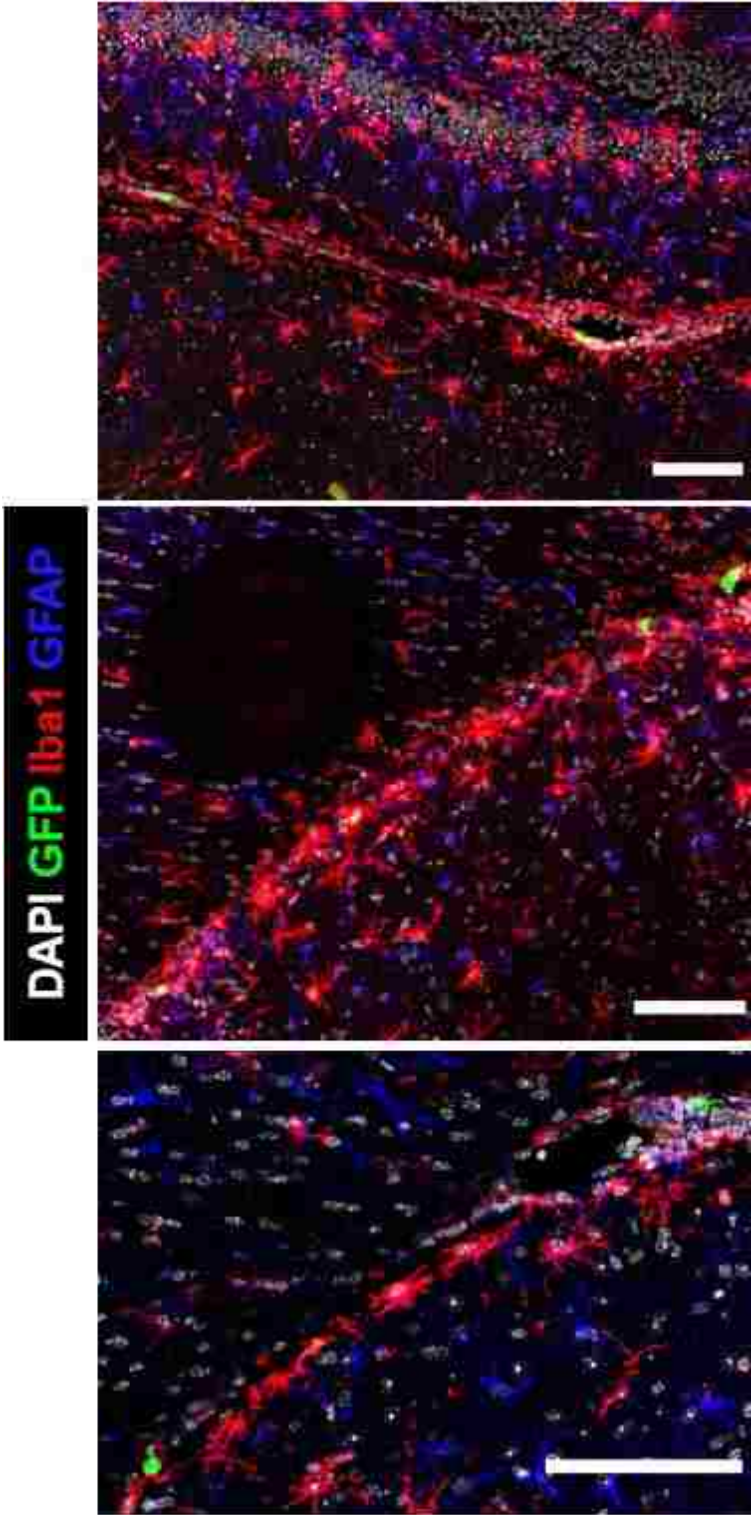
Supplemental Figure 3.8 Transfected cells were never Iba1+ but some GFAP+ cells were observed.
Scale bar = 25 µm.
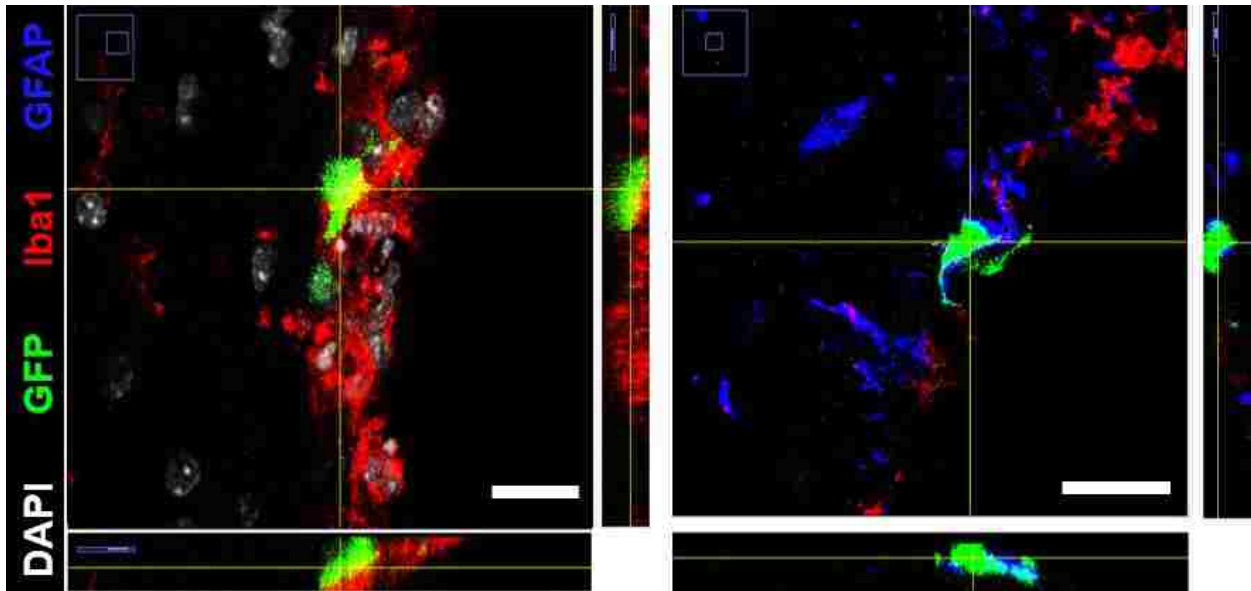
Supplemental Figure 3.9 Representative flow cytometry histograms of VIPER/QD585-plasmid polyplex uptake.
VIPER polyplexes were prepared at N/P 5 with 1 µg QD585-pLuciferase and incubated with various CHO cell lines for either 2, 4, or 8 h. Cells were washed twice with PBS before being lifted for analysis by flow cytometry. Singlet cell event QD585 signal is shown below.

Sample Name	QDot585+ :: Freq. of Paren	Median : VL3-A
A0h1.fcs	0.21	191
A2h1.fcs	78.2	2395
A4h1.fcs	90.8	3965
A8h1.fcs	94.9	5600

Sample Name	QDot585+ :: Freq. of Paren	Median : VL3-A
B0h1.fcs	0.085	230
B2h1.fcs	81.0	2678
B4h1.fcs	90.8	4602
B8h1.fcs	91.7	5872

Sample Name	QDot585+ :: Freq. of Paren	Median : VL3-A
C0h1.fcs	0.072	189
C2h1.fcs	5.31	408
C4h1.fcs	10.5	505
C8h1.fcs	18.4	596
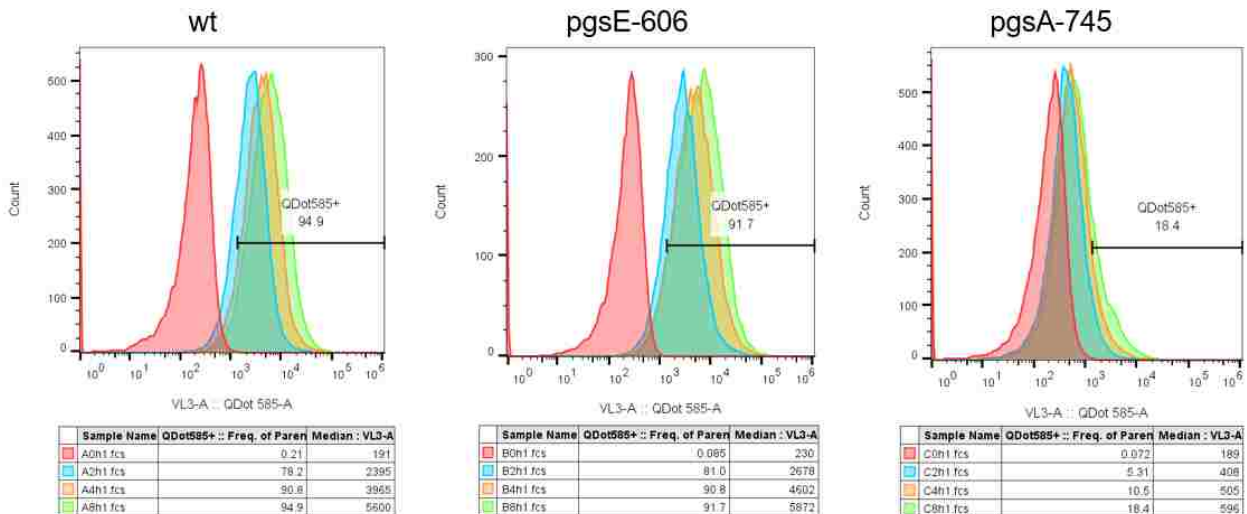
Supplemental Figure 3.10 Polyplex unpackaging by various sulfated ECM components. VIPER or bPEI polyplexes were formulated with pLuciferase at N/P 10 and incubated in the presence of various concentrations of heparan sulfate or chondroitin sulfate sodium salt for 30 min at 37 °C. Samples were then loaded onto a 0.5% agarose gel containing TAE buffer and ethidium bromide, and were electrophoresed at 110 V for 30 min before imaging on a UV transilluminator.
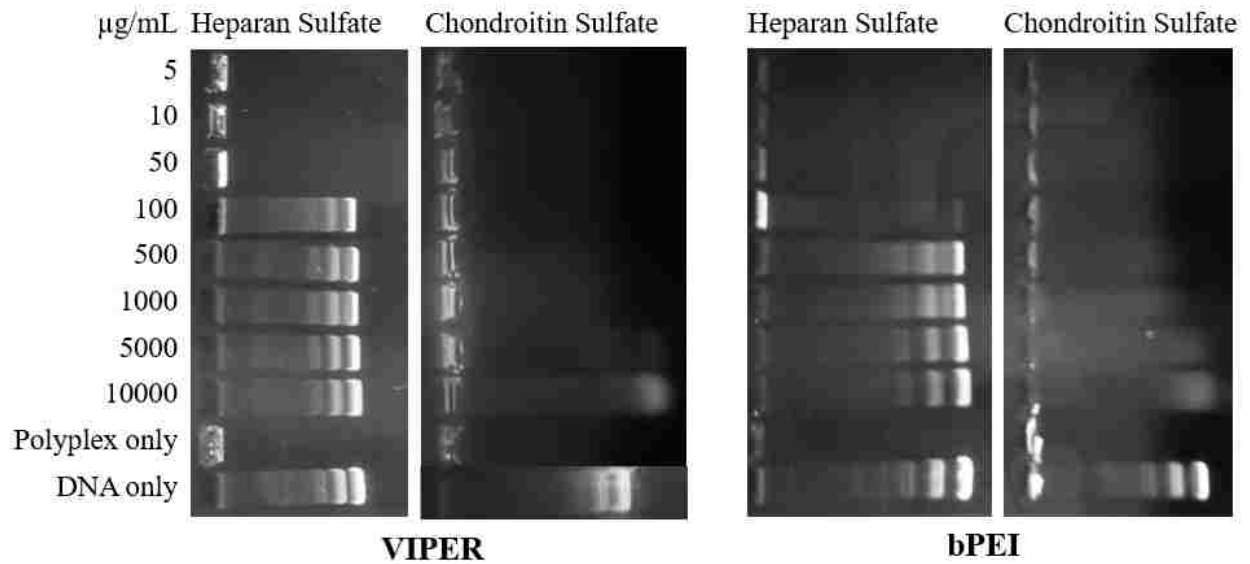
BIBLIOGRAPHY

(1)   J.D. Corrigan, TBI at the Centers for Disease Control and Prevention, J. Head Trauma Rehabil. 30 (2015) 147. doi:10.1097/HTR.0000000000000157.

[2]   D.J. Thurman, The epidemiology of traumatic brain injury in children and youths: A review of research since 1990, J. Child Neurol. 31 (2016) 20–27. doi:10.1177/0883073814544363.

[3]   R.M. Chesnut, R.M. Chesnut, L.F. Marshall, M.R. Klauber, B.A. Blunt, N. Baldwin, H.M. Eisenberg, J.A. Jane, A. Marmarou, M.A. Foulkes, The role of secondary brain injury in determining outcome from severe head injury, J. Trauma - Inj. Infect. Crit. Care. 34 (1993) 216. doi:10.1097/00005373-199302000-00006.

[4]   J. Lu, K.W. Gary, J.P. Neimeier, J. Ward, K.L. Lapane, Randomized controlled trials in adult traumatic brain injury, Brain Inj. 26 (2012) 1523–1548. doi:10.3109/02699052.2012.722257.

[5]   T. Savio, M.E. Schwab, Rat CNS white matter, but not gray matter, is nonpermissive for neuronal cell adhesion and fiber outgrowth., J. Neurosci. 9 (1989) 1126–33. http://www.ncbi.nlm.nih.gov/pubmed/2467969 (accessed November 6, 2018).

[6]   Z. Wang, Y. Luo, L. Chen, W. Liang, Safety of neural stem cell transplantation in patients with severe traumatic brain injury., Exp. Ther. Med. 13 (2017) 3613–3618. doi:10.3892/etm.2017.4423.

[7]   J. Larouche, C.A. Aguilar, New Technologies To Enhance In Vivo Reprogramming for Regenerative Medicine, Trends Biotechnol. (2018). doi:10.1016/j.tibtech.2018.11.003.

[8]   S. Gascón, G. Masserdotti, G.L. Russo, M. Götz, Direct Neuronal Reprogramming: Achievements, Hurdles, and New Roads to Success, Cell Stem Cell. 21 (2017) 18–34. doi:10.1016/j.stem.2017.06.011.

[9]   C. Heinrich, F.M. Spagnoli, B. Berninger, In vivo reprogramming for tissue repair, Nat Cell Biol. 17 (2015) 204–211. http://dx.doi.org/10.1038/ncb3108.

[10]   R.A. Barker, M. Götz, M. Parmar, New approaches for brain repair - from rescue to reprogramming, Nature. 557 (2018) 329–334. doi:10.1038/s41586-018-0087-1.

[11]   S. Chirumamilla, D. Sun, M.R. Bullock, R.J. Colello, Traumatic Brain Injury Induced Cell Proliferation in the Adult Mammalian Central Nervous System, J. Neurotrauma. 19 (2002) 693–703. doi:10.1089/08977150260139084.

[12]   G.E. Goings, V. Sahni, F.G. Szele, Migration patterns of subventricular zone cells in adult mice change after cerebral cortex injury, Brain Res. 996 (2004) 213–226. doi:10.1016/j.brainres.2003.10.034.

[13]   B. Saha, S. Peron, K. Murray, M. Jaber, A. Gaillard, Cortical lesion stimulates adult subventricular zone neural progenitor cell proliferation and migration to the site of injury, Stem Cell Res. 11 (2013) 965–977. doi:10.1016/j.scr.2013.06.006.

[14]   W. Zheng, Q. ZhuGe, M. Zhong, G. Chen, B. Shao, H. Wang, X. Mao, L. Xie, K. Jin, Neurogenesis in adult human brain after traumatic brain injury., J. Neurotrauma. 30 (2013) 1872–80. doi:10.1089/neu.2010.1579.

[15]   C.A. Blaiss, T.-S. Yu, G. Zhang, J. Chen, G. Dimchev, L.F. Parada, C.M. Powell, S.G. Kernie, Temporally specified genetic ablation of neurogenesis impairs cognitive recovery after traumatic brain injury., J. Neurosci. 31 (2011) 4906–16. doi:10.1523/JNEUROSCI.5265-10.2011.

[16]   K.W.A. Bang, S. Gasco, C.M. Morshead, A. Nagy, K.W.A. Bang, C.M. Morshead, A.

Nagy, Adult Neural Stem Cells from the Subventricular Zone Give Rise to Reactive Astrocytes in the Cortex after Stroke, Cell Stem Cell. (2015). doi:10.1016/j.stem.2015.08.002.

[17]   S. Peron, L.M. Miyakoshi, M.S. Brill, F. Ortega, M. Karow, S. Gascon, B. Berninger, Programming of neural progenitors of the adult subependymal zone towards a glutamatergic identity by neurogenin2, BioRxiv. (2017) 171686. doi:10.1101/171686.

[18]   I. Lostalé-seijo, J. Montenegro, Synthetic materials at the forefront of gene delivery, Nat. Rev. Chem. 2 (2018). doi:10.1038/s41570-018-0039-1.

[19]   L. Peng, E. Wagner, Polymeric Carriers for Nucleic Acid Delivery: Current Designs and Future Directions, Biomacromolecules. 20 (2019) 3613–3626. doi:10.1021/acs.biomac.9b00999.

[20]   J.-K.Y. Tan, B. Pham, Y. Zong, C. Perez, D.O. Maris, A. Hemphill, C. Miao, T.J. Matula, P.D. Mourad, H. Wei, D.L. Sellers, P.J. Horner, S.H. Pun, Microbubbles and ultrasound increase intraventricular polyplex gene transfer to the brain, J. Control. Release. (2016). doi:10.1016/j.jconrel.2016.02.003.

[21]   D.J. Peeler, S.N. Thai, Y. Cheng, P.J. Horner, D.L. Sellers, S.H. Pun, pH-sensitive polymer micelles provide selective and potentiated lytic capacity to venom peptides for effective intracellular delivery, Biomaterials. 192 (2019) 235–244. doi:10.1016/J.BIOMATERIALS.2018.11.004.

[22]   Y. Cheng, R.C. Yumul, S.H. Pun, Virus-Inspired Polymer for Efficient In Vitro and In Vivo Gene Delivery, Angew. Chemie - Int. Ed. 55 (2016) 12013–12017. doi:10.1002/anie.201605958.

[23]   Y.P. Zhang, J. Cai, L.B.E. Shields, N. Liu, X.M. Xu, C.B. Shields, Traumatic Brain Injury Using Mouse Models, Transl. Stroke Res. 5 (2014) 454–471. doi:10.1007/s12975-014-0327-0.

[24]   Y. Xiong, A. Mahmood, M. Chopp, Animal models of traumatic brain injury, Nat. Rev. Neurosci. 14 (2013) 128–42. doi:10.1038/nrn3407.

[25]   L.B. Jakeman, D.M. McTigue, P. Walters, B.T. Stokes, The Ohio state university ESCID spinal cord contusion model, in: Anim. Model. Acute Neurol. Inj., Humana Press, Totowa, NJ, 2009: pp. 433–447. doi:10.1007/978-1-60327-185-1_37.

[26]   M. Ghorbani, P. Shahabi, A. Ebrahimi-Kalan, H. Soltani-Zangbar, J. Mahmoudi, S. Bani, B. Sadeghzadeh-Oskouei, Y. Rafiee-Byraami, O. Salimi, Induction of traumatic brain and spinal cord injury models in rat using a modified impactor device, Physiol. Pharmacol. 22 (2018) 228–239. http://ppj.phypha.ir/article-1-1410-en.html&sw=Induction+of+Traumatic+Brain+and+Spinal+Cord+Injury+Models+in+Rat+Using+A+Modified+Impactor+Device (accessed October 4, 2019).

[27]   S. Zhang, L. Kojic, M. Tsang, P. Grewal, J. Liu, D. Namjoshi, C.L. Wellington, W. Tetzlaff, M.S. Cynader, W. Jia, Distinct roles for metalloproteinases during traumatic brain injury, Neurochem. Int. 96 (2016) 46–55. doi:10.1016/j.neuint.2016.02.013.

[28]   J.R. Basford, L.-S. Chou, K.R. Kaufman, R.H. Brey, A. Walker, J.F. Malec, A.M. Moessner, A.W. Brown, An assessment of gait and balance deficits after traumatic brain injury, Arch. Phys. Med. Rehabil. 84 (2003) 343–349. doi:10.1053/apmr.2003.50034.

[29]   Y. Cheng, H. Wei, J.Y. Tan, D.J. Peeler, D.O. Maris, D.L. Sellers, P.J. Horner, S.H. Pun, Nano-Sized Sunflower Polycations As Effective Gene Transfer Vehicles, Small. (2016) 1–9. doi:10.1002/smll.201502930.

[30]   A. Salic, T.J. Mitchison, A chemical method for fast and sensitive detection of DNA

synthesis in vivo., Proc. Natl. Acad. Sci. U. S. A. 105 (2008) 2415–2420. doi:10.1073/pnas.0712168105.

[31]   R.S. Burke, S.H. Pun, Extracellular barriers to in vivo PEI and PEGylated PEI polyplex-mediated gene delivery to the liver, Bioconjug. Chem. 19 (2008) 693–704. doi:10.1021/bc700388u.

[32]   M.C. Morganti-Kossmann, M. Rancan, P.F. Stahel, T. Kossmann, Inflammatory response in acute traumatic brain injury: a double-edged sword, Curr. Opin. Crit. Care. 1 (2002). doi:10.1073/pnas.1011199107.

[33]   S. Ramaswamy, G.E. Goings, K.E. Soderstrom, F.G. Szele, D.A. Kozlowski, Cellular proliferation and migration following a controlled cortical impact in the mouse, Brain Res. 1053 (2005) 38–53. doi:10.1016/j.brainres.2005.06.042.

[34]   B.D. White, R.J. Nathe, D.O. Maris, N.K. Nguyen, J.M. Goodson, R.T. Moon, P.J. Horner, β-catenin signaling increases in proliferating NG21 progenitors and astrocytes during post-traumatic gliogenesis in the adult brain, Stem Cells. 28 (2010) 297–307. doi:10.1002/stem.268.

[35]   D.J. Peeler, D.L. Sellers, S.H. Pun, pH-sensitive polymers as dynamic mediators of barriers to nucleic acid delivery, Bioconjug. Chem. (2018).

[36]   J. Casaca-Carreira, Y. Temel, S.-A. Hescham, A. Jahanshahi, Transependymal Cerebrospinal Fluid Flow: Opportunity for Drug Delivery?, Mol. Neurobiol. (2017). doi:10.1007/s12035-017-0501-y.

[37]   B. Bedussi, M.G.J.T.B. van Lier, J.W. Bartstra, J. de Vos, M. Siebes, E. VanBavel, E.N.T.P. Bakker, Clearance from the mouse brain by convection of interstitial fluid towards the ventricular system., Fluids Barriers CNS. 12 (2015) 23. doi:10.1186/s12987-015-0019-5.

[38]   T. Brinker, E. Stopa, J. Morrison, P. Klinge, A new look at cerebrospinal fluid circulation., Fluids Barriers CNS. 11 (2014) 10. doi:10.1186/2045-8118-11-10.

[39]   H.P. Song, J.Y. Yang, S.L. Lo, Y. Wang, W.M. Fan, X.S. Tang, J.M. Xue, S. Wang, Gene transfer using self-assembled ternary complexes of cationic magnetic nanoparticles, plasmid DNA and cell-penetrating tat peptide, Biomaterials. 31 (2010) 769–778. doi:10.1016/j.biomaterials.2009.09.085.

[40]   C. Helmschrodt, S. Höbel, S. Schöniger, A. Bauer, J. Bonicelli, M. Gringmuth, S.A. Fietz, A. Aigner, A. Richter, F. Richter, Polyethylenimine Nanoparticle-Mediated siRNA Delivery to Reduce α-Synuclein Expression in a Model of Parkinson's Disease, Mol. Ther. - Nucleic Acids. 9 (2017) 57–68. doi:10.1016/j.omtn.2017.08.013.

[41]   K.T. Householder, S. Dharmaraj, D.I. Sandberg, R.J. Wechsler-Reya, R.W. Sirianni, Fate of nanoparticles in the central nervous system after intrathecal injection in healthy mice, Sci. Rep. 9 (2019). doi:10.1038/s41598-019-49028-w.

[42]   J.A. Varela, J.P. Dupuis, L. Etchepare, A. Espana, L. Cognet, L. Groc, Targeting neurotransmitter receptors with nanoparticles in vivo allows single-molecule tracking in acute brain slices, Nat. Commun. 7 (2016). doi:10.1038/ncomms10947.

[43]   Y.-P. Ho, H.H. Chen, K.W. Leong, T.-H. Wang, Evaluating the intracellular stability and unpacking of DNA nanocomplexes by quantum dots-FRET, J. Control. Release. 116 (2006) 83–89. doi:10.1016/j.jconrel.2006.09.005.

[44]   J.D. Esko, T.E. Stewart, W.H. Taylor, Animal cell mutants defective in glycosaminoglycan biosynthesis., Proc. Natl. Acad. Sci. 82 (1985) 3197–3201. doi:10.1073/pnas.82.10.3197.

[45]   K.J. Bame, J.D. Esko, Undersulfated heparan sulfate in a Chinese hamster ovary cell mutant defective in heparan sulfate N-sulfotransferase., J. Biol. Chem. 264 (1989) 8059–65. http://www.ncbi.nlm.nih.gov/pubmed/2524478 (accessed October 7, 2019).

[46]   M. Ruponen, S. Ylä-Herttuala, A. Urtti, Interactions of polymeric and liposomal gene delivery systems with extracellular glycosaminoglycans: Physicochemical and transfection studies, Biochim. Biophys. Acta - Biomembr. 1415 (1999) 331–341. doi:10.1016/S0005-2736(98)00199-0.

[47]   K.A. Mislick, J.D. Baldeschwieler, Evidence for the role of proteoglycans in cation-mediated gene transfer, Proc. Natl. Acad. Sci. U. S. A. 93 (1996) 12349–12354. doi:10.1073/pnas.93.22.12349.

[48]   Y. Xu, F.C. Szoka, Mechanism of DNA release from cationic liposome/DNA complexes used in cell transfection, Biochemistry. 35 (1996) 5616–5623. doi:10.1021/bi9602019.

[49]   P.M. Carlson, J.G. Schellinger, J. a Pahang, R.N. Johnson, S.H. Pun, Comparative Study of guanidine-based and lysine-based brush copolymers for plasmid delivery, Biomater. Sci. (2013) 736–744. doi:10.1039/c3bm60079c.

[50]   H. Wei, L.R. Volpatti, D.L. Sellers, D.O. Maris, I.W. Andrews, A.S. Hemphill, L.W. Chan, D.S.H. Chu, P.J. Horner, S.H. Pun, Dual responsive, stabilized nanoparticles for efficient in vivo plasmid delivery, Angew. Chemie - Int. Ed. 52 (2013) 5377–5381. doi:10.1002/anie.201301896.

Chapter 4. TRANSPLANTATION OF ENGINEERED NEURAL PROGENITOR CELLS TO REPAIR TRAUMATIC BRAIN INJURY

Abstract

Transplantation of engineered stem cells has emerged over the past few decades as one of the most promising avenues towards therapeutic regeneration of central nervous system function after traumatic injury.[1–5] Thus far, induced neurons (iN) have been derived from three main transplant sources: neural, embryonic, or induced pluripotent stem cells.[6–9] These studies have demonstrated that stem cells can be programmed by transcription factors to induce neurogenesis in the injured brain; however, strategies to ensure proper function and nerve-circuit repair are needed to advance these potential therapies into reliable regenerative medicines. We seek to generate new neurons in the traumatically injured mouse cortex through transplantation of neural progenitor cells (NPCs) transduced with neuronal-fate biasing transcription factor lentivirus *ex vivo*. We hypothesize that constitutive Neurogenin-2 (Ngn2) signaling in transplanted NPCs will result in improved motor function as a result of limited glial and improved neural differentiation relative to cells expressing cell-cycle dependent Ngn2 or non-programmed, naïve NPCs. In this chapter, we present preliminary data comparing the *in vitro* and *in vivo* differentiation capacity of Ngn2-programmed and naïve NPCs. We report that constitutive Ngn2 programming imbues NPCs with a resistance to glial differentiation *in vitro* and increases neuronal morphological phenotypes in cells transplanted to mice with traumatic brain injury. We conclude with a plan for future investigations of NPC fate *in vivo*, as well as strategies that could improve NPC survival and neuroregeneration.

4.1   RESEARCH APPROACH AND RATIONALE

Human neural stem cell (NSC) transplants have already demonstrated improved neurological function in humans with severe TBI[10] and spinal cord injury (SCI)[11] and are being evaluated in ongoing clinical trials (e.g. NCT03296618). However, the relative therapeutic importance of neuronal differentiation and the derivation of specific cellular subtypes (versus the secretion of paracrine neurotrophic factors, etc.) is not well characterized. This is in part because the specification of a particular cell fate in a particular brain circuit requires a balance between extrinsic (i.e. environmental) and intrinsic (i.e. genetic) factors that are unique to the development of that region.[12] For example, the inflammatory milieu of the injured CNS environment directs transplanted naïve embryonic stem cells to become scar tissue;[8] conversely, iN that are fully differentiated *ex vivo* into a single subtype are unable to integrate into local circuits upon transplantation.[13] Thus, there remains a need for transplant studies that 1) balance intrinsic and extrinsic differentiation signals and 2) correlate differentiated cellular subtypes with functional recovery. We have therefore chosen to investigate the differentiation of transplanted neural progenitor cells (NPCs) that have been transduced with lentivirus encoding a neuron-specifying transcription factor but cultured in proliferation media until time of transplant.

We have chosen to employ ectopic expression of neurogenin-2 (Ngn2), a pioneer transcription factor that has been used for direct neuronal conversion of fibroblasts *in vitro* and reactive astrocytes *in vivo,* as well as the differentiation of various transplanted stem cells *in vivo*.[14–20] Thus far, only one study has tested Ngn2-programmed NPCs for the repair of traumatic injury in the CNS.[21] The authors showed that NPC Ngn2 expression increased functional recovery after traumatic SCI as result of limited glial differentiation, enhanced myelination, and increased neuronal differentiation. We hypothesize that Ngn2-programmed NPCs will similarly resist

inflammation-induced glial differentiation bias when transplanted into the traumatically injured brain, leading to greater neuronal differentiation and improved recovery of neural function compared to non-programmed naïve NPCs. A previously reported phosphorylation-incompetent mutant of Ngn2 remains constitutively activated despite cell cycling (Ngn2^{S9A}), altering NPC glial differentiation potential and neuronal subtype specification.[22] We have therefore transduced murine NPCs to express either Ngn2^{wt} or Ngn2^{S9A} for comparison to naïve, non-programmed NPCs, and further hypothesize that Ngn2^{S9A} cells will yield the greatest therapeutic benefit. Herein, we first compare the differentiation status of these three NPC cell lines under various culture conditions *in vitro* and then report preliminary observations of NPC survival following transplant into the dentate gyrus of CCI-injured mice. We propose future work to quantify differentiation of these cells and ultimately compare the motor function recovery of injured animals through various behavioral assessments. Finally, we suggest a few strategies to improve NPC survival and differentiation following transplantation.

4.2 PRELIMINARY DATA

4.2.1 *Primary NPC isolation, culture, and transduction*

Primary neural progenitor cells (NPCs) were isolated from dissociated adult Ai14 mouse (Gt(ROSA)26Sor$^{tm14(CAG-tdTomato)Hze}$/J) brain tissue and cultured in proliferative media as previously described.[23] Cells were transduced with neomycin-resistant retrovirus encoding Cre and grown under G418 selection to generate polyclonal populations of fluorescently labeled naïve NPCs. Cells were separately transduced with lentivirus encoding Ngn2^{wt}-T2A-Cre or Ngn2^{S9A}-T2A-Cre and sorted with FACS to generate polyclonal populations of tdTomato-labeled Ngn2 NPCs, which were expanded and cryopreserved for future use. All cultures were utilized for *in vitro* differentiation or *in vivo* transplant before passage 20.

94

4.2.2 In vitro *characterization of NPC differentiation potential*

We hypothesized that intrinsic Ngn2-programming might confer resistance to extrinsic glial differentiation signals and/or enhance response to extrinsic neurogenic signals. Thus, NPC culture conditions were crafted *in vitro* to institute neurogenic (NPC growth media + 1X B27 + 20 ng/mL BDNF + 20 ng/mL NGF + 10 ng/mL FGF2) or gliogenic (NPC growth media + 10% FBS) differentiation bias in NPCs cultured for 14 days in glass chamber slides. NPC fate choices were evaluated through immunocytochemistry for GFAP and Tuj1 with imaging performed at 20X magnification on an epifluorescence microscope.

As shown in **Figure 4.1** below, we observed that naïve NPCs differentiated into mixed GFAP+/Tuj1+ populations under neurogenic conditions, whereas both Ngn2-programmed NPCs yielded highly pure Tuj1+ neuronal cultures almost entirely devoid of GFAP staining. Moreover, Ngn2^{S9A} NPCs qualitatively appeared to possess characteristics of more fuller neuronal differentiation compared to Ngn2^{wt} NPCs, including longer neuronal processes with more branching and more intense Tuj1 staining.[16] Ongoing work seeks to quantify Tuj1+ neurite length and complexity under these differentiation conditions through image analysis. When cultured in gliogenic media, naïve NPCs became morphologically flat and wide, upregulated GFAP, and downregulated Tuj1 as expected of cells committing to astrocytic fate. Some cells in both Ngn2-programmed NPC cultures also adopted astrocytic morphology and stained GFAP+; however, most cells retained intense Tuj1 expression and extended a small number of Tuj1+ processes that appear more like neurites in morphology. No apparent difference between Ngn2^{wt} and Ngn2^{S9A} NPCs was discernible, although more characterization could reveal differences in cell identity. Thus, Ngn2-programming enhances resistance to gliogenic cues, as reported,[21] and enhances

commitment to neuronal differentiation. Although programming with Ngn2[S9A] seems to provide more complete neuronal maturation than Ngn2[wt], more work is required to both qualitatively and quantitatively assess these differences.
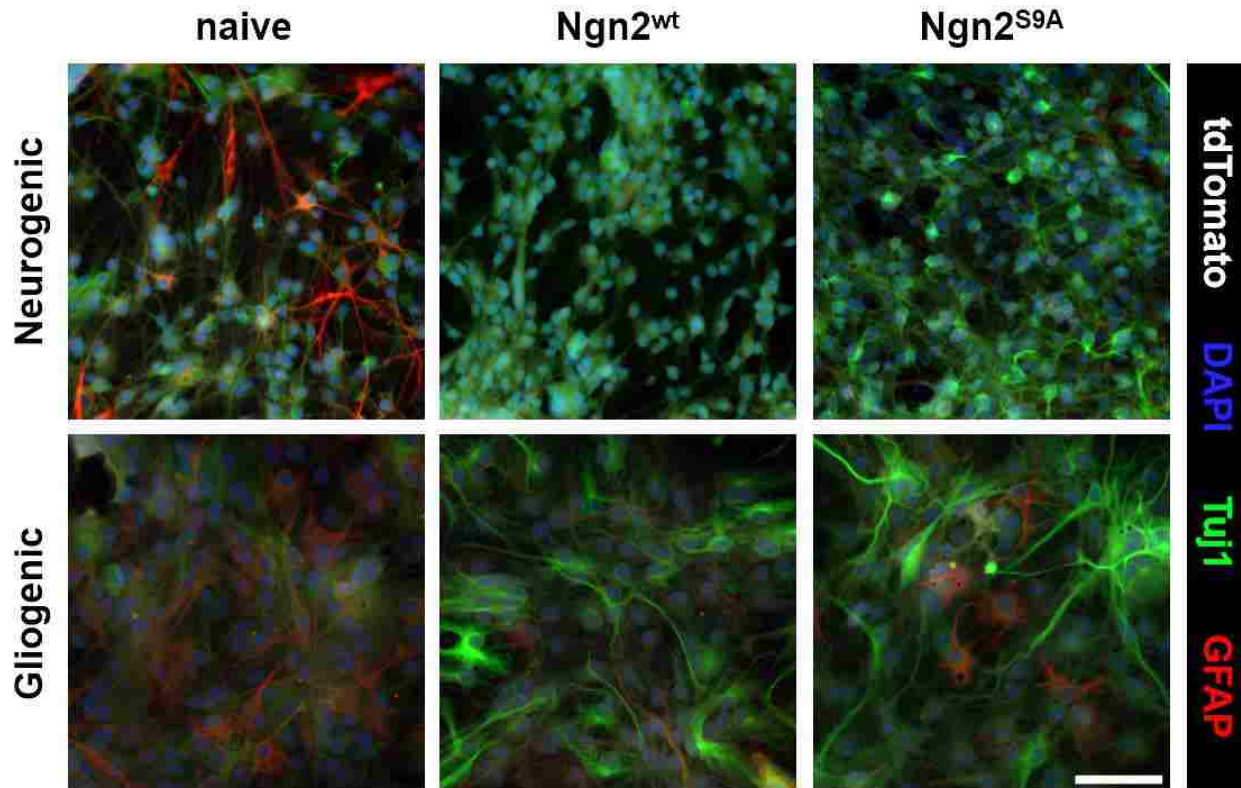
Figure 4.1 *In vitro* differentiation of naïve, wt, and S9A NPCs in neurogenic (top row) or gliogenic (bottom row) media.
Scale bar = 100 µm

4.2.3 *Transplant survival in CCI mice*

Having demonstrated variations in differentiation potential *in vitro*, we sought to compare the survival and differentiation status of various NPCs in the brains of traumatically injured mice. Controlled cortical impact (CCI) was performed on 8 wk old female C57Bl/6 mice as described in **Chapter 3.2.2**. Three days after injury, NPCs were lifted from culture and resuspended in ice cold HBSS supplemented with 5 mM EDTA (to prevent aggregation) and 5% glucose (to enhance survival) at a concentration of 1-6 x10^5 viable NPCs/µL and injected slowly (2 µL at 1 µL/min) 1

mm below the initial impact depth (1.8 mm ventral). The needle was allowed to rest for 5 min before removal and the wound closed with gel foam as before. Cell viability among was confirmed to be >90% at the beginning and end of the procedure using trypan blue staining. Uninjured mice were also given transplants so that neuronal differentiation and viability may be quantified in the absence of confounding hostile environment. (N = 5 mice per treatment; N = 30 total) Mice were sacrificed 4 weeks after injury and brains processed into floating sections for antibody staining as described in **Chapter 3.2.4**. Alternating tissue sections of a 1:6 series of the brain were imaged with epifluorescent microscopy in order to quantify NPC survival.

We observed that overall Ngn2^{wt} NPC survival was significantly lower than that of both naïve and Ngn2^{S9A} NPCs. (**Figure 4.2**) However, due to variation in injected concentration of NPCs, percent survival was not significantly different between any group. These approximations of survival, although not fully quantitative due to a lack of stereological projection software, indicate lower overall survival compared to other transplant studies in moderate-to-severe TBI even though our injection parameters and cellular dosage are very similar (~2-5% injected dose regardless of programming).[6,7,9,24–26] By binning NPC counts by hippocampal anatomical region, we also determined that programming with Ngn2 does not have a major effect on the rostral-caudal NPC migration or distribution away from the injection site. (**Figure 4.3**)
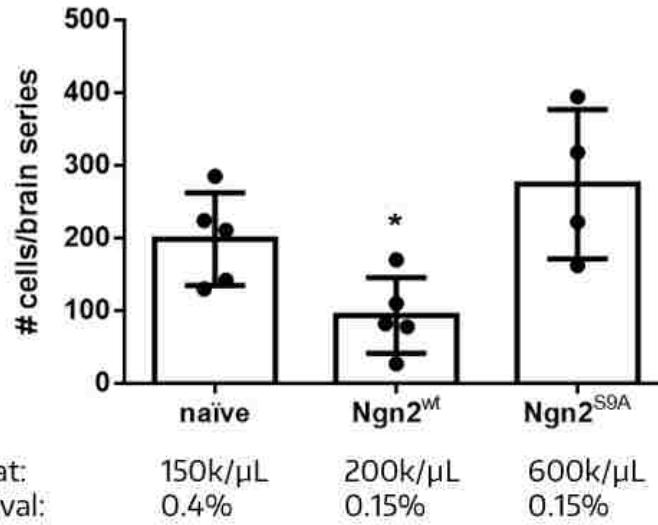
Figure 4.2 Survival of various NPCs transplanted in CCI injured mice
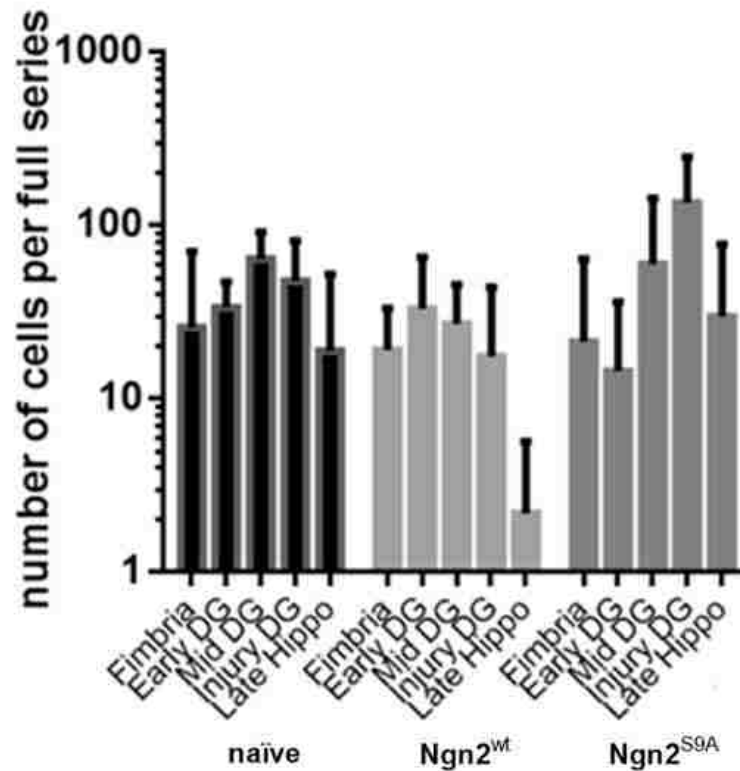
Figure 4.3 Distribution of transplanted NPCs along the rostral-caudal axis near the injection site. tdTomato+ NPC counts were binned at 0.5 mm intervals throughout the hippocampus. DG = dentate gyrus; Hippo = hippocampus.

We observed that, regardless of programming, surviving NPCs mainly engrafted at regional interfaces between the dentate gyrus (DG) of the hippocampus and either the white matter tract above the DG, the ventricle lateral to the DG, or the posterior nuclei below the DG. (**Figure 4.4A-C**) To a lesser degree, all NPC types also demonstrated some promising engraftment within and extension of processes throughout the granule cell layer of the DG. (**Figure 4.4D**) Unfortunately, surviving Ngn2^{S9A} NPCs in this area were often found on the edge of a clumps of dead cells due to high cell concentration during injection. (**Figure 4.4E**) Several Ngn2^{S9A} transplants displayed engraftment along the needle track (which passes through the injury site) and at the site of injury itself. (**Figure 4.5**) In summary, our preliminary survey of NPCs transplanted in CCI brains reveals that overall survival and location of engraftment does not vary greatly between naïve and Ngn2-programmed cells, and that engraftment largely occurs in and around the DG with some cells found along the needle track and in the site of CCI.
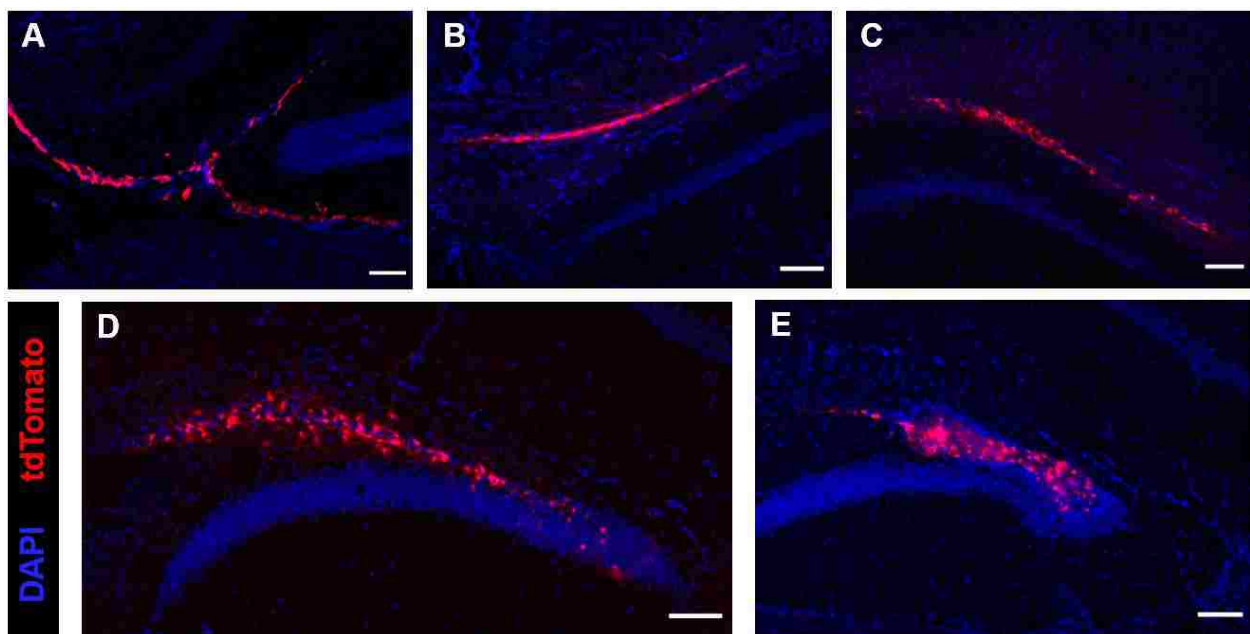
Figure 4.4 Anatomical distribution of transplanted NPCs does not depend on programming. Naïve (A), Ngn2^{wt} (B) and Ngn2^{S9A} (C) NPCs found at the interface of the DG with other tissues. Naïve NPC integration (D) and Ngn2^{S9A} NPC death (E) in the DG. Scale bar = 100 um.
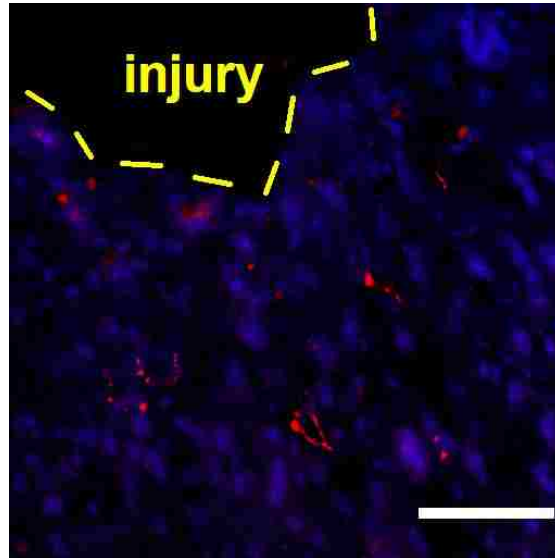
Figure 4.5 Ngn2^{S9A} NPCs found in proximity of injury.
Blue = DAPI; Red = tdTomato; Scale bar = 100 um.

4.3   FUTURE DIRECTIONS

4.3.1   *Quantification of transplant differentiation through immunohistochemistry*

Methods: In order to investigate whether Ngn2-programming restricts glial fate and enhanced neural fate commitment of transplanted NPCs, tissue sections were also immunostained for neuronal (Tuj1) or astrocyte (GFAP) markers in alternate tissue series derived from the study described in **Section 4.2.3**. Work is ongoing to quantify the co-localization of these stains with reporter cell tdTomato through confocal microscopy. We propose that quantification of neuronal Nissl bodies through cresyl violet staining may also provide useful metrics for evaluating the extent of neural tissue loss and repair generated by the various treatments in future work. Taken together, these experiments should determine whether Ngn2^{wt} or Ngn2^{S9A} NPCs should be compared to naïve NPCs in the behavioral studies described later.

Expected outcomes: We expect that mice treated with Ngn2[S9A] NPCs will display the highest percentage of neuronally differentiated cell types (tdTomato+/Tuj1+ cells) due to their constitutive expression of active Ngn2[7,22] and that mice treated with naïve NPCs will display the highest percentage of glial differentiated cell types (tdTomato+/GFAP+) due to their lack of programming and the influence of the injury environment.[12,25] Animals receiving Ngn2 NPCs may or may not demonstrate more neuronal tissue sparing than animals receiving naïve NPCs as indicated by an increase in the number of cresyl violet labeled Nissl bodies in the region surrounding the CCI impact. Through this experiment, we will identify the transplant treatment that provides the greatest overall neuronal differentiation and survival so that we can compare the behavioral recovery achieved by this treatment to *in vivo* reprogramming in later aims.

Potential pitfalls: The specific analyses we have chosen may fail to detect differences between treatment groups. For example, if all transplanted NPCs have differentiated to an extent that Tuj1 staining is detectable, we may instead quantify the extent of neuronal differentiation by staining for NeuN, a marker that is expressed later in neuronal differentiation than Tuj1. Additional stains to visualize neural progenitor marker Sox2 or proliferation marker Ki67 may provide insight into variations of transplant "stemness" as an alternative to evaluations of differentiation. Furthermore, it has been shown Ngn2-transduced NSCs transplanted into the injured spinal cord primarily generated oligodendroglial cells with limited neuronal differentiation, a phenomena attributed to the gliogenic cues in the injury environment.[21] In keeping with prior demonstrations that Ngn2 suppresses astrocyte fate commitment,[27] animals receiving Ngn2-NSCs in this study also displayed significantly reduced GFAP expression and improved motor function compared to animals receiving naïve NSCs.[21] Thus, if little Tuj1 or NeuN expression is observed in transplanted cells,

reduced GFAP expression and increased NG2 expression compared to naïve cells may be considered an alternative route to future success in functional recovery experiments.

4.3.2 *Behavioral studies to assess transplant impact on motor function*

Although the clinical etiology of TBI is extremely diverse and patient outcomes are notoriously difficult to predict, acute locomotor functional assessments have been clinically validated (in addition to neurocognitive measures) as predictors of long term vocational outcomes in TBI patients.[28,29] Importantly, CCI leads to quantifiable cognitive and motor deficits in mice that mimic acute symptoms experienced by human TBI patients.[30] Thus, much preclinical research on regenerative therapies has focused on demonstrating improved performance in a variety of motor function tests that are performed during the first month after injury.[25,31–36] We hypothesize that transplant of Ngn2 NPCs will enhance neurogenesis in the injured mouse motor cortex and result in recovery of motor function after injury. To evaluate this hypothesis, we will assess changes in gross and fine motor function following injury and treatment using rotarod and CatWalk tests, respectively. In addition, we will analyze tissue generated in this study with histology in order to correlate the generation of specific cell types with any behavioral changes observed.

Strategy: In order to understand the therapeutic impact of neurogenesis, injuries will be performed on 8 wk old female mice as previously described and transplants will be given at optimized times post-injury. In addition, EdU will be injected on days 0-7 post-injury in order to facilitate detection of all cells generated in the acute injury phase. Neuromotor functional testing will be performed in the Mouse Behavior Laboratory of the UW Center on Human Development and Disability Animal Behavior Core as described below. Study design is summarized in **Figure**

4.6 below. Injured mice receiving Ngn2-programmed NPCs will be compared to injured mice receiving either a naïve NPCs or no treatment (N = 10 each; N = 30 total).
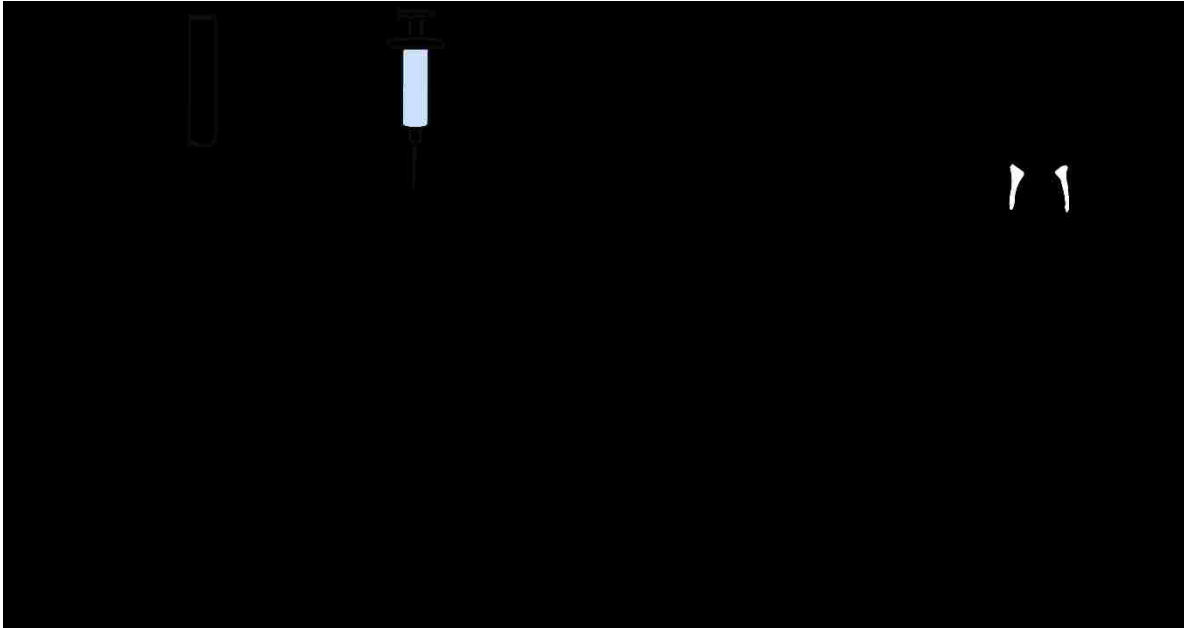
Figure 4.6 Experimental timeline of training, injury, treatment, and data collection. (CCI = Controlled cortical impact; RR = Rotarod; CW = CatWalk)

CatWalk: The CatWalk gait analysis system (Noldus Information Technology) quantifies a broad range of clinically relevant locomotion parameters in an unbiased fashion.[34–36] Briefly, as animals cross a glass walkway, light shining through the glass illuminates paw contact with the surface for video recording of footprints. Three days prior to injury, animals will be trained to cross the walkway and baseline data collected. Data will then be collected on the days 3, 7, 14, and 28 post-injury (on days coinciding with treatment, data will be collected prior to surgery). During each session, each animal will be required to cross 3 times without pausing and averages of these 3 trials will be used for data analysis of each timepoint. After processing videos with Noldus CatWalk software, we will quantify the following parameters: step sequence pattern regularity index, print area, maximum contact area, base of support, stride length, and limb swing duration.

Rotarod: The rotarod apparatus (Columbus Instruments, Columbus, OH) will be used to measure motor coordination and balance.[25,31–33] In this test, mice are placed on a 36-mm diameter rod with a rubber surface which is then rotated at one of two different rotational accelerations (slow or fast). The time it takes the mouse to fall off or grip and rotate with the rotarod during acceleration is recorded. For slow acceleration, the device is accelerated from 1 rpm to 18 rpm over 90 s, with each trial lasting a maximum of 120 s. For fast acceleration, the device is accelerated from 1 rpm to 30 rpm over 90 s, with each trial again lasting a maximum of 120 s.[31,33] Mice receive four training trials per day with a 2 min inter-trial interval for 3 consecutive days leading up to injury to obtain baseline performance data. Data will then be collected on the days 3, 7, 14, and 28 post-injury (on days coinciding with treatment, data will be collected prior to surgery). On testing days, each mouse will receive three trials at each rotational acceleration. The mean latency to fall off the rotarod at each acceleration will be recorded and reported as a percent of that individual's baseline latency in subsequent analysis.

Histology: Sections will be stained to identify reporter cells as astrocytes (GFAP), glial progenitor cells (NG2), immature or mature neurons (Tuj1 or NeuN), and oligodendrocytes (CNPase). Chemical EdU labeling will be performed to detect cells born during the first week of injury.

Expected outcomes: We predict that Ngn2 expression will suppress astrocytic fate and generate new neurons in the injured somatosensory cortex that will result in observable improvement in motor function. We expect that latency to recovery will vary between tests, even in mice receiving no therapy, as shown in previous work.[37–39] For example, data collected during CatWalk testing is

expected to show that TBI significantly affects fine motor coordination in terms of forepaw usage (intensity, maximal area), temporal parameters (swing duration, stance, stride length) and velocity related parameters (cadence, walk speed, swing speed).[34–36] Pronounced deficits in these functions in injured mice are especially likely at early timepoints (3, 7 dpi); however, statistical significance may not be reached at later timepoints (14, 28 dpi) due to natural recovery of fine motor function in the CCI model.[32] In contrast, we expect that performance in the Rotarod test will reveal a significant loss of gross motor ability in injured mice compared with baseline at all timepoints post-injury.[25,31–33] Thus, while our measurement of fine motor coordination offers a highly sensitive, unbiased indicator of recovery, we may find that differences in gross motor function are more dramatic between treated and untreated animals.

Finally, we expect that the histological outcomes of this study will support findings from previous aims—that forced Ngn2 expression increases neuronal markers and decreases glial markers in programmed NPC progeny.[27,40] Importantly, we will be able to draw correlations between newly generated cellular phenotypes and recovery of locomotor function as in previous work with Ngn2-programmed human embryonic stem cells in spinal cord injury.[7] We expect that animals displaying a larger percentage of neuronally differentiated NPCs (Tuj1 or NeuN) will demonstrate better recovery than animals with NPC fates skewed towards glial subtypes (GFAP, NG2, CNPase).

Potential pitfalls and alternative approaches: Although most previously cited studies conclude at one month post-injury, the time course planned may not be long enough to observe substantial differences in functional outcomes between treated animals and/or untreated animals. If recovery of neither gross nor fine motor function has occurred by 28 dpi, we may extend observation of

animals for an additional 2 weeks before sacrifice. If significant differences are not observed between treatments in these evaluations of motor function, cognitive testing such as the adhesive removal test[33] or Morris Water Maze may provide more obvious differences in future studies.[42]

Lastly, our assumptions about which cellular phenotypes will correlate with recovery may not hold true. Although we hypothesize that recovery will be contingent on neurogenesis at the injury site, enhanced generation of oligodendrocytes or NG2 glial progenitors may also contribute to recovery through myelination and tissue sparing.[38,39,43] Ngn2 therapy may contribute to this mechanism of recovery by suppressing astrocyte fate commitment, which has been shown to permit more NG2 glia to form.[21] Moreover, even if we do enhance neurogenesis, it may not be therapeutic, which will manifest as a lack of change in motor function or even a decline in function. If we see a decline in function, new neurons may have formed a neuronal subtype that disrupts the cortical circuitry or formed inappropriate connections.[44]

4.3.3 *Strategies to enhance NPC survival and differentiation*

Although several studies beyond our own have conducted transplants 2 or 3 days post-injury (DPI),[6,45] delaying cell delivery may improve engraftment. Other groups have demonstrated that transplantation between 2–7 DPI is optimal[25] in part because the injury cavity may be more stable and hospitable for transplants 7 DPI.[7,26,46] By 7 DPI, peak toxicity due to necrotic cell death[47,48] and inflammation[49] have passed, thus potentially aiding transplant survival. Systemic administration of anti-inflammatory drugs[50,51], or encapsulation of NPCs within bio-derived matrices displaying growth or differentiation cues on hydrogels composed of laminin/collagen,[26] chondroitin sulfate,[6] or hyaluronic acid[52–55] may also allow for more permissive engraftment.

BIBLIOGRAPHY

(1)   Goldman, S. Stem and Progenitor Cell-Based Therapy of the Human Central Nervous System. *Nat. Biotechnol.* **2005**, *23* (7), 862–871.

(2)   Goldman, S. A. Stem and Progenitor Cell-Based Therapy of the Central Nervous System: Hopes, Hype, and Wishful Thinking. *Cell Stem Cell* **2016**, *18* (2), 174–188.

(3)   Kim, J.; Schafer, J.; Ming, G. New Directions in Neuroregeneration. *Expert Opin. Biol. Ther.* **2006**, *6* (8), 735–738.

(4)   Lu, J.; Gary, K. W.; Neimeier, J. P.; Ward, J.; Lapane, K. L. Randomized Controlled Trials in Adult Traumatic Brain Injury. *Brain Injury*. December 19, 2012, pp 1523–1548.

(5)   Xiong, Y.; Mahmood, A.; Chopp, M. Emerging Treatments for Traumatic Brain Injury. *Expert Opin. Emerg. Drugs* **2009**, *14* (1), 67–84.

(6)   Betancur, M. I.; Mason, H. D.; Alvarado-Velez, M.; Holmes, P. V; Bellamkonda, R. V; Karumbaiah, L. Chondroitin Sulfate Glycosaminoglycan Matrices Promote Neural Stem Cell Maintenance and Neuroprotection Post-Traumatic Brain Injury. *ACS Biomater. Sci. Eng.* **2017**, *3* (3), 420–430.

(7)   Perrin, F. E.; Boniface, G.; Serguera, C.; Lonjon, N.; Serre, A.; Prieto, M.; Mallet, J.; Privat, A. Grafted Human Embryonic Progenitors Expressing Neurogenin-2 Stimulate Axonal Sprouting and Improve Motor Recovery after Severe Spinal Cord Injury. *PLoS One* **2010**, *5* (12).

(8)   Falkner, S.; Grade, S.; Dimou, L.; Conzelmann, K.-K.; Bonhoeffer, T.; Götz, M.; Hübener, M. Transplanted Embryonic Neurons Integrate into Adult Neocortical Circuits. *Nature* **2016**.

(9)   Carlson, A. L.; Bennett, N. K.; Francis, N. L.; Halikere, A.; Clarke, S.; Moore, J. C.; Hart, R. P.; Paradiso, K.; Wernig, M.; Kohn, J.; et al. Generation and Transplantation of Reprogrammed Human Neurons in the Brain Using 3D Microtopographic Scaffolds. *Nat Commun* **2016**, *7*.

(10)   Wang, Z.; Luo, Y.; Chen, L.; Liang, W. Safety of Neural Stem Cell Transplantation in Patients with Severe Traumatic Brain Injury. *Exp. Ther. Med.* **2017**, *13* (6), 3613–3618.

(11)   Curtis, E.; Martin, J. R.; Gabel, B.; Sidhu, N.; Rzesiewicz, T. K.; Mandeville, R.; Van Gorp, S.; Leerink, M.; Tadokoro, T.; Marsala, S.; et al. A First-in-Human, Phase I Study of Neural Stem Cell Transplantation for Chronic Spinal Cord Injury. *Cell Stem Cell* **2018**, *22* (6), 941-950.e6.

(12)   Grande, A.; Sumiyoshi, K.; Lopez-Juarez, A.; Howard, J.; Sakthivel, B.; Aronow, B.; Campbell, K.; Nakafuku, M. Environmental Impact on Direct Neuronal Reprogramming in Vivo in the Adult Brain. *Nat. Commun.* **2013**, *4*, 2373.

(13)   Steinbeck, J. A.; Studer, L. Moving Stem Cells to the Clinic: Potential and Limitations for Brain Repair. *Neuron* **2015**, *86* (1), 187–206.

(14)   Heinrich, C.; Blum, R.; Gascón, S.; Masserdotti, G.; Tripathi, P.; Sánchez, R.; Tiedt, S.; Schroeder, T.; Götz, M.; Berninger, B. Directing Astroglia from the Cerebral Cortex into Subtype Specific Functional Neurons. *PLoS Biol.* **2010**, *8* (5).

(15)   Chen, X.; Lepier, A.; Berninger, B.; Tolkovsky, A. M.; Herbert, J. Cultured Subventricular Zone Progenitor Cells Transduced with Neurogenin-2 Become Mature Glutamatergic Neurons and Integrate into the Dentate Gyrus. *PLoS One* **2012**, *7* (2), e31547.

(16)   Zhang, Y.; Pak, C.; Han, Y.; Ahlenius, H.; Zhang, Z.; Chanda, S.; Marro, S.; Patzke, C.;

Acuna, C.; Covy, J.; et al. Rapid Single-Step Induction of Functional Neurons from Human Pluripotent Stem Cells. *Neuron* **2013**, *78* (5), 785–798.

(17) Su, Z.; Niu, W.; Liu, M.-L.; Zou, Y.; Zhang, C.-L. In Vivo Conversion of Astrocytes to Neurons in the Injured Adult Spinal Cord. *Nat. Commun.* **2014**, *5*, 3338.

(18) Smith, D. K.; Yang, J.; Liu, M.-L.; Zhang, C.-L. Small Molecules Modulate Chromatin Accessibility to Promote NEUROG2-Mediated Fibroblast-to-Neuron Reprogramming. *Stem Cell Reports* **2016**.

(19) Dai, X.; Lu, X.; Cheng, F.; Hao, H.; Qian, T.; Yu, W.; Tang, L.; Li, L. Neurogenin 2 Enhances the Neuronal Differentiation of Skin-Derived Precursors. *Int. J. Neurosci.* **2014**, *7454* (December), 1–24.

(20) Liu, M.-L.; Zang, T.; Zou, Y.; Chang, J. C.; Gibson, J. R.; Huber, K. M.; Zhang, C.-L. Small Molecules Enable Neurogenin 2 to Efficiently Convert Human Fibroblasts into Cholinergic Neurons. *Nat. Commun.* **2013**, *4* (May), 2183.

(21) Hofstetter, C. P.; Holmström, N. A. V.; Lilja, J. A.; Schweinhardt, P.; Hao, J.; Spenger, C.; Wiesenfeld-Hallin, Z.; Kurpad, S. N.; Frisén, J.; Olson, L. Allodynia Limits the Usefulness of Intraspinal Neural Stem Cell Grafts; Directed Differentiation Improves Outcome. *Nat. Neurosci.* **2005**, *8* (3), 346–353.

(22) Ali, F.; Hindley, C.; McDowell, G.; Deibler, R.; Jones, A.; Kirschner, M.; Guillemot, F.; Philpott, A. Cell Cycle-Regulated Multi-Site Phosphorylation of Neurogenin 2 Coordinates Cell Cycling with Differentiation during Neurogenesis. *Dev.* **2011**, *138* (19), 4267–4277.

(23) Reynolds, B. A.; Weiss, S. Generation of Neurons and Astrocytes from Isolated Cells of the Adult Mammalian Central Nervous System. *Science (80-.).* **1992**, *255* (5052), 1707–1710.

(24) Yamashita, T.; Liu, W.; Matsumura, Y.; Miyagi, R.; Zhai, Y.; Kusaki, M.; Hishikawa, N.; Ohta, Y.; Kim, S. M.; Kwak, T. H.; et al. Novel Therapeutic Transplantation of Induced Neural Stem Cells for Stroke. *Cell Transplant.* **2017**, *26* (3), 461–467.

(25) Shear, D. A.; Tate, C. C.; Tate, M. C.; Archer, D. R.; Laplaca, M. C.; Stein, D. G.; Dunbar, G. L. Stem Cell Survival and Functional Outcome after Traumatic Brain Injury Is Dependent on Transplant Timing and Location. *Restor. Neurol. Neurosci.* **2011**, *29* (4), 215–225.

(26) Tate, C. C.; Shear, D. A.; Tate, M. C.; Archer, D. R.; Stein, D. G.; LaPlaca, M. C. Laminin and Fibronectin Scaffolds Enhance Neural Stem Cell Transplantation into the Injured Brain. *J. Tissue Eng. Regen. Med.* **2009**, *3* (3), 208–217.

(27) Sun, Y.; Nadal-Vicens, M.; Misono, S.; Lin, M. Z.; Zubiaga, A.; Hua, X.; Fan, G.; Greenberg, M. E. Neurogenin Promotes Neurogenesis and Inhibits Glial Differentiation by Independent Mechanisms. *Cell* **2001**, *104* (3), 365–376.

(28) Cifu, D. X.; Keyser-Marcus, L.; Lopez, E.; Wehman, P.; Kreutzer, J. S.; Englander, J.; High, W. Acute Predictors of Successful Return to Work 1 Year after Traumatic Brain Injury: A Multicenter Analysis. *Arch. Phys. Med. Rehabil.* **1997**, *78* (2), 125–131.

(29) Keyser-Marcus, L. A.; Bricout, J. C.; Wehman, P.; Campbell, L. R.; Cifu, D. X.; Englander, J.; High, W.; Zafonte, R. D. Acute Predictors of Return to Employment after Traumatic Brain Injury: A Longitudinal Follow-Up. *Arch. Phys. Med. Rehabil.* **2002**, *83* (5), 635–641.

(30) Basford, J. R.; Chou, L.-S.; Kaufman, K. R.; Brey, R. H.; Walker, A.; Malec, J. F.; Moessner, A. M.; Brown, A. W. An Assessment of Gait and Balance Deficits after

Traumatic Brain Injury. *Arch. Phys. Med. Rehabil.* **2003**, *84* (3), 343–349.

(31)   Nakamura, M.; Saatman, K. E.; Galvin, J. E.; Scherbel, U.; Raghupathi, R.; Trojanowski, J. Q.; McIntosh, T. K. Increased Vulnerability of NFH-LacZ Transgenic Mouse to Traumatic Brain Injury-Induced Behavioral Deficits and Cortical Damage. *J. Cereb. Blood Flow Metab.* **1999**, *19* (7), 762–770.

(32)   Brickler, T. R.; Hazy, A.; Guilhaume Correa, F.; Dai, R.; Kowalski, E. J. A.; Dickerson, R.; Chen, J.; Wang, X.; Morton, P. D.; Whittington, A.; et al. Angiopoietin/Tie2 Axis Regulates the Age-at-Injury Cerebrovascular Response to Traumatic Brain Injury. *J. Neurosci.* **2018**, *38* (45), 9618–9634.

(33)   Liu, N.-K. K.; Zhang, Y.-P. P.; O'Connor, J.; Gianaris, A.; Oakes, E.; Lu, Q.-B. B.; Verhovshek, T.; Walker, C. L.; Shields, C. B.; Xu, X.-M. M. A Bilateral Head Injury That Shows Graded Brain Damage and Behavioral Deficits in Adultmice. *Brain Res.* **2013**, *1499*, 121–128.

(34)   Hamers, F. P. T.; Lankhorst, A. J.; van Laar, T. J.; Veldhuis, W. B.; Gispen, W. H. Automated Quantitative Gait Analysis During Overground Locomotion in the Rat: Its Application to Spinal Cord Contusion and Transection Injuries. *J. Neurotrauma* **2001**, *18* (2), 187–201.

(35)   Schira, J.; Gasis, M.; Estrada, V.; Hendricks, M.; Schmitz, C.; Trapp, T.; Kruse, F.; Kögler, G.; Wernet, P.; Hartung, H.-P.; et al. Significant Clinical, Neuropathological and Behavioural Recovery from Acute Spinal Cord Trauma by Transplantation of a Well-Defined Somatic Stem Cell from Human Umbilical Cord Blood. *Brain* **2012**, *135* (2), 431–446.

(36)   Neumann, M.; Wang, Y.; Kim, S.; Hong, S. M.; Jeng, L.; Bilgen, M.; Liu, J. Assessing Gait Impairment Following Experimental Traumatic Brain Injury in Mice. *J. Neurosci. Methods* **2009**, *176* (1), 34–44.

(37)   Petit, A.; Sellers, D. L.; Liebl, D. J.; Tessier-Lavigne, M.; Kennedy, T. E.; Horner, P. J. Adult Spinal Cord Progenitor Cells Are Repelled by Netrin-1 in the Embryonic and Injured Adult Spinal Cord. *Proc. Natl. Acad. Sci.* **2007**, *104* (45), 17837–17842.

(38)   Powers, B. E.; Sellers, D. L.; Lovelett, E. A.; Cheung, W.; Aalami, S. P.; Zapertov, N.; Maris, D. O.; Horner, P. J. Remyelination Reporter Reveals Prolonged Refinement of Spontaneously Regenerated Myelin. *Proc. Natl. Acad. Sci.* **2013**, *110* (10), 4075–4080.

(39)   Sellers, D. L.; Maris, D. O.; Horner, P. J. Postinjury Niches Induce Temporal Shifts in Progenitor Fates to Direct Lesion Repair after Spinal Cord Injury. *J. Neurosci.* **2009**, *29* (20), 6722–6733.

(40)   Morrison, S. J. Neuronal Differentiation: Proneural Genes Inhibit Gliogenesis. *Curr. Biol.* **2001**, *11* (9), 349–351.

(41)   Rosenberg, A. B.; Roco, C. M.; Muscat, R. A.; Kuchina, A.; Sample, P.; Yao, Z.; Graybuck, L. T.; Peeler, D. J.; Mukherjee, S.; Chen, W.; et al. Single-Cell Profiling of the Developing Mouse Brain and Spinal Cord with Split-Pool Barcoding. *Science (80-.).* **2018**, *360* (6385), 176–182.

(42)   SMITH, D. H.; SOARES, H. D.; PIERCE, J. S.; PERLMAN, K. G.; SAATMAN, K. E.; MEANEY, D. F.; DIXON, C. E.; McINTOSH, T. K. A Model of Parasagittal Controlled Cortical Impact in the Mouse: Cognitive and Histopathologic Effects. *J. Neurotrauma* **1995**, *12* (2), 169–178.

(43)   White, B. D.; Nathe, R. J.; Maris, D. O.; Nguyen, N. K.; Goodson, J. M.; Moon, R. T.; Horner, P. J. β-Catenin Signaling Increases in Proliferating NG21 Progenitors and

Astrocytes during Post-Traumatic Gliogenesis in the Adult Brain. *Stem Cells* **2010**, *28* (2), 297–307.

(44)   Neuberger, E. J.; Swietek, B.; Corrubia, L.; Prasanna, A.; Santhakumar, V. Enhanced Dentate Neurogenesis after Brain Injury Undermines Long-Term Neurogenic Potential and Promotes Seizure Susceptibility. *Stem Cell Reports* **2017**, *9*.

(45)   Riess, P.; Zhang, C.; Saatman, K. E.; Laurer, H. L.; Longhi, L. G.; Raghupathi, R.; Lenzlinger, P. M.; Lifshitz, J.; Boockvar, J.; Neugebauer, E.; et al. Transplanted Neural Stem Cells Survive, Differentiate, and Improve Neurological Motor Function after Experimental Traumatic Brain Injury. *Neurosurgery*. October 2002, pp 1043–1052; discussion 1052-4.

(46)   HOVDA, D. A.; LEE, S. M.; SMITH, M. L.; VONSTUCK, S.; BERGSNEIDER, M.; KELLY, D.; SHALMON, E.; MARTIN, N.; CARON, M.; MAZZIOTTA, J.; et al. The Neurochemical and Metabolic Cascade Following Brain Injury - Moving From Animal-Models To Man. *J. Neurotrauma* **1995**, *12* (5), 903–906.

(47)   McIntosh, T. K.; Saatmann, K. E.; Raghupathi, R.; Graham, D. I.; Smith, D. H.; Lee, V. M. Y.; Trojanowski, J. Q. The Dorothy Russell Memorial Lecture. The Molecular and Cellular Sequelae of Experimental Traumatic Brain Injury: Pathogenetic Mechanisms. *Neuropathology and Applied Neurobiology*. Wiley/Blackwell (10.1111) August 1, 1998, pp 251–267.

(48)   Newcomb, J. K.; Zhao, X.; Pike, B. R.; Hayes, R. L. Temporal Profile of Apoptotic-like Changes in Neurons and Astrocytes Following Controlled Cortical Impact Injury in the Rat. *Exp. Neurol.* **1999**, *158* (1), 76–88.

(49)   Morganti-Kossmann, M. C.; Rancan, M.; Stahel, P. F.; Kossmann, T. Inflammatory Response in Acute Traumatic Brain Injury: A Double-Edged Sword. *Curr. Opin. Crit. Care* **2002**, *1* (6).

(50)   Wallenquist, U.; Holmqvist, K.; Hnell, A.; Marklund, N.; Hillered, L.; Forsberg-Nilsson, K. Ibuprofen Attenuates the Inflammatory Response and Allows Formation of Migratory Neuroblasts from Grafted Stem Cells after Traumatic Brain Injury. *Restor. Neurol. Neurosci.* **2012**, *30* (1), 9–19.

(51)   Monje, M. L.; Toda, H.; Palmer, T. D. Inflammatory Blockade Restores Adult Hippocampal Neurogenesis. *Science (80-.).* **2003**, *302* (5651), 1760–1765.

(52)   Führmann, T.; Obermeyer, J.; Tator, C. H.; Shoichet, M. S. Click-Crosslinked Injectable Hyaluronic Acid Hydrogel Is Safe and Biocompatible in the Intrathecal Space for Ultimate Use in Regenerative Strategies of the Injured Spinal Cord. *Methods* **2015**, *84*, 60–69.

(53)   Ballios, B. G.; Cooke, M. J.; Donaldson, L.; Coles, B. L. K.; Morshead, C. M.; van der Kooy, D.; Shoichet, M. S. A Hyaluronan-Based Injectable Hydrogel Improves the Survival and Integration of Stem Cell Progeny Following Transplantation. *Stem cell reports* **2015**, *4* (6), 1031–1045.

(54)   Segura, T.; Anderson, B. C.; Chung, P. H.; Webber, R. E.; Shull, K. R.; Shea, L. D. Crosslinked Hyaluronic Acid Hydrogels: A Strategy to Functionalize and Pattern. *Biomaterials* **2005**, *26* (4), 359–371.

(55)   Sideris, E.; Griffin, D. R.; Ding, Y.; Li, S.; Weaver, W. M.; Di Carlo, D.; Hsiai, T.; Segura, T. Particle Hydrogels Based on Hyaluronic Acid Building Blocks. *ACS Biomater. Sci. Eng.* **2016**, *2* (11), 2034–2041.

Chapter 5. ENDOSOMAL ESCAPE ENHANCES CYTOTOXIC T CELL RESPONSE TO POLYMER-MEDIATED PEPTIDE VACCINATION

Abstract

Nanobiomaterials empower fundamental and applied immunology research by enabling control over key temporal and spatial contexts of vaccine delivery. In particular, recent work has shown that membrane-disrupting endosomal escape strategies can potentiate cellular immune responses critical for therapeutic vaccination against cancer and other chronic diseases. Our lab has developed a cationic polymer-lytic peptide conjugate (VIPER) that greatly improves endosomal escape and intracellular activity of nucleic acid cargoes; furthermore, we hypothesize that VIPER's unique mechanism of endosomal disruption can increase cytoplasmic delivery of other biomacromolecules (e.g. peptides). Herein, we formulate VIPER as a nanoparticulate subunit vaccine composed of conjugated peptide antigens and electrostatically complexed poly(I:C) nucleic acid adjuvant and evaluate whether the presence of a lytic peptide in the pH-responsive micelle core improves vaccination outcomes. After demonstrating that formulation with lytic peptide is critical for VIPER-mediated endosomal disruption and antigen cross-presentation *in vitro*, we show that VIPER vaccine formulations generate potent antigen-specific cytotoxic T-cell responses *in vivo* and prolong melanoma survival in subset of therapeutically vaccinated mice. These results demonstrate that cellular immune responses to vaccination can be enhanced by endosomal disruption in peripheral cells and promote VIPER as a platform technology for the study of intracellular antigen delivery.

5.1   INTRODUCTION

Therapeutically-administered subunit peptide vaccines hold great promise in cancer treatment as a relatively low cost approach to self-elicited immunotherapy that can be customized to patient-specific targets or specific adaptive immune phenotypes by judicious peptide epitope and adjuvant selection.[1,2] However, peptide subunit vaccines have only achieved modest benefit in anticancer clinical trials thus far, in part because the immunological relationships that govern the success of therapeutic vaccination against chronic disease remain undefined.[3] Among other challenges, an effective anticancer peptide vaccine provokes potent antiviral-like adaptive cellular responses from cytotoxic (CD8$^+$) T lymphocytes (CTLs) that are ultimately critical for the elimination of cancer cells.[2] While advances in the design of synthetic vaccine adjuvants (e.g. TLR agonists[4]) have enabled the stimulation of antigen presenting cell (APC) maturation and secretion of antiviral/pro-inflammatory cytokines, there remains a need for vaccine designs that concomitantly enhance MHC class I (MHCI) antigen presentation in order to elicit a potent antigen-specific CTL response.[5,6]

Nanoscale vaccine formulations ("nanovaccines") offer many strategic opportunities to address the current shortcomings of soluble vaccines.[7–10] Polymers are particularly promising nanovaccine vectors because they may be designed with diverse and responsive chemical properties to navigate extracellular and intracellular barriers impeding delivery of antigen and adjuvant cargo.[9–13] For example, loading polymeric nanoparticles with both antigen and adjuvant facilitates co-delivery of these biomacromolecules into the same APC, which is difficult to achieve with soluble vaccine formulations, and which limits toxicity associated with systemic adjuvant biodistribution.[10] Furthermore, while most conventional subunit vaccines suffer from rapid clearance and poor

lymph node (LN) accumulation, the dimensions and surface chemistries of polymeric nanoparticles can be designed to enhance APC uptake and lymphatic transport.[13,14] Once internalized by APCs, polymeric delivery systems with endosomolytic properties can also enhance the cross-presentation of exogenous peptide antigens on APC MHCI receptors, which is required for the generation of a CTL response.[15–17]

Tuning the endosomal release of vaccines in APCs remains a largely untapped strategy for increasing potency of vaccine-induced cellular immune responses. While much research in the field of nucleic acid delivery has focused on developing methods that increase rates of endosomal escape, comparatively few strategies have been developed for vaccine cargo.[18–20] Endosomal disruption in APCs has been hypothesized to increase the generation of cellular immune responses by enhancing cross-presentation via improved cytoplasmic antigen delivery[21] and/or by releasing inflammasome-activating molecules from endosomal compartments.[22–24] While initial studies performed by the Stayton group have correlated delayed endosomolysis with increased cross-presentation,[16,25–27] early escape has also been correlated with more productive antigen presentation,[21] and the role of phagocytic disruption in APC stimulation remains a topic of debate.[10,24] Thus, there remains a need for drug delivery technologies that enable investigation of how endosomal escape alters antigen presentation and the resulting adaptive immune responses.

We recently reported a polymer (VIPER, "Virus-Inspired Polymer for Endosomal Release") that facilitates efficient endosomal escape of nucleic acid cargo through selective display of membrane lytic peptides as a result of pH-triggered micelle disassembly.[28,29] We have further demonstrated that VIPER micelles can encapsulate a wide variety of peptides regardless of peptide

hydrophobicity or charge.[30] Inspired by these observations and prior applications of cationic polymers for co-delivery of nucleic acid adjuvants and protein antigens,[16,31] we hypothesized that VIPER could be used to deliver all necessary vaccine components in endosomolytic mixed micelle formulations.

In this work, we synthesize VIPER polymers that co-deliver peptide antigen via a reversible disulfide bond and nucleic acid adjuvant via electrostatic complexation. We demonstrate that inclusion of a membrane-lytic peptide within the VIPER formulation is critical for endosomal disruption and antigen cross-presentation *in vitro*. The VIPER formulation also generates potent antigen-specific cytotoxic T-cell responses *in vivo* and prolongs melanoma survival in subset of therapeutically vaccinated mice. These results indicate that cellular immune responses to vaccination are augmented by endosomal disruption in peripheral cells and further promote VIPER as a platform technology for intracellular antigen delivery.

5.2   EXPERIMENTAL SECTION

5.2.1   *Materials*

All chemicals used for polymer and peptide synthesis were purchased from either Sigma Aldrich or Thermo Fisher Scientific and used without further purification as previously described.[30] All media and cell culture reagents were purchased from Gibco. Endotoxin-free plasmid pmaxGFP™ (Lonza) were purified with the Qiagen Plasmid Giga kit (Qiagen) according to the manufacturer's protocol. Incomplete Freund's adjuvant (InvivoGen) was stored at 4 °C until emulsification with control antigen and adjuvant according to the manufacturer's protocol. Endotoxin-free SIINFEKL peptide (InvivoGen) was dissolved in endotoxin-free 5% glucose (Sigma) and stored at -20 °C

until further usage. Endotoxin-free high molecular weight poly(I:C) (InvivoGen) was annealed in sterile saline according to the manufacturer's protocol and then buffer exchanged into 5% glucose via centrifugal filtration (10 kDa cutoff; Amicon) before sterile filtration with a 0.22 µm pore filter (Millipore) and storage at -20 °C until further usage. All antibodies were purchased from Invitrogen unless otherwise specified, and the SIINFEKL tetramer was a gift of the NIH tetramer core (see acknowledgements).

5.2.2 *Peptide synthesis*

Lytic (melittin; GIGAVLKVLTTGLPALISWIKRKRQQC) and antigen (CSSSIINFEKL) peptides were synthesized through solid phase peptide synthesis using a Liberty Blue microwave peptide synthesizer (CEM) at 0.25 mmol scale using standard Fmoc amino acids and NovaPEG Rink Amide Resin (Millipore). Peptides were cleaved from the resin in a trifluoroacetic acid (TFA) cocktail with 5% dimethoxybenzene, 2.5% triisopropylsilane, and 2.5% ethanedithiol. Water was included at 2.5% for peptides containing arginine. Crude peptide was precipitated twice in cold diethyl ether and purified by reverse-phase HPLC using 0.1% TFA water and acetonitrile to > 98% purity. Peptide molecular mass was determined by MALDI-TOF at the University of Washington Department of Medicinal Chemistry Mass Spectrometry Center. Rhodamine-CSSSIINFEKL was generated by reaction of Rhodamine-NHS (Thermo Scientific) with Fmoc-deprotected peptide N-terminal amines through EDC/NHS chemistry on resin, followed by cleavage and purification as with the other peptides.

5.2.3 *Polymer synthesis, peptide conjugation, and micelle formation*

Block copolymer p(OEGMA$_{8.6}$-*co*-DMAEMA$_{50.0}$)-*bl*-p(DIPAMA$_{25.3}$-*co*-PDSEMA$_{1.0}$) ("control polymer" CP) was prepared with RAFT polymerization, purified by dialysis, and characterized with ^{1}H NMR and GPC in previous work.[30] Synthesized peptides were conjugated to CP through disulfide exchange between cysteine and PDSEMA and conjugates were purified as in previous work.[30] Mixed micelles were formed by mixing various polymers dissolved in acidic phosphate buffer at defined ratios before forming micelles through rapid pH shift as previously described.[28,30] Micelles were allowed to form overnight before buffer exchange to 5% glucose in water on a 10 kDa cutoff Amicon centrifugal filter (Millipore), sterile filtered using a 0.22 µm pore filter (Millipore), and stored at 4 °C as a 0.5 µg CSSSIINFEKL/µL solution until use in future experiments.

5.2.4 *Preparation and characterization of polyplexes*

Polyplexes were formed by adding polymer micelles to either plasmid DNA or poly(I:C) solution followed by 30 min incubation at room temperature before further use or characterization. For the gel retardation assay, polyplexes with various N/P ratios were loaded onto a 1% agarose gel containing TAE buffer (40 µM tris-acetate, 1 mM EDTA) and 0.5 µg/mL ethidium bromide. Polyplexes were then electrophoresed at 100 V for 40 min before imaging on a UV transilluminator. The size and surface charge of the polyplexes were also tested on a Malvern Zetasizer instrument; polyplexes (1 µg poly(I:C), 20 µL solution) were diluted in 800 µL in 10 mM NaCl and measured in triplicate.

The morphology and size of polyplex under dried state was imaged by transmission electron microscopy on a hydrophilic surface. Copper/Formvar grids (400-mesh) were treated with glow discharge for 45 s to create a hydrophilic surface. Twenty microliters of polyplex (in dH_2O) was applied to the Formvar-side of the grid for 30 min. Then the grid was washed three times with dH_2O, followed by dipping in 4% (w/v) uranyl acetate (in dH_2O) to negatively stain the sample. Excess solution was wicked off the grid with filter paper, and the grid was allowed to dry overnight in a desiccator prior to imaging. Images of the sample grids were taken with a JEOL 1010 transmission electron microscope (Electron Microscopy Facility, Fred Hutchinson Cancer Research Center).

5.2.5 *Cell culture*

The DC2.4 mouse dendritic cell line (gift of Prof. Kim Woodrow) was cultured in RPMI supplemented with 10% heat-inactivated fetal bovine serum (HIFBS), L-glutamine, 1X penicillin/streptomycin (P/S), 10 mM HEPES buffer, 1X non-essential amino acids, and 55 µM β-mercaptoethanol (BME). The Gal8-DC2.4 cell line was generated by co-transfecting plasmids containing a transposable Gal8-GFP construct and PiggyBac transposon (gifts of Prof. Jordan Green) using Lipofectamine 2000 and then sorting for the top 5% brightest GFP+ singlet cell events using a custom FACS Aria sorter (BD). Transfected cells were expanded and sorted a total of three times to yield a polyclonal population of Gal8-GFP^{high} cells. The B3Z mouse CD8+ T-cell hybridoma line (gift of Prof. Nilabh Shastri) was cultured in RPMI supplemented with 10% HIFBS, L-glutamine, 1X P/S, 1 mM sodium pyruvate, and 50 µM BME. The NIH/3T3 mouse fibroblast line was cultured in DMEM supplemented with 10% HIFBS, L-glutamine, 4.5 g/L D-glucose, 1X P/S, and 110 mg/mL sodium pyruvate. The B16-OVA mouse melanoma line (gift of

Prof. Amanda Lund) was cultured in DMEM supplemented with 10% FBS, L-glutamine, 4.5 g/L D-glucose, and 1X P/S. DC2.4, NIH/3T3, and B16-OVA cells were passaged every three days or when 75% confluent and seeded to reach 75-100% confluency at time of treatment or harvest. B3Z cells were passaged no more than 10 times and maintained at a cell density under 700,000 cells/mL.

5.2.6   In vitro *dendritic cell transfection*

For pmaxGFP™ transfection, DC2.4 cells were seeded at a density of 25,000 cells/well in complete cell culture medium in 24-well plates. Cells were first incubated at 37 °C, 5% CO_2 for 16 h. Polyplexes were prepared at different N/P ratios using either VIPER or CP micelles and 1 μg of pmaxGFP™ pDNA (0.1 mg/mL) and allowed to rest for at least 10 min. Each polyplex solution was then added dropwise directly to each well (in triplicate). After 4 h, cells were washed with phosphate-buffered saline (PBS) and resuspended in fresh complete cell culture medium. After 40 additional hours, cells were lifted by scraping, stained with Zombie Violet™ viability dye (BioLegend), and analyzed using an Attune NxT flow cytometer (Thermo Fisher). Transfection efficiency is reported as the mean percentage of single cells that were GFP[+]/Violet[-].

5.2.7   *Gal8 endosomal disruption assay*

Gal8-DC2.4 were seeded in glass bottom half-area 96 well plates at 10^4 cells/well and incubated overnight. Mixed micelles with varying molar ratios of antigen-conjugated polymer (AP) relative to either melittin-conjugated polymer (MP) or control polymer without peptide (CP) were formulated to yield 1:1, 2:1, 3:1, and 4:1 AP:MP (VIPER-Vax treatments) or AP:CP (Control-Vax treatments). Micelles were mixed with poly(I:C) to form N/P 10 polyplexes and added to wells to a final antigen concentration of 2 μg/mL. After 8 h incubation, culture media was

removed and replaced with imaging media (FluoroBrite DMEM supplemented with 25 mM HEPES, 10% FBS, and Hoechst 33342). Live cell imaging was performed using a 20X objective on a custom Leica SP8X laser scanning confocal microscope to capture > 20,000 cells per condition. Summation of punctate Gal8 pixel area and normalization to cell count was performed using a slightly modified version of the original MATLAB code provided by Kilchrist, et al,[32] and is available upon request. Each experiment was repeated three times on different passages of the same cell line and data are presented as the average of these three experiments.

5.2.8   In vitro *dendritic cell uptake*

DC2.4 cells were incubated with 2 µg/mL rhodamine-conjugated CSSSIINFEKL delivered as soluble peptide, VIPER-Vax micelles, or N/P 10 VIPER-Vax polyplexes for various durations before uptake was quantified by flow cytometry.

5.2.9   *DC2.4 cross-presentation and viability assays*

DC2.4 cells were seeded into 96-well U-bottom tissue culture plates at 50,000 cells/well. 24 h after seeding, DC2.4 cells were pulsed for 2 h with 2.5 µg/mL CSSSIINFEKL in 100 µL culture media, administered directly as soluble peptide or loaded into N/P 10 VIPER-Vax or Control-Vax polyplexes. After the 2 h pulse, DC2.4 cells were washed 2 times with PBS and co-cultured for an additional 20-24 h with B3Z cells (mouse CD8^{+} T-cell hybridomas that produce β-galactosidase upon binding of SIINFEKL-MHCI complexes) at 100,000 B3Z cells/well in 200 µL B3Z media.[33] After 20 h of co-culture, cells were centrifuged at 500 rcf for 7 m and culture media was removed. Cells were subsequently resuspended in 150 µL/well of CPRG lysis buffer (0.15 mM chlorophenol red-β-D-galactopyranoside (Roche), 0.1% Triton X-100, 9 mM $MgCl_2$, and 100 µM BME in PBS)

and incubated in the dark at 37 °C for 1.5 h. After 1.5 h of incubation, cross-presentation levels were quantified by measuring the absorbance of chlorophenol red at 570 nm (reference 650 nm) using a Tecan Infinite M200 plate reader. To assess DC2.4 cell viability after polyplex treatment, DC2.4 cells were first seeded into tissue culture plates and pulsed with vaccine formulations as described above. 20-24 h after pulsing, an MTS assay (Promega) was performed in accordance with manufacturer protocol to measure cell viability.

5.2.10 *NIH/3T3-DC2.4 cross-presentation and viability assays*

NIH/3T3 cells were seeded into 96-well U-bottom tissue culture plates at 2,100 cells/well. 24 h after seeding, NIH/3T3 cells were pulsed for 4 h with 0.625, 1.25, 2.5, or 5.0 µg/mL CSSSIINFEKL in 100 µL culture media, administered directly as soluble peptide or loaded into N/P 10 VIPER-Vax or Control-Vax polyplexes. After the 4 h pulse, polyplex-containing media was removed and fresh culture media was added without any PBS washes. NIH/3T3 cells were subsequently co-cultured with DC2.4 cells (50,000 cells/well) in 100 µL NIH/3T3 media supplemented with 10 mM HEPES buffer. Note that DC2.4 cells were maintained in NIH/3T3 media supplemented with 10 mM HEPES buffer for at least 3 days prior to co-culture with NIH/3T3 cells. After 24 h of DC2.4 co-culture, cross-presentation levels were quantified using the same B3Z co-culture assay described in the previous section. To assess NIH/3T3 cell viability after polyplex treatment, NIH/3T3 cells were first seeded into tissue culture plates and pulsed with vaccine formulations as described above, with the addition of two PBS washes after pulsing. 24 h after pulsing, an MTS assay (Promega) was performed in accordance with manufacturer protocol to measure cell viability.

5.2.11 *Immunization of mice*

All animal procedures were performed in accordance with protocols approved by the Institutional

Animal Care and Use Committee at the University of Washington. Female C57Bl/6 mice (Jackson

Laboratory), 6-8 weeks old, were immunized via intradermal injection at the right base of the tail

in a total volume of 50 µL. In all studies comparing polyplex formulations, mice were immunized

with 10 µg antigen (SIINFEKL or CSSSIINFEKL) and 17.5 µg poly(I:C). All formulations were

prepared < 1 h prior to injection.

5.2.12 *Splenocyte surface staining, restimulation, intracellular cytokine staining, and flow*
cytometry

Female C57Bl/6 mice, 6 weeks old, were immunized intradermally on D0 and D21 with either (i)

glucose, (ii) SIINFEKL + poly(I:C), (iii) CSSSIINFEKL + poly(I:C), (iv) Control-Vax polyplexes,

or (v) VIPER-Vax polyplexes using antigen and adjuvant doses described above (N = 6). On D28,

mice were killed by Avertin overdose and spleens placed in complete RPMI media (+10% FBS;

cRPMI) on ice. Spleens were mechanically dissociated into a single cell suspensions using a

syringe plunger and a 40 µm cell strainer, which was rinsed with media and replaced after each

spleen. Splenocytes were pelleted by centrifugation at 800 x *g* and resuspended in cRPMI with

100 U/mL DNAse I (Worthington) for 5 minutes before lysis of red blood cells with ACK buffer

(Gibco). Following a PBS wash, splenocytes were split for either immediate surface staining or

SIINFKEL restimulation followed by surface and intracellular cytokine staining (ICCS). Surface

staining of 200,000 splenocytes per mouse was conducted at room temperature beginning with

Zombie NIR viability staining (1:500; Biolegend), two washes with PBS + 1% BSA (PBSA), 15

m room temperature incubation with PE H-2K(b) SIINFEKL tetramer (1:200; NIH Tetramer

121

Core), two washes with PBSA, 30 m incubation on ice with antibody cocktail (eFluor450 CD3e [1:100; clone 145-2C11; Invitrogen], FITC CD8α [1:1000; clone KT-15; ProImmune], APC CD19 [1:1000; clone 1D3; Invitrogen]), and three final washes with PBSA before analysis by flow cytometry. For SIINFEKL restimulation, 200,000 splenocytes were plated per well in cRPMI with 20 µg/mL SIINFEKL peptide and incubated 1 h at 37 °C and 5% CO_2, after which Protein Transport Inhibitor Cocktail (eBioscience) was added to 1X and cells were incubated an additional 8 h to accumulate intracellular cytokines. Following a PBSA wash, cells were stained for viability, CD3e, CD8α, and CD19 as described above and then fixed and permeabilized using the Cytofix/Cytoperm kit (BD) according to the manufacturer's instructions. Finally, ICCS was performed on ice for 30 m with antibody cocktail (PerCP-710 TNFα [1:50; clone MP6-XT22; Invitrogen], PE-Cy7 IFNγ [1:50; clone XMG1.2; Invitrogen]), followed by three washes with Perm/Wash buffer and analysis on an Attune NxT Flow Cytometer (ThermoFisher).

5.2.13 *Tumor inoculation and monitoring*

Female C57Bl/6 mice, 6-8 weeks old, were inoculated subcutaneously with 100,000 B16-OVA cells in the right hind flank and randomized into various treatment groups (N = 8). Animal weight was recorded immediately prior to tumor inoculation and every two days thereafter. Once tumors were palpable, tumor dimensions were measured by caliper every two days, and tumor volumes were calculated using the equation $V = (W^2 \times L) / 2$. Mice were euthanized when tumor mass exceeded 10% of body weight, when body weight loss exceeded 20%, or when severe tumor ulceration was observed.

5.2.14 *Tumor dissociation and analysis of tumor-infiltrating lymphocytes*

Mice were overdosed with Avertin upon reaching tumor volume criteria for euthanasia (N = 3; D42). Tumors were resected and minced with a scalpel in a dissociation cocktail of 1 mM L-cysteine, 0.5 mM EDTA, 20 U/mL papain, 20 U/mL collagenase D, and 125 U/mL DNAse I (Worthington) in 5 mL RPMI per tumor. Each tumor was placed in a C-tube and subjected to two "imp_tumor" dissociations cycles performed by a gentleMACS machine (Miltenyi) separated by a 40 m incubation at 37 °C before being filtered through a 70 µm cell strainer into a 50 mL tube. Single cell suspensions were washed three times with 50 mL PBS before 200,000 cells per tumor were stained for analysis by flow cytometry. Antibody staining and flow cytometry was performed as described above for splenocytes with the addition of mouse Fc block (1:100; Biolegend) before staining with eFluor506 PD-1 [1:100; clone J43; Invitrogen] and PE CD45 [1:500; clone REA737; Miltenyi] in addition to the eFluor450 CD3e and FITC CD8a described earlier.

5.2.15 *Statistical analysis*

All statistical analyses were performed in Prism software (GraphPad Software, La Jolla, CA) For analysis of *in vitro* data, a two-tailed Student's t-test with unequal variance and Welch's correction or a one-way ANOVA with post-hoc Tukey HSD test were used. For analysis of survival data, a logrank test was used.

5.3 RESULTS AND DISCUSSION

5.3.1 *Design of comprehensive delivery platform for subunit antigen and adjuvant*

Peptide epitopes from tumor-associated antigens and neoantigens have been investigated as cancer vaccines in clinical trials, but despite some promising results have not been broadly effective.[3] The importance of eliciting MHCI presentation and subsequent CTL response in addition to MHCII/helper (CD4^{+}) T cell response for prolonged anti-tumor response is now recognized.[1,5,6] While the specific trafficking profiles required for MHCI presentation of antigens are not yet fully understood, proteasome processing after cytosolic delivery is one demonstrated route.[34–36] For example, Moore and colleagues demonstrated that a CTL response could be elicited by incubation of an ovalbumin-derived peptide with APCs followed by osmotic lysis of pinosomes for release into the cytosol.[37] Antigen delivery and MHCI/II presentation alone is rarely efficacious due to the immunosuppressive environment of most solid tumors that biases adaptive immune responses towards tumor tolerance.[2] Thus, adjuvants that stimulate APCs through the activation of danger-sensing signaling pathways in the context of antigens are often required to shift adaptive responses towards tumor rejection for vaccine efficacy.[4] We therefore designed a VIPER-based formulation with the goal of using a polymer to facilitate cytosolic delivery for MHCI peptide antigen presentation while providing co-delivery of an immunostimulatory adjuvant to the same cells receiving antigen (**Figure 5.1**).
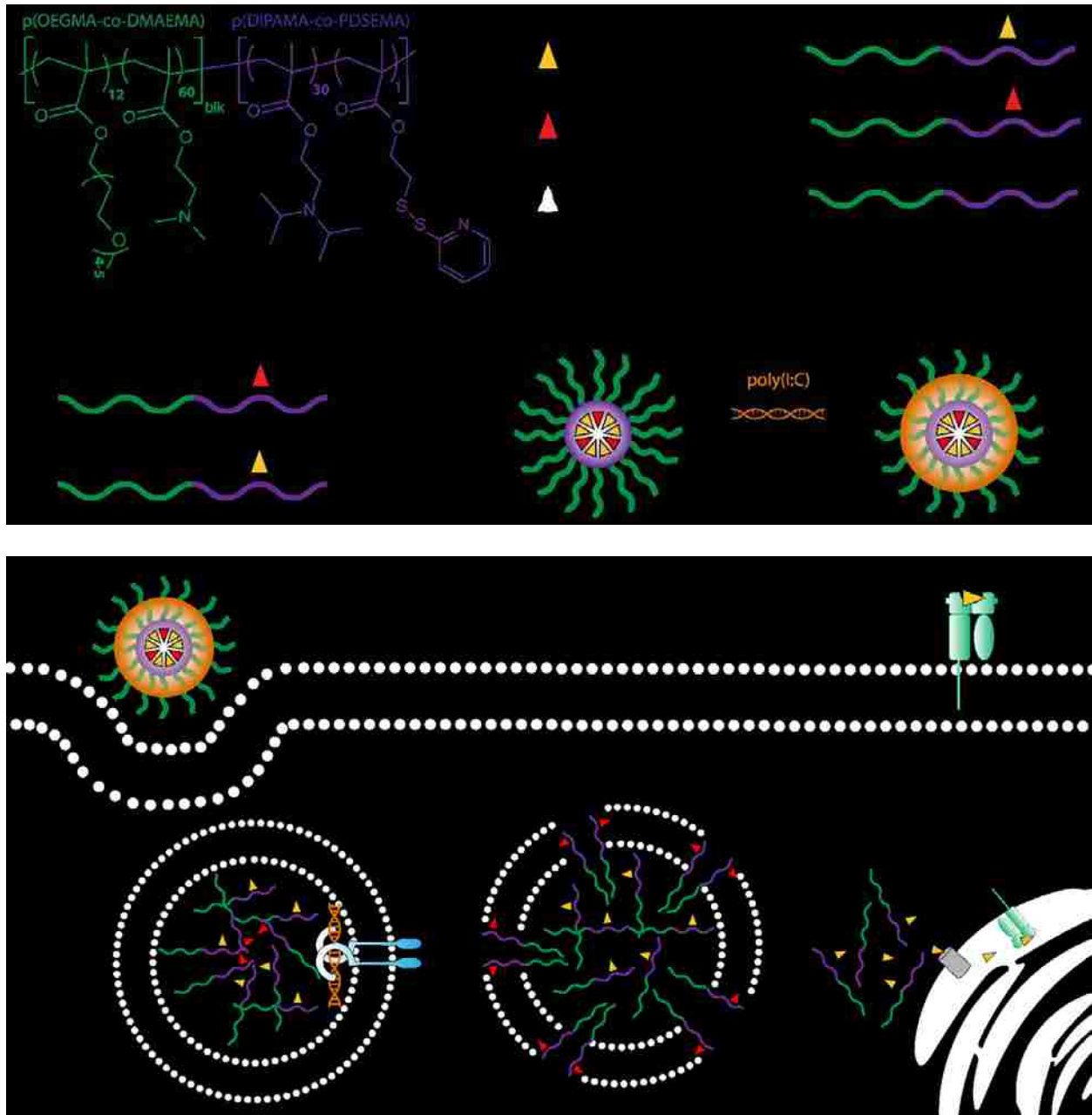
Figure 5.1 VIPER-Vax chemical structure, formulation, and mechanism of dual TLR3 agonism and enhanced antigen cross presentation through the cytosolic MHCI loading pathway.
Mixed micelles composed of pH-sensitive polymers conjugated to either lytic or antigen peptides are formulated as poly(I:C) vaccine polyplexes through simple mixing. Polyplexes undergo endocytosis followed by pH-triggered endosomal disassembly, which enables TLR3 agonism (blue) as well as cytoplasmic antigen delivery for TAP-assisted (grey) loading into MHCI (light green) in the endoplasmic reticulum.

We synthesized VIPER as a diblock copolymer with a hydrophilic, cationic block for adjuvant loading and a pH-sensitive block for either endosomal release or peptide antigen delivery. The pH-sensitive block is comprised primarily of 2-diisopropylaminoethyl methacrylate (DIPAMA)[38,39] copolymerized with pyridyl disulfide ethyl methacrylate (PDSEMA) for conjugation to thiolated peptides. The DIPAMA-rich block transitions sharply from hydrophobic to hydrophilic upon decreasing pH below 6.4. Consequently, the block copolymers self-assemble into core-shell structures at physiological, extracellular pH (pH > 7.0) but dissemble into individual polymer chains in acidic environments (pH < 6.5). Peptides conjugated to the DIPAMA block are thus protected by polymer micellization in extracellular environments but are exposed after cell internalization into endosomes.

The exogenous antigen ovalbumin is a popular model system for cancer vaccine delivery because of its high immunogenicity and well-characterized MHCI and MHCII peptide epitopes.[40] We selected CSSSIINFEKL, a variant of the ovalbumin MCHI epitope SIINFEKL, as a model antigen because it bears an N-terminal cysteine for conjugation and exhibited more efficient MCHI presentation than SIINFEKL in other reported work.[41,42] For endosomal release, the bee venom-derived peptide melittin was selected based on our previous work where we screened a panel of lytic peptides for endosomolytic activity. [30] The resulting polymers used in micelle formulation for this work were: Control Polymer (p(OEGMA$_{8.6}$-co-DMAEMA$_{50.0}$)-b-p(DIPAMA$_{25.3}$-co-PDSEMA$_{1.0}$)) without peptide (CP), CSSSIINFEKL Antigen-conjugated Polymer (AP), and Melittin-conjugated Polymer (MP, a.k.a. VIPER). Defined ratios of polymer chains—separately conjugated with lytic or antigen peptide—are mixed prior to micellization by combining polymers

in acidic buffer at a defined molar ratios of antigen-containing to non-antigen containing polymer (either lytic or control) followed by neutralization to induce micellization.

We selected the TLR3 agonist poly(I:C) as an adjuvant because of its cost-effective, potent ability to stimulate APC maturation and inflammatory cytokine production.[4] Importantly, localized delivery of poly(I:C) via nanovaccine systems has been shown to limit its systemic toxicity while also increasing on-target effects in APCs.[43,44] Poly(I:C) was incorporated into the vaccine formulation by electrostatic complexation with VIPER's cationic micelle shell, similar to previous work using PEI and cationic liposomes.[31,45,46] Adjuvant incorporation was efficient and complete adjuvant encapsulation could be achieved at polymer to adjuvant N/P ratios of 5 (polymer DMAEMA to adjuvant phosphate) (**Supplemental Figure 5.8**). We chose to proceed with N/P 10 polyplexes in order to maximize polymer-mediated resistance to polyplex unpackaging by extracellular matrix components while still delivering poly(I:C) doses comparable to those used in other *in vivo* studies.[43,45–47] The resulting +10-12 mV zeta potential complexes were ~ 150 nm in diameter as determined by dynamic light scattering, while transmission electron microscopy revealed highly monodisperse micelle structures ~ 26 nm (±4 nm) in diameter were preserved in both polyplex formulations (**Figure 5.2**). We confirmed that the size and surface charge of these VIPER/poly(I:C) polyplexes mediate efficient cellular uptake of rhodamine-labeled antigen peptide *in vitro* (**Supplemental Figure 5.9**).
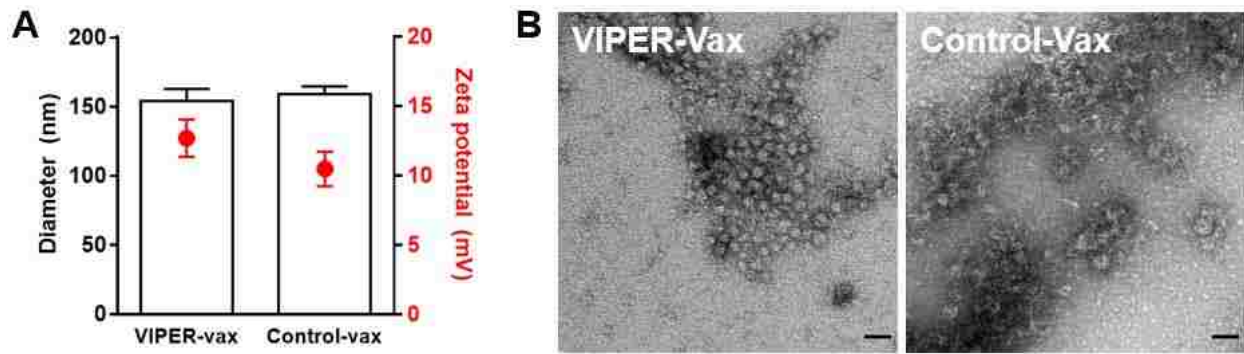
Figure 5.2 Polyplex characterization

Cationic mixed micelles with (VIPER-Vax) or without (Control-Vax) melittin were mixed with poly(I:C) at N/P 10 to form polyplexes. Polyplex diameter and surface charge were evaluated by dynamic light scattering and zeta potential measurements (**A**). Polyplex morphology and size were also confirmed by transmission electron microscopy (**B**). Data in (A) are plotted as mean + SD of three independent measurements. Scale bar = 50 nm

5.3.2   *Intracellular antigen delivery and MHCI presentation*

We first evaluated the ability of mixed micelle VIPER formulations to mediate endosomal disruption in Gal8-GFP expressing DC2.4 cells. Kilchrist et al. recently developed a high throughput confocal microscopy-based assay that correlates Galectin8 (Gal8) recruitment to disrupted endosomes with endosomal escape and intracellular cargo delivery.[32] In this assay, the total pixel area of bright, punctate Gal8-GFP signal in a given image is summed and divided by the number of cells in that image, such that greater GFP pixel area per cell correlates with a greater number of disrupted endosomes. We generated a Gal8-DC2.4 cell line and used it to define the minimum ratio of MP to AP in micelle formulations required for efficient endosomal disruption. Gal8-DC2.4 cells were treated with poly(I:C) polyplexes consisting of 1:1, 2:1, 3:1, or 4:1 AP:MP (VIPER-Vax) or AP:CP (Control-Vax) mixed micelles and Gal8 signal was quantified through live cell imaging after 8 h incubation (**Figure 5.3A-B**). Increasing MP content correlated with increased endosomal disruption induced by VIPER-Vax formulations (ΣGal8/cell = 650 vs. 102 for 1:1 vs 4:1 AP:MP) and all Control-Vax formulations rarely induced detectable endosomal

disruption. Because both 1:1 and 2:1 AP:MP formulations induced significantly greater ΣGal8/cell compared to Control-Vax formulations, we proceeded with 2:1 mixed micelles in order to maximize micelle antigen concentration (5% w/w) while retaining potent endosomal escape functionality.
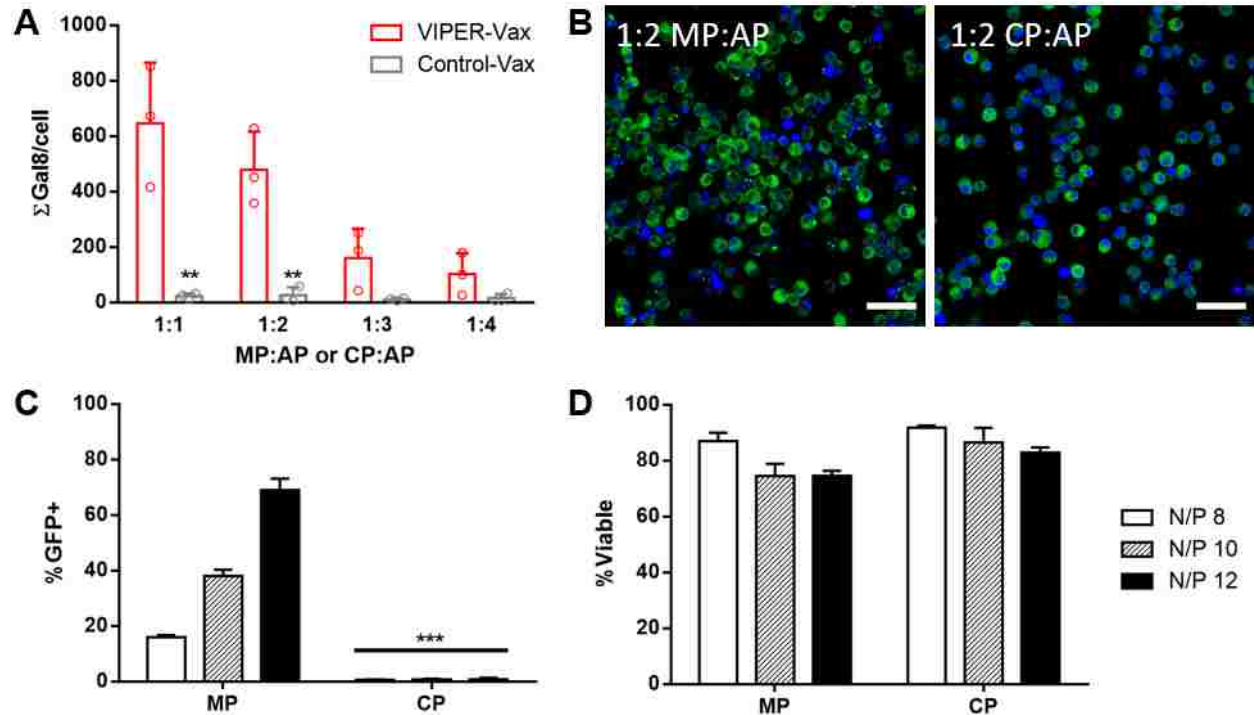

Figure 5.3 Melittin is essential for endosomal disruption and plasmid transfection in DC2.4 cells. **(A)** Gal8-DC2.4 cells were treated with poly(I:C) polyplexes consisting of 1:1, 2:1, 3:1, or 4:1 AP:MP (VIPER-Vax) or AP:CP (Control-Vax) mixed micelles and Gal8 signal was quantified through live cell imaging after 8 h incubation. Data are plotted as the mean + SD of three independent experiments and statistical significance is derived from Student's T-test comparing VIPER-Vax to Control-Vax at each mixed micelle ratio (** $p < 0.01$) **(B)** Representative images of Gal8-DC2.4 cells treated with the mixed micelle formulations carried forward in this work. Hoescht stained nuclei appear in blue and cytoplasmic Gal8-GFP appears in green; punctate Gal8-GFP is localized to disrupted endosomes. Scale bar is 50 µm. **(C)** GFP expression and **(D)** cell viability were analyzed by flow cytometry 48 h after transfection of DC2.4 cells with polyplexes composed of pMAX-GFP plasmid DNA and either MP or CP. Data are plotted as the mean + SD of three independent experiments and statistical significance is derived from Student's T-test comparing each N/P (*** $p < 0.001$)

After confirming enhanced endosomal disruption in dendritic cells, we evaluated cytosolic delivery of biological cargo. We substituted the poly(I:C) adjuvant for a transgene reporter plasmid, pmaxGFP™. Similar to poly(I:C), this plasmid is encapsulated by electrostatic interactions.[30] Cytosolic and subsequent nuclear delivery of this plasmid results in expression of green fluorescence protein (GFP) which is assessed by flow cytometry analysis. We observed that MP transfected much better than CP (69% vs. 0.77% GFP$^+$ at N/P 12) even in the presence of serum proteins, confirming results from our previous work that pH-dependent display of the lytic peptide is required for efficient transfection.[28–30] (**Figure 5.3C-D**).

Finally, we confirmed that cytosolic delivery mediated by VIPER improves antigen cross-priming. The B3Z cell line is a mouse CD8$^+$ T-cell hybridoma that produces β-galactosidase upon binding of its T-cell receptor to the mouse SIINFEKL-MHCI complex.[33] Therefore, cross-presentation by mouse APCs can be indirectly quantified by co-culturing antigen-pulsed APCs with B3Z cells and performing a colorimetric β-galactosidase assay. With this colorimetric assay, we demonstrated that pulsing DC2.4 cells directly with endosomolytic VIPER-Vax polyplexes consistently yielded the highest level of cross-presentation, which we attribute to enhanced access of antigen cargo to cytoplasmic proteasomes and MHCI loading machinery (**Figure 5.4A**).[34,35] However, this level of cross-presentation was not statistically different from those obtained with Control-Vax polyplexes and free CSSSIINFEKL (**Figure 5.4B**).

In preliminary B3Z co-culture assays, we detected significant cross-presentation after pulsing DC2.4 cells with micelle dosages that resulted in widespread DC2.4 cell death (data not shown). We hypothesized that cross-presentation may have been partly mediated by apoptotic "bystander"

cells, where antigen-loaded apoptotic bodies from micelle-pulsed DC2.4 cells were processed by their viable counterparts for antigen cross-presentation.[48] To explore this hypothesis, we pulsed NIH/3T3 fibroblasts with cytotoxic doses of polyplexes (0.625, 1.25, 2.5, and 5.0 µg/mL antigen doses) and subsequently co-cultured the fibroblasts with DC2.4 cells (**Supplemental Figure 5.10**).[48] Using this bystander co-culture assay, we confirmed that polyplex-pulsed bystander cells indeed serve as an antigen source for nearby APCs (**Figure 5.4C**). We also observed ~7.3-, ~2.7-, and ~1.5-fold increases in cross-presentation when melittin was included in the polyplexes, at 1.25, 2.5, and 5 µg/mL antigen, respectively (**Figure 5.4C**). These increases in cross-presentation may be due to not only the cytotoxic effect of melittin on NIH/3T3 fibroblasts, which drives production of apoptotic bodies, but also greater cytoplasmic delivery of antigen by melittin-loaded apoptotic bodies following endocytosis by APCs (**Supplemental Figure 5.10**).

Taken altogether, these results suggest that our polyplex formulations stimulate antigen cross-presentation through two distinct pathways: polyplexes may deliver vaccine cargo directly into APCs, or APCs may uptake vaccine-loaded apoptotic bodies produced by polyplex-pulsed bystander cells. Importantly, inclusion of melittin into the polyplex formulation significantly increases antigen cross-presentation through the latter pathway, and this increase in cross-presentation may be partially attributed to enhanced endosomal disruption by melittin after uptake of apoptotic bodies. As APCs are relatively rare in the intradermal space, we expect bystander-mediated cross-presentation to be the primary mechanism by which our polyplexes potentiate cellular immunity.[48] It is worth noting that MHCI loading may also take place within endosomes,[35] and thus efficient endosomal peptide delivery alone may account for the cross-presentation observed in Control-Vax–treated DC2.4 cells.
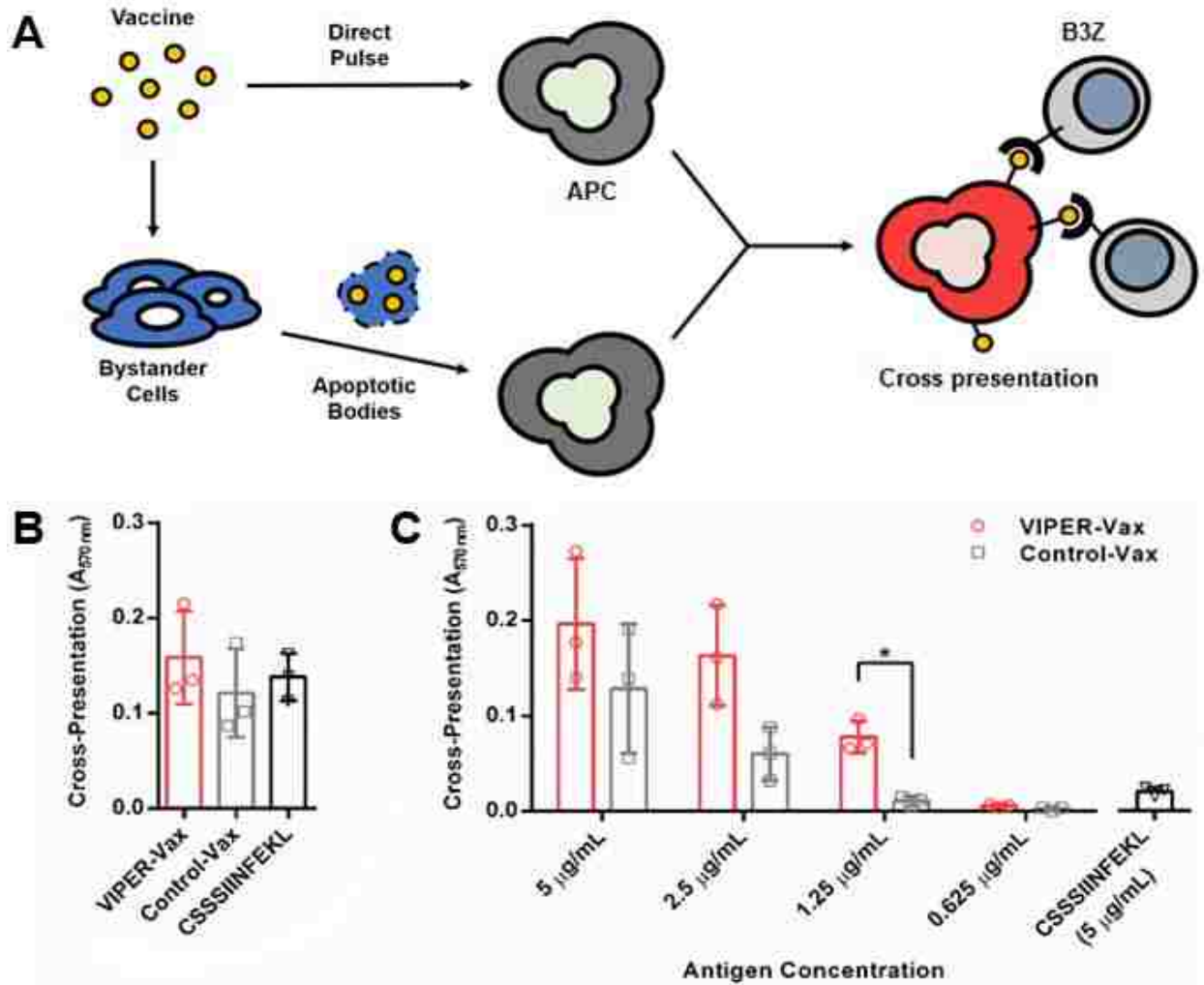
Figure 5.4 Active endosomal escape potentiates MHC class I antigen cross-presentation in vitro. **(A)** Cross-priming may occur after direct vaccine transfer into APCs or APC uptake of vaccine-loaded apoptotic bodies from bystander cells. **(B)** DC2.4 cells were pulsed with 2.5 µg/mL SIINFEKL delivered as either soluble CSSSIINFEKL peptide, VIPER-Vax polyplex, or Control-Vax polyplex for 2 h and subsequently co-cultured for 20-24 h with B3Z T-cell hybridoma cells. Production of β-galactosidase by B3Z cells upon recognition of MHCI SIINFEKL antigen presentation by DC2.4 cells was detected using a lysis buffer containing a colorimetric substrate with an absorbance maximum at 570 nm. Data expressed as mean $\pm$ SD; N = 3 independent experiments. **(C)** NIH/3T3 cells were pulsed with VIPER-Vax polyplex or Control-Vax polyplex for 4 h at cytotoxic polyplex doses (0.626, 1.25, 2.5, and 5 µg/mL antigen doses). NIH/3T3 cells were subsequently co-cultured for 24 h with DC2.4 cells. B3Z cells were added after 24 h of NIH/3T3-DC2.4 co-culture, and the same colorimetric assay from (B) was used to quantify cross-presentation 20-24 h after addition of B3Z cells. Data expressed as mean $\pm$ SD; N = 3 independent experiments. Statistical significance was determined using a two-tailed Student's t-test with unequal variance and Welch's correction (*$p \leq 0.05$).

132

5.3.3 *Cytotoxic T cell response in healthy mice*

Armed with a dual antigen/adjuvant delivery system capable of inducing efficient cross-presentation of peptide antigens *in vitro*, we sought to establish whether VIPER-Vax could elicit a therapeutically relevant antigen-specific CTL response in tumor-naïve mice. Inspired by the body of nanovaccine literature, we hypothesized that nanoformulation of antigen and adjuvant would lead to a greater adaptive immune response compared to injections of soluble mixtures of vaccine components due to enhanced vaccine co-delivery to APCs and reduced lymphatic clearance.[8–10] We further hypothesized that delivery of poly(I:C) in the context of VIPER-enhanced antigen cross-presentation would result in greater expansion and functional maturation of anti-SIINFEKL CTLs than that achieved with the Control-Vax formulation lacking endosomal escape. In contrast to previously reported endosomolytic vaccine vectors,[15,16,22,23,49] the VIPER platform enables an isolated investigation of the impact of antigen delivery location on vaccine productivity, which is solely dictated by the presence (cytoplasmic delivery) or absence (endosomal delivery) of melittin in the micelle core. Thus, VIPER-Vax offers the opportunity to study T cell responses generated by antigens primarily processed through the cytosolic cross-presentation pathway, whereas Control-Vax antigens are more likely to be processed through the vacuolar cross-presentation pathway.[34,35]

As a first step towards characterizing the cellular immune responses generated by our endosomolytic nanovaccine, we intradermally vaccinated healthy mice with various [CSS]SIINFEKL/poly(I:C) formulations on days 1 and 21 and analyzed splenocyte CTLs using tetramer staining and ICCS on day 28 (**Figure 5.5**; **Supplemental Figure 5.11**). Compared to mice vaccinated with soluble CSSSIINFEKL/poly(I:C), mice vaccinated with VIPER-Vax had

significantly more tetramer$^+$ CD8$^+$ T cells (4.57% vs. 2.55%) and significantly more antigen-specific IFN-γ^+ CTLs (6.85% vs. 1.86%). While mice treated with Control-Vax also exhibited an increased antigen-specific CTL response relative to mice treated with soluble CSSSIINFEKL/poly(I:C), this increase was not significant. Surprisingly, vaccination with SIINFEKL/poly(I:C) yielded no detection of antigen specific T cells beyond assay background established by vehicle treated mice.
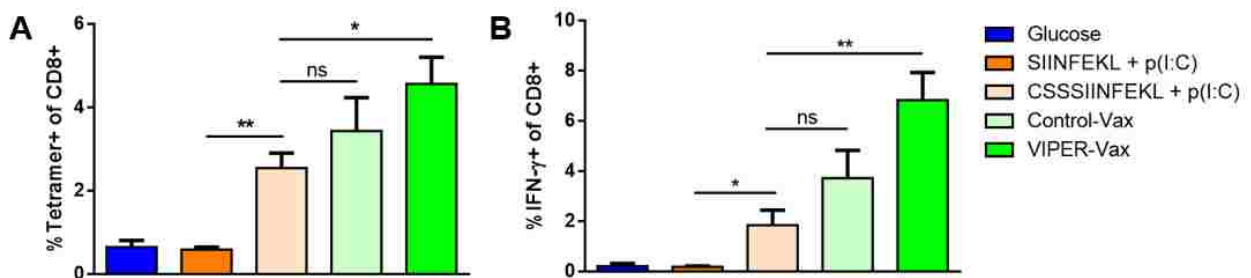

Figure 5.5 Polyplex vaccination enhances the generation of antigen-specific cytotoxic T cells. On D1 and D21, 6 week old female C57Bl/6 (N=6) were vaccinated intradermally at the base of the tail with various formulations containing 10 µg antigen and 17.5 µg poly(I:C) in 50 µL of 5% glucose or with 5% glucose alone. On D28, spleens were harvested and dissociated splenocytes were either directly stained with H-2K(b) SIINFEKL Tetramer **(A)** or restimulated in culture with 20 µg/mL SIINFEKL for 8 h before intracellular cytokine staining for IFN-γ **(B)**. Data are plotted as the mean + SEM and significance derived from Student's t-test. (* $p < 0.05$, ** $p < 0.01$)

These results benchmark VIPER-Vax among the most potent SIINFEKL vaccines reported to date and strongly reinforce the correlation between APC cross-presentation efficiency and antigen-specific CTL response levels.[16,41,50,51] Vaccination with VIPER-Vax not only generated the largest number of anti-SIINFEKL CD8$^+$ T cells of any formulation tested in this study as measured by surface tetramer staining (4.6%), it generated an even more dramatic increase in the number of CD8$^+$ T cells with antigen-specific CTL effector phenotype (> 3.5-fold increase in %IFN-γ^+ vs. CSSSIINFEKL). Both VIPER-Vax and Control-Vax formulations tested herein generated a greater antigen-specific cellular immune response than either soluble antigen/adjuvant mixture,

corroborating the importance of co-delivering antigens and adjuvants to individual APCs. The poor performance of SIINFEKL/poly(I:C) relative to CSSSIINFEKL/poly(I:C) has been reported in a previous study[41] and is attributed to less efficient MHCI loading in the absence of the CSS linker.[42] Overall, these data show that VIPER-Vax immunization produces large quantities of antigen-specific CTLs with robust IFN-γ expression and that inclusion of melittin in the VIPER formulation is necessary to significantly enhance adaptive immune responses over those elicited by traditional vaccine formulations.

5.3.4   *Therapeutic vaccination and tumor survival*

Having validated that VIPER-Vax induces a potent anti-SIINFEKL CTL response, we sought to evaluate the therapeutic relevance of this response in mice bearing syngeneic B16-OVA flank tumors. B16 tumors display rapid subcutaneous growth, metastatic-like engraftment after intravenous injection, and expression of several well-defined endogenous neoantigens that render the tumor susceptible to vaccination-induced immunity.[52] Because B16 neoantigens are typically poorly immunogenic, B16 cells expressing highly immunogenic exogenous ovalbumin (B16-OVA) are often used for initial *in vivo* screens of vaccine efficacy, where ovalbumin or its epitopes are administered as antigens to tumor-bearing mice.[40] It has also been demonstrated that strong anti-SIINFEKL CTL responses can be sufficient for total prophylactic protection from B16-OVA tumors.[41]

Therapeutic vaccination with VIPER-Vax was performed on days 4 and 11 after B16-OVA tumor inoculation with dosing equivalent to our previous study in healthy mice (**Figure 5.6A**). Average tumor growth rates and the survival of VIPER-Vax–vaccinated mice were benchmarked against

those of mice vaccinated with (i) soluble mixture SIINFEKL and poly(I:C), (ii) SIINFEKL and poly(I:C) emulsified in IFA, or (iii) vehicle (5% glucose). All vaccine formulations delayed tumor growth and statistically prolonged survival relative to vehicle (**Figure 5.6B-C**). Notably, vaccination with VIPER-Vax dramatically delayed tumor growth in a subset of mice (3 of 8 mice) and extended their survival beyond all other mice in the study (**Figure 5.6C**, **Supplemental Figure 5.12**). Terminal analysis in this subset of mice further showed that only 0.75% of $CD8^+$ splenocytes were IFN-γ^+ and that 44% of tumor-infiltrating $CD45^+CD8^+$ lymphocytes (TILs) were PD-1^+ (**Supplemental Figure 5.13**). While vaccination improved survival compared to control mice, survival rates between the vaccine treatment groups were not statistically different (**Figure 5.6C**).
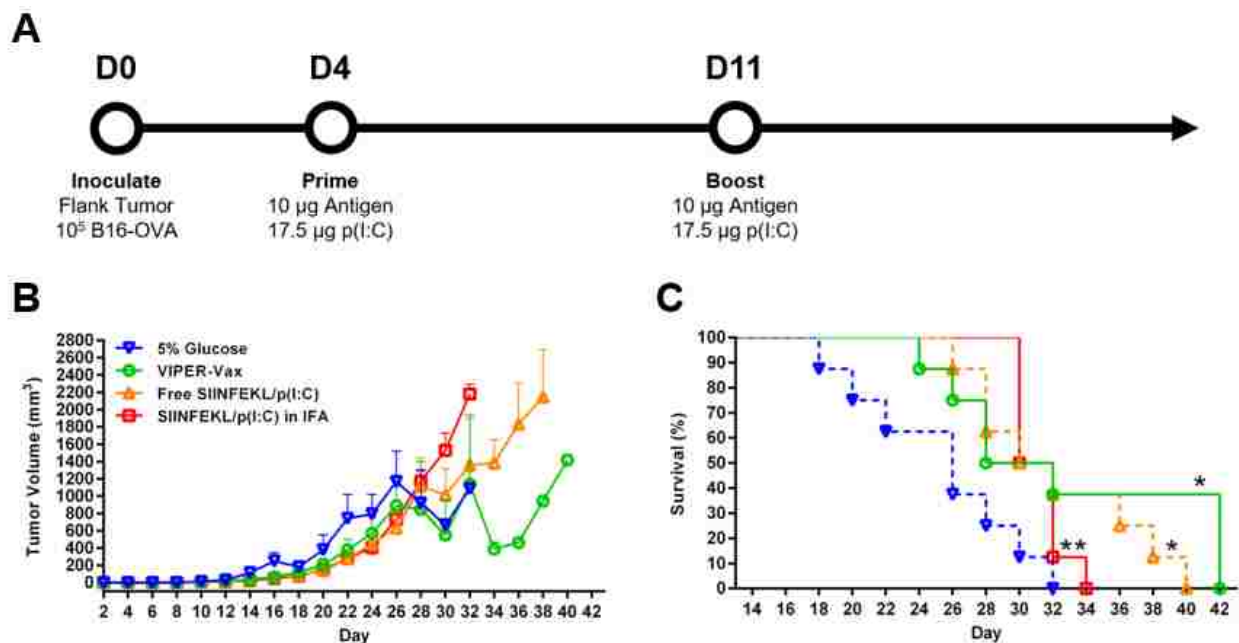

Figure 5.6 Therapeutic polyplex vaccination delays tumor growth and prolongs survival of a subset of B16-OVA tumor-bearing mice.
(A) 6- to 8-week–old female C57BL/6 mice were subcutaneously inoculated with 105 B16-OVA cells and randomized into various treatment groups (N = 8). On D4 and D11, mice were vaccinated intradermally at the right base of the tail with various formulations containing 10 µg antigen and 17.5 µg poly(I:C). 5% glucose was used as a vehicle control. Tumor volume and animal weight were measured every other day. Animals were euthanized when tumor mass exceeded 10% body weight, when body weight loss exceeded 20%, or when severe tumor ulceration was observed. **(B)** Average tumor volumes as measured over the course of 42 days. Data expressed as mean + SEM. **(C)** Kaplan-Meyer survival curves for mice immunized with vehicle in comparison to vaccine

formulations. All vaccine formulations prolonged survival relative to vehicle. VIPER-Vax extends survival in a subset of mice (3/8). Statistical significance was determined using a logrank test (*p-value ≤ 0.05; **p-value ≤ 0.01).

Although immunization with VIPER-Vax generated strong anti-SIINFEKL CTL responses in healthy mice, therapeutic vaccination with VIPER-Vax in B16-OVA–bearing mice failed to significantly improve survival outcomes over vaccination with conventional formulations. Although we did not perform terminal flow cytometry analysis on all tumor-bearing mice, analyzing the CTL content of tumors from the three longest-surviving VIPER-Vax–treated mice provided some insight into limitations of our nanovaccine formulation. These mice displayed high rates of TIL exhaustion and relatively low surviving numbers of antigen-specific CTLs compared to those generated in healthy mice, characteristics commonly observed in T cell populations that have been defeated by immunosuppressive solid tumors.[2,5]

Prior work has also shown that cationic polyplexes aggregate after injection into the dermis, likely because of charge interactions between cationic polymer side groups and anionic extracellular matrix (ECM) components.[53,54] We suspect this aggregation may slow uptake of polyplexes by skin-resident APCs, reducing the rate of antigen transport to LNs. Thus, intradermal vaccination with VIPER-Vax may not prime a sufficiently rapid immune response against aggressive cancers like B16 melanoma. The persistence of antigen in peripheral tissue may also result in antigen tolerance or CTL fratricide, a documented disadvantage of slow-releasing vaccine formulations like IFA.[5] Indeed, immunization with an IFA emulsion of antigen and adjuvant provided the least therapeutic benefit of the vaccine formulations tested in this study. Given these results, we expect that VIPER-Vax would perform better as a prophylactic vaccine, but that its therapeutic efficacy could also be improved by the addition of MHCII antigen epitopes to stimulate a T_H1 CD4 T cell

response or by co-administration of immune checkpoint inhibiting antibodies.[1,55] Future work in our laboratory is focused on altering the surface chemistry of VIPER micelles to enable rapid trafficking to LN APCs to address these issues.

5.4   CONCLUSION

We present VIPER-Vax, a polymer micelle/poly(I:C) polyplex nanovaccine that leverages endosomal pH-sensitive exposure of encapsulated lytic peptides to achieve cytoplasmic delivery of peptide antigens. In an effort to define the impact of endosomal disruption on antigen cross presentation and resulting cellular immune responses, we first optimized design parameters governing endosomal escape functionality and verified that enhanced endosomal disruption correlates with increased cross-presentation *in vitro*. Both endosomolytic (VIPER-Vax) and non-lytic (Control-Vax) polyplex nanovaccines evaluated herein mediated cross-presentation *in vitro* and generated larger numbers of CTLs *in vivo* than soluble antigen/adjuvant mixtures, but only VIPER-Vax achieved statistically significant improvements in these metrics. While therapeutic vaccination with VIPER-Vax delayed B16-OVA tumor growth in a subset of mice, it ultimately did not consistently outperform traditional antigen/adjuvant mixtures. This lack of therapeutic efficacy was likely due to slow T cell priming kinetics, which may be caused by polyplex depot formation after intradermal VIPER-Vax administration. In summary, we have provided direct evidence that melittin-mediated endosomal disruption increases cross-presentation and improves the quantity and quality of antigen-specific CTLs. Future work will focus on new micelle surface chemistries that facilitate rapid trafficking of VIPER-Vax to APCs *in vivo*, thereby enabling further investigation of how cytosolic antigen localization in APCs affects therapeutic CTL responses in aggressive cancer models.

**Supplemental Figure 5.7** Polyplex characterization
Cationic polymer micelles were mixed with the dsRNA adjuvant high molecular weight poly(I:C) at various N/P ratios. Nucleic acid packaging efficiency was characterized by gel retardation **(A)** and polyplex size was evaluated by dynamic light scattering (DLS; **B**). Data are plotted as mean + SD of three independent measurements.
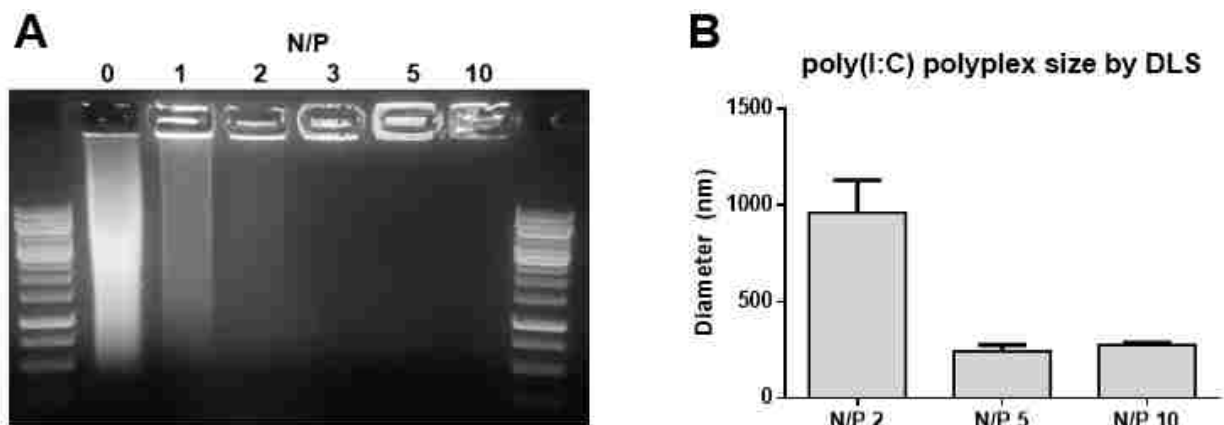
**Supplemental Figure 5.8** Uptake of fluorescently labeled antigen in DC2.4 cells
DC2.4 cells were incubated with 2 µg/mL rhodamine-conjugated CSSSIINFEKL delivered in various formulations (soluble peptide, cationic micelle, or N/P 10 poly(I:C) polyplex) for various times before uptake was quantified by flow cytometry. Data are plotted as mean + SD from three independent experiments and statistical significance derived from Student's t-test. (* $p < 0.05$, ** $p < 0.01$)
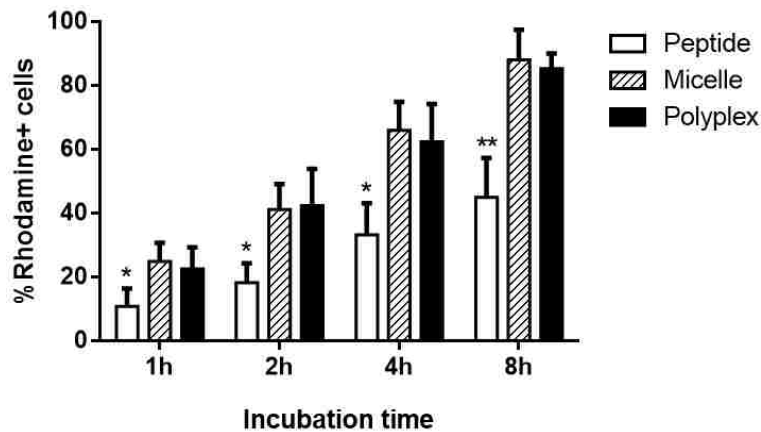
Supplemental Figure 5.9 Cell viability in B3Z assays
(A) DC2.4 cells were pulsed with 2.5 µg/mL SIINFEKL delivered as either soluble CSSSIINFEKL peptide, VIPER-Vax polyplex, or Control-Vax polyplex for 2 h. An MTS assay was used to measure cell viability 20-24 h after pulsing. Data expressed as mean ± SD; N = 3 independent experiments. **(B)** NIH/3T3 cells were pulsed with VIPER-Vax polyplex or Control-Vax polyplex for 4 h at the indicated antigen doses. An MTS assay was used to measure cell viability 24 h after pulsing. Data expressed as mean ± SD; N = 3 independent experiments.
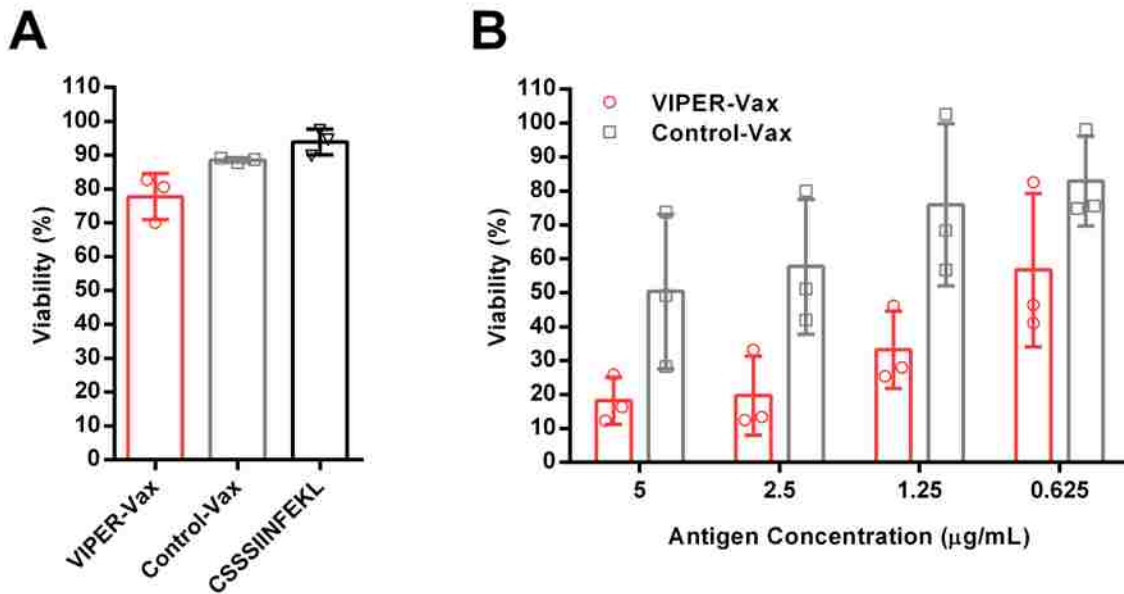
Supplemental Figure 5.10 Representative scatter plots of CD8 and IFN-γ staining in SIINFEKL-restimulated splenocytes
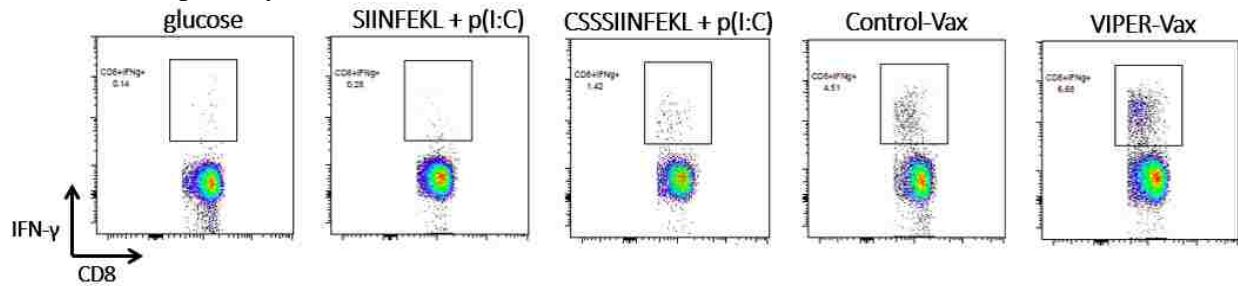
Supplemental Figure 5.11 Spider plots of B16-OVA tumor growth in individual mice.
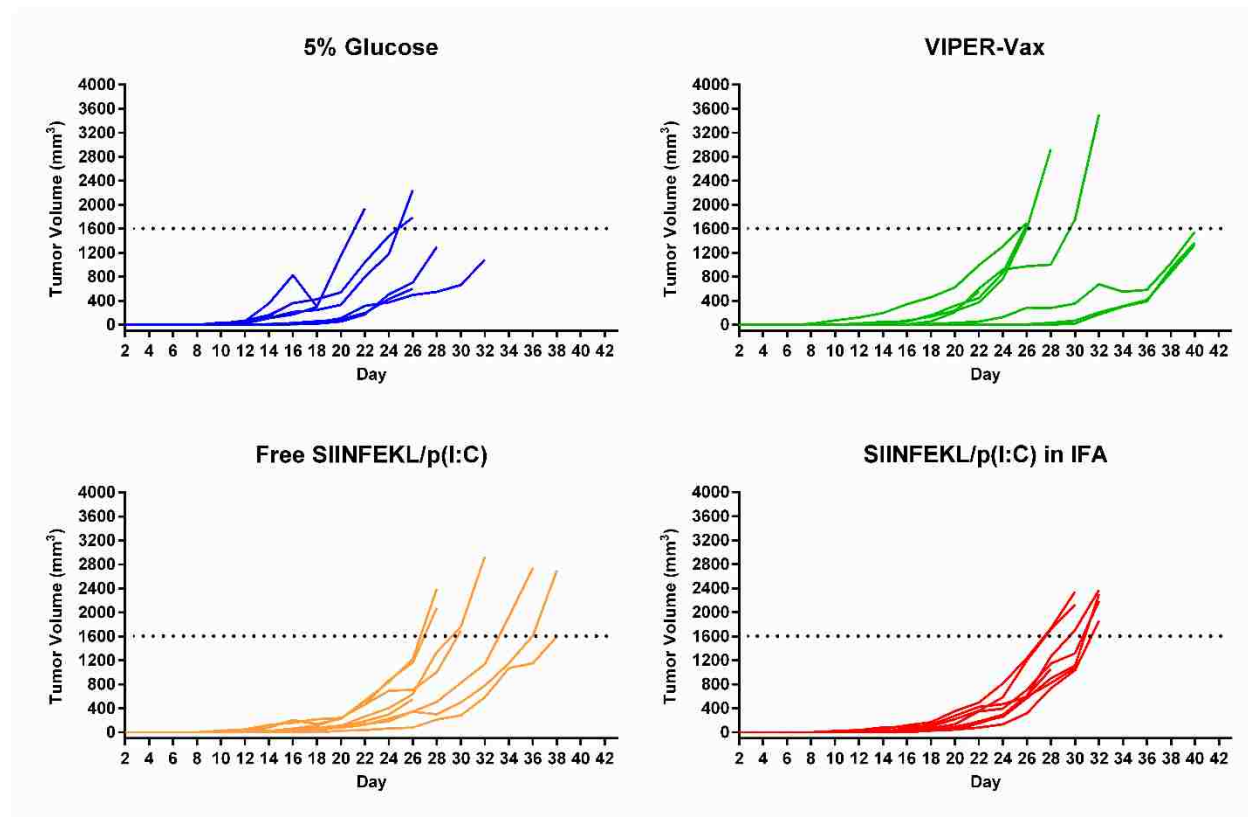
Supplemental Figure 5.12 At time of sacrifice, tumorbearing mice have relatively few CTLs and their tumor infiltrating lymphocytes express PD-1.

(A) On D42 of the tumor survival study, spleens were harvested from final surviving VIPER-vax mice (N =3) and naïve mice (N = 3). Dissociated splenocytes were restimulated in culture with 20 µg/mL SIINFEKL for 8 h before intracellular cytokine staining for IFN-γ. Data are plotted as the mean + SD and statistical significance derived from Student's t-test. (* $p < 0.05$) **(B)** On D42 of the tumor study described in Figure 7, tumors were harvested from final surviving VIPER-vax mice (N =3) and dissociated into single cell suspensions for flow cytometry. Histograms of PD-1 expression in tumor infiltrating CD45$^+$/CD8$^+$ cells from a VIPER-Vax treated mouse intended to show the gating strategy for determining %PD-1$^+$.
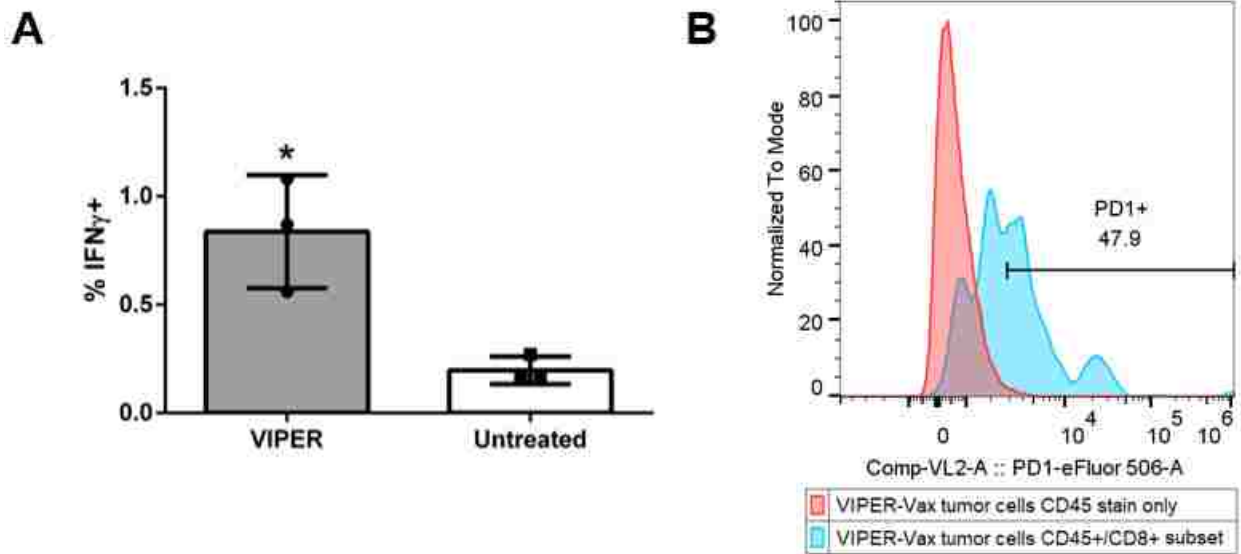
BIBLIOGRAPHY

(1)   Hu, Z.; Ott, P. A.; Wu, C. J. Towards Personalized, Tumour-Specific, Therapeutic Vaccines for Cancer. *Nature Reviews Immunology*. Nature Publishing Group December 11, 2018, pp 168–182.

(2)   Chen, D. S. S.; Mellman, I. Oncology Meets Immunology: The Cancer-Immunity Cycle. *Immunity* **2013**, *39* (1), 1–10.

(3)   Bezu, L.; Kepp, O.; Cerrato, G.; Pol, J.; Fucikova, J.; Spisek, R.; Zitvogel, L.; Kroemer, G.; Galluzzi, L. Trial Watch: Peptide-Based Vaccines in Anticancer Therapy. *Oncoimmunology* **2018**, *7* (12), e1511506.

(4)   O'Neill, L. A. J.; Hennessy, E. J.; Parker, A. E. Targeting Toll-like Receptors: Emerging Therapeutics? *Nature Reviews Drug Discovery*. Nature Publishing Group April 1, 2010, pp 293–307.

(5)   Melief, C. J. M.; Van Der Burg, S. H. Immunotherapy of Established (Pre)Malignant Disease by Synthetic Long Peptide Vaccines. *Nature Reviews Cancer*. May 2008, pp 351–360.

(6)   Deres, K.; Schild, H.; Wiesmüller, K.-H.; Jung, G.; Rammensee, H.-G. In Vivo Priming of Virus-Specific Cytotoxic T Lymphocytes with Synthetic Lipopeptide Vaccine. *Nature* **1989**, *342* (6249), 561–564.

(7)   Hong, E.; Dobrovolskaia, M. A. Addressing Barriers to Effective Cancer Immunotherapy with Nanotechnology: Achievements, Challenges, and Roadmap to the next Generation of Nanoimmunotherapeutics. *Adv. Drug Deliv. Rev.* **2019**, *141*, 3–22.

(8)   Zhang, R.; Billingsley, M. M.; Mitchell, M. J. Biomaterials for Vaccine-Based Cancer Immunotherapy. *J. Control. Release* **2018**, *292*, 256–276.

(9)   Zhu, G.; Zhang, F.; Ni, Q.; Niu, G.; Chen, X. Efficient Nanovaccine Delivery in Cancer Immunotherapy. *ACS Nano* **2017**, *11* (3), 2387–2392.

(10)   Irvine, D. J.; Swartz, M. A.; Szeto, G. L. Engineering Synthetic Vaccines Using Cues from Natural Immunity. *Nat. Mater.* **2013**, *12* (11), 978–990.

(11)   Yoon, H. Y.; Selvan, S. T.; Yang, Y.; Kim, M. J.; Yi, D. K.; Kwon, I. C.; Kim, K. Engineering Nanoparticle Strategies for Effective Cancer Immunotherapy. *Biomaterials* **2018**, *178*, 597–607.

(12)   Goldberg, M. S. Immunoengineering: How Nanotechnology Can Enhance Cancer Immunotherapy. *Cell*. Elsevier April 9, 2015, pp 201–204.

(13)   Hubbell, J. A.; Thomas, S. N.; Swartz, M. A. Materials Engineering for Immunomodulation. *Nature*. November 26, 2009, pp 449–460.

(14)   Ali, O. A.; Huebsch, N.; Cao, L.; Dranoff, G.; Mooney, D. J. Infection-Mimicking Materials to Program Dendritic Cells in Situ. *Nat. Mater.* **2009**, *8* (2), 151–158.

(15)   Yuhua, H.; Litwin, T.; Nagaraja, A. R.; Kwong, B.; Katz, J.; Watson, N.; Irvine, D. J.; Hu, Y.; Litwin, T.; Nagaraja, A. R.; et al. Cytosolic Delivery of Membrane-Impermeable Molecules in Dendritic Cells Using PH-Responsive Core-Shell Nanoparticles. *Nano Lett.* **2007**, *7* (10), 3056–3064.

(16)   Wilson, J. T.; Keller, S.; Manganiello, M. J.; Cheng, C.; Lee, C.-C.; Opara, C.; Convertine, A.; Stayton, P. S. PH-Responsive Nanoparticle Vaccines for Dual-Delivery of Antigens and Immunostimulatory Oligonucleotides. *ACS Nano* **2013**, *7* (5), 3912–3925.

(17)   Shen, H.; Ackerman, A. L.; Cody, V.; Giodini, A.; Hinson, E. R.; Cresswell, P.; Edelson, R. L.; Saltzman, W. M.; Hanlon, D. J. Enhanced and Prolonged Cross-Presentation

Following Endosomal Escape of Exogenous Antigens Encapsulated in Biodegradable Nanoparticles. *Immunology* **2006**, *117* (1), 78–88.

(18) Varkouhi, A. K.; Scholte, M.; Storm, G.; Haisma, H. J. Endosomal Escape Pathways for Delivery of Biologicals. *J. Control. Release* **2011**, *151* (3), 220–228.

(19) Lönn, P.; Kacsinta, A. D.; Cui, X.-S.; Hamil, A. S.; Kaulich, M.; Gogoi, K.; Dowdy, S. F. Enhancing Endosomal Escape for Intracellular Delivery of Macromolecular Biologic Therapeutics. *Nat. Publ. Gr.* **2016**, *6* (March), 32301.

(20) Stewart, M. P.; Lorenz, A.; Dahlman, J.; Sahay, G. Challenges in Carrier-Mediated Intracellular Delivery: Moving beyond Endosomal Barriers. *Wiley Interdisc. Rev. Nanomedicine Nanobiotechnology* **2016**, *8* (3), 465–478.

(21) Howland, S. W.; Wittrup, K. D. Antigen Release Kinetics in the Phagosome Are Critical to Cross-Presentation Efficiency. *J. Immunol.* **2008**, *180* (3), 1576–1583.

(22) Hornung, V.; Bauernfeind, F.; Halle, A.; Samstad, E. O.; Kono, H.; Rock, K. L.; Fitzgerald, K. A.; Latz, E. Silica Crystals and Aluminum Salts Activate the NALP3 Inflammasome through Phagosomal Destabilization. *Nat. Immunol.* **2008**, *9* (8), 847–856.

(23) Demento, S. L.; Eisenbarth, S. C.; Foellmer, H. G.; Platt, C.; Caplan, M. J.; Mark Saltzman, W.; Mellman, I.; Ledizet, M.; Fikrig, E.; Flavell, R. A.; et al. Inflammasome-Activating Nanoparticles as Modular Systems for Optimizing Vaccine Efficacy. *Vaccine* **2009**, *27* (23), 3013–3021.

(24) Baljon, J. J.; Dandy, A.; Wang-Bishop, L.; Wehbe, M.; Jacobson, M. E.; Wilson, J. T. The Efficiency of Cytosolic Drug Delivery Using PH-Responsive Endosomolytic Polymers Does Not Correlate with Activation of the NLRP3 Inflammasome. *Biomater. Sci.* **2019**.

(25) Foster, S.; Duvall, C. L.; Crownover, E. F.; Hoffman, A. S.; Stayton, P. S. Intracellular Delivery of a Protein Antigen with an Endosomal-Releasing Polymer Enhances CD8 T-Cell Production and Prophylactic Vaccine Efficacy. *Bioconjug. Chem.* **2010**, *21* (12), 2205–2212.

(26) Wilson, J. T.; Postma, A.; Keller, S.; Convertine, A. J.; Moad, G.; Rizzardo, E.; Meagher, L.; Chiefari, J.; Stayton, P. S. Enhancement of MHC-I Antigen Presentation via Architectural Control of PH-Responsive, Endosomolytic Polymer Nanoparticles. *AAPS J.* **2015**, *17* (2), 358–369.

(27) Keller, S.; T.wilson, J.; Patilea, G. I.; Kern, H. B.; Convertine, A. J.; Stayton, P. S. Neutral Polymer Micelle Carriers with PH-Responsive, Endosome-Releasing Activity Modulate Antigen Trafficking to Enhance CD8+T Cell Responses. *J. Control. Release* **2014**, *191*, 24–33.

(28) Cheng, Y.; Yumul, R. C.; Pun, S. H. Virus-Inspired Polymer for Efficient In Vitro and In Vivo Gene Delivery. *Angew. Chemie - Int. Ed.* **2016**, *55* (39), 12013–12017.

(29) Feldmann, D. P.; Cheng, Y.; Kandil, R.; Xie, Y.; Mohammadi, M.; Harz, H.; Sharma, A.; Peeler, D. J.; Moszczynska, A.; Leonhardt, H.; et al. In Vitro and in Vivo Delivery of SiRNA via VIPER Polymer System to Lung Cells. *J. Control. Release* **2018**, *276*, 50–58.

(30) Peeler, D. J.; Thai, S. N.; Cheng, Y.; Horner, P. J.; Sellers, D. L.; Pun, S. H. PH-Sensitive Polymer Micelles Provide Selective and Potentiated Lytic Capacity to Venom Peptides for Effective Intracellular Delivery. *Biomaterials* **2019**, *192*, 235–244.

(31) Shir, A.; Ogris, M.; Wagner, E.; Levitzki, A. EGF Receptor-Targeted Synthetic Double-Stranded RNA Eliminates Glioblastoma, Breast Cancer, and Adenocarcinoma Tumors in Mice. *PLoS Med.* **2006**, *3* (1), 125–135.

(32) Kilchrist, K. V.; Dimobi, S. C.; Jackson, M. A.; Evans, B. C.; Werfel, T. A.; Dailing, E.

A.; Bedingfield, S. K.; Kelly, I. B.; Duvall, C. L. Gal8 Visualization of Endosome Disruption Predicts Carrier-Mediated Biologic Drug Intracellular Bioavailability. *ACS Nano*. American Chemical Society January 18, 2019, p acsnano.8b05482.

(33) Karttunen, J.; Sanderson, S.; Shastri, N. Detection of Rare Antigen-Presenting Cells by the LacZ T-Cell Activation Assay Suggests an Expression Cloning Strategy for T-Cell Antigens. *Proc. Natl. Acad. Sci. U. S. A.* **1992**, *89* (13), 6020–6024.

(34) Sánchez-Paulete, A. R.; Teijeira, A.; Cueto, F. J.; Garasa, S.; Pérez-Gracia, J. L.; Sánchez-Arráez, A.; Sancho, D.; Melero, I. Antigen Cross-Presentation and T-Cell Cross-Priming in Cancer Immunology and Immunotherapy. *Annals of Oncology*. Oxford University Press December 1, 2017, pp xii44–xii55.

(35) Joffre, O. P.; Segura, E.; Savina, A.; Amigorena, S. Cross-Presentation by Dendritic Cells. *Nat. Rev. Immunol.* **2012**, *12* (8), 557–569.

(36) Mantegazza, A. R.; Magalhaes, J. G.; Amigorena, S.; Marks, M. S. Presentation of Phagocytosed Antigens by MHC Class I and II. *Traffic* **2013**, *14* (2), 135–152.

(37) Moore, M. W.; Carbone, F. R.; Bevan, M. J. Introduction of Soluble Protein into the Class I Pathway of Antigen Processing and Presentation. *Cell* **1988**, *54* (6), 777–785.

(38) Li, Y.; Zhao, T.; Wang, C.; Lin, Z.; Huang, G.; Sumer, B. D.; Gao, J. Molecular Basis of Cooperativity in PH-Triggered Supramolecular Self-Assembly. *Nat. Commun.* **2016**, *7*, 13214.

(39) Zhou, K.; Wang, Y.; Huang, X.; Luby-Phelps, K.; Sumer, B. D.; Gao, J. Tunable, Ultrasensitive PH-Responsive Nanoparticles Targeting Specific Endocytic Organelles in Living Cells. *Angew. Chem. Int. Ed. Engl.* **2011**, *50* (27), 6109–6114.

(40) Bellone, M.; Cantarella, D.; Castiglioni, P.; Crosti, M. C.; Ronchetti, A.; Moro, M.; Garancini, M. P.; Casorati, G.; Dellabona, P. Relevance of the Tumor Antigen in the Validation of Three Vaccination Strategies for Melanoma. *J. Immunol.* **2000**, *165* (5), 2651–2656.

(41) Kuai, R.; Ochyl, L. J.; Bahjat, K. S.; Schwendeman, A.; Moon, J. J. Designer Vaccine Nanodiscs for Personalized Cancer Immunotherapy. *Nat. Mater.* **2017**, *16* (4), 489–496.

(42) Hirosue, S.; Kourtis, I. C.; van der Vlies, A. J.; Hubbell, J. A.; Swartz, M. A. Antigen Delivery to Dendritic Cells by Poly(Propylene Sulfide) Nanoparticles with Disulfide Conjugated Peptides: Cross-Presentation and T Cell Activation. *Vaccine* **2010**, *28* (50), 7897–7906.

(43) Hafner, A. M.; Corthésy, B.; Merkle, H. P. Particulate Formulations for the Delivery of Poly(I:C) as Vaccine Adjuvant. *Adv. Drug Deliv. Rev.* **2013**, *65* (10), 1386–1399.

(44) Jewell, C. M.; Bustamante Lopez, S. C.; Irvine, D. J. In Situ Engineering of the Lymph Node Microenvironment via Intranodal Injection of Adjuvant-Releasing Polymer Particles. *Proc. Natl. Acad. Sci.* **2011**, *108* (38), 15745–15750.

(45) Zaks, K.; Jordan, M.; Guth, A.; Sellins, K.; Kedl, R.; Izzo, A.; Bosio, C.; Dow, S. Efficient Immunization and Cross-Priming by Vaccine Adjuvants Containing TLR3 or TLR9 Agonists Complexed to Cationic Liposomes. *J. Immunol.* **2006**, *176* (12), 7335–7345.

(46) Schaffert, D.; Kiss, M.; Rödl, W.; Shir, A.; Levitzki, A.; Ogris, M.; Wagner, E. Poly(I:C)-Mediated Tumor Growth Suppression in EGF-Receptor Overexpressing Tumors Using EGF-Polyethylene Glycol-Linear Polyethylenimine as Carrier. *Pharm. Res.* **2011**, *28* (4), 731–741.

(47) Nordly, P.; Rose, F.; Christensen, D.; Nielsen, H. M.; Andersen, P.; Agger, E. M.; Foged,

C. Immunity by Formulation Design: Induction of High CD8+ T-Cell Responses by Poly(I:C) Incorporated into the CAF01 Adjuvant via a Double Emulsion Method. *J. Control. Release* **2011**, *150* (3), 307–317.

(48) Palumbo, R. N.; Zhong, X.; Wang, C. Polymer-Mediated DNA Vaccine Delivery via Bystander Cells Requires a Proper Balance between Transfection Efficiency and Cytotoxicity. *J. Control. Release* **2012**, *157* (1), 86–93.

(49) Murthy, N.; Xu, M.; Schuck, S.; Kunisawa, J.; Shastri, N.; Fréchet, J. M. A Macromolecular Delivery Vehicle for Protein-Based Vaccines: Acid-Degradable Protein-Loaded Microgels. *Proc. Natl. Acad. Sci.* **2003**, *100* (9), 4995–5000.

(50) Luo, M.; Wang, H.; Wang, Z.; Cai, H.; Lu, Z.; Li, Y.; Du, M.; Huang, G.; Wang, C.; Chen, X.; et al. A STING-Activating Nanovaccine for Cancer Immunotherapy. *Nat. Nanotechnol.* **2017**, No. April.

(51) Wilson, D. S.; Hirosue, S.; Raczy, M. M.; Bonilla-Ramirez, L.; Jeanbart, L.; Wang, R.; Kwissa, M.; Franetich, J.-F.; Broggi, M. A. S.; Diaceri, G.; et al. Antigens Reversibly Conjugated to a Polymeric Glyco-Adjuvant Induce Protective Humoral and Cellular Immunity. *Nat. Mater.* **2019**, *18* (2), 175–185.

(52) Overwijk, W. W.; Restifo, N. P. B16 as a Mouse Model for Human Melanoma. In *Current Protocols in Immunology*; NIH Public Access, 2001; Vol. Chapter 20, p Unit 20.1.

(53) Zhong, X.; Han, W.; Wang, C.; Ji, W.; Palumbo, R. N.; Panus, D. Transgene Expression and Local Tissue Distribution of Naked and Polymer-Condensed Plasmid DNA after Intradermal Administration in Mice. *J. Control. Release* **2012**, *159* (2), 232–239.

(54) Burke, R. S.; Pun, S. H. Extracellular Barriers to in Vivo PEI and PEGylated PEI Polyplex-Mediated Gene Delivery to the Liver. *Bioconjug. Chem.* **2008**, *19* (3), 693–704.

(55) Nam, J.; Son, S.; Park, K. S.; Zou, W.; Shea, L. D.; Moon, J. J. Cancer Nanomedicine for Combination Cancer Immunotherapy. *Nat. Rev. Mater.* **2019**, *4* (6), 398–414.

Chapter 6. POLYMERIC STRATEGIES TO IMPROVE DRUG DELIVERY IN CANCER IMMUNOTHERAPY

Abstract

Our previous work shows that the pH-responsive, lytic peptide-concealing micelle core of the VIPER system can efficiently navigate endosomal barriers to the cytosolic delivery of both nucleic acids and subunit vaccines. However, we have also shown that VIPER's cationic corona strongly interacts with components of the extracellular matrix, and have posited that these interactions restrict the speed of innate immune responses to VIPER vaccination. In this chapter, we describe our efforts to refine the surface chemistry of VIPER micelles to enable rapid transport to the antigen presenting cells of the lymph nodes following intradermal or subcutaneous vaccination. We also describe a next-generation polymer incorporating the small molecule adjuvant resiquimod, and propose a high-throughput method for the identification of future polymer architectures that maximize *in vivo* immune responses.

6.1 SYNTHESIS OF NEUTRALLY CHARGED VIPER VARIANTS

6.1.1 *Motivation*

As described earlier (**Chapter 5.1**), productive therapeutic vaccination against cancer requires rapid cross-presentation of antigens by professional antigen presenting cells (APCs) to CD8^{+} T cells in the lymph node (LN). Cross-presentation is performed nearly exclusively by specific subsets of dendritic cells (DCs) that are either lymphoid resident (CD8+CD11b- and CD8-CD11b+ DCs) or migrate to the lymph node from peripheral tissue (CD103+CD11b- and CD103-CD11b+).[1,2] Nanovaccines have been developed to target cells in each of these locations following subcutaneous or intradermal injection.[3–6] For example, nanoparticles with "stealth" steric shields have been shown to drain to the LN for uptake by LN resident DCs,[7,8] while functionalization with mannose has been shown to improve uptake by DCs[9,10] and transport to lymph nodes[11] through active targeting of peripheral DCs. While we have demonstrated that cationic VIPER-Vax polyplexes elicit potent CD8^{+} T cell responses, we showed that these responses were generated insufficiently rapidly to provide therapeutic benefit against an aggressive xenograft melanoma tumor. We hypothesize that APC uptake of these cationic materials is slow, indirect (bystander effect[12]), and spatially restricted (due to electrostatic interactions in the interstitial space[3–5]). Thus, we sought to examine whether endowing VIPER micelles with "active" (mannose) or "stealth" (PEG, HPMA) surface chemistries could enhance both the speed and magnitude of antigen accumulation in LN APCs, and whether these improvements translate into more productive T cell responses.

6.1.2 *Polymer synthesis and characterization*

In order to investigate the impact of micelle surface chemistry on VIPER micelle accumulation in lymph node resident APCs, we synthesized a panel of VIPER micelles bearing either cationic (DMAEMA), steric stealth (PEG or HPMA), or actively-targeted (MMA) shells (**Table 6.1**). RAFT polymerization conditions were optimized to yield a panel of diblock copolymers with similar molecular weights and second block structure (**Supplemental Table 6.3**). Polymer monomer composition was determined with nuclear magnetic resonance (^{1}H NMR; **Table 6.1**; **Supplemental Figure 6.7**), dispersity analyzed by aqueous gel permeation chromatography (GPC; data not shown), and micelle size characterized with dynamic light scattering (DLS; **Table 6.1**). Additionally, the Nile Red encapsulation assay described in **Chapter 2.2.7** was utilized to compare pH-responsive micelle unpackaging.

Table 6.1 VIPER variations synthesized to compare impact of micelle surface chemistry

Surface Chemistry	Structure (via ^{1}H NMR)	Micelle diameter (nm)
Cationic	p(OEGMA$_{8.6}$-*co*-DMAEMA$_{54.2}$)-*bl*-p(DIPAMA$_{25}$-*co*-PDSEMA$_1$)	25
PEG	PEG5k-*bl*-p(DIPAMA$_{35}$-*co*-PDSEMA$_2$)	28
HPMA	pHPMA$_{70}$-*bl*-p(DIPAMA$_{34}$-*co*-PDSEMA$_{2.2}$)	60
MMA	pMMA$_{35}$-*bl*-p(DIPAMA$_{55}$-*co*-PDSEMA$_8$)	90

OEGMA = oligo(ethylene glycol) methacrylate; MW = 300
DMAEMA= 2-(dimethylamino) ethyl methacrylate; MW = 157.2
DIPAMA = diisopropyl(amino) ethyl methacrylate; MW = 213.3
PDSEMA = pyridyl disulfide ethyl methacrylate; MW = 255.4
PEG5k = methoxy poly(ethylene glycol); MW = 5000
HPMA = N-(2-hydroxylpropyl) methacrylamide; MW = 143.2
MMA = mannose ethyl methacrylate; MW = 292.3

Owing to the flexibility of controlled free radical polymerization afforded by RAFT, all polymers were synthesized with low dispersity and with similar molecular weights. All micelle diameters were on the order of 20-100 nm; importantly, this size range has been shown to be ideal for passive

lymphatic transport and LN retention.[3,4] Moreover, all neutrally charged micelles unpackaged ~pH 6.2, which is nearly identical to the pKa of previously characterized[13] cationic micelles and should mediate melittin exposure in the early endosome (**Figure 6.1**). It is worth noting that polymers synthesized from 5 kDa and 10 kDa macro-CTAs composed of p(OEGMA300) were found to be largely insoluble in micelle form, highlighting the difference in solubility between PEG and OEGMA brushes. (data not shown)
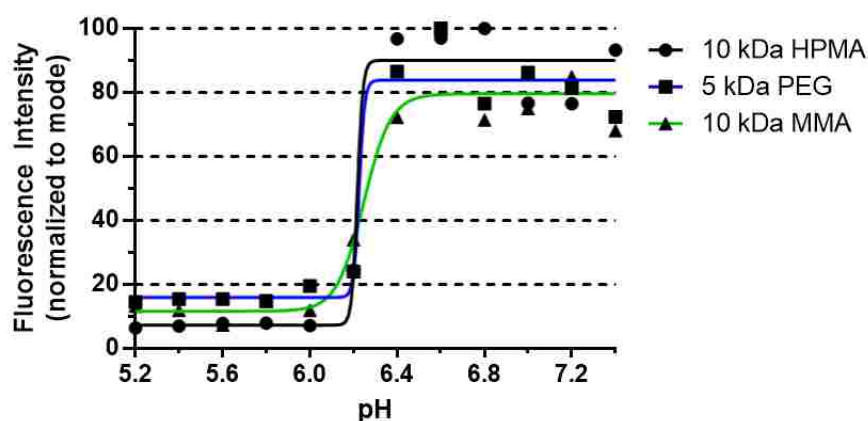

Figure 6.1 Determination of neutral VIPER pKa via Nile Red micellization assay. Neutral VIPER micelles were incubated at 0.2 mg/mL in phosphate buffer with 3 µM Nile Red for 24 h at various pH before fluorescence was determined using a plate reader. Increased fluorescence indicates that micelles are present and permitting Nile Red partitioning into their micelle core.

6.1.3 *Antigen uptake* in vitro

In order to facilitate detection of antigen transport *in vitro* and *in vivo*, all VIPER variants were conjugated with 10% rhodamine-labeled CSSSIINFEKL antigen peptide at either 1 (cationic) or 2 (all others) peptides per polymer chain as described in **Chapter 5.2.3**. In separate reactions, 1 melittin was conjugated per polymer chain in all cases (higher melittin loading is not advisable due to solubility concerns; data not shown). Mixed micelles were then formed using 2:1 antigen-polymer:melittin-polymer as described in **Chapter 5.2.3.**

All attempts to detect significant uptake of non-cationic micelles *in vitro* were unsuccessful, with no formulation achieving uptake in >20% of cells after 8 h incubation at 4 µg/mL CSSSIINFEKL. (data not shown) Uptake did not vary with cell type: we tested primary bone marrow-derived dendritic cells (BMDCs) in addition to both RAW264.7 and DC2.4 cells with or without 48 h pre-conditioning in 20 ng/mL IL-4. We were unable to induce CD206 upregulation in immortal RAW264.7 and DC2.4 cell lines; however, treatment of BMDCs with IL-4 might yet yield CD206^{high} populations capable of mannose receptor-mediated uptake of mannose VIPER formulations. Because others have previously shown that *in vitro* uptake of mannose micelles is not representative of uptake *in vivo*, we decided to move forward with *in vivo* studies.[14]

6.1.4 *Evaluation of polymer-mediated antigen uptake* in vivo

Based on prior work that demonstrates differential vaccine uptake based on particle surface chemistry and route of administration, we chose to compare LN DC uptake of cationic, PEG, HPMA, and MMA micelles following either subcutaneous (SQ) or intradermal (ID) injection.[15–17] Thus, 6-8 week old female C57Bl/6 mice were injected SQ or ID at the base of the tail with 20 µg rhodamine-CSSSIINFEKL in 5% glucose as either free peptide or micelle (N=3 per formulation per route of administration; 30 total). A Xenogen instrument was used to perform live whole body fluorescent imaging 0, 24, and 48 h after injection and to image excised inguinal LN after sacrifice at 48 h post-injection. Draining lymph nodes were dissociated into single cell suspensions using a 40 µm cell strainer and analyzed for DC (MHCII^{high}/CD11c^{high}) uptake using flow cytometry. (**Supplemental Figure 6.8**)

We observed that both route of administration and micelle formulation chemistry had an impact on LN antigen trafficking from the injection site. Whole body Xenogen imaging showed that SQ but not ID freely soluble peptide was rapidly drained from the injection site, likely due to enhanced access to lymphatic drainage in the SQ space (**Supplemental Figure 6.9**).[4] Increased retention of PEG and MMA through ID *vs.* SQ injection was also observed. As expected, cationic micelles were not noticeably cleared from either SQ or ID injection sites at 48 h. Among the neutrally charged micelle formulations, SQ injected MMA and HPMA cleared from the injection site most rapidly, with near total loss of rhodamine signal at 48 h for both formulations. Xenogen imaging of dissected lymph nodes confirmed all neutral VIPER formulations achieved greater total LN uptake compared to cationic VIPER, but did not show clear differences between routes of administration (**Figure 6.2**). Mannose VIPER clearly demonstrated the greatest uptake of all formulations tested; in addition, LN from Mannose VIPER-treated animals were substantially larger than LN from other mice, indicating preferential immune activation by these formulations.
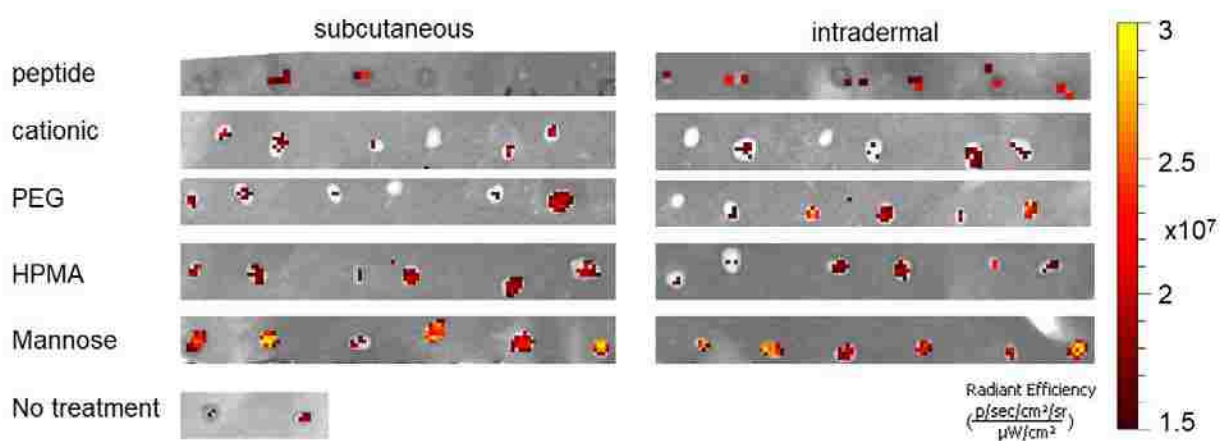

Figure 6.2 Xenogen imaging of dissected inguinal lymph nodes
Left and right inguinal lymph nodes were dissected 48 h after vaccination with rhodamine-CSSSIINFEKL in various formulations and imaged prior to dissociation for flow cytometry.

Overall, flow cytometry data echoed those obtained through Xenogen imaging. Very few rhodamine+ DCs were detected in mice treated with soluble peptide or cationic VIPER, but all neutral VIPER formulations mediated improved uptake in LN DCs relative to soluble peptide. (**Figure 6.3**; **Supplemental Figure 6.10**) Antigen uptake was higher in all cases in the right inguinal LN (ipsilateral to injection), with only mannose VIPER formulations achieving notable uptake in the left LN. (**Supplemental Figure 6.10**) While PEG and HPMA VIPER formulations showed increased LN DC uptake following ID injection relative to SQ injection, MMA VIPER was taken up to the same degree through both routes of administration and achieved the highest uptake overall (~12% of all LN DCs; **Figure 6.3**).
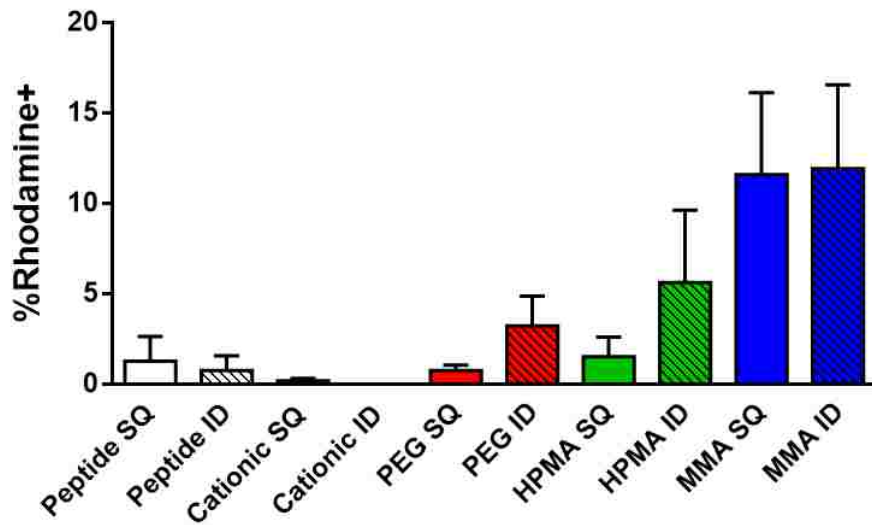

Figure 6.3 Flow cytometry of dissociated right inguinal lymph nodes assessing rhodamine-labeled antigen uptake in $CD45^{+}/MHCII^{high}/CD11c^{high}$ dendritic cells 48 h after vaccination through either intradermal (ID) or subcutaneous (SQ) injection. (N = 3 mice per bar)

Taken together, these results posit VIPER formulations with mannose surface chemistry as attractive vaccine vectors that achieve rapid delivery to LN DCs. Future studies will be needed to determine whether uptake occurs in the periphery or in the lymph node itself; additional co-staining for CD8, CD103, CD11b, and CD206 should reveal the DC subsets that are responsible

for uptake. These studies will provide additional kinetic information related to APC activation and LN trafficking, and may inform the design of micelles that can potentiate antigen cross-presentation in specific cell types.[1,2,18–21]

6.1.5 *Pilot* in vivo *T cell activation studies with mannose VIPER*

Encouraged by mannose VIPER's superior antigen delivery capabilities, we included a small number of mannose VIPER-treated animals in the T cell activation study described in **Chapter 5.3.3**. We formulated mannose VIPER mixed micelle equivalents of VIPER-Vax and Control-Vax, termed "MMA VIPER-Vax" (2:1 antigen-polymer:melittin-polymer) and "MMA Control-Vax" (2:1 antigen-polymer:control polymer) and vaccinated naïve mice with these micelle formulations as described in **Chapter 5.2.11** (N = 2). Both surface tetramer staining and intracellular IFN-γ staining showed that MMA VIPER formulations induce high levels of antigen specific T cells among CD8$^+$ splenocytes (**Figure 6.4**). Although the number of mice evaluated is far too low to consider statistical analysis, it is encouraging that MMA VIPER-Vax outperformed all other vaccine formulations by these metrics in this preliminary study, even in the absence of any poly(I:C) adjuvant. These results motivate future work that will compare the impact of melittin on vaccine productivity in the context of a mannose-targeted VIPER that incorporates adjuvant.
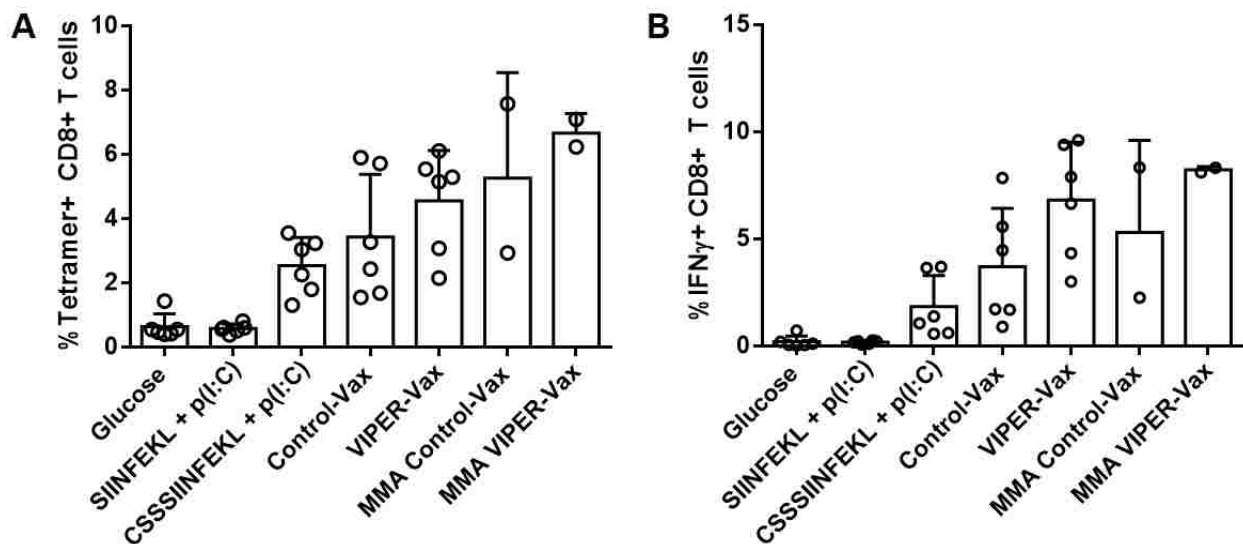
Figure 6.4 Flow cytometry of splenocytes from naïve mice vaccinated with various [CSS]SIINFEKL vaccine formulations.
All data except that from MMA mice are identical to that shown in **Figure 5.6**. Mice were immunized intradermally on D0 and D21 with 10 µg [CSS]SIINFEKL in various formulations. Terminal splenocyte analysis was conducted on D28 prior to (**A**, tetramer staining) or after (**B**, intracellular cytokine staining) SIINFEKL restimulation. (N = 6 for previously reported data; N = 2 per MMA formulation)

6.2 SYNTHESIS OF RESIQUIMOD VIPER

6.2.1 *Motivation*

Agonists of toll-like receptors (TLRs) and the stimulator of interferon genes (STING) complex are perhaps the most commonly employed anti-cancer vaccine adjuvants.[11,15,16,22–26] In short, these adjuvants initiate robust type I interferon and proinflammatory cytokine production by APCs which results in the generation of T_H1 and T_H2 responses that potentiate cellular and humoral anti-tumor activity.[22,27] Because electrostatic complexation of nucleic acid adjuvants like poly(I:C) is not readily achievable with mannose VIPER, we sought to incorporate the small molecule TLR agonist resiquimod (a.k.a. R848) into VIPER through direct polymerization of a custom self-immolative resiquimod carbamate methacrylate (SRCMA) monomer synthesized by the Stayton lab (**Figure 6.5**). Resiquimod is a potent ssRNA mimetic TLR7/8 agonist (TLR7/8a) that has been

primarily studied clinically for the activation of cellular immunity against chronic viral infections and in topical formulations for the treatment of cancers of viral origin.[28,29] While a growing body of research has sought to limit the systemic toxicity associated with oral TLR7/8a dosing through nanoformulation,[23,25,30–32] no one has utilized a drug linker that connects to the nucleobase primary amine. We hypothesize that SRCMA may not be able to activate TLRs until hydrolytic cleavage of its phenyl ester bond leads to beta-elimination of the linker and release of native resiquimod, allowing us to control the timing of TLR activation and further limit off-target effects by refining drug linker cleavage rate. Thus, we set out to incorporate SRCMA into mannose VIPER formulations with the goal of developing a targeted nanovaccine with controlled adjuvant pharmacokinetic properties and efficient endosomal escape of antigen cargo.
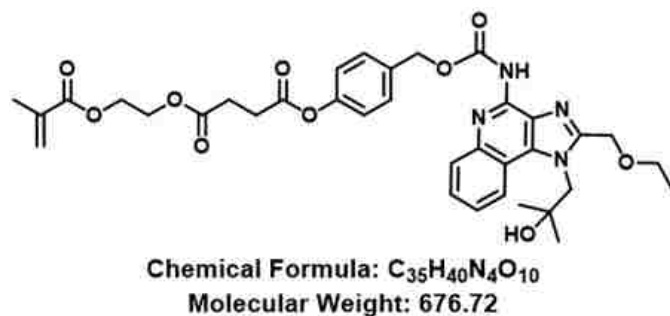

Chemical Formula: $C_{35}H_{40}N_4O_{10}$
Molecular Weight: 676.72

Figure 6.5 Structure of self-immolative resiquimod carbamate methacrylate (SRCMA) Courtesy of Selvi Srinavisan, Stayton lab (UW).

6.2.2 *Synthetic strategy and results*

Drawing on lessons from other polymeric TLR7/8a strategies, we reasoned that incorporating more than 20 mol% SRCMA in the final VIPER construct would likely limit overall solubility.[24,31] Moreover, we reasoned that co-polymerizing SRCMA with MMA as a macro-CTA (instead of incorporating it in the second block) would improve solubility and better preserve the all-or-nothing pH-responsive behavior conveyed by the DIPAMA block.[33] Thus, we designed RAFT

polymerization conditions (**Supplemental Table 6.4**) to yield full length VIPER polymers with either 10 or 20 mol% SRCMA, varying MMA monomer feeds inversely proportional to SRCMA feeds to maintain first block molecular weight at 10 kDa as in previous VIPER polymers. Of note, we employed low temperature initiation of the first block reaction and high initiator content in the second reaction in an effort to limit SRCMA cleavage during polymerizations while still achieving DIPAMA polymerization.

Our NMR data demonstrate that we have achieved the desired drug content and successfully reproduced the VIPER second block structure necessary for micelle formulation and peptide conjugation (**Table 6.5**; **Supplemental Figure 6.11**). Although we have not yet characterized the molecular weight dispersity of these polymers by aqueous GPC, we did confirm that both polymers form micelles <100 nm in diameter when dialyzed against water, reinforcing the success of the second block reaction (data not shown). Initial attempts to conjugate melittin-Cys and CSSSIINFEKL revealed that neither polymer is soluble in methanol (the solvent used in all past VIPER conjugations), and that while both polymers dissolve very well in N-methyl-2-pyrolidone (NMP), the pyridyl disulfide conjugation reaction does not proceed as determined by Abs_{343nm} measurement (data not shown).

Table 6.2 Mannose-targeted VIPER polymers containing various compositions of SRCMA. The calculation for *wt% R848 in micelle* assumes all chains are conjugated with one melittin.

Polymer chemical structure (via ^{1}H NMR)	MW (kDa)	mol% SRCMA	wt% R848 in micelle
p(MMA$_{22.1}$-*c*-SRCMA$_{8.0}$)-*bl*-p(DIPAMA$_{27.3}$-*c*-PDSEMA$_{2.0}$)	18.5	13	12
p(MMA$_{12.7}$-*c*-SRCMA$_{11.8}$)-*bl*-p(DIPAMA$_{26.7}$-*c*-PDSEMA$_{2.5}$)	18.4	22	18

6.2.3 *Future work*

Immediate next steps for this work include: optimization of solvent conditions for peptide conjugation; full characterization of the polymers by GPC; determination of micelle unpackaging pKa through a Nile Red assay; and an assessment of drug release kinetics in serum. Based on preliminary observations, it is likely that this characterization will reveal that polymers with 20 mol% SRCMA are insufficiently water soluble and that only 10 mol% SRCMA polymers should be carried forward. If solubility fully limits polymer utility, polymerization of SRCMA in the second block may improve this property. Once drug release kinetics are understood, we may optimize *in vivo* dosing through an experiment that measures total inflammatory cytokine production (e.g. IL-12p40, IP-10) achieved by various doses of SRCMA VIPER *vs.* soluble resiquimod at various times using ELISA.[24] Armed with a nanovaccine targeted with mannose and adjuvanted with resiquimod, we will be equipped to ask many meaningful questions about the timing of adjuvant release and the impact of pH-responsive endosomal escape on therapeutic innate and adaptive immune responses against cancer.

6.3 HIGH THROUGHPUT SYNTHESIS AND SCREENING OF GENETICALLY BARCODED DRUGAMERS FOR IMPROVED ADJUVANT DELIVERY IN BREAST CANCER

6.3.1 *Motivation*

Biomaterials tailored with physiochemical properties that enable controlled drug delivery to key cell types, such as antigen presenting cells (APCs) or myeloid-derived suppressor cells (MDSCs), have been sought for many years.[34–36] While basic principles that govern drug delivery to these populations have been elucidated through empirical investigations spanning the past several

decades, there remains a need for high throughput methods that can correlate high dimensional multi-parameter formulation data with cell type-specific delivery in relevant models of human disease. Dahlman et al have made important progress towards this goal by pioneering methods to quantify the biodistribution of genetically-barcoded libraries of lipid nanoparticle formulations through PCR.[37–39] However, these methods are limited by the overall narrow biodistribution of lipid nanoparticles and a reliance on FACS for the detection of cell type-specific delivery. We propose to extend material barcoding methods to the much vaster realm of polymeric delivery systems while also enabling the simultaneous scRNA-seq based identification of cell types that uptake barcoded formulations. We hypothesize that high throughput *in vivo* screening of rationally diversified polymer-drug conjugate libraries in mouse models of breast cancer will identify formulations capable of efficient resiquimod delivery to clinically relevant cell types. Beyond immediate impact in cancer immunotherapy, establishing this platform technology for *in vivo* formulation screening will dramatically expand the breadth and pace of innovation in drug delivery for any disease.

6.3.2   *Rationale and approach: Screening polymer libraries in vivo by sequencing DNA barcodes*

Our research approach leverages molecular genetic technologies to screen cutting-edge polymer-drug conjugate libraries produced in the Pun/Stayton lab in syngeneic mouse models of HER2/neu+ breast cancer in the Disis lab. (**Figure 6.6**) An ongoing collaboration between the Pun and Stayton labs has begun to reveal properties that target resiquimod-conjugated polymer to antigen presenting cells in lymph nodes following subcutaneous injection. (**Figure 6.3**) By expanding the range of formulation parameters we can screen in a single experiment, we expect that this method will not only refine our current designs for lymph node delivery but also uncover

designs that preferentially deliver to tumor cells or tumor-associated immune cells. Unpublished research performed in the Pun lab has utilized next generation sequencing for co-detection of DNA-barcoded antibodies and cellular cDNA within a scRNA-seq workflow developed by the Seelig lab (UW).[40] Conjugating similar barcode constructs to polymers should enable highly sensitive and cell-type specific biodistribution analyses based on unbiased sequencing data instead of relatively limited flow cytometry panels. Encouraged by preliminary data from our polymeric and genetic technologies, we further aim to evaluate their co-application in the syngeneic HER2/neu+ breast cancer model used in the Disis lab to test therapeutic breast cancer vaccines. The Disis lab's expertise in cancer biology will be critical for the identification of cell types retrieved from our biodistribution studies, which we expect to directly inform iterative rounds of screening and design centered on clinically meaningful targets. Excitingly, the Stayton lab has drug monomers that will enable the extension of this screening method to the delivery of chemotherapeutics or peptide vaccines in the future.[41] Thus, in pursuit of targeted small molecule cancer immunotherapy, we aim to synthesize a large, chemically diverse library of genetically barcoded polymers (Aim 1) and to demonstrate high throughput biodistribution analysis of this library in a translationally relevant model of breast cancer (Aim 2).
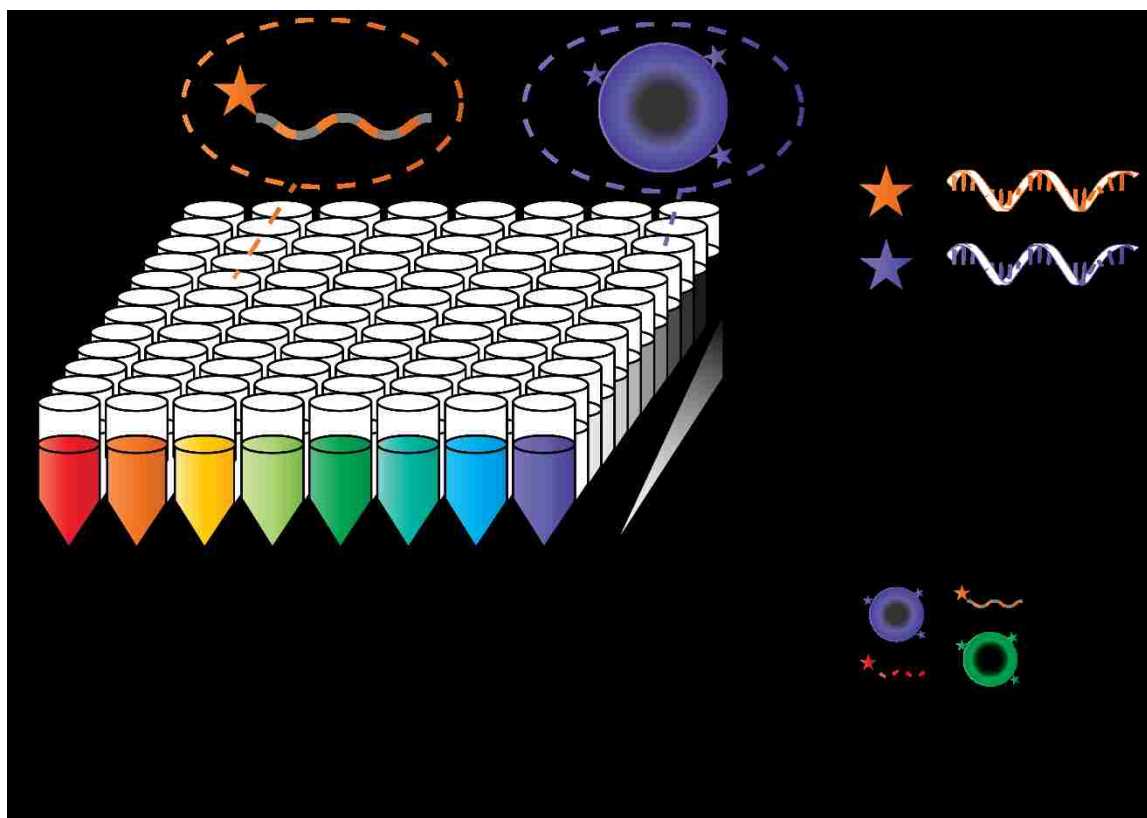
Figure 6.6 Drugamer library production and screening workflow.
We will synthesize a combinatorial drugamer library with variations in overall drug content, excipient co-monomer chemistry, and blocking orders (architectures) using high throughput controlled free radical techniques at RAMP. This array will be conjugated with an array of ssDNA barcodes, characterized for solubility, and pooled for biodistribution screening in mice.

6.3.3   *Aim 1: Synthesize a library of genetically barcoded polymer-drug conjugates*

Our synthetic strategy in Aim 1 will take advantage of the Stayton lab's access to groundbreaking

robotic machinery developed for high throughput polymer synthesis in collaboration with the

Rapid Automated Materials Processing (RAMP) laboratory of the Australian CSIRO. We will

utilize the RAMP facility to perform a large array of controlled free radical polymerizations with

unique reactant compositions, purify the resulting polymers, and conjugate DNA barcodes unique

to each polymer composition. (**Figure 6.6**) We will then characterize the library using high

throughput light scattering and absorption measurements to select non-aggregating, nanometer-

scale formulations for *in vivo* testing. Importantly, the Stayton lab has also developed a panel of drug-monomers (including resiquimod-methacrylate and galunisertib-methacrylate) that can be directly polymerized into "drugamers" alongside excipient monomers,[42–44] obviating the need for inefficient drug loading processes in our synthetic workflow. Building on our significant experience in polymer synthesis for targeted drug delivery, we will design reaction conditions to yield a library of drugamers with varying molecular weight, drug content, excipient monomer chemistry (e.g. mannose, PEG), and macromolecular architecture (linear unimers vs. self-assembled micelles). We expect *in vitro* characterization to identify solubility thresholds in high drug content formulations that are dependent on all other parameters varied. Indeed, this library approach is uniquely well suited to the exploration of diverse polymer property combinations that can enable high drug loading without compromising solubility.

6.3.4   *Aim 2: Identify drugamer properties that result in resiquimod delivery to desirable cell types in vivo*

HER2/neu is an oncogenic self-antigen overexpressed on approximately 30% of all breast cancers and a promising target for therapeutic vaccines, including those developed in the Disis lab.[45,46] Performing direct *in vivo* screening of our drugamer library in TgMMTV-neu mice will enable us to identify formulations that target resiquimod to relevant cell types associated with spontaneous, luminal breast tumors.[47] Because resiquimod is used clinically to either inflame and activate cells in the tumor microenvironment (TME) or potentiate the response of antigen presenting cells (APCs) to tumor antigens, we are most interested in designs from this library that accumulate in tumor-associated, lymph resident, and circulating myeloid cells (e.g. TAMs, MDSCs, DCs).[48,49] We have already shown that micelles with mannose surface chemistry are efficiently taken up by

MHCII^{high}/CD11c^{high} APCs in the inginual lymph nodes after subcutaneous or intradermal injection at the base of the tail. Thus, preliminary experiments will employ FACS of lymph node APCs to validate the retrieval of drugamer DNA barcodes delivered by first generation mannose polymers. Briefly, we will sort MHCII^{high}/CD11c^{high} cells into fixative and perform *in situ* reverse transcription on cellular RNA and barcode ssDNA, followed by tagmentation and PCR to generate cDNA and barcode libraries for sequencing as in previous work.[40] After validating our ability to retrieve polymer barcodes in parallel with cellular cDNA, we will inject the drugamer library in tumor-bearing mice and perform scRNA-seq on circulating leukoctyes and cells dissociated from tumors and lymph nodes. In addition to generating a multi-dimensional understanding of drugamer properties that lead to cell-type specific uptake, our scRNA-seq approach will also enable future investigations into the impact of resiquimod delivery on the gene expression of cells in the TME.

6.4 CONCLUSION

In this chapter, we have shown that the pH-responsive VIPER system is amenable to modifications of its micelle corona that enhance antigen uptake in target cells and enable the incorporation of drugamer adjuvants. In particular, we have established the means for replacement of cationic monomers and electrostatically complexed nucleic acid adjuvants used in the original VIPER-Vax formulation with mannose and resiquimod monomers, and have piloted studies that show the superiority of these next generation vaccine formulations. We further propose a molecular genetic technique to streamline the development of adjuvant drugamer delivery platforms, but conclude with optimism that the pH-responsive micelle structures we have pioneered show great promise as vehicles for both fundamental and applied research in cancer immunology.

6.5 SUPPLEMENTAL INFORMATION

Supplemental Table 6.3 Reaction parameters of neutral VIPER polymers

Polymer	PEG VIPER bl1 (courtesy Shixian Lv)	
		Feed
CTA	CCP	2
Initiator	n/a (this is a coupling reaction)	n/a
Monomer 1	mPEG-OH, 5000 g/mol	1
Monomer 2	DIC/DMAP	3/0.1
Monomer/solvent wt/wt%	1 g PEG / 10 mL DCM	
Solvent	DCM	
Reaction time / Temp	Overnight / room temperature	
Targeted conversion %	100	
Purification	Multiple precipitations in diethyl ether	

Polymer	PEG VIPER bl2	
		Feed
CTA	PEG VIPER bl1	1
Initiator	AIBN	0.1
Monomer 1	DIPAMA	35
Monomer 2	PDSEMA	5
Monomer/solvent wt/wt%	20	
Solvent	DMAc	
Reaction time / Temp	24 h / 70 °C	
Targeted conversion %	85	
Purification	Dialysis in MeOH then water	

Polymer	HPMA VIPER bl1	
		Feed
CTA	CCC	1
Initiator	AIBN	0.1
Monomer 1	HPMA	80
Monomer 2	n/a	
Monomer/solvent wt/wt%	25	
Solvent	DMAc	
Reaction time / Temp	12 h / 70 °C	
Targeted conversion %	95	
Purification	Dialysis in water	

Polymer	HPMA VIPER bl2	
		Feed
CTA	HPMA VIPER bl1	1
Initiator	AIBN	0.11
Monomer 1	DIPAMA	200
Monomer 2	PDSEMA	20
Monomer/solvent wt/wt%	20	
Solvent	DMAc	
Reaction time / Temp	24 h / 70 °C	
Targeted conversion %	15	
Purification	Dialysis in MeOH then water	

Polymer	MMA VIPER bl1	
		Feed
CTA	CCC	1
Initiator	ABCVA	0.1
Monomer 1	MMA	38
Monomer 2	n/a	
Monomer/solvent wt/wt%	25	
Solvent	DMSO	
Reaction time / Temp	7 h / 70 °C	
Targeted conversion %	90	
Purification	Dialysis in water	

| Polymer	MMA VIPER bl2	
		Feed
CTA	MMA VIPER bl1	1
Initiator	AIBN	0.25*
Monomer 1	DIPAMA	200
Monomer 2	PDSEMA	20
Monomer/solvent wt/wt%	25	
Solvent	NMP	
Reaction time / Temp	3 h / 70 °C*	
Targeted conversion %	10-15	
Purification	Dialysis in NMP then water	

*Note: Lower AIBN concentration (0.1 feed) and shorter reaction time (1 h) may be plenty if new AIBN powder is used. I found that I had to use more initiator and run the reaction longer as the stock of AIBN powder I had increased in age.

Supplemental Figure 6.7 Characterization of neutral VIPER polymers by ^{1}H NMR
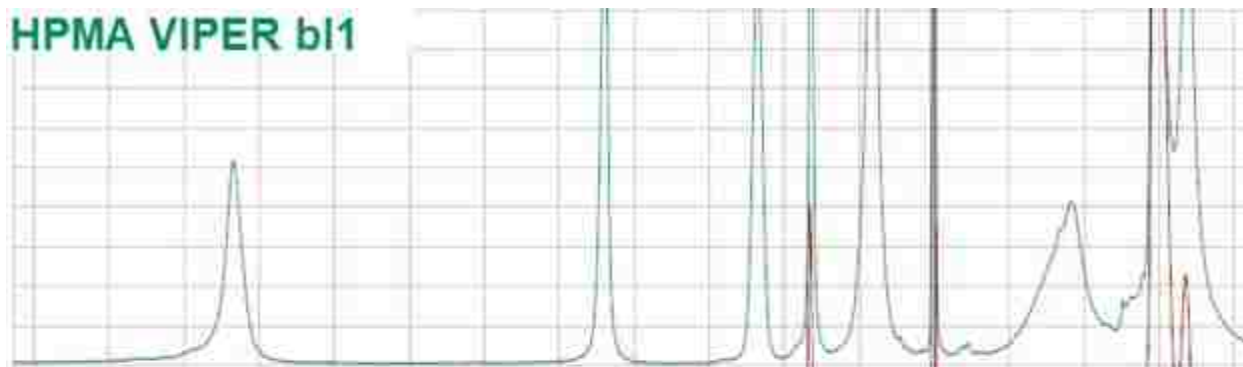Characteristic DIPAMA peaks appear at 1.2, 3.0, and 3.8 ppm.
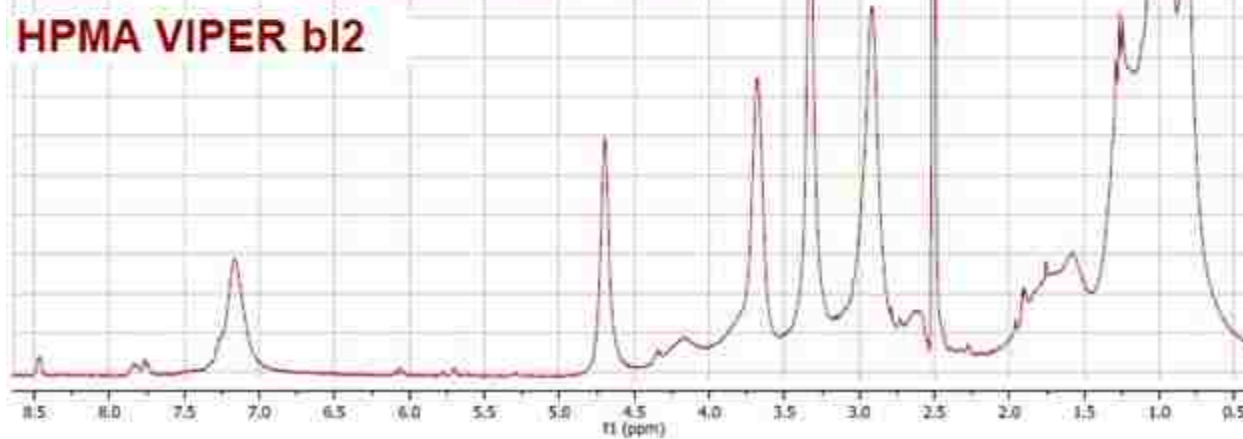Characteristic PDSEMA peaks appear at 7.2, 7.75, and 8.4 ppm.
PEG VIPER spectra were recorded CDCl$_3$, HPMA VIPER spectra were recorded in DMSO-d6, and MMA VIPER spectra were recorded in DMSO-d6 and D$_2$O + 1% TFA-d (bl1 and bl2, respectively).
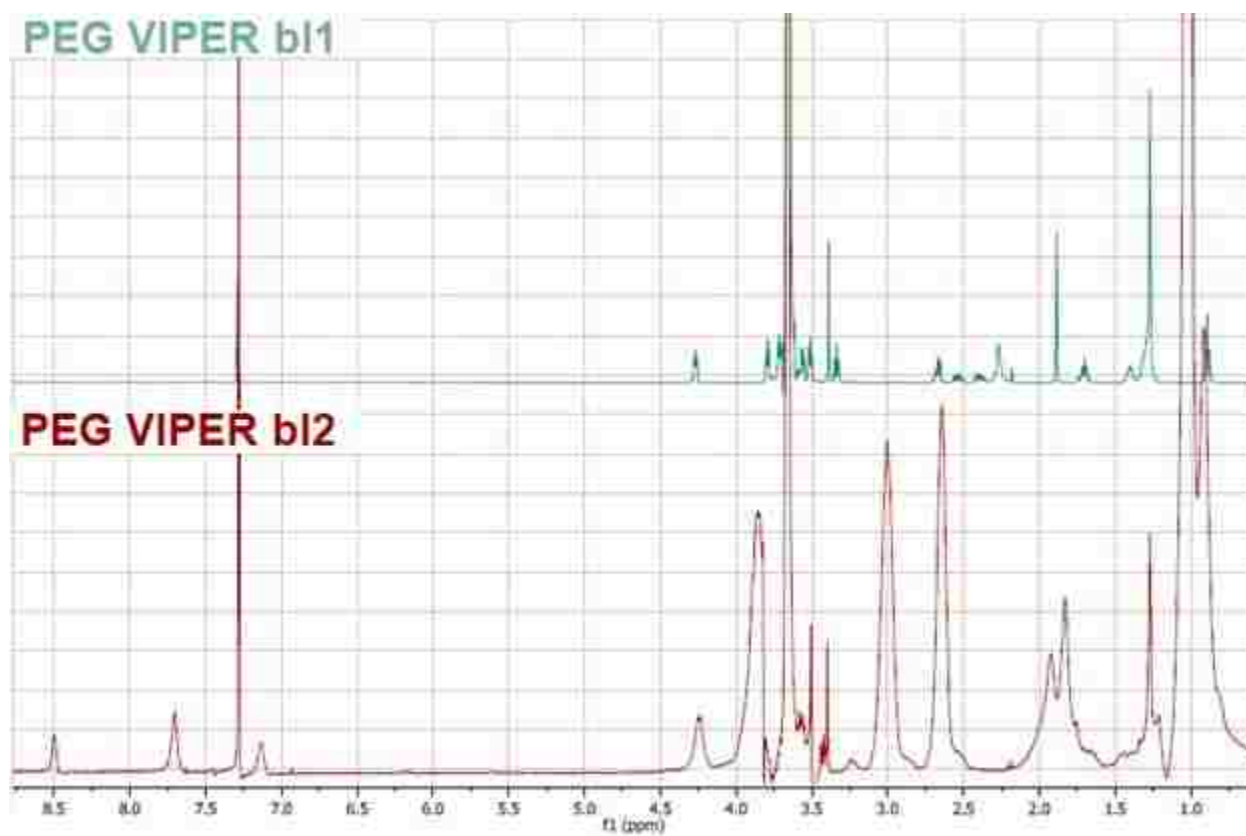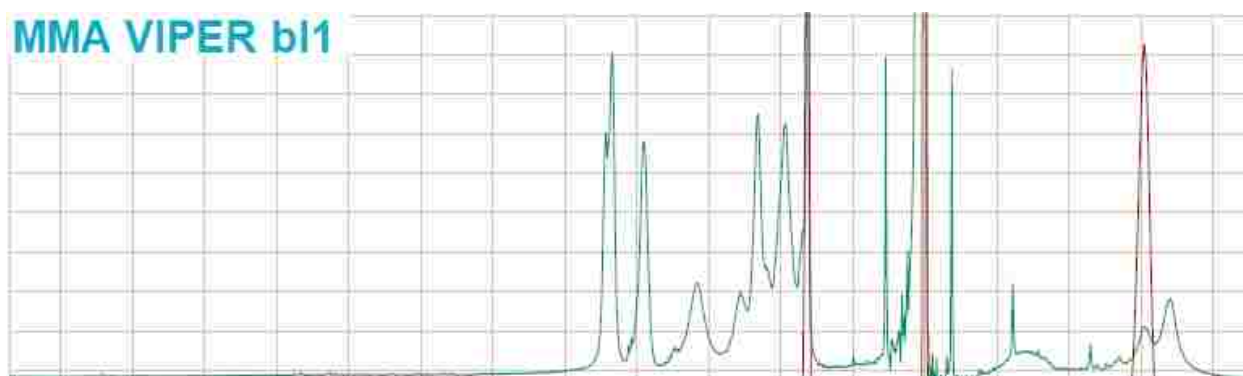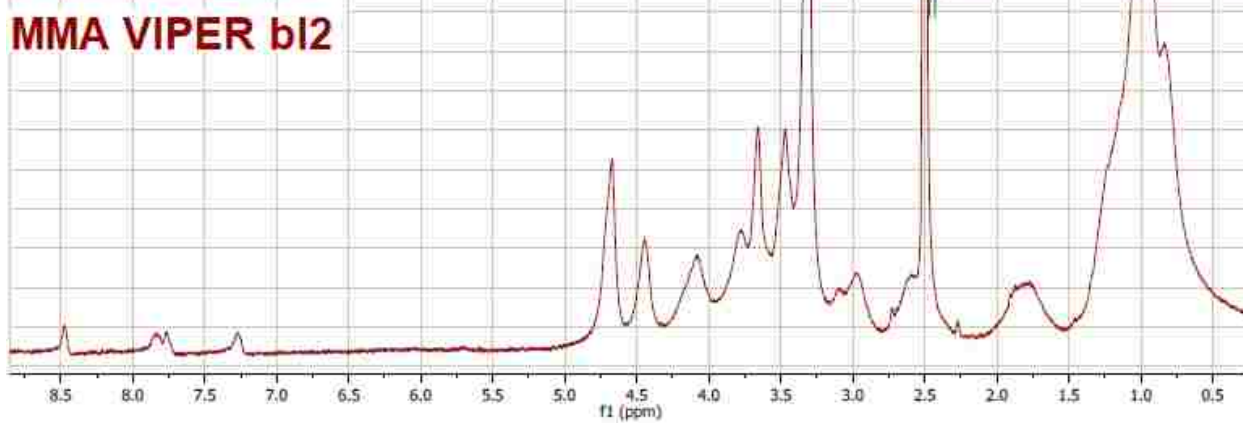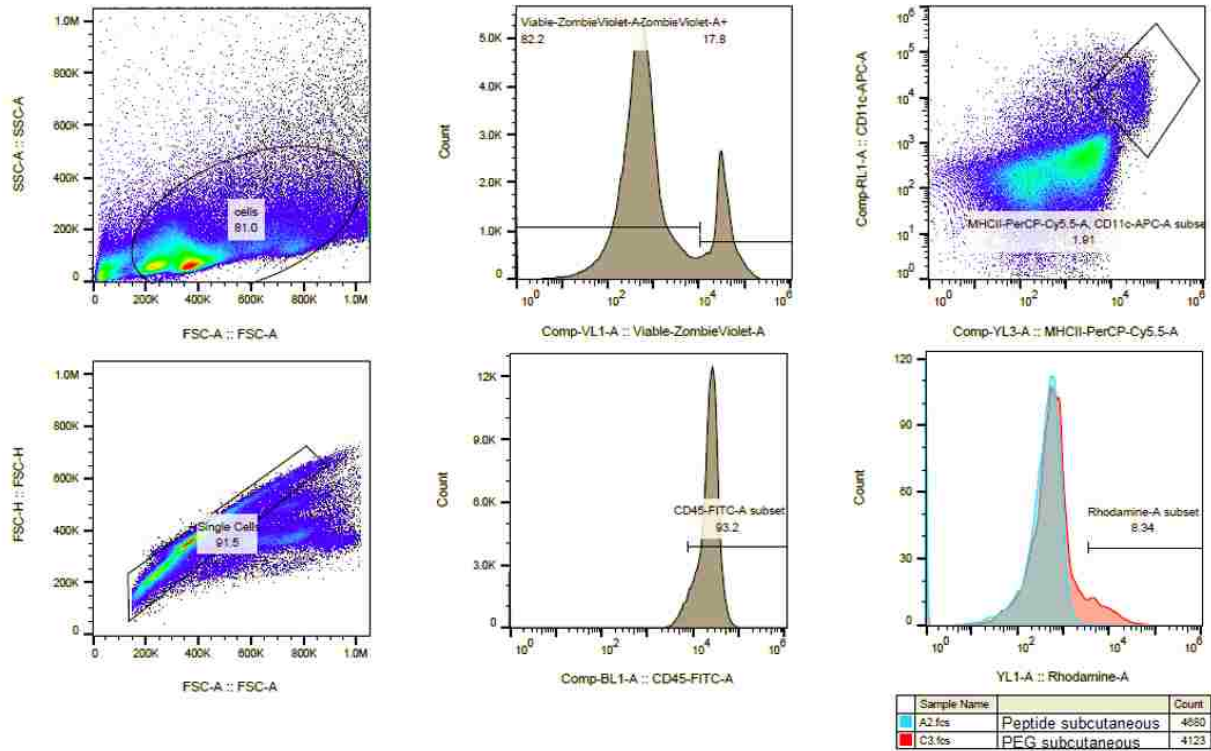
HPMA VIPER bl1

HPMA VIPER bl2

MMA VIPER bl1

MMA VIPER bl2

Supplemental Figure 6.8 Flow cytometry gating strategy for the detection of rhodamine-CSSSIINFEKL+ DCs.

Singlet cell events were gated using FSC/SSC, viable as Zombie Violet^{-}, lymphocytes as CD45 [+], dendritic cells as MHCII^{high}/CD11c^{high}, and then rhodamine+ through comparison to untreated controls.

Supplemental Figure 6.9 Whole body Xenogen imaging of rhodamine signal in mice treated with various VIPER formulations.
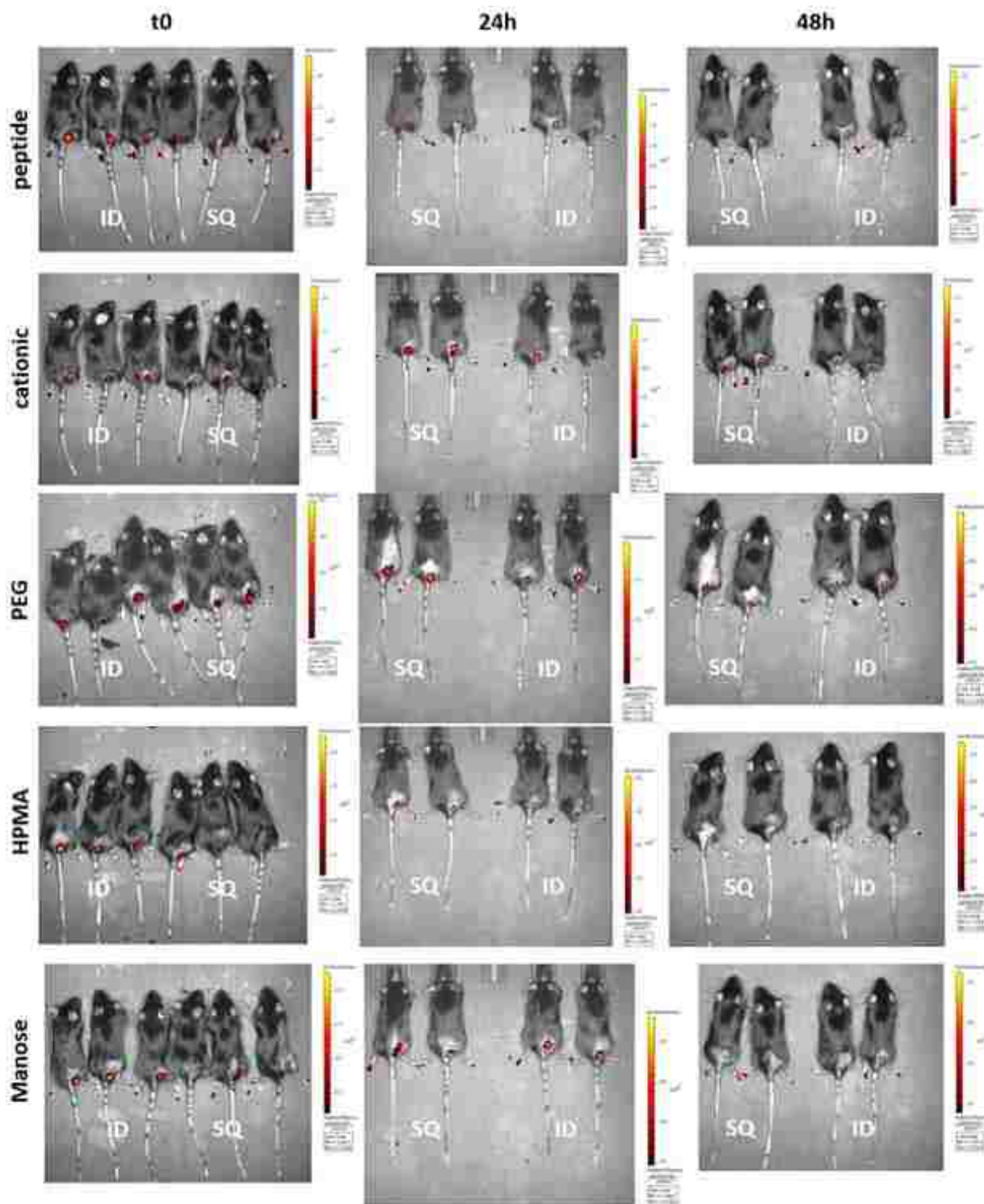
Supplemental Figure 6.10 Inguinal lymph node DC uptake of rhodamine-CSSSIINFEKL administered in various formulations and administration routes.
L = left inguinal lymph node; R = right inguinal lymph node; ID = intradermal; SQ = subcutaneous
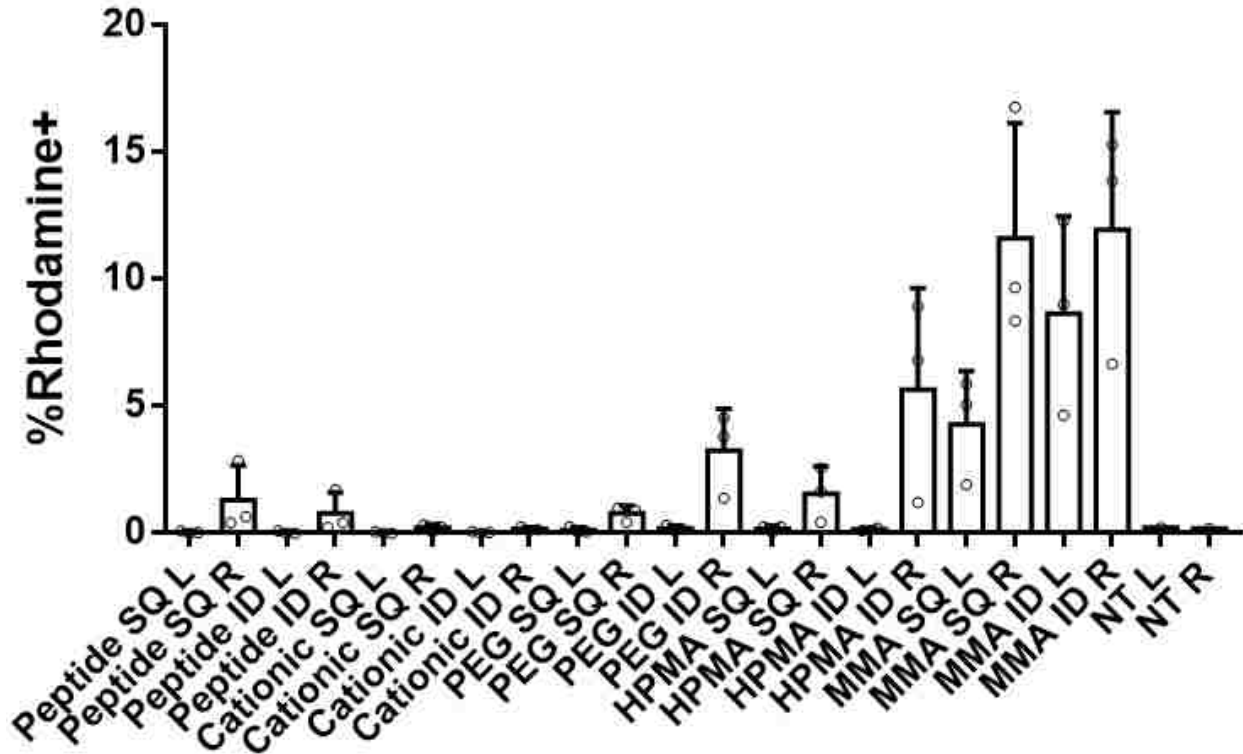
Supplemental Table 6.4 Reaction parameters of SRCMA VIPER polymers

Polymer	SRCMA VIPER 10 mol%	
		Feed
CTA	CCC	1
Initiator	V70	0.1
Monomer 1	SRCMA	7
Monomer 2	MMA	24
Monomer/solvent wt/wt%	25	
Solvent	DMSO	
Reaction time / Temp	22 h / 35 °C	
Targeted conversion %	90	
Purification	Dialysis in DMSO at RT then water at 4 °C	

Polymer	SRCMA VIPER 20 mol%	
		Feed
CTA	CCC	1
Initiator	V70	0.1
Monomer 1	SRCMA	12
Monomer 2	MMA	14
Monomer/solvent wt/wt%	25	
Solvent	DMSO	
Reaction time / Temp	22 h / 35 °C	
Targeted conversion %	90	
Purification	Dialysis in DMSO at RT then water at 4 °C	

Polymer	SRCMA VIPER block 2	
		Feed
CTA	Either SRCMA VIPER macro-CTA	1
Initiator	AIBN	0.25
Monomer 1	DIPAMA	12
Monomer 2	PDSEMA	14
Monomer/solvent wt/wt%	25	
Solvent	NMP	
Reaction time / Temp	3 h / 70 °C	
Targeted conversion %	10-15	
Purification	Dialysis in NMP at RT then water at 4 °C	

Supplemental Figure 6.11 Characterization of SRCMA VIPER by ^{1}H NMR. Perforemed in DMSO-d6.
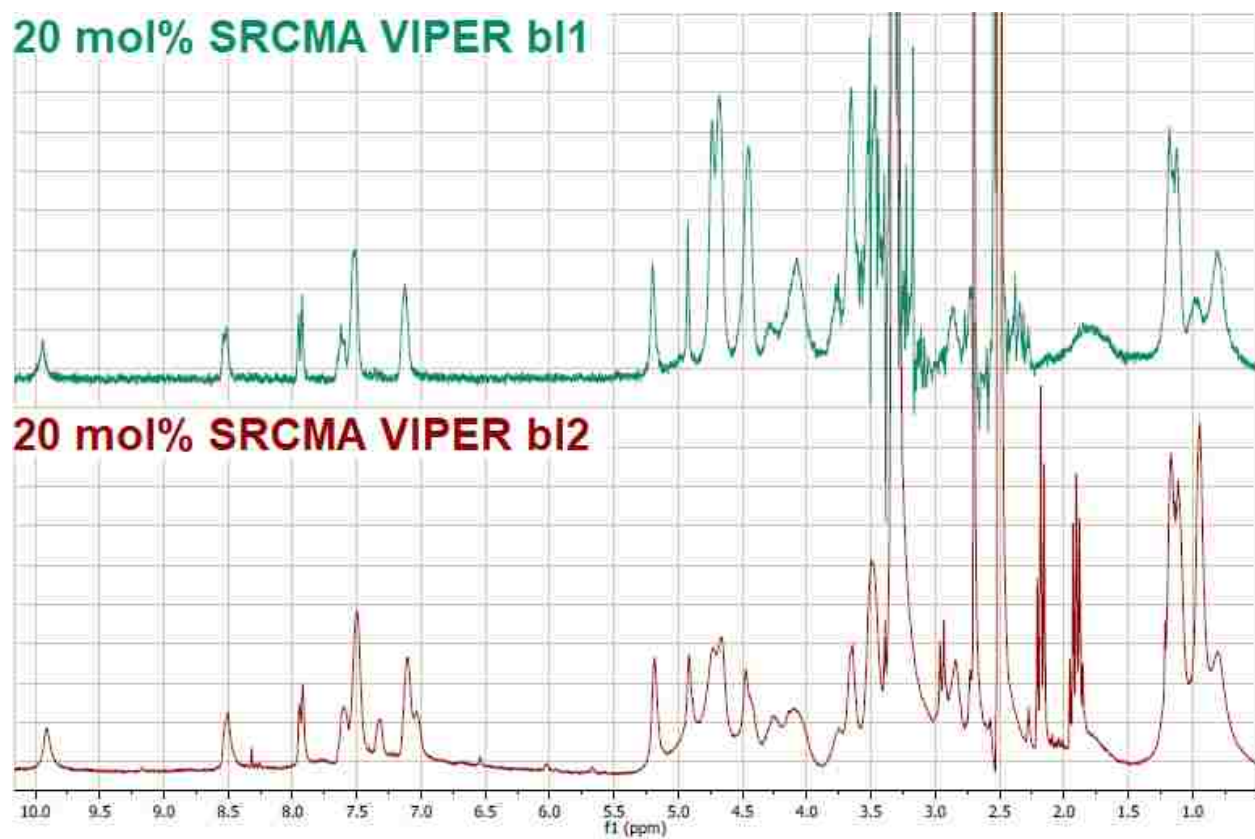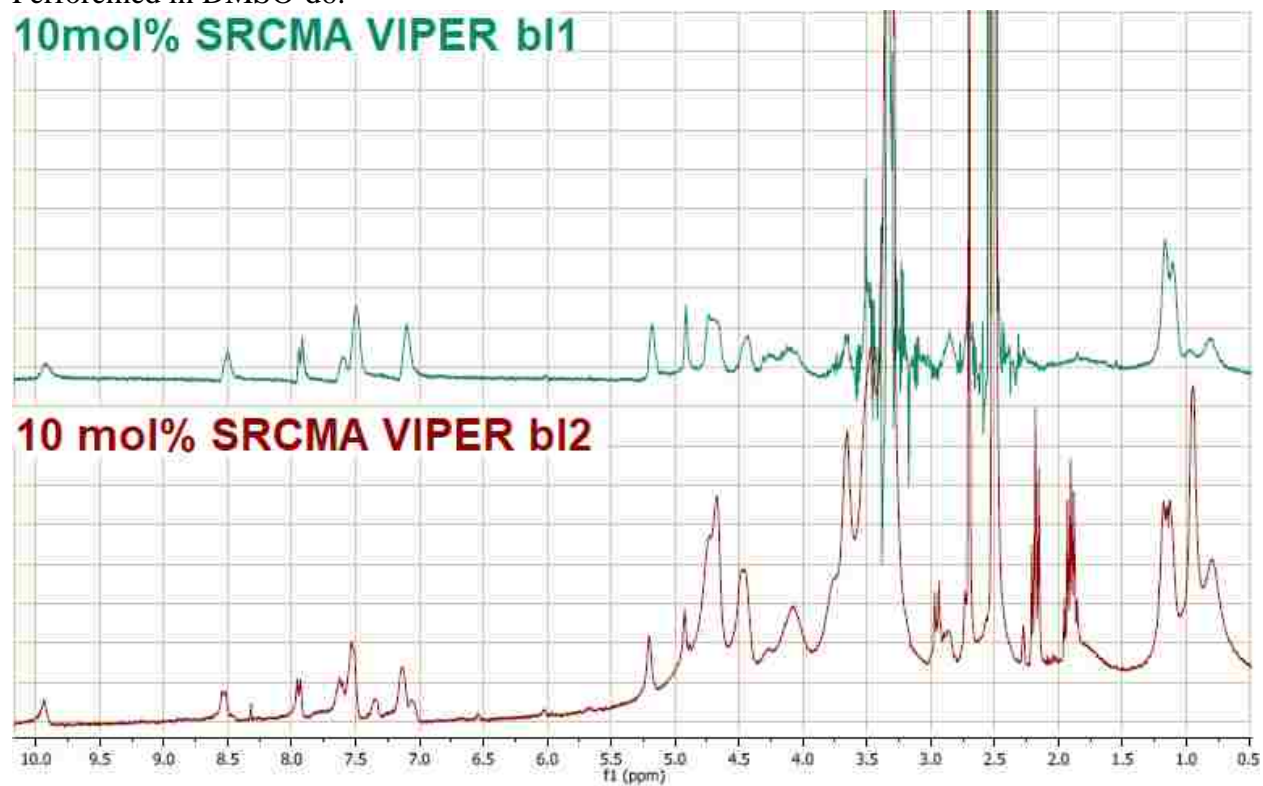
BIBLIOGRAPHY

(1) Sánchez-Paulete, A. R.; Teijeira, A.; Cueto, F. J.; Garasa, S.; Pérez-Gracia, J. L.; Sánchez-Arráez, A.; Sancho, D.; Melero, I. Antigen Cross-Presentation and T-Cell Cross-Priming in Cancer Immunology and Immunotherapy. *Annals of Oncology*. Oxford University Press December 1, 2017, pp xii44–xii55.

(2) Joffre, O. P.; Segura, E.; Savina, A.; Amigorena, S. Cross-Presentation by Dendritic Cells. *Nat. Rev. Immunol.* **2012**, *12* (8), 557–569.

(3) Bachmann, M. F.; Jennings, G. T. Vaccine Delivery: A Matter of Size, Geometry, Kinetics and Molecular Patterns. *Nature Reviews Immunology*. Nature Publishing Group November 15, 2010, pp 787–796.

(4) Thomas, S. N.; Rohner, N. A.; Edwards, E. E. Implications of Lymphatic Transport to Lymph Nodes in Immunity and Immunotherapy. *Annu. Rev. Biomed. Eng.* **2016**, *18* (1), 207–233.

(5) Thomas, S. N.; Schudel, A. Overcoming Transport Barriers for Interstitial-, Lymphatic-, and Lymph Node-Targeted Drug Delivery. *Curr. Opin. Chem. Eng.* **2015**, *7*, 65–74.

(6) Liu, H.; Moynihan, K. D.; Zheng, Y.; Szeto, G. L.; Li, A. V.; Huang, B.; Van Egeren, D. S.; Park, C.; Irvine, D. J. Structure-Based Programming of Lymph-Node Targeting in Molecular Vaccines. *Nature* **2014**, *507* (7493), 519–522.

(7) Eby, J. K.; Dane, K. Y.; O'Neil, C. P.; Hirosue, S.; Swartz, M. A.; Hubbell, J. A. Polymer Micelles with Pyridyl Disulfide-Coupled Antigen Travel through Lymphatics and Show Enhanced Cellular Responses Following Immunization. *Acta Biomater.* **2012**, *8* (9), 3210–3217.

(8) Thomas, S. N.; Vokali, E.; Lund, A. W.; Hubbell, J. A.; Swartz, M. A. Targeting the Tumor-Draining Lymph Node with Adjuvanted Nanoparticles Reshapes the Anti-Tumor Immune Response. *Biomaterials* **2014**, *35* (2), 814–824.

(9) Wattendorf, U.; Coullerez, G.; Vörös, J.; Textor, M.; Merkle, H. P. Mannose-Based Molecular Patterns on Stealth Microspheres for Receptor-Specific Targeting of Human Antigen-Presenting Cells. *Langmuir* **2008**, *24* (20), 11790–11802.

(10) Kempe, K.; Xiang, S. D.; Wilson, P.; Rahim, M. A.; Ju, Y.; Whittaker, M. R.; Haddleton, D. M.; Plebanski, M.; Caruso, F.; Davis, T. P. Engineered Hydrogen-Bonded Glycopolymer Capsules and Their Interactions with Antigen Presenting Cells. *ACS Appl. Mater. Interfaces* **2017**, *9* (7), 6444–6452.

(11) Yang, R.; Xu, J.; Xu, L.; Sun, X.; Chen, Q.; Zhao, Y.; Peng, R.; Liu, Z. Cancer Cell Membrane-Coated Adjuvant Nanoparticles with Mannose Modification for Effective Anticancer Vaccination. *ACS Nano* **2018**, *12* (6), 5121–5129.

(12) Palumbo, R. N.; Zhong, X.; Wang, C. Polymer-Mediated DNA Vaccine Delivery via Bystander Cells Requires a Proper Balance between Transfection Efficiency and Cytotoxicity. *J. Control. Release* **2012**, *157* (1), 86–93.

(13) Peeler, D. J.; Thai, S. N.; Cheng, Y.; Horner, P. J.; Sellers, D. L.; Pun, S. H. PH-Sensitive Polymer Micelles Provide Selective and Potentiated Lytic Capacity to Venom Peptides for Effective Intracellular Delivery. *Biomaterials* **2019**, *192*, 235–244.

(14) Manganiello, M. J. Development of PH-Responsive, Glycopolymer Micelles for DNA Delivery, University of Washington, 2013.

(15) Wilson, J. T.; Keller, S.; Manganiello, M. J.; Cheng, C.; Lee, C.-C.; Opara, C.; Convertine, A.; Stayton, P. S. PH-Responsive Nanoparticle Vaccines for Dual-Delivery of Antigens and Immunostimulatory Oligonucleotides. *ACS Nano* **2013**, *7* (5), 3912–3925.

(16) Hanson, M. C.; Crespo, M. P.; Abraham, W.; Moynihan, K. D.; Szeto, G. L.; Chen, S. H.; Melo, M. B.; Mueller, S.; Irvine, D. J. Nanoparticulate STING Agonists Are Potent Lymph Node-Targeted Vaccine Adjuvants. *J. Clin. Invest.* **2015**, *125* (6), 2532–2546.

(17) Luo, M.; Wang, H.; Wang, Z.; Cai, H.; Lu, Z.; Li, Y.; Du, M.; Huang, G.; Wang, C.; Chen, X.; et al. A STING-Activating Nanovaccine for Cancer Immunotherapy. *Nat. Nanotechnol.* **2017**, No. April.

(18) Cohn, L.; Chatterjee, B.; Esselborn, F.; Smed-Sörensen, A.; Nakamura, N.; Chalouni, C.; Lee, B.-C.; Vandlen, R.; Keler, T.; Lauer, P.; et al. Antigen Delivery to Early Endosomes Eliminates the Superiority of Human Blood BDCA3 + Dendritic Cells at Cross Presentation. *J. Exp. Med.* **2013**, *210* (5), 1049–1063.

(19) Segura, E.; Durand, M.; Amigorena, S. Similar Antigen Cross-Presentation Capacity and Phagocytic Functions in All Freshly Isolated Human Lymphoid Organ-Resident Dendritic Cells. *J. Exp. Med.* **2013**, *210* (5), 1035–1047.

(20) Howland, S. W.; Wittrup, K. D. Antigen Release Kinetics in the Phagosome Are Critical to Cross-Presentation Efficiency. *J. Immunol.* **2008**, *180* (3), 1576–1583.

(21) den Haan, J. M. M.; Bevan, M. J. Constitutive versus Activation-Dependent Cross-Presentation of Immune Complexes by CD8(+) and CD8(-) Dendritic Cells in Vivo. *J. Exp. Med.* **2002**, *196* (6), 817–827.

(22) O'Neill, L. A. J.; Hennessy, E. J.; Parker, A. E. Targeting Toll-like Receptors: Emerging Therapeutics? *Nature Reviews Drug Discovery*. Nature Publishing Group April 1, 2010, pp 293–307.

(23) Nuhn, L.; Vanparijs, N.; De Beuckelaer, A.; Lybaert, L.; Verstraete, G.; Deswarte, K.; Lienenklaus, S.; Shukla, N. M.; Salyer, A. C. D.; Lambrecht, B. N.; et al. PH-Degradable Imidazoquinoline-Ligated Nanogels for Lymph Node-Focused Immune Activation. *Proc. Natl. Acad. Sci.* **2016**, *113* (29), 8098–8103.

(24) Lynn, G. M.; Laga, R.; Darrah, P. A.; Ishizuka, A. S.; Balaci, A. J.; Dulcey, A. E.; Pechar, M.; Pola, R.; Gerner, M. Y.; Yamamoto, A.; et al. In Vivo Characterization of the Physicochemical Properties of Polymer-Linked TLR Agonists That Enhance Vaccine Immunogenicity. *Nat. Biotechnol.* **2015**, *33* (11), 1201–1210.

(25) Van Herck, S.; Deswarte, K.; Nuhn, L.; Zhong, Z.; Portela Catani, J. P.; Li, Y.; Sanders, N. N.; Lienenklaus, S.; De Koker, S.; Lambrecht, B. N.; et al. Lymph-Node-Targeted Immune Activation by Engineered Block Copolymer Amphiphiles–TLR7/8 Agonist Conjugates. *J. Am. Chem. Soc.* **2018**, jacs.8b08595.

(26) Kuai, R.; Ochyl, L. J.; Bahjat, K. S.; Schwendeman, A.; Moon, J. J. Designer Vaccine Nanodiscs for Personalized Cancer Immunotherapy. *Nat. Mater.* **2017**, *16* (4), 489–496.

(27) Fu, J.; Kanne, D. B.; Leong, M.; Glickman, L. H.; McWhirter, S. M.; Lemmens, E.; Mechette, K.; Leong, J. J.; Lauer, P.; Liu, W.; et al. STING Agonist Formulated Cancer Vaccines Can Cure Established Tumors Resistant to PD-1 Blockade. *Sci. Transl. Med.* **2015**, *7* (283), 283ra52.

(28) Pockros, P. J.; Guyader, D.; Patton, H.; Tong, M. J.; Wright, T.; McHutchison, J. G.; Meng, T. C. Oral Resiquimod in Chronic HCV Infection: Safety and Efficacy in 2 Placebo-Controlled, Double-Blind Phase IIa Studies. *J. Hepatol.* **2007**, *47* (2), 174–182.

(29) Engel, A. L.; Holt, G. E.; Lu, H. The Pharmacokinetics of Toll-like Receptor Agonists and the Impact on the Immune System. *Expert Rev. Clin. Pharmacol.* **2011**, *4* (2), 275–289.

(30) Lu, R.; Groer, C.; Kleindl, P. A.; Moulder, K. R.; Huang, A.; Hunt, J. R.; Cai, S.; Aires, D. J.; Berkland, C.; Forrest, M. L. Formulation and Preclinical Evaluation of a Toll-like

Receptor 7/8 Agonist as an Anti-Tumoral Immunomodulator. *J. Control. Release* **2019**, *306*, 165–176.

(31)   Wilson, D. S.; Hirosue, S.; Raczy, M. M.; Bonilla-Ramirez, L.; Jeanbart, L.; Wang, R.; Kwissa, M.; Franetich, J.-F.; Broggi, M. A. S.; Diaceri, G.; et al. Antigens Reversibly Conjugated to a Polymeric Glyco-Adjuvant Induce Protective Humoral and Cellular Immunity. *Nat. Mater.* **2019**, *18* (2), 175–185.

(32)   Lynn, G. M.; Chytil, P.; Francica, J. R.; Lagová, A.; Kueberuwa, G.; Ishizuka, A. S.; Zaidi, N.; Ramirez-Valdez, R. A.; Blobel, N. J.; Baharom, F.; et al. Impact of Polymer-TLR-7/8 Agonist (Adjuvant) Morphology on the Potency and Mechanism of CD8 T Cell Induction. *Biomacromolecules* **2019**, *20* (2), 854–870.

(33)   Li, Y.; Zhao, T.; Wang, C.; Lin, Z.; Huang, G.; Sumer, B. D.; Gao, J. Molecular Basis of Cooperativity in PH-Triggered Supramolecular Self-Assembly. *Nat. Commun.* **2016**, *7*, 13214.

(34)   Goldberg, M. S. Immunoengineering: How Nanotechnology Can Enhance Cancer Immunotherapy. *Cell*. Elsevier April 9, 2015, pp 201–204.

(35)   Hubbell, J. A.; Thomas, S. N.; Swartz, M. A. Materials Engineering for Immunomodulation. *Nature*. November 26, 2009, pp 449–460.

(36)   Yoon, H. Y.; Selvan, S. T.; Yang, Y.; Kim, M. J.; Yi, D. K.; Kwon, I. C.; Kim, K. Engineering Nanoparticle Strategies for Effective Cancer Immunotherapy. *Biomaterials* **2018**, *178*, 597–607.

(37)   Dahlman, J. E.; Kauffman, K. J.; Xing, Y.; Shaw, T. E.; Mir, F. F.; Dlott, C. C.; Langer, R.; Anderson, D. G.; Wang, E. T. Barcoded Nanoparticles for High Throughput in Vivo Discovery of Targeted Therapeutics. *Proc. Natl. Acad. Sci.* **2017**, *114* (8), 2060–2065.

(38)   Paunovska, K.; Gil, C. J.; Lokugamage, M. P.; Sago, C. D.; Sato, M.; Lando, G. N.; Gamboa Castro, M.; Bryksin, A. V.; Dahlman, J. E. Analyzing 2,000 in Vivo Drug Delivery Data Points Reveals Cholesterol Structure Impacts Nanoparticle Delivery. *ACS Nano*. American Chemical Society July 20, 2018, p acsnano.8b03640.

(39)   Lokugamage, M. P.; Sago, C. D.; Dahlman, J. E. Testing Thousands of Nanoparticles in Vivo Using DNA Barcodes. *Curr. Opin. Biomed. Eng.* **2018**, *7*, 1–8.

(40)   Rosenberg, A. B.; Roco, C. M.; Muscat, R. A.; Kuchina, A.; Sample, P.; Yao, Z.; Graybuck, L. T.; Peeler, D. J.; Mukherjee, S.; Chen, W.; et al. Single-Cell Profiling of the Developing Mouse Brain and Spinal Cord with Split-Pool Barcoding. *Science (80-.).* **2018**, *360* (6385), 176–182.

(41)   Freeman, H.; Srinivasan, S.; Das, D.; Stayton, P. S.; Convertine, A. J. Fully Synthetic Macromolecular Prodrug Chemotherapeutics with EGFR Targeting and Controlled Camptothecin Release Kinetics. *Polym. Chem.* **2018**, *9* (42), 5224–5233.

(42)   Das, D.; Srinivasan, S.; Kelly, A. M.; Chiu, D. Y.; Daugherty, B. K.; Ratner, D. M.; Stayton, P. S.; Convertine, A. J. RAFT Polymerization of Ciprofloxacin Prodrug Monomers for the Controlled Intracellular Delivery of Antibiotics. *Polym. Chem.* **2016**, *7* (4), 826–837.

(43)   Das, D.; Chen, J.; Srinivasan, S.; Kelly, A. M.; Lee, B.; Son, H.-N.; Radella, F.; West, T. E.; Ratner, D. M.; Convertine, A. J.; et al. Synthetic Macromolecular Antibiotic Platform for Inhalable Therapy against Aerosolized Intracellular Alveolar Infections. *Mol. Pharm.* **2017**, *14* (6), 1988–1997.

(44)   Su, F.-Y.; Srinivasan, S.; Lee, B.; Chen, J.; Convertine, A. J.; West, T. E.; Ratner, D. M.; Skerrett, S. J.; Stayton, P. S. Macrophage-Targeted Drugamers with Enzyme-Cleavable

Linkers Deliver High Intracellular Drug Dosing and Sustained Drug Pharmacokinetics against Alveolar Pulmonary Infections. *J. Control. Release* **2018**, *287*, 1–11.

(45) Knutson, K. L.; Disis, M. L. Expansion of HER2/Neu-Specific T Cells Ex Vivo Following Immunization with a HER2/Neu Peptide-Based Vaccine. *Clin. Breast Cancer* **2001**, *2* (1), 73–79.

(46) Disis, M. L.; Dang, Y.; Coveler, A. L.; Marzbani, E.; Kou, Z. C.; Childs, J. S.; Fintak, P.; Higgins, D. M.; Reichow, J.; Waisman, J.; et al. HER-2/Neu Vaccine-Primed Autologous T-Cell Infusions for the Treatment of Advanced Stage HER-2/Neu Expressing Cancers. *Cancer Immunol. Immunother.* **2014**, *63* (2), 101–109.

(47) Fry, E. A.; Taneja, P.; Inoue, K. Clinical Applications of Mouse Models for Breast Cancer Engaging HER2/Neu. *Integr. cancer Sci. Ther.* **2016**, *3* (5), 593–603.

(48) Gajewski, T. F.; Schreiber, H.; Fu, Y.-X. Innate and Adaptive Immune Cells in the Tumor Microenvironment. *Nat. Immunol.* **2013**, *14* (10), 1014–1022.

(49) Gardner, A.; Ruffell, B. Dendritic Cells and Cancer Immunity. *Trends Immunol.* **2016**, *37* (12), 855–865.